7.8 CONCLUSIONS AND SUMMARY

The basis and calculational method used to determine the amount of water that is evaporated from the AP600 containment steel shell during the operation of the passive containment water cooling system is conservative; both with respect to the individual elements of the WGOTHIC code and the PCS film coverage model, as well as the method of combining these elements in the Evaluation Model.

The amount of water that can be evaporated is the important input parameter to the WGOTHIC portion of the Evaluation Model. The amount of water evaporated determines the effectiveness of the PCS in limiting peak containment pressure, as well as the capability of the PCS to reduce and maintain low containment pressure following postulated limiting design basis events.

The basis for determining the evaporation-limited PCS flow rate input for WGOTHIC has been developed based on PCS test data and observations, and includes the following:

- The portion of the containment shell perimeter that is wetted versus the amount of water being delivered from the PCS water storage tank to the containment dome has been based on data from the Phase 3 Water Distribution Test. This test was performed with prototypic water distribution devices on a full sized segment of the dome and top of sidewall.

- The relationship of wetted perimeter to delivered flow is conservatively bounded by the linear equation,

  Γ_{dist} = Delivered Flow/Wetted Perimeter

  where: Γ_{dist} is a constant = [ ]^{a,c} lb_m/hr-ft for PCS flow rates less than 220 gpm

  The wetted perimeter used in the PCS film coverage model is limited to [ ]^{a,c} percent of the containment circumference.

- The several PCS tests performed with hot evaporating surfaces have demonstrated that the value for Γ_{dist} obtained with cold water on a cold surface conservatively bounds the Γ_{dist} that will occur with heated water on a heated surface during operation of the PCS.

- In the heat flux range of PCS operation, water streams on the containment surface are observed to become narrower in width only when most of the water in the stream has been evaporated. The Evaluation Model uses a Γ_{min} of [ ]^{a,c} lb_m/hr-ft, as the film flow rate at which water streams will become narrower. This minimum film flow rate conservatively bounds the observed minimum film flow rates observed in the PCS tests over the entire range of anticipated heat fluxes.

- Water or streams of water on the containment below the second water distribution weir ring and on the vertical containment sidewall are always observed to flow downward, following the natural fall

line of the dome surface.

The calculational methods for determining the amount of water evaporated have been developed and are consistent with or conservatively bound PCS test data and observations, and include the following:

- The evaporation of water due to the conduction of heat in the circumferential direction through the containment steel shell has been calculated for the alternating, vertical, wetted and dry stripes that were observed in the PCS testing at reduced delivered water flow rates.

- The reduction in dry surface convective and radiative heat transfer that is calculated to occur with alternating, vertical, wet and dry stripes on the containment shell has been determined to be conservatively considered in the WGOTHIC portion of the Evaluation Model.

Bounding assumptions and conservatisms for the operational characteristics of the PCS delivering and applying water to the containment surface have been incorporated in the Evaluation Model including:

- The portion of the containment shell surface wetted by the initial delivered PCS water flow rate is conservatively assumed to be [ ]^{a,c} percent, although, at the high initial flow rate, 100 percent coverage is expected. A sensitivity study has shown that the containment design pressure will not be exceeded when only 70 percent of the containment surface is wetted. Coverage at lower flow rates is based on cold water data, which are believed to underestimate the coverage area.

- The minimum delivered PCS flow rate used in the Evaluation Model assumes the single failure of one of two parallel valves in the PCS water storage tank discharge flow path to open.

- A 337-second delay time is used to account for filling the water distribution devices and for establishing steady-state water coverage over the containment shell. No credit is taken for any containment heat removal due to heating the delivered water or due to evaporation, prior to the time when the steady-state water coverage is established.

- The temperature of the delivered PCS water is assumed to be 120°F, 5°F higher than the design basis maximum ambient temperature, to minimize the amount of containment heat removed in heating the water to the temperature at which it is being evaporated.

- The evaporation-limited PCS water flow rate calculated by the PCS film coverage model neglects the subcooled heat capacity of the runoff flow.

7.9 NOMENCLATURE

Dimensionless Groups

Biot Number: $$Bi = \frac{\text{Convection}}{\text{Conduction}} = \frac{hL}{k}$$

Marangoni Number: $$Ma = \frac{\text{Surface Tension Force}}{\text{Viscous Force}} = \frac{\partial\sigma}{\partial T}\frac{\partial T}{\partial L}\frac{\delta^2}{\mu\alpha}$$

Reynold Number: $$Re = \frac{\text{Momentum Force}}{\text{Viscous Force}} = \frac{4\Gamma}{\mu}$$

Parameters

g	=	gravitational constant
h	=	convection heat transfer coefficient
k	=	conductivity
L	=	characteristic length,
$\dot{m}$	=	mass flow rate
M	=	multiplier representing the ratio of 2-D to 1-D heat transfer
$\dot{q}''$	=	surface heat flux
T	=	film temperature;
W	=	width of water film stripe
Z	=	vertical distance from top of sidewall

Greek Characters

α	=	thermal diffusivity,
β	=	surface angle of inclination relative to horizontal
Γ	=	film flow rate = mass flow rate per unit width of film,
δ	=	film thickness,
ρ	=	liquid density
σ	=	liquid surface tension
φ	=	heat or mass flux
θ	=	contact angle between the surface and film
μ	=	liquid viscosity

7.10 REFERENCES

7.1 A. T. Pieczynski, W. A. Stewart, WCAP-13884, "Water Film Formation on AP600 Reactor Containment Surface," February 1988

7.2 J. E. Gilmore, WCAP-13960, "PCS Water Distribution Phase 3 Test Data Report," December 1993

7.3 W. A. Stewart, A. T. Pieczynski, L. E. Conway, WCAP-12665 Rev 1, "Tests of Heat Transfer and Water Film Evaporation on a Heated Plate Simulating Cooling of the AP600 Reactor Containment," April 1992

7.4 R. E. Batiste, WCAP-14134, "AP600 Passive Containment Cooling System Integral Small-Scale Tests Final Report," August 1994

7.5 R. P. Ofstun and D. R. Spencer, PCS-T2R050, "Large-Scale Test Data Evaluation," May 1995, Westinghouse Electric Corporation

7.6 F. E. Peters, WCAP-13566, "AP600 1/8th Large-Scale Passive Containment Cooling System Heat Transfer Test Baseline Data Report," October 1992

7.7 F. E. Peters, WCAP-14135, Rev. 1, "Final Data Report for PCS Large-Scale Tests, Phase 2 and Phase 3," April 1997

7.8 D. R. Spencer, WCAP-14845, Rev. 3, "Scaling Analysis for AP600 Containment Pressure During Design Basis Accidents," March 1998

7.9 Frank Kreith, *"Principles of Heat Transfer,"* 3rd Edition, 1973

7.10 M. S. Bohn and S. H. Davis, "Thermocapillary breakdown of Falling Liquid Films at High Reynolds Numbers," *International Journal of Heat and Mass Transfer*, Vol. 36, pp 1875-1881 (1993)

7.11 F. Delose, R. P. Ofstun, D. R. Spencer, WCAP-14326, Rev. 2, "Experimental Basis for the AP600 Containment Vessel Heat and Mass Transfer Correlations,"April 1998, Westinghouse Electric Corporation

7.12 T. Fujita and T. Ueda, "Heat Transfer to Falling Liquid Films and Film Breakdown Parts I and II," *International Journal of Heat and Mass Transfer*, Vol. 21, pp. 97-108 and 109-118 (1978)

APPENDIX 7A

PHYSICS OF LIQUID FILMS ON THE AP600 AND AP1000 CONTAINMENT SHELLS

TABLE OF CONTENTS

7.A.1 INTRODUCTION 7.A-2

7.A.2 SUMMARY OF GENERAL LIQUID FILM BEHAVIOR 7.A-3

7.A.3 CONTACT ANGLE AND SURFACE WETTABILITY 7.A-8

7.A.4 DESCRIPTION OF LST OBSERVATIONS 7.A-14

7.A.5 CONCLUSIONS 7.A-19

7.A.6 REFERENCES 7.A-20

LIST OF TABLES

Table 7.A-1 Summary of Test Results to Determine Static Contact Angle 7.A-12

LIST OF FIGURES

Figure 7.A-1 Variation in Surface Tension Over the Surface of a Heated Liquid Film 7.A-6

Figure 7.A-2 Typical Qualitative Contact Angles for Advancing and Receding Contact Lines 7.A-10

Figure 7.A-3 Sketch of Qualitative Wavy Laminar Film Flow Characteristics on Heated LST Shell Water Stripe 7.A-15

Figure 7.A-4 Large-Scale Test Water Coverage Pattern at High PCS Flows 7.A-17

Figure 7.A-5 Sketch of LST Observation of Vessel Exterior at Water Flows Similar to LST 213.1 Showing Complete Dryout of Some Stripes 7.A-18

7.A.1 INTRODUCTION

The total evaporation from the external shell is the parameter of interest for mass transfer, the dominant means of removing heat from the containment. Total evaporation is equal to the integral of the mass flux over the covered, or wetted, area. The mass flux for a given set of parameters (surface and film temperature, film flow rate, annulus conditions) is given by correlations presented in Reference 7.A.1. The subject of this appendix is the wetted area of the external shell surface, and how the wetted area is limited by film stability effects.

Note that the initial application of water to the external surface at safety analysis basis surface temperatures is discussed in Section 7.6.5, so that quasi-steady water coverage is assumed to be established in the discussions of this appendix.

The introduction and Section 7.2 provide a brief overview of the PCS design, as it relates to film stability considerations. The test program is discussed in Section 7.6, where it is shown that the range of nondimensional parameters for AP600 and AP1000 is adequately covered in the test program. Subsequent Appendix 7A sections give a summary of literature findings on film stability, a discussion of the contact wetting angle that addresses the wettability of the coated surface in the context of surfaces studied in the literature, and a description of LST observed liquid film behavior for high and low flow tests. The physics summarized in this appendix were considered in the development of the PCS film coverage model. The PCS film coverage model is biased to conservatively bound test data that include cold full-scale tests and smaller-scale heated surface tests.

The double dam-weir system is designed to evenly distribute the PCS water onto the surface of the dome. The elliptical shape of the dome and corresponding area divergence helps spread the stripes of water flowing from the individual V-notches in the weirs. Water coverage on the top of the dome is the most difficult to quantify, but water coverage on this portion of the dome is also the least important to the successful operation of the PCS; the area between the top of the dome and the second weir is only about 20 percent of the total shell external surface area and is neglected in the PCS film coverage model calculation of the evaporation-limited PCS flow rate input for the WGOTHIC model.

The distribution system applies water to the shell in discrete, evenly spaced streams. Water from the PCCWST discharge header falls into a bucket suspended just above the center of the dome. Slots on the side of the bucket allow water to spill at discrete locations around the circumference onto the containment dome. From there, the water flows outward and downward, spreading due to the area divergence, until it is collected and redistributed by a series of two weir rings. Weir outflow rates as a function of time, including the initial filling of the bucket and dams, are shown in Figure 7-3. The method of water application, by weir slots, induces discrete water streams that can remain discrete at low PCS water flow rates and merge to form continuous circumferential water coverage at higher PCS water flow rates.

The initial application of water flowing from a weir slot hits the surface and spreads until surface tension and skin friction dissipate the momentum. If the film is significantly subcooled relative to the surface at that point, thermocapillary effects (see Section 7.A.2.2) may also affect how wide the stripe is as it flows down from the point of application. The PCS water distribution system employs two weir rings on the dome. By the time the water exits the second weir ring, the water has been heated to a temperature relatively close to that of the shell, so that thermocapillary effects are less important. Therefore, the focus for film stability is on evaporating film stability.

Evaporation of the PCS water results in a reduction of the mass flow rate as the film advances down the containment structure from the second weir. As the mass flow rate decreases, the wetted perimeter of the stable film also changes. From observation of tests, the wetted perimeter typically decreases only after the mass flow rate decreases below a certain point. The physical processes that limit the amount of stable film coverage on the containment shell are discussed in this appendix.

7.A.2 SUMMARY OF GENERAL LIQUID FILM BEHAVIOR

This section provides a summary of available literature on models and data for liquid films and provides a discussion of the various aspects of liquid film behavior.

7.A.2.1 Literature Summary

The study of movement in a fluid interface has been studied over 150 years. In studying the spreading of a drop of alcohol on the surface of water, British engineer and physicist James Thompson correctly explained the phenomena as a surface-tension-driven flow. The name of Italian physicist Carlo Marangoni has been associated with two distinct but related surface effects. The first is motion in a fluid interface caused by local variations in interfacial tension which were, in turn, caused by differences in composition or temperature. The second phenomenon is a conjugate of the first; it is the departure from equilibrium surface tension that is produced by the extension or contraction of an interface. Both of these phenomena are important to the understanding of the behavior of liquid films.

The stability of liquid films has been studied by many analysts and experimenters within the last 50 years. These studies may be grouped in two general categories;

1. Determining the minimum flow rate required to rewet a stable dry patch.
2. Examining the thermocapillary breakdown of a thin film.

Films are generally categorized as saturated films or subcooled films, due to differences in stability, or wetting performance. Films that are applied at or near the temperature of the surface are typically referred to as "saturated films." Such films, when applied to heated surfaces as is done on AP600 and AP1000, have a significant evaporation component and are thus called "evaporating films." Norman and McIntyre (Ref 7.A.2) reported data showing that a large increase in the minimum film wetting rate was required as the temperature difference between the surface and film was increased (that is, subcooling of the liquid film relative to the surface was increased). Hallet (Ref. 7.A-3) also observed this phenomenon and developed a film breakdown correlation that was related to the film surface tension difference, the wave number, and the heat transfer coefficient. Fujita and Ueda (Ref. 7.A-4) measured the breakdown of both subcooled and saturated liquid films on heated, vertical, polished, stainless steel tubes. A comparison of the results from their tests also showed that the highly subcooled films are unstable at flow rates several times higher than that observed for saturated films. More recently, Bohn and Davis (Ref. 7.A-5) measured the breakdown of subcooled water films on heated, vertical, polished, stainless steel tubes and developed a film breakdown correlation that was dependent on thermocapillary effects. Thus, there is clearly a basis for separately considering film stability for subcooled and evaporating films.

The conclusion that thermocapillary effects influence the early breakdown of subcooled films is based on the following. Subcooled films having liquid temperatures much lower than the solid surface temperature absorb heat, causing the film temperature to increase. Evaporating films that are more nearly in thermal equilibrium with the solid surface, transfer mass and energy from the film surface to the gas atmosphere. Thus, one explanation for the apparent reduced stability of subcooled films is the existence of significantly higher temperature gradients through the film that give rise to increased thermocapillary forces (see Section 7.A.2.2).

The manner in which data has been presented in the literature is also of interest. In general, the surface heat flux is recognized as the dominant independent parameter, and properties have a strong influence on film behavior. The literature presents data most often as film flow rate (mass flow rate per unit wetted perimeter) versus heat flux. To account for the effect of viscosity on wettability, the Westinghouse test data reduction uses film Reynold's number as the dependent parameter, with surface heat flux as the independent parameter.

The performance of the coated surface to be used for AP600 and AP1000 can be compared to the performance of the typical surfaces studied in the literature, polished steel and polished copper. The use of polished materials in laboratory tests allows careful characterization of the important parameter, the wetting angle. The coated surface does not lend itself to characterization of a single local wetting angle (Section 7.A.3.2). Therefore, the data for film flow rate versus heat flux give an appropriate means of comparison of film stability data. Stable film flow rates on the order of 20 to 50 lb_m/hr-ft are noted on the LST and other test surfaces, even with heat fluxes up to 10,000 Btu/hr-ft^2. Comparison to Fujita-Ueda data shows that the coated surface is significantly better at wetting, and is less sensitive to heat flux than the polished surfaces.

The list of papers reviewed and considered for application to the containment Evaluation Model is extensive and will not be given here. However, in a summary article (Ref. 7.A-6), Bankoff provided an extensive list of relevant papers. The current state of the art is focused on the "moving contact line," which was also considered for application to the containment Evaluation Model, but is generally not very practical for engineering application.

7.A.2.2 Thermocapillary Effect

Based on discussions with Bankoff (Reference 7.A-8), the thermocapillary effect is a result of the variation of surface tension with temperature in moving from the contact line to the free film surface (see Figure 7.A-1). For a stable stripe shape, the forces in the horizontal direction must sum to zero. The surface tension decreases as temperature increases, so the minimum stable film flow rate has to be greater to prevent the hotter liquid at the surface from causing the film stripe width to contract. The thermocapillary effect on the force balance is sometimes estimated (as in equation 7.A-2) by replacing the actual $\sigma(T)$ function with a much simpler function using the temperature drop through the film which can be related to the heat flux as

$$\sigma_{surf} - \sigma_{film} \approx \sigma_{surf} - (\sigma_{surf} + \frac{d\sigma}{dT}\Delta T_{film}) \approx -\frac{d\sigma}{dT}\frac{q''}{k_{film}} \qquad (7.A\text{-}1)$$

This simplification becomes increasingly inaccurate as the film subcooling increases, since the sensible temperature increase of the film invalidates the approximation q"/k, used to estimate the film surface temperature.

Overall, investigators have identified momentum, surface tension, body (hydrostatic) force, thermocapillary, and vapor thrust as the dominant forces affecting film stability. These forces are typically expressed as functions of flow rate, heat flux, fluid properties, and wetting angle. Vapor thrust can be neglected in AP600 and AP1000 because the heat flux is low, less than 10,000 BTU/hr-ft^2. Consequently, film stability may be considered to be controlled by a balance between momentum, surface tension, hydrostatic, and thermocapillary forces.

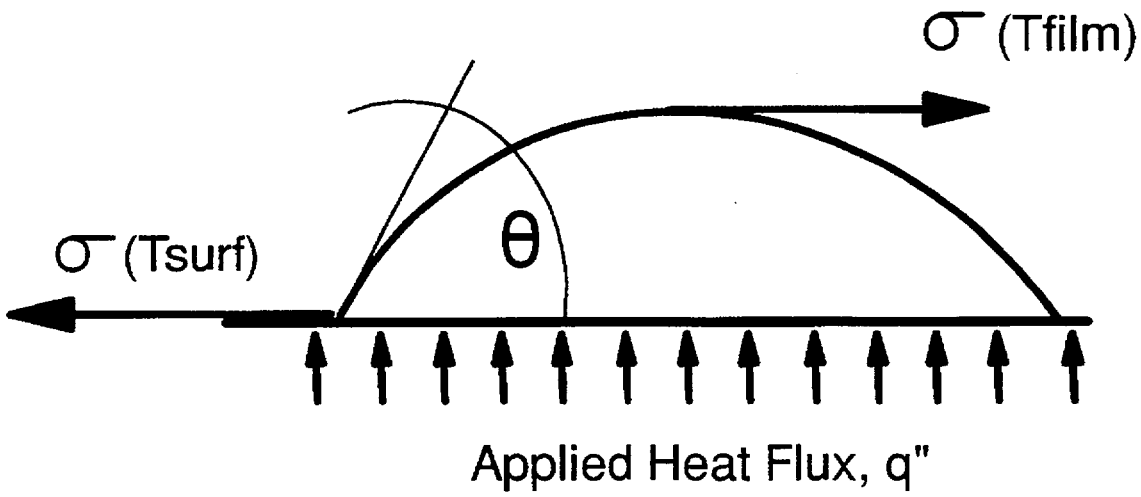

$$T_{surf} > T_{film}$$

$$\sigma_{surf} < \sigma_{film}$$

Figure 7.A-1 Variation in Surface Tension Over the Surface of a Heated Liquid Film

7.A.2.3 Available Theoretical Analytical Models

The available analytical theoretical models have not been found to be practical for determining the film coverage on the passive containment design. Rather, the Evaluation Model includes a film coverage model that is consistent with the physics of liquid films, and is developed to provide a conservatively bounded total water coverage. However, models proposed in the literature can be used to gain insight into film behavior.

The Zuber-Staub model (Ref. 7.A-7) considers the stability of a dry patch located within a uniform, flowing film, i.e., the inability of the liquid film to rewet the dry patch. The mathematical formulation of the model includes three of the dominant terms identified above: momentum, surface tension, and thermocapillary. The model uses a vertical force balance at the tip of a postulated dry patch to determine the minimum uniform film thickness required to rewet the dry patch. This minimum film thickness is a function of the surface heat flux, the film properties (including the contact angle between the film and surface).

One of the Zuber-Staub formulations treats the film thickness as the dependent parameter from which film stability criteria can be derived. Although film thickness is not easily measured, film thickness is related to the film flow rate through continuity. Therefore, the discussions that follow will treat the film flow rate as the controlling parameter from which film stability criteria may be derived.

According to the Zuber-Staub model, if the film flow rate is greater than the minimum stability value, any dry patch created in the film would be washed over and would readily disappear after formation due to the momentum of the flowing film. Conversely, if the film flow rate was equal to or less than the minimum stability value, a dry patch, if formed, would be predicted to be stable (i.e., the film would not be able to recover the dry patch). The Zuber-Staub model does not consider the effects of waves in recovering the dry patch.

The concept of a force balance can be used to develop insight into controlling parameters for film stability. A force balance more specific to the passive containment design that includes momentum, surface tension, thermocapillary, and body forces (and thus, surface inclination angle, β) to account for spreading on the inclined surface of the elliptical dome, but neglects the vapor thrust term, may be written in terms of the film flow rate, Γ. Since the relationship is for a stable film width, equilibrium between the various forces is assumed. If the film flow rate is greater than the value of Γ in the equation, the film will wash over any dry patch which happens to form. The equation, which can be used to examine the minimum stable film flow, Γ_{min}, is:

$$\frac{1}{15}\left[\frac{9g\ \sin\beta\ \Gamma_{min}^2}{\rho\mu}\right]^{\frac{2}{3}} + \left[\frac{3\rho g^2\ \cos^3\beta\ \mu\Gamma_{min}}{8\ \sin\beta}\right]^{\frac{1}{3}} = \frac{\sigma(1-\cos\theta)}{\left[\frac{3\mu\Gamma_{min}}{g\ \sin\beta\ \rho^2}\right]^{\frac{1}{3}}} - \frac{d\sigma}{dT}\frac{q''}{k}\cos\theta \qquad (7.A\text{-}2)$$

Note that the formulation given above assumes a laminar film with uniform film thickness and does not consider the effect of waves in wavy laminar flow. Waves in wavy laminar flow typically have a peak to valley distance of about 3 times the average film thickness, but occupy only a small fraction of the flowing volume. Waves carry momentum as they pass, but do not significantly affect the calculated average film thickness. Waves will wash through the region of flowing film, effectively wiping out any history effect of the method of application or other upstream effects. Therefore, film stability can be considered to be a local phenomenon, governed by local force balances at the point of interest on the contact line.

Equation 7.A-2 predicts higher values for the minimum stable film flow rate on surfaces that wet poorly, that is, those that have large contact angles, than for surfaces that wet readily. For surfaces that are heated, heat flux is destabilizing. The equation also shows that as the film heats up, it becomes more stable due to property changes.

Since the theoretical models available in the literature are not practical for determining the film coverage on the passive containment design, the insight gained from examining those approaches is used to support development of an empirical bulk coverage model. That is, the film stability can be characterized using a criterion for a minimum film flow rate, Γ_{min}, that will maintain a stable stripe. Data from tests at different scales, wherein the range of AP600 and AP1000 dimensionless parameters is sufficiently covered, can be used to empirically derive a bounding value for Γ_{min}. As discussed in 7.A.2.1, data can be represented using the film flow rate, and plotted against the dominant independent parameter, heat flux.

7.A.3 CONTACT ANGLE AND SURFACE WETTABILITY

A discussion of contact angles in general and observations from test coupons are provided to gain insight into the performance of the coated surface relative to surfaces in the literature. Finally, factors which can affect surface wettability are discussed.

7.A.3.1 Advancing and Receding Contact Angles

The place where the wet and dry regions intersect is called the contact line. For example, in a liquid film flowing down a wall in a constant width stripe, the contact lines are the two vertical lines defining the width of the stripe. The contact angle is defined as the angle between the solid and the liquid surface at the contact line. The contact angle between a water film and the surface to which it is applied is an indication of the surface wettability. Typically, better wetting occurs on surfaces with small contact angles. In practice, contact angles are measured for both advancing and receding films. Usually the two values are quite different, with the advancing contact angle being much larger than the receding contact angle. The relation between contact angle and velocity is qualitatively depicted in Figure 7.A-2. Of interest is the hysteresis between advancing and receding contact angles. There is actually a range of stable contact angles for a static contact line. Thus, if a droplet starts out by spreading, such as when it is dropped onto the surface, it will spread to a diameter governed by the advancing contact angle. Then as the droplet evaporates, it may be expected to remain at a constant diameter, with the contact line anchored, until the mass lost contracts the

droplet such that the receding contact angle is reached. Further evaporation would then cause the droplet diameter to decrease.

It is general practice to measure contact angles of a liquid on a smooth or polished surface, such as glass or polished steel having surface profiles measured in microns. High magnification is used to measure the contact angle as it meets the surface. The surface on the external containment shell is an inorganic zinc coating applied on a carbon steel structure. The surface of the inorganic zinc coating is not smooth, having a surface profile of several mils. With a surface profile of several mils, the magnified image shows significant peaks and valleys, making it impossible to measure a single contact angle that is applicable over the entire surface. Thus, the significance of a representative contact angle for the organic zinc coating used for the exterior of the containment shell is diminished. The interest is on bulk coverage performance over a large surface area, so larger scale integral tests are used. It is desired, however, to understand and relate the bulk wetting performance of the coated surface to that of surfaces in the literature. Therefore, measurements were taken to characterize a bulk static contact angle on the prototypic surface by observing a drop on sample coupons under various conditions as described below.

7.A.3.2 Static Contact Angle Measurements of Coated Surface

The bulk contact angle for a drop of water was measured as a function of temperature and age of the surface coating selected for the AP600 and AP1000. Two samples were prepared for these measurements. The first test coupon was supplied to Westinghouse by the coating vendor. This sample was prepared by the vendor and was not subjected to weathering. The second sample was a 12-in^2 section of a steel plate that was painted by Westinghouse and weathered for two years.

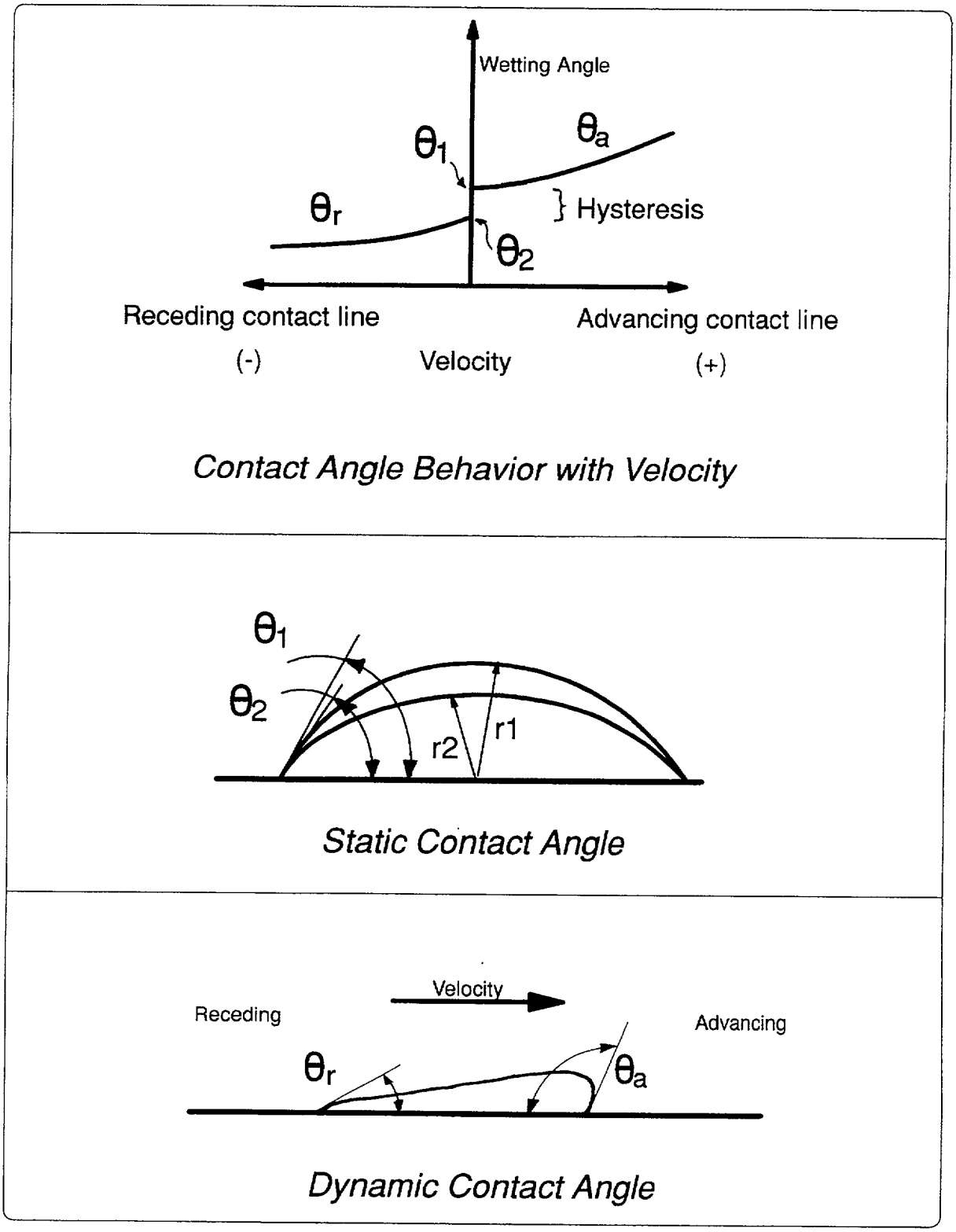

Figure 7.A-2 Typical Qualitative Contact Angles for Advancing and Receding Contact Lines

The following procedure was used to determine the static contact angle for both samples at ambient conditions:

- The test coupons were cleaned per coating vendor specifications and dried.
- The test coupon was placed in a horizontal position.
- A drop of water was placed on the test coupon.
- Using an optical comparator, the average angle between the sample surface and the drop at the interface.
- Measurements were repeated using several drops to ensure repeatability and consistency in the measurements.

Additional measurements were taken with the test coupons held at different temperatures. This was done to evaluate the effect of the surface temperature on the contact angle. The test coupons were heated with either hot water or a heat gun.

The static contact angle measurements taken are summarized in Table 7.A-1. They show that the contact angle for inorganic zinc coated surface decreases both with an increase in age and an increase in temperature. At high temperatures, the contact angle was observed to be initially larger than that observed for lower temperatures. It was observed, however, that the drops quickly spread and flattened out to a quasi-steady shape, thereby reducing the measured contact angle.

From the measurements listed in Table 7.A-1, it is concluded that a representative bulk or average contact angle for the inorganic zinc coated containment shell surface is between [ ]^{a,c} for a new surface, and between [ ]^{a,c} after just two years of weathering.

a,

A small drop of water spread around on the inorganic zinc-coated surface was not observed to contract, or snap back into a drop. This observation indicates that the receding contact angle for this surface is nearly zero. These observations also suggest that the film breakdown to form a dry spot occurs at a lower film Reynolds number than the critical Reynolds number for rewetting.

Static wetting angle measurements indicate that the coated surface is clearly more wettable than surfaces reported in the literature, and based on the force balance it is expected to be less sensitive to heat flux.

7.A.3.3 Relative Magnitude of Surface Tension Effects

A solid surface will be wet with liquid if the free surface energy of the solid is greater than the free surface energy of the liquid. Surface tension, σ, is defined as the work required to expand the surface of a liquid by a unit of area. It is a measure of the strength of the intermolecular forces in the fluid, similar to the latent heat of vaporization.

Hydrogen bonding is the strongest type of intermolecular force. Liquid water has relatively strong intermolecular forces due to the strong hydrogen bonds; 80 percent of the intermolecular attraction in water is attributed to hydrogen bonding. In a water molecule, the electrons spend more time in the vicinity of the oxygen atom than the hydrogen atoms because oxygen is more electro-negative than hydrogen (3.5 versus 2.1 for hydrogen on a scale of 4.0). This results in an electric dipole within the molecule. For this reason water is said to be a polar molecule.

As its temperature increases, the mean spacing between molecules in a liquid increases, causing the density to decrease and a reduction in the intermolecular forces. Therefore, both surface tension, σ, and the latent heat of vaporization, h_{fg}, decrease with increasing liquid temperature. For example, the surface tension of water is about 4.97×10^{-3} lbf/ft and the latent heat of vaporization is about 1054 BTU/lbm at room temperature. The value of these two parameters decreases to 4.0×10^{-3} lbf/ft and 970 BTU/lbm, respectively, at 212°F.

7.A.3.4 Factors Affecting Surface Wettability

The wetting of a solid surface by water is improved by reducing the surface tension of the water (by use of a wetting agent such as a detergent), by making the surface more porous (to improve the spreading by capillary action), or by using a polar surface (increasing the intermolecular forces between the surface and the polar liquid water). The use of a surfactant was examined during the Water Distribution Tests. It was found that surfactants offered no effective improvement in coverage. This has been postulated to be due to the turbulence of the flowing film which would not allow the surfactant to influence the surface of the film significantly. The porosity of the inorganic zinc coating is believed to be the primary factor affecting wetting early in the coating's life, adding a significant capillary effect at the contact line. It was postulated that the buildup of polar molecules (e.g., oxides of zinc) on the solid surface improved its wettability with age. Photographs were taken of both new and weathered surface coating samples using a scanning electron microscope with an energy dispersive X-ray spectrometer to identify the chemical species present on the surface. More oxides of zinc were found on the weathered surface than the new surface, supporting the hypothesis that the increase in wetting is due to the surface becoming more polar as it ages.

A buildup of some surface contaminants can result in a reduction in wettability. The worst surface contaminant for the inorganic zinc coating is silicone; it has both low surface energy and low polarity. Sources of silicone in air pollution are rare. Other surface contaminants that could result in reduced wetting include hydrocarbons such as oils, members of the PTFE family (Teflon), polypropylene, and polyethylene residues. To combat surface contaminants, the coatings vendor has developed and made available a standard cleaning procedure and a specially developed detergent that emulsifies these types of surface contaminants so they can be washed away.

Although the number of potential contaminants that would adversely affect wetting of the inorganic zinc coating surface is probably limited to a dozen or so, it would be very difficult to analytically predict the wetting degradation over time. The degradation of surface wettability would have to be estimated as a function of the concentration of each potential contaminant, the deposition rate of each as a function of the local or worst case atmospheric conditions, and the assumption that the degradation is additive, etc. Therefore, periodic in-service inspections will be performed to look for corrosion and surface contaminant buildups to assure surface wettability. The frequency and procedures for testing and the minimum acceptance criteria prior to cleaning the surface are defined in the Reliability Assurance Program.

7.A.3.5 Summary of Wetting Angle Assessment

The contact angle between a water film and the surface to which it is applied is an indication of the surface wettability. Although the surface provided by the inorganic zinc coating applied to the external surface of the containment is not smooth relative to other materials used to measure contact angles such as glass or polished steel, measurements were taken to characterize a bulk static contact angle of a spreading film on the prototypic surface to relate to literature data. The static angle was measured by observing the spreading of a drop on two coupons, one weathered and one not weathered, under ambient and heated conditions. Results showed that a surface weathered for two years is significantly more wettable [ ]^{a,b} than surfaces for which data exists in the literature (in the range of 60 degrees).

7.A.4 DESCRIPTION OF LST OBSERVATIONS

LST observations to characterize wetting behavior were made during shakedown tests, video tapes were recorded, and sketches were made for the test records. During these shakedown tests, quasi-steady heat flux and water flow rate conditions were achieved, and then water flow was slowly valved down in stages with constant steam flow. At each stage, when quasi-steady conditions again were reached, observations and notes were taken. Subsequent similar cycles were done at several steam flows (heat fluxes). The objective was to observe the behavior of the liquid film as it varied from a moderately high flow down to nearly complete evaporation. Since the majority of the LST matrix tests were run with a high flow rate, the qualitative discussion starts with a description of water coverage on a high flow test. Finally, the water coverage on a low flow test is described. Observations are consistent with the physics of liquid films discussed above.

7.A.4.1 High Flow LST

As discussed in Section 7.6.3, the water is applied to the shell in stripes around the circumference of the test vessel. Stripe widths for a given steady state test were relatively constant, varying by fractions of an inch as the delivered flow rate varied (see Section 7.6.3). Based on Reynolds number, the flow regime is wavy laminar, which has been confirmed by test observations. The wavy laminar regime is discussed in the literature. A simple sketch is provided in Figure 7.A-3, showing qualitative characteristics observed for a representative film stripe on a heated LST surface with a high flow rate. High flow rate LST typically exhibited constant width stripes, as discussed further below. Stripe widths varied from an inch or an inch or less to complete circumferential coverage, depending on the test delivered flow and heat flux. Within a stripe, the majority of the width is flowing water with wavy laminar conditions. In that portion, waves are generated by upstream disturbances and advance down the stripe with a velocity faster than the average film speed, consistent with continuity flow theory. The waves generally alternate with slight left and right horizontal velocity components.

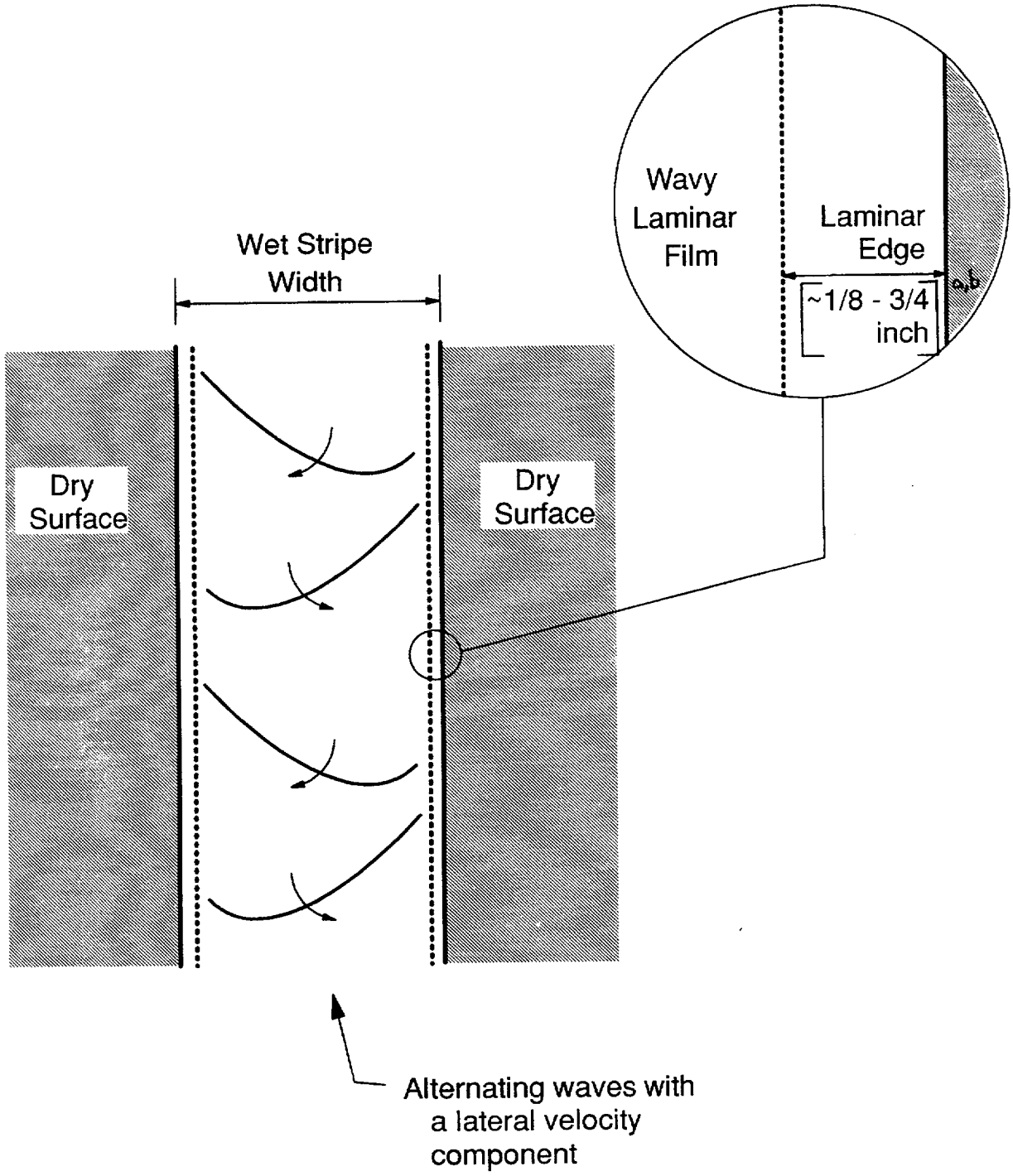

Figure 7.A-3 Sketch of Qualitative Wavy Laminar Film Flow Characteristics on Heated LST Shell Water Stripe

Water stripe edges exhibited a narrow [ ]^{a,b} region of laminar flow. Visual observation indicated that the edges were wetted but not obviously flowing. When an obstruction was placed within a wet edge, a "bow wave" built up above the obstruction, confirming that indeed liquid was flowing downward in that region. The film flow, and thus thickness, in that region is small enough that viscous forces damp out any disturbances. For example, the waves are damped by viscous forces in the stripe edge. Note that the laminar edge was also observed to occur on stripes which narrowed as their film flow rates decreased due to evaporation. This indicates that there is a very thin layer near a stripe edge, or in fact the equivalent wetting angle at the contact line is very small. This is consistent with the consideration in 7.A.3 that the receding wetting angle likely governs film stability of an evaporating stripe on the containment shell.

Since the water is applied as stripes at the dome with J-tubes (see Figure 7.A-4), and there is significant liquid film subcooling over much of the LST dome for high flow tests, the width of stripes that reach the vertical sidewall is less than can be supported by a stable film at the given film flow rate. Therefore, it can be postulated that the initial width at the top of the vertical sidewall is sufficiently greater than the evaporating film stability limit and that evaporation from the stripes does not cause the receding contact angle to be reached. Rather the film stripes in high flow LST tests are believed to remain within the region of hysteresis over the entire height, consistent with the observed constant width stripes.

7.A.4.2 Low Flow LST

Figure 7.A-5 shows a composite of typical film characteristics on a portion of the LST shell at relatively low flows typical of the water flow applied to LST 213.1. The tests described here have film flows that are low enough that evaporation causes the receding contact angle to be reached, and further evaporation leads to narrowing of the stripes.

As for the high flow LST, the water is delivered to the vessel shell surface via J-tubes, as a subcooled film. The application method and subcooled film stability set the initial stripe width, similar to the high flow tests. However, the film heats up to become an evaporating film before it reaches the sidewall. Observations were made of shakedown tests at conditions (steam flow, external water flow) similar to those for LST 213.1. During the initial setup prior to heating the vessel, the film flow was established and gradually valved down. As very low flows were reached, some J-tubes were seen to stop delivering water before others, indicating that there was some asymmetry in delivered flow per stream. This is consistent with observations of heated tests that indicated stripe widths and vertical extents varied around the circumference of the vessel.

In Figure 7.A-5 the width of the two outer stripes shown remain approximately constant down to a certain elevation, varying only as the delivered flow rate varied. At some elevation on the sidewall, which may be different for different stripes, the film width began to narrow until the gutter was reached.

For some stripes, shown as the two innermost stripes in Figure 7.A-5, the delivered flow was low enough that the stripes completely evaporated before reaching the gutter elevation.

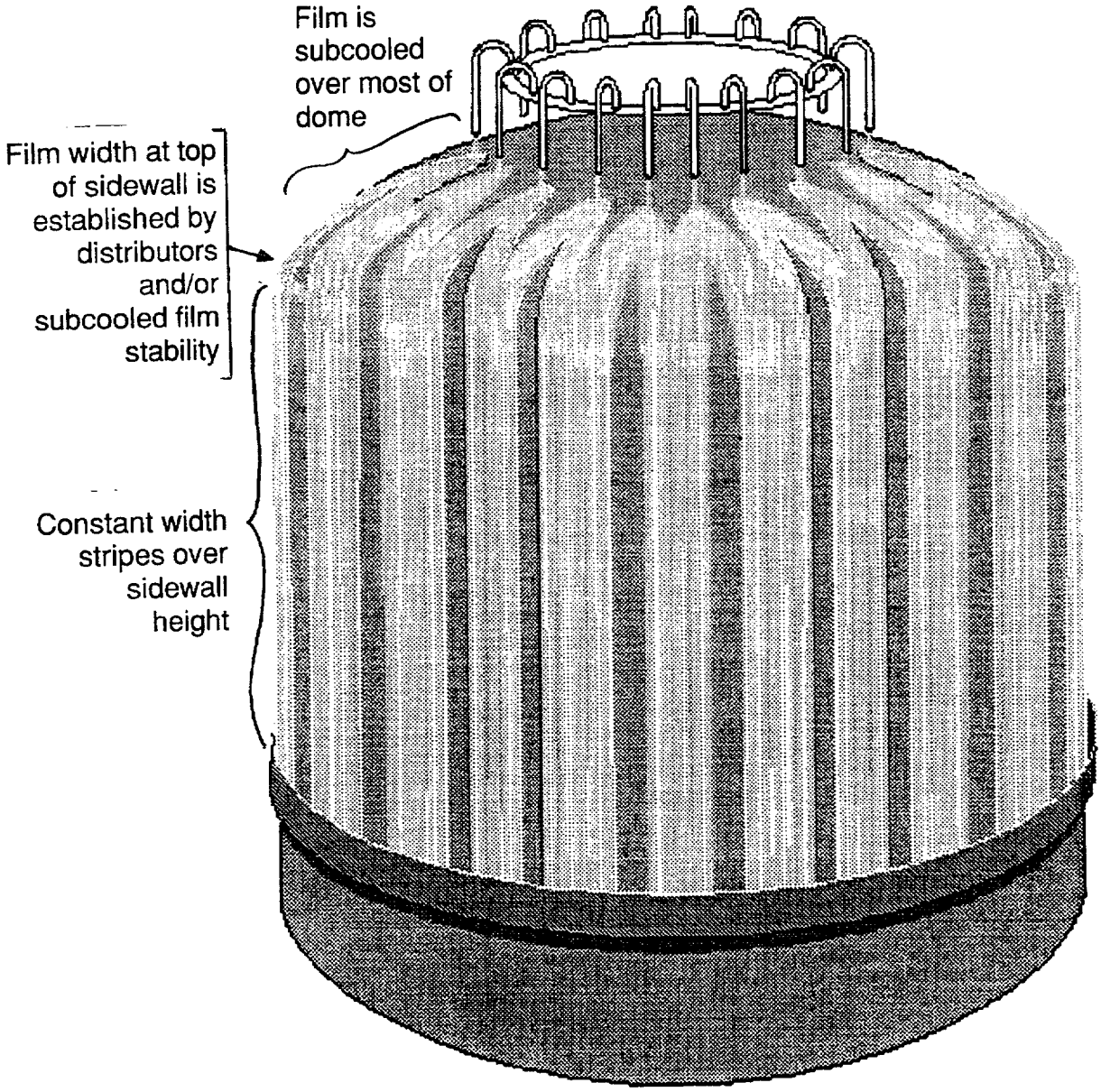

Figure 7.A-4 Large-Scale Test Water Coverage Pattern at High PCS Flows

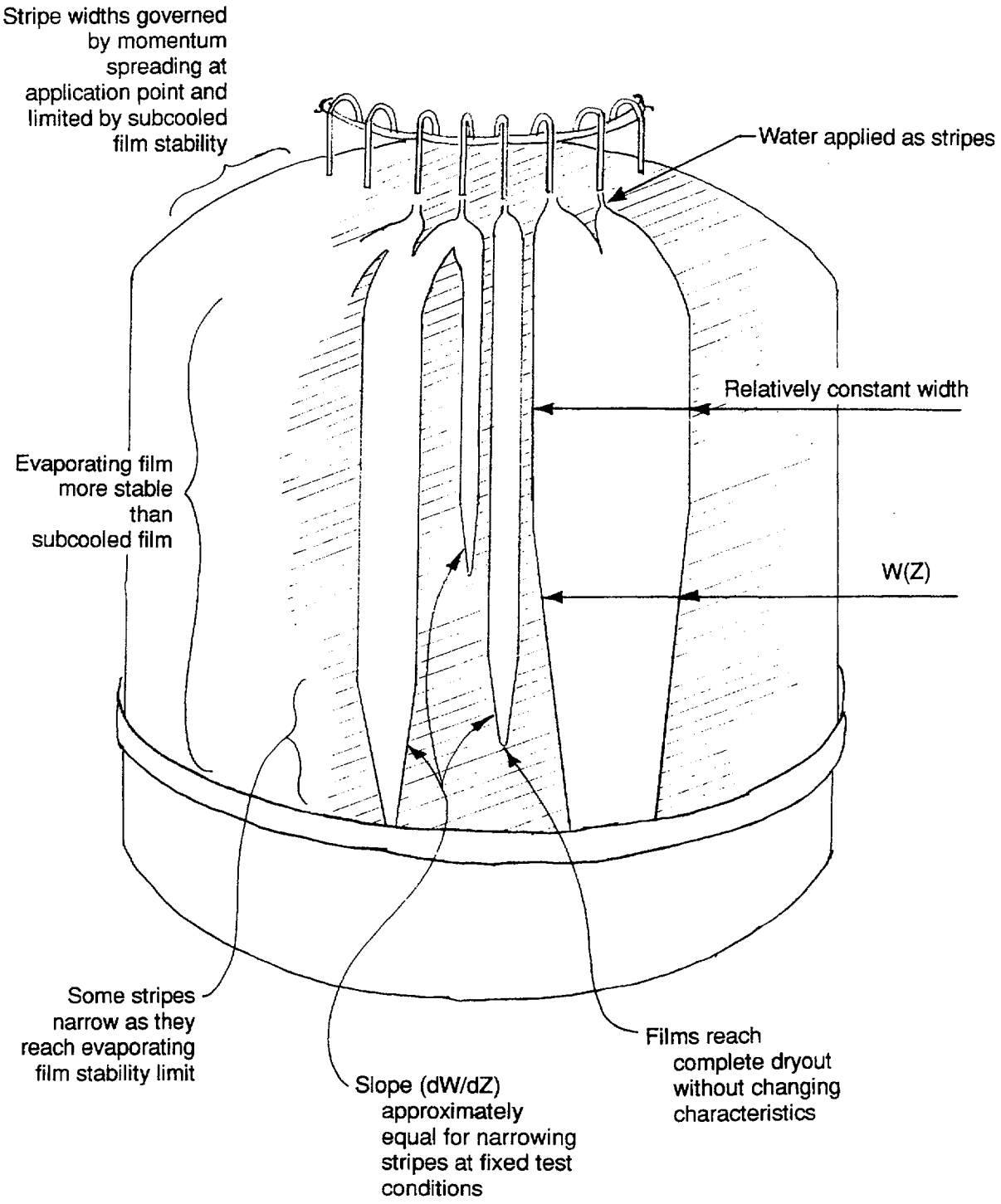

Figure 7.A-5 Sketch of LST Observation of Vessel Exterior at Water Flows Similar to LST 213.1 Showing Complete Dryout of Some Stripes

The slope of the changing width as a function of height, dW/dZ, was carefully observed. Qualitative observation indicated that the dW/dZ of each stripe around the circumference was nearly constant at a specific quasi-steady-state test condition.

Of most interest in these tests, relative to water coverage, is the fact that stripes that evaporated completely did so without changing their characteristics near the point of complete dryout. Thus, for the surface tested, the liquid films did not snap, or draw up, into a thick film. The edges of the film, including the bottom edge remained as wavy laminar film up to within a fraction of an inch from the edge, including the lower edge. As the water flow rate was valved down, the bottom edge moved gradually up, and when the flow was increased to its original value, the vertical extent of the stripe returned to a consistent elevation. Therefore, the film was well behaved as it completely evaporated.

7.A.5 CONCLUSIONS

A comparison of coated surface data with polished surface data from the literature shows the coated surface is more wettable.

Models from the literature are not sufficiently developed to be considered reliable. The literature provides an indication of the appropriate parameters to study film breakdown data: Re_{film} or Γ and heat flux. A practical approach taken to bound the data from the various tests is to establish a minimum stable film flow rate, Γ, that can be used to define a minimum coverage.

History effects are washed out by waves, so breakdown can be considered to be a local phenomenon. Therefore, LST (Section 7.6.3), SST (Section 7.6.2), and heated flat plate tests (Section 7.6.1) can be said to represent the bottom portions of liquid film stripes on the containment shell that dry out due to evaporation.

Observations of tests are explained based on physics of liquid films on heated surfaces. At high enough applied flows, the applied stripe maintains constant width until the film stability limit is reached, governed by the receding contact angle, then the stripe begins to narrow consistent with the minimum film flow rate required to maintain a stable film.

Observations of tests show that complete dryout occurs while maintaining a stable stripe geometry, gradually decreasing in width until it disappears.

7.A.6 REFERENCES

7.A.1 WCAP-14326, Revision 2, "Experimental Basis for the AP600 Containment Vessel Heat and Mass Transfer Correlations," April 1998.

7.A.2 W. S. Norman and V. McIntyre, "Heat Transfer to a Liquid Film on a Vertical Surface," *Trans. Inst. Chem. Engrs.* Vol. 38, pp 301-307 (1960).

7.A-3 V. A. Hallett, "Surface Phenomena Causing Breakdown of Falling Liquid Films During Heat Transfer," *International Journal of Heat and Mass Transfer*, Vol. 9, pp 283-294 (1966).

7.A-4 T. Fujita and T. Ueda, "Heat Transfer to Falling Liquid Films and Film Breakdown Parts I and II," *International Journal of Heat and Mass Transfer*, Vol. 21, pp 97-108 and 109-118 (1978).

7.A-5 M. S. Bohn and S. H. Davis, "Thermocapillary breakdown of Falling Liquid Films at High Reynolds Numbers," *International Journal of Heat and Mass Transfer*, Vol. 36, pp 1875-1881 (1993).

7.A-6 S. G. Bankoff, "Dynamics and Stability of Thin Heated Liquid Films," *Transactions of the ASME – Journal of Heat Transfer*, Vol. 112, pp 538-546, (1990).

7.A-7 N. Zuber and F. W. Staub, "Stability of Dry Patches Forming in Liquid Films Flowing over Heated Surfaces," *International Journal of Heat and Mass Transfer*, Vol. 9, pp 897-905 (1966).

7.A-8 Dr. S. G. Bankoff, discussions held at Westinghouse Science and Technology Center during observations of LST, 1996.

Section 8

Containment Pressure Sensitivity During Blowdown

TABLE OF CONTENTS

LIST OF FIGURES iii

8.1 INTRODUCTION 8-1

8.2 METHOD 8-1

8.3 ANALYSIS 8-2

8.4 CONCLUSIONS 8-2

LIST OF FIGURES

Figure 8-1 Comparison of Single-Node Model with EM Pressure Curve 8-3

Figure 8-2 Comparison of Response with No Heat Sinks to EM Response 8-4

8.1 INTRODUCTION

The purpose of performing the single-node WGOTHIC analysis is to show that the containment pressure during the blowdown phase (predicted using the WGOTHIC code) is essentially the same as if Standard Review Plan (SRP) methodologies were utilized for the analysis. This comparison supports the use of WGOTHIC during the analysis of the blowdown phase of the transient, since it is expected that the presence of external heat removal from the containment shell during the first 50 seconds of the transient has little impact on the pressure transient. The containment shell time constant is long, as compared to the transient time, and passive cooling system (PCS) film flow is assumed to be delayed until well after the end of blowdown.

The purpose of performing the sensitivity to heat sinks during blowdown is to confirm that volume compliance is the dominant means of mitigating pressure increase during blowdown.

8.2 METHOD

The AP600 evaluation model (EM) described in Section 4 was used for comparison in this study. The EM was converted to a single-node containment model, consistent with SRP 6.2.1 methodology and comparable to the licensed Westinghouse methodology by the following input modifications:

- All of the climes were removed.
- All of the flow paths, except for those associated with the mass and energy release forcing functions, were deleted. The mass and energy forcing functions were not changed.
- All control volumes which represent the outside containment regions were deleted.
- A single-node containment control volume, containing all of the thermal conductors from the base case and the two mass and energy release forcing functions, was created.
- A conductor representing the containment shell was added to the single-node containment control volume.
- The Uchida heat transfer correlation with revaporization was used on the shell and conductors.

The EM was modified to eliminate heat removal from the containment gas volume by internal heat sinks and the steel shell. The only modification to the EM was to delete all thermal conductors within containment and to effectively eliminate the clime conductors for the shell itself by assuming an adiabatic inner surface.

8.3 ANALYSIS

The blowdown phase pressure results for the single-node analysis are compared to the EM containment pressure in Figure 8-1.

The blowdown phase pressure response without heat sinks is compared to the EM results in Figure 8-2.

8.4 CONCLUSIONS

The conclusion of the blowdown noding sensitivity is that the single-node model (utilizing SRP 6.2.1 methodologies) essentially provides the same results during the blowdown phase as the EM.

The conclusion of the sensitivity to eliminating heat sinks during blowdown shows a relative pressure increase at the end of blowdown of only 3.6 psi relative to the EM. This compares to the EM pressure increase of about 33 psi during the blowdown phase, which confirms the dominant pressure mitigation during blowdown is energy storage due to pressure increase of the volume, or volume compliance.

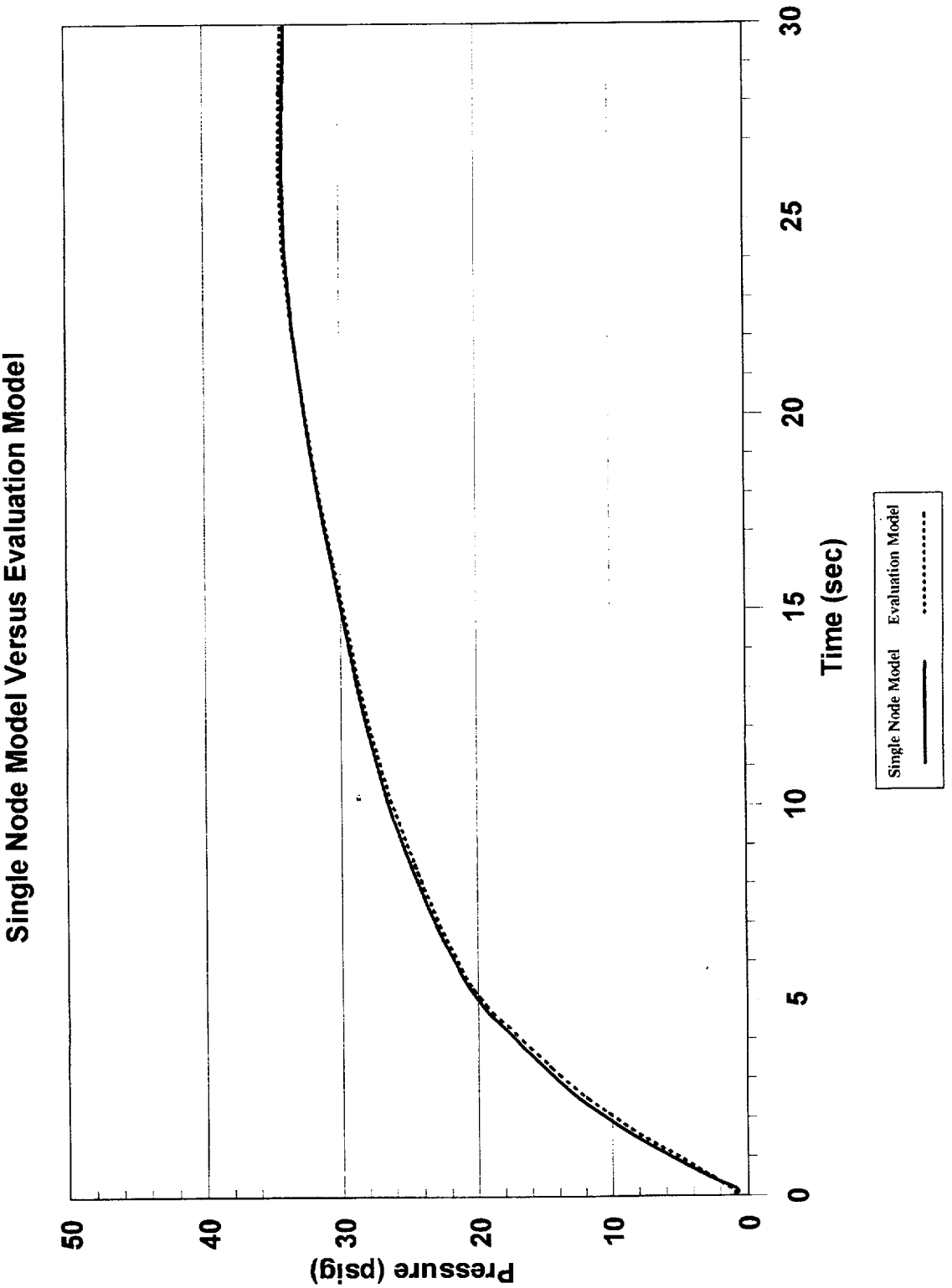

Figure 8-1 Comparison of Single-Node Model with EM Pressure Curve

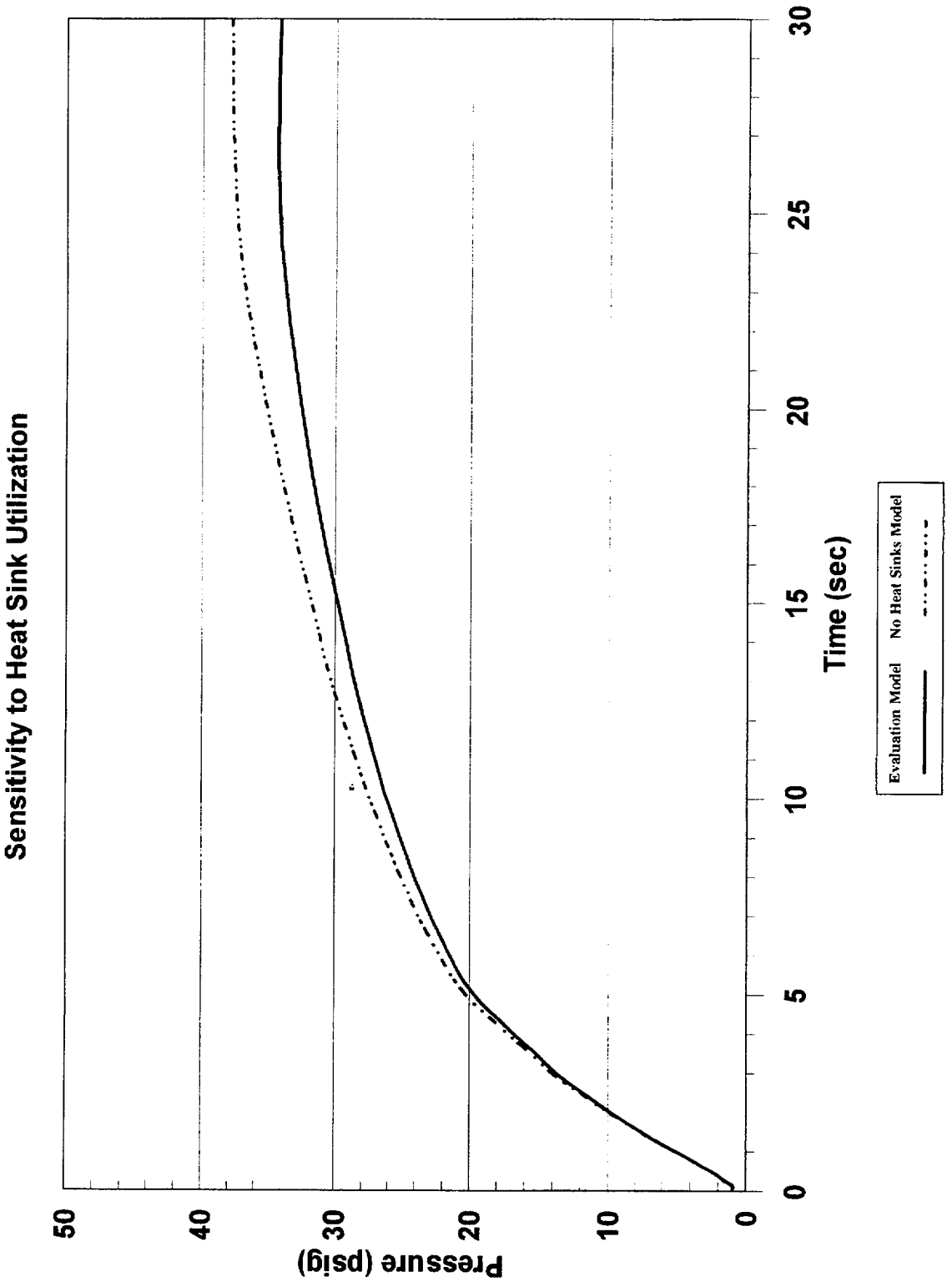

Figure 8-2 Comparison of Response with No Heat Sinks to EM Response

Section 9

Circulation and Stratification Within Containment

TABLE OF CONTENTS

LIST OF TABLES iv
LIST OF FIGURES v

9 CIRCULATION AND STRATIFICATION WITHIN CONTAINMENT 9-1

9.1 INTRODUCTION 9-4
9.1.1 Definitions 9-14
9.1.2 Lumped Parameter Biases and Capabilities 9-14

9.2 LARGE-SCALE TEST RESULTS 9-17
9.2.1 LOCA Configuration 9-18
9.2.2 MSLB Configuration 9-19
9.2.3 Method to Address Distortions in LST Stratification Data 9-20
9.2.4 Application of Modeling Methods Developed for NUPEC M-4-3 Lumped Parameter Model 9-22

9.3 CIRCULATION AND STRATIFICATION ASSESSMENT FOR THE LOSS-OF-COOLANT ACCIDENT 9-26
9.3.1 LOCA Break Scenarios 9-27
9.3.2 WGOTHIC Containment Evaluation Model for LOCA 9-34

9.4 MAIN STEAMLINE BREAK (MSLB) 9-44
9.4.1 Break Locations 9-44
9.4.2 WGOTHIC Containment Evaluation Model for MSLB 9-45
9.4.3 MSLB Sensitivity Results 9-46

9.5 CONCLUSIONS 9-48

9.6 REFERENCES 9-50

APPENDIX 9A THERMAL AND CIRCULATION EFFECTS OF DROPS DURING A LOCA 9A-1

APPENDIX 9B EFFECTS OF STRATIFICATION ON HEAT SINK UTILIZATION 9B-1

APPENDIX 9C ADDITIONAL INFORMATION ON AP600 CONTAINMENT CIRCULATION AND STRATIFICATION 9C-1

TABLE OF CONTENTS (Cont.)

APPENDIX 9D BASIS FOR ASSUMING HOMOGENEOUS BULK CONDITIONS FOR AP6000 AND AP1000 CONTAINMENT PRESSURE DESIGN BASIS ANALYSIS 9D-1

LIST OF TABLES

Table 9-1 Circulation and Stratification Evaluation Summary 9-5

Table 9-2 Flow Areas Connecting to North and South CMT Compartments (excluding Dead-Ended Compartment Connections) 9-24

LIST OF FIGURES

Figure 9-1 Measured Steam Concentrations for LST 9-52

Figure 9-2 LST with Diffuser Under Steam Generator - Steam Flow 0.11-0.17 lb/sec - Internal Fluid Temperature - Group 1 9-53

Figure 9-3 LST with Diffuser Under Steam Generator - Steam Flow 0.11-0.17 lb/sec - Saturation Temperature - Group 1 9-54

Figure 9-4 LST with Diffuser Under Steam Generator - Steam Flow 0.11-0.17 lb/sec - Internal Steam Pressure Ratio - Group 1 9-55

Figure 9-5 LST with Diffuser Under Steam Generator - Steam Flow 0.11-0.17 lb/sec - Internal Fluid Temperature - Group 2 9-56

Figure 9-6 LST with Diffuser Under Steam Generator - Steam Flow 0.11-0.17 lb/sec - Saturation Temperature - Group 2 9-57

Figure 9-7 LST with Diffuser Under Steam Generator - Steam Flow 0.11-0.17 lb/sec - Internal Steam Pressure Ratio - Group 2 9-58

Figure 9-8 LST with Diffuser Under Steam Generator - Steam Flow 0.27-0.36 lb/sec - Internal Fluid Temperature 9-59

Figure 9-9 LST with Diffuser Under Steam Generator - Steam Flow 0.27-0.36 lb/sec - Saturation Temperature 9-60

Figure 9-10 LST with Diffuser Under Steam Generator - Steam Flow 0.27-0.36 lb/sec - Internal Steam Pressure Ratio 9-61

Figure 9-11 LST with Diffuser Under Steam Generator - Steam Flow 0.49-0.62 lb/sec - Internal Fluid Temperature - Group 1 9-62

Figure 9-12 LST with Diffuser Under Steam Generator - Steam Flow 0.49-0.26 lb/sec - Saturation Temperature - Group 1 9-63

Figure 9-13 LST with Diffuser Under Steam Generator - Steam Flow 0.49-0.62 lb/sec - Internal Steam Pressure Ratio - Group 1 9-64

Figure 9-14 LST with Diffuser Under Steam Generator - Steam Flow 0.49-0.62 lb/sec - Internal Fluid Temperature - Group 2 9-65

Figure 9-15 LST with Diffuser Under Steam Generator - Steam Flow 0.49-0.62 lb/sec - Saturation Temperature - Group 2 9-66

Figure 9-16 LST with Diffuser Under Steam Generator - Steam Flow 0.49-0.62 lb/sec - Internal Steam Pressure Ratio - Group 2 9-67

LIST OF FIGURES (Cont.)

Figure 9-17 LST with Diffuser Under Steam Generator - Steam Flow 0.76-0.84 lb/sec - Internal Fluid Temperature 9-68

Figure 9-18 LST with Diffuser Under Steam Generator - Steam Flow 0.76-0.84 lb/sec - Saturation Temperature 9-69

Figure 9-19 LST with Diffuser Under Steam Generator - Steam Flow 0.76-0.84 lb/sec - Internal Steam Pressure Ratio 9-70

Figure 9-20 LST with Diffuser Under Steam Generator - Steam Flow 1.10-1.20 lb/sec - Internal Fluid Temperature 9-71

Figure 9-21 LST with Diffuser Under Steam Generator - Steam Flow 1.10-1.20 lb/sec - Saturation Temperature 9-72

Figure 9-22 LST with Diffuser Under Steam Generator - Steam Flow 1.10-1.20 lb/sec - Internal Steam Pressure Ratio 9-73

Figure 9-23 LST with Diffuser Under Steam Generator - Steam Flow 1.54-1.68 lb/sec - Internal Fluid Temperature 9-74

Figure 9-24 LST with Diffuser Under Steam Generator - Steam Flow 1.54-1.68 lb/sec - Saturation Temperature 9-75

Figure 9-25 LST with Diffuser Under Steam Generator - Steam Flow 1.54-1.68 lb/sec - Internal Steam Pressure Ratio 9-76

Figure 9-26 LST with Diffuser Up 6 Feet - Steam Flow 0.76 & 1.68 lb/sec - Internal Fluid Temperature 9-77

Figure 9-27 LST with Diffuser Up 6 Feet - Steam Flow 0.76 & 1.68 lb/sec - Saturation Temperature 9-78

Figure 9-28 LST with Diffuser Up 6 Feet - Steam Flow 0.76 & 1.68 lb/sec - Internal Steam Pressure Ratio 9-79

Figure 9-29 LST with Steam Injection: 3 Inch Pipe - Steam Flow 0.76 - 0.95 lb/sec - Internal Fluid Temperature 9-80

Figure 9-30 LST with Steam Injection: 3 Inch Pipe - Steam Flow 0.76 - 0.95 lb/sec - Saturation Temperature 9-81

Figure 9-31 LST with Steam Injection: 3 Inch Pipe - Steam Flow 0.76 - 0.95 lb/sec - Internal Steam Pressure Ratio 9-82

LIST OF FIGURES (Cont.)

Figure 9-32 LST with Steam Injection: 3 Inch Pipe - Steam Flow 1.25 - 1.31 lb/sec - Internal Fluid Temperature 9-83

Figure 9-33 LST with Steam Injection: 3 Inch Pipe - Steam Flow 1.25 - 1.31 lb/sec - Saturation Temperature 9-84

Figure 9-34 LST with Steam Injection: 3 Inch Pipe - Steam Flow 1.25 - 1.31 lb/sec - Internal Steam Pressure Ratio 9-85

Figure 9-35 CMT Compartment Layout 9-86

Figure 9-36 Simplified AP600 Containment Diagram 9-87

Figure 9-37 WGOTHIC Calculated LOCA Blowdown Steam Pressure Ratio for Jet Momentum Dissipated in SG East Compartment 9-88

Figure 9-38 WGOTHIC Calculated AP600 Containment Pressure - Sensitivity to Loss Coefficients for LOCA Jet Momentum Dissipated in SG East Compartment 9-89

Figure 9-39 WGOTHIC Calculated Flow Pattern - Sensitivity to Loss Coefficients for LOCA Jet Momentum Dissipated in SG East Compartment at 20 Seconds 9-90

Figure 9-40 WGOTHIC Calculated Flow Pattern - Sensitivity to Loss Coefficients for LOCA Jet Momentum Dissipated in SG East Comp. at 1000 Seconds 9-91

Figure 9-41 WGOTHIC Calculated Flow Pattern - Sensitivity to Loss Coefficients for LOCA Jet Momentum Dissipated in SG East Comp. at 1550 Seconds 9-92

Figure 9-42 WGOTHIC Calculated Flow Pattern - Sensitivity to Loss Coefficients for LOCA Jet Momentum Dissipated in SG East Comp. at 80050 Seconds 9-93

Figure 9-43 WGOTHIC Calculated AP600 Containment Heat Removal Rates - LOCA Jet Momentum Dissipated in SG East Compartment 9-94

Figure 9-44 WGOTHIC Calculated AP600 Containment Steam Pressure Ratio for LOCA Jet Momentum Dissipated in SG East Compartment 9-95

Figure 9-45 WGOTHIC Calculated AP600 Cont. Pressure - Sensitivity to Heat Transfer Coefficient for Study of Undissipated Jet Effects During a LOCA 9-96

Figure 9-46 WGOTHIC Calculated AP600 Containment Pressure-LOCA Jet Momentum Dissipated in SG East Compartment 9-97

LIST OF FIGURES (Cont.)

Figure 9-46A WGOTHIC Calculated AP600 Containment Below-Deck Compartment Pressure for LOCA Jet Momentum Dissipated in SG East Compartment 9-98

Figure 9-47 WGOTHIC Calculated Flow Pattern - LOCA Jet Momentum Dissipated in SG East Compartment at 20 Seconds 9-99

Figure 9-48 WGOTHIC Calculated Flow Pattern - LOCA Jet Momentum Dissipated in SG East Compartment at 1000 Seconds 9-100

Figure 9-49 WGOTHIC Calculated Flow Pattern - LOCA Jet Momentum Dissipated in SG East Compartment at 1500 Seconds 9-101

Figure 9-50 WGOTHIC Calculated Flow Pattern - LOCA Jet Momentum Dissipated in SG East Compartment at 8000 Seconds 9-102

Figure 9-51 Details of WGOTHIC Flow Paths to Above-Deck Region from CMT, Refueling Canal, and IRWST 9-103

Figure 9-52 WGOTHIC Calculated AP600 Containment Pressure - LOCA Plume Rising into CMT Room 9-104

Figure 9-53 WGOTHIC Calculated Flow Pattern - LOCA Plume Rising into CMT Room at 1000 Seconds 9-105

Figure 9-54 WGOTHIC Calculated Flow Pattern - LOCA Plume Rising into CMT Room at 1400 Seconds 9-106

Figure 9-55 WGOTHIC Calculated AP600 Containment Heat Removal Rates - LOCA Plume Rising into CMT Room 9-107

Figure 9-56 WGOTHIC Calculated AP600 Containment Pressure - LOCA Plume Rising into CMT Room and SG Compartments 9-108

Figure 9-57 WGOTHIC Calculated Flow Pattern - LOCA Plume Rising into CMT Room and SG Compartments at 1000 Seconds 9-109

Figure 9-58 WGOTHIC Calculated Flow Pattern - LOCA Plume Rising into CMT Room and SG Compartments at 1500 Seconds 9-110

Figure 9-59 WGOTHIC Calculated AP600 Containment Heat Removal Rates - LOCA Plume Rising into CMT Room and SG Compartments 9-111

Figure 9-60 WGOTHIC Calculated AP600 Containment Steam Pressure Ratio for MSLB Above-Deck 9-112

LIST OF FIGURES (Cont.)

Figure 9-61 WGOTHIC Calculated AP600 Containment Pressure - MSLB Above Operating Deck 9-113

Figure 9-62 WGOTHIC Calculated AP600 Containment Pressure - MSLB in CMT Room 9-114

9 CIRCULATION AND STRATIFICATION WITHIN CONTAINMENT

Design basis accident (DBA) evaluations of AP600 and AP1000 containment pressurization transients follow an approach that bounds uncertainties in parameters important for containment response. In this regard, the assessment of circulation and stratification examined a range of possible break elevations, orientations, and momentum to determine the worst case set of assumptions. A summary of the evaluation results and a cross reference to supporting subsections is given in Table 9-1.

The effect of break parameters on mass transfer to heat sinks, the dominant means of pressure mitigation, is evaluated. The evaluation results in both the selection of a limiting scenario for large-scale circulation, and also a conservative handling of potential effects of stratification. The objective is to perform a bounding, or worst case analysis. The effects of circulation and stratification do not lend themselves readily to quantification of a bias and distribution for uncertainty, such as would be done for a best-estimate analysis. For example, it would be very difficult to quantify the probability of a break being directed in any particular direction. Rather the simplest DBA approach is to examine the range of possible break conditions, to select a limiting scenario, and use modeling techniques to bound the potential for reduced heat sink mass transfer.

For equipment qualification (SSAR Appendix 3D.5.5.1.5), the simple bounding approach is taken which uses the temperature in the break compartment as input to the qualification envelope. This temperature is the maximum value in containment. For containment pressure, the evaluation in this section has been performed, summarized as follows.

The containment pressure transient is potentially affected by parameters which influence the dominant heat removal mechanism, mass transfer. Mass transfer has as its primary parameters steam concentration, and, in the case of forced convection conditions, velocity. Large-scale circulation and entrainment into jets or plumes can drive circulation and can affect local values of steam concentration and velocity near heat transfer surfaces. Jet and plume entrainment within compartments or the above-deck region can also result in stratification, or the existence of a vertical steam concentration gradient. Therefore, an assessment of the effects of circulation and stratification should focus on how the steam concentration and velocity are affected. Since the Evaluation Model assumes only free convection inside the containment, the potential benefit of forced convection, when it exists, is neglected. Therefore, the assessment can be further focused on the potential effects on steam concentration distributions.

For the main steamline break (MSLB), the containment vessel shell never becomes the dominant heat removal mechanism before break releases are over; therefore, known biases inherent in the lumped parameter Evaluation Model are used to minimize the internal heat sink effectiveness. Lumped parameter model biases, supported with LST comparisons, are used to impose a conservative break release boundary condition location in the Evaluation Model for MSLB pressure responses.

For the loss of coolant accident double-ended cold leg guillotine break (LOCA DECLG), temporal partitioning has been used to further refine the evaluation for blowdown (0-30 sec.), refill (30 to 90 sec.), peak pressure (90 to 1200 sec.), and long-term (1200 sec. and beyond). During blowdown, volume pressurization is the dominant energy absorber, so the details of mixing and stratification effects are not dominant. During the long-term, the passive containment cooling system (PCS) is the dominant heat removal mechanism, so that increasing the concentration of noncondensables in the above-deck region would reduce the PCS heat removal capability and result in higher calculated containment pressures. The peak pressure period, where both the below-deck heat sinks and the PCS surface are significant contributors, has been assessed by examining extreme release scenarios and examining the range of conditions to select a limiting scenario for peak pressure. The evaluation includes a logical sorting and organization of extreme break scenarios that are quantified by various analytical models and selected experimental results. The analytical models include hand calculations and the use of the WGOTHIC AP600 Containment Evaluation Model for sensitivities to the range of the extreme break scenarios considered.

Entrainment into a jet or plume and large-scale, density-driven circulation between compartments can force some degree of homogenization between and within compartments. Entrainment into a jet or plume can reduce the vertical density gradient occurring due to stratification because of the induced circulation. The assessment of large-scale circulation and compartment density gradients is summarized below.

Large-scale circulation is evaluated by examining a range of extreme release scenarios, including break location, elevation, orientation, and momentum. A limiting, large-scale circulation scenario for the peak pressure period can be shown to result from the assumption of dissipation of the break momentum within the steam generator compartment, at the elevation of the primary system pipe. The scenario is limiting because other scenarios were shown to have improved heat sink utilization, and thus lower peak pressures. For example, the extreme postulated scenario of an undissipated forced jet exiting the upper steam generator compartment opening would drive significantly more convection on the steel shell (PCS) surface, and data indicates that the kinetic energy exiting the steam generator compartment would drive circulation below deck. Mass transfer would be greater than that for a buoyant plume. For a buoyant source and a break low in containment, it is reasonable to use a lumped parameter formulation to model the large-scale, or intercompartment circulation. A review of possible release locations and the expected circulation patterns led to the selection of four potentially limiting cases for further evaluation. The lumped parameter WGOTHIC AP600 Containment Evaluation Model was then used to examine those potentially limiting buoyant source release locations. Results from the sensitivity cases were consistent with the expected circulation patterns in each case, which supports the use of the WGOTHIC lumped parameter model for those sensitivities. Results also showed that the postulated scenarios examined a wide range of possible transient evolutions of steam concentrations throughout the dominant circulating compartments. An assumption of a buoyant release within the broken steam generator compartment reduced the steam access to a large fraction of heat sinks compared to the other locations for a buoyant release, which reduced below-deck heat sink effectiveness and led to the maximum calculated containment pressure.

The use of lumped parameter models can introduce a bias in heat and mass transfer calculations when details within a compartment or region may be important. The simplified momentum formulation can lead to overmixing when multiple lumped parameter nodes are used to represent a single region, such as is done for the above-deck region in the Evaluation Model. Thus, density gradients larger than those predicted by the model in the above-deck region are expected and are assessed independently from the Evaluation Model. The calculation uses a single calculational node to represent each below-deck compartment. The single node representing each compartment allows only an average value of steam concentration for that compartment. For both above- and below-deck regions, density gradients larger than those predicted by the Evaluation Model are evaluated to gain insight into the effects of extreme gradients on heat sink utilization. Showing how sensitive the heat sink utilization is to extreme gradients provides greater confidence that the simplifications inherent in the Evaluation Model have been conservatively bounded.

Since stratification within compartments is not considered explicitly in the WGOTHIC lumped parameter model, it has been evaluated for its effect on total compartment heat sink utilization. The potential for degraded heat sink effectiveness has been examined using a simple calculation for the vertical heat sink distribution and an extreme vertical density gradient. Results show that the total heat sink effectiveness within a compartment or region is affected by the assumed vertical gradients. Evaluations also showed that mass transfer to upward facing surfaces in circulating compartments may be degraded very early in the transient, and heat sink effectiveness within dead-ended compartments may be overestimated by the lumped parameter model after blowdown. Biases have been introduced into the Evaluation Model to bound these effects.

The conclusion of the circulation and stratification assessment provides specific guidelines for the Evaluation Model to bound the effects. The guidelines are summarized in Table 9-1, noted in the conclusions in Section 9.5, and are implemented as noted in Section 4 in the Special Modeling Assumptions subsection for each compartment or region.

9.1 INTRODUCTION

The rupture of the primary system or main steamline piping has the potential to release a significant amount of mass and energy into the containment atmosphere. The passive containment is designed to withstand a loss-of-coolant accident (LOCA) or a main steamline break (MSLB) through a combination of a high containment design pressure and passive heat removal mechanisms. The passive heat removal systems include energy absorption by internal heat sinks as well as heat removal by the passive containment cooling system (PCS).

A containment analysis is performed to verify the adequacy of the containment heat removal mechanisms to maintain post-accident containment pressure below the design limit. In this regard, the WGOTHIC code (Reference 9.1) has been developed as the containment code for performing the design basis containment analysis. Appropriate Evaluation Models (Sections 4 and 13) have been created. These models consider important input parameters such as mass and energy releases, containment volume, internal heat sinks, and PCS heat removal to calculate post-LOCA and post-MSLB containment pressure and temperature response.

To obtain a conservative containment analysis, the effects of circulation and stratification must be bounded by the Evaluation Model. Circulation and stratification are natural processes that occur inside the passive containment during postulated containment pressurization transients and have been identified as important phenomena to be addressed in support of the Evaluation Model for containment pressure calculations (Reference 9.2). The circulation and stratification that occur during a high energy pipe break transient, have the potential to reduce heat and mass transfer rates by transporting and concentrating noncondensables. The degradation of heat and mass transfer may reduce the effectiveness of the heat sinks and the PCS at mitigating the peak containment pressure. The effects of circulation and stratification must be addressed to justify the approach used in the containment Evaluation Model.

This section presents an overview of the effects of circulation and stratification for the containment Evaluation Model for the LOCA and MSLB events. The evaluation results are summarized in Table 9-1. As the table shows, the LOCA and MSLB events are evaluated separately. The LOCA event is divided into four temporal phases based on heat sink utilization: the blowdown phase, the refill phase, the peak pressure phase, and the long-term phase. During each of these phases, important phenomena, such as mass and energy release rates, break source direction, and heat removal mechanisms are considered for impact on circulation and stratification. Unlike the LOCA events, the MSLB events are not divided into temporal phases. The MSLB is characterized by a single, high-intensity blowdown phase. However, different piping rupture locations are considered in the MSLB evaluation.

Table 9-1 Circulation and Stratification Evaluation Summary

Element	Summary of Evaluation	Relevant PIRT Parameter [1]	WCAP-14407 Section Reference
General Approach			
	Circulation and stratification evaluated because of the potential to degrade heat sink effectiveness via the condensation parameters: • Steam concentration • Velocity	Circulation/ stratification (2A), condensation (3F, 7C)	9.0
	High kinetic energy sources, such as during LOCA blowdown and MSLB result in forced convection component of mass transfer	Circulation (2A), condensation (3F)	9.0
	Effects of velocity eliminated in calculation by assuming only free convection internally. Focus, therefore, is on impact of circulation and stratification on steam and noncondensible distributions	Circulation/ stratification (2A)	9.0
	Equipment qualification temperature is conservatively taken from the break compartment (containment pressure is therefore, the focus of the evaluation in Section 9)	Circulation/ stratification (2A)	9.0
	For the DBA LOCA, volume compliance is the primary pressure mitigator during blowdown, internal heat sinks and the containment steel shell are the primary mitigators during the peak pressure phase, and the steel shell surface is the dominant mitigator during the long-term phase	Gas compliance (2C), condensation (3F, 7C)	9.0, 9.3, 9.3.2.1, 9.3.2.4
	For the DBA MSLB, the internal heat sinks are the dominant pressure mitigators.	Condensation (3F)	9.0, 9.4.3

Table 9-1 (cont.) Circulation and Stratification Evaluation Summary			
Test Data			
A. Method to Address Distortions in the LST for Circulation and Stratification Assessment	Power to volume ratio: using only quasi-steady-state data for circulation and stratification, therefore, no impact of this distortion on these results.	Stratification (2A), int. heat sink conduction (3D), shell conduction (7F)	9.2.3
	Power to area ratio: • Steam flow was ranged and external boundary conditions were ranged • Considering the matrix of the LST, a range of power-to-area (or condensation rate) ratios were considered, which minimizes the degree of the distortion • Distortion addressed by considering stratification and condensation data from LST matrix tests and supplementing LST with assessment of international test data for stratification	Circulation/ Stratification (2A)	9.2.3, 1.4.1
	Circulation path impact on *circulation* : cannot use the LST data for assessment of circulation. Addressed by supplementing LST with assessment of international test data for circulation	Circulation (2A), intercmprt flow (2B)	9.2.3
	Circulation path impact on *stratification* : • Lack of LST SG compartment circulation results in LST stratification more extreme than if a circulation path existed • Addressed by supplementing LST with assessment of using international test data for stratification	Stratification (2A), intercmprt flow (2B)	9.2.3

Table 9-1 (cont.) Circulation and Stratification Evaluation Summary			
B. Usage of LST Data for Circulation and Stratification Assessment	LST above-deck separate effects style data for condensation and stratification is considered	Mass and energy (1A), direction and elevation (1B), momentum (1C), Circulation/ stratification (2A)	9.2.1, 9.2.2
	LOCA - applicable tests had diffuser under the SG, reference case had elevated diffuser. Key LST result - above-deck stratification data used to support development of a bounding stratification gradient for evaluation of heat sink utilization for peak pressure/long-term phases	Stratification (2A)	9.2.1
	MSLB - applicable tests had elevated 3" pipe pointing vertically/horizontally. Key LST results - kinetic energy drives circulation below-deck, forced convection significantly enhances mass transfer (factor of 1 to 10 over shell surface relative to free convection mass transfer)	Circulation/ stratification (2A)	9.2.2
Lumped Parameter Biases Implemented in WGOTHIC Evaluation Model			
A. International/ Industry Experience	Lumped-parameter modeling uses a simplified momentum formulation, which biases calculated pressure with respect to circulation and stratification. These biases are evaluated and bounded by the Evaluation Model.	Circulation/ stratification (2A)	9.1.2
	NUPEC modeling experience is applied to Evaluation Model compartment flow connections, resulting in reasonably predicted circulation patterns.	Circulation (2A) Inter-compartment Flow (2B)	9.2.4, Appendix C Section 9.C.3

Table 9-1 (cont.) Circulation and Stratification Evaluation Summary

B. LOCA Biases	The effects of stratification on heat sink utilization are negligible for compartments experiencing downflow of heavier ambient atmosphere mixture	Stratification (2A)	9.3.1.1
	• Dead-ended compartments with no assumed thermal gradients stratify • Condensation and convective heat transfer turned off in dead-ended compartments after 30 seconds	Stratification (2A)	9.3.2.1
	• Effect of stratification on steel shell condensation assessed with extreme gradient • Stratification effect bounded by removing upward facing surface of operating deck as a heat sink	Stratification (2A)	9.3.1.1
	• Effect of stratification on heat sinks in a below-deck compartment assessed with extreme gradient • CMT room (most heat sinks) evaluated for case in which LOCA plume is rising in room • Stratification effect bounded by removing floor as heat sink (bias applied in all compartments regardless of assumed break location)	Stratification (2A)	9.3.1.3
C. MSLB Biases	LST data indicates: • Kinetic energy drives some circulation below-deck • Forced convection is driven by high kinetic energy jet above-deck • No significant stratification above-deck, therefore no bias required	Circulation/ stratification (2A)	9.4.2

Table 9-1 (cont.) Circulation and Stratification Evaluation Summary

	Lumped parameter model code biases: • Evaluation Model places break node at operating deck level minimizing circulation and steam access to below-deck heat sinks • Momentum dissipated in each node (Evaluation Model uses only free convection) • Density-driven circulation as plume rises resulting in relatively homogeneous region above modeled break node – results in steam-rich region above modeled break node and steam-deficient region below modeled break node, which bounds effects of stratification – conservatively, the LOCA stratification biases are included for the MSLB Evaluation Model	Circulation/ stratification (2A)	9.4.2
LOCA Evaluation Results			
A. Considerations by Time Phase for Evaluation Model	LOCA blowdown (0 to 30 seconds): • Blowdown pressurizes compartments and drives significant circulation above and below-deck • Lumped parameter modeling adequate for pressure-driven flow • Containment pressure insensitive to noding (multi-node vs. one-node model) • Low sensitivity to heat sinks because volume storage is dominant pressure mitigator • Fr indicates significant forced convection on steel shell, Evaluation Model conservatively assumes only free convection • Steam driven into dead-ended compartments. Assuming thermally uniform heat sinks results in no circulation, therefore, condensation and convection heat transfer in dead-ended compartments neglected after 30 seconds.	Intercompart-ment Flow (2B) Gas compliance (2C) Break source momentum (1C)	9.3.2, 9.3.2.1 9.2.2
	LOCA refill (30 to 90 seconds): • Break releases are negligible • Containment depressurizes during this phase • Conservatively ignore containment pressure reduction by neglecting this phase to maximize initial pressure for the peak pressure phase	Break source mass and energy (1A)	9.3.2.2

Table 9-1 (cont.) Circulation and Stratification Evaluation Summary

	LOCA peak pressure (90 to 1200 seconds): • Steam source location changes to ADS Stage 4 valves in both SG compartments at approximately 1000 seconds • Condensation on steel shell becomes dominant heat removal mechanism towards end of peak pressure phase • Compartment filling reduces heat transfer for affected compartments during peak pressure phase and long-term phase (compartment filling is modeled by code)	Break source (1B, 1C)	9.3.2.3
	LOCA long-term (1200 seconds to 24 hours): • Condensation on steel shell remains dominant heat removal mechanism • WGOTHIC predicted steam gradient becomes essentially homogeneous in less than 24 hours, excluding the SG compartments (due to ADS Stage 4 valves releasing steam) • Evaluation using extreme stratification gradient shows nearly negligible increase in heat removal by the steel shell relative to homogeneous steam concentration case - bounded by removing the non-grating operating deck floors • Evaluation using extreme stratification gradient shows a decrease in heat removal by the below-deck compartment heat sinks relative to the homogeneous steam concentration case - bounded by removing the compartment floor.	Condensation (7C) Break pool filling (5F) Stratification (2A)	9.3.2.4 9.3.1.3
B. Range of Break Scenarios and Effects	Jet dissipated in SG East compartment • Limiting scenario • Post-blowdown flow into CMT room is downward with steam/air mixture	Break source (1B, 1C)	9.3.1.1, 9.3.2.5
	Undissipated jet in SG East compartment • Forced convection above-deck improves condensation on containment shell • Significant kinetic energy-driven circulation below-deck • Minimal stratification in above-deck region	Break source (1B, 1C)	9.3.1.2

Table 9-1 (cont.) Circulation and Stratification Evaluation Summary

	Jet to RCDT cavity - dissipated plume rises in CMT North room • Good steam access to below-deck room with most internal heat sinks	Break source (1B, 1C)	9.3.1.3
	Jet to RCDT cavity - dissipated plume rises in SG West compartment • Same scenario as dissipated jet rising in SG East compartment	Break source (1B, 1C)	9.3.1.3
	Jet dissipates in RCDT cavity • Flow split based on flow area and loss coefficients • Better steam access to CMT room and SG West compartment compared to break in SG East compartment	Break source (1B, 1C)	9.3.1.3
C. Sensitivity Cases Run with the Evaluation Model	Break locations (all located low in containment): • Jet undissipated in SG East compartment - forced convection benefit on steel shell assessed to estimate effect of undissipated jet • Jet dissipated in SG East compartment - limiting case for maximum containment pressure • Jet into RCDT cavity - plume rises in CMT North room • Jet dissipated in RCDT cavity - plume rise determined by flow path resistances	Intercompart-ment Flow (2B)	9.3.2.5
	Loss coefficients: • Loss coefficients for several flow paths changed to modify blowdown-predicted flow direction • Modeled dissipated jet in SG East compartment • End of blowdown conditions changed with negligible change to maximum containment pressure	Intercompart-ment Flow (2B)	9.3.2.1

Table 9-1 (cont.) Circulation and Stratification Evaluation Summary

	Thermal and circulation effects of drops: • Drops only created during LOCA blowdown • Thermal effects - 5 percent drop formation enough to saturate containment atmosphere - 0 percent drops less limiting for maximum containment pressure - Negligible change in containment pressure between 100 percent drops and Evaluation Model (approximately 50 percent drops) • Circulation effects examined for 0 and 100 percent drop formation - Presence of drops increases density of atmosphere increasing relative buoyancy of plume - Containment atmosphere entrainment into plume is significant for both 0 and 100 percent cases	Break source droplet/liquid flashing (1E) Stratification (2A) Intercompart-ment Flow (2B) Containment volume fog (2D)	9.2.3.6 5.8 9.2.3.6
D. Conclusions	• Evaluation Model with dissipated break in SG East compartment is the limiting scenario - Calculated containment pressure is not very sensitive to break location due to heat sink utilization prior to maximum pressure • Biases included in Evaluation Model to bound effects of stratification		9.2.3.5, 9.5
MSLB Evaluation Results			
A. Break Location Scenarios and Effects	• Selected based on routing of steamline pipe • MSLB above-deck - High kinetic energy release with relatively short duration, which drives circulation below the source - High Fr number (comparison provided to LST Fr number) - LST data indicates forced convection enhancement to mass transfer (only free convection modeled) - Break in MSLB Evaluation Model located in node just above-deck, which limits steam access to below-deck heat sinks	Stratification (2A) Intercompart-ment Flow 2B) Break source (1B, 1C)	9.4, 9.4.1, 9.4.1.1, 9.4.2

Table 9-1 (cont.) Circulation and Stratification Evaluation Summary

	• MSLB in CMT North room - Break in CMT room would significantly dissipate due to equipment in room and rise as a plume - CMT room contains most of the internal heat sinks - Good steam access to CMT room heat sinks, therefore case is expected to be less limiting		9.4.1.2
B. Sensitivity Cases	• MSLB located just above deck • MSLB in CMT North room		9.4.3
C. Conclusions	• MSLB in CMT North room calculated containment pressure significantly less limiting • MSLB located just above-deck used for the MSLB Evaluation Model		9.4.3, 9.5

(1) PIRT parameters are identified in Reference 9.2, Table 4-1

9.1.1 Definitions

Several terms used to discuss circulation and stratification are defined, as they relate to containment analysis.

Stratification is a state characterized by strata, or horizontal layers, of different density. Stratification is stable when the lower layers are increasingly dense due to composition and/or temperature. The term stratification does not indicate the magnitude of the density gradient.

Mixing is a collective term for convective transport processes that reduce temperature and/or concentration differences within a volume or between volumes. Convective transport processes in containment include jets, plumes, wall layers, turbulent diffusion, and entrained flow. Molecular diffusion also contributes to mixing but is considerably less effective than convection, except in boundary layers. Diffusion also contributes to mixing in stratified conditions.

Circulation is a term used to describe gross, overall convective flow patterns that occur on a compartment scale and on a large scale (or containment scale). The compartment-scale circulation is due to wall layers, jets, plumes, and entrained flow. The large-scale circulation is due to interactions between compartments induced by pressure, density, elevation, and momentum differences such as intercompartment flow. The break source jet or plume can induce both compartment-scale and large-scale circulation.

Segregation is a state characterized by a different air/steam concentration in one compartment than in another. For example, the heavier air may reach different concentrations in separate compartments, especially the dead-ended compartments if the intercompartment circulation is low.

9.1.2 Lumped Parameter Biases and Capabilities

Lumped parameter biases and capabilities have been identified based on industry experience, as documented in the literature (Appendix 9.C, Section 9.C.3.4). The documented experience base includes facilities at different geometric scales, from that of the LST to nearly full-scale AP600 height (Appendix 9.C, Figure 9.C.2-1). The lumped parameter biases and capabilities, summarized below, have been reported consistently across the range of facilities, indicating that the biases and capabilities are applicable to the Containment Evaluation Model. The consistency across scales also indicates that the LST facility is a reasonable basis on which to study the biases and capabilities as they apply to AP600, reported in WCAP-14382 (Reference 9.1). The following provides a summary of the method used in the development of the Containment Evaluation Model to address each documented bias and capability.

1. Single node models were not capable of modeling stratification, or the passing of a stratification front through horizontal vents.

(a,c)

[ ]

2. Sump liquid level and sump temperature were not well predicted (a,c)

[ ]

3. Some codes produced results which were not correct due to missing or oversimplifying buoyancy terms (a,c)

[ ]

4. To account for recirculation flows, the applied lumped parameter model used double junctions in the horizontal direction. (This did not help in the case of an elevated release and resulting stratified containment.)

See discussion for item 3 above regarding the impact of lumped volume static pressure profile on the use of double junctions in the Evaluation Model. All of the LOCA cases have releases in the lower compartments (below the operating deck). This break location results in good circulation throughout containment. The main steamline break releases contain high kinetic energy. Therefore, the break node used in the lumped parameter model is a node that minimizes kinetic energy driven circulation to below-deck heat sinks, thus overestimating calculated containment pressure.

5. For releases low in containment, typical for the LOCA DECLG, the lumped parameter model well-predicted pressure, temperature, and helium concentrations inside the compartments, which were affected by the global circulation loop, while predictions needed improvements to account for postulated circulation effects inside dead-ended compartments (a,c)

[ ]

6. Scenarios with homogeneous containment atmosphere (like HDR E11.4 and E11.5) can be simulated successfully with lumped parameter models. (Such conditions typically result from breaks located within the bottom 20 percent of the containment height.)

See discussion for item 5 regarding the use of lumped parameter models for bounding design basis analyses.

7. Circulation effects due to sump boiling (releases generated at the bottom of containment) were well-simulated.

Sump boiling is not a consideration for containment DBA, since long-term primary system energy rejection is through the ADS Stage 4 valves and the sump is therefore a relatively insignificant heat source.

8. The order of magnitude of computed velocities matches data and it can be concluded that trends in the direction of the flow are predicted well; however, predicted velocities differ by as much as a factor of two.

Calculated velocities using lumped parameter codes are strongly dependent on the noding used. Experience with validating the WGOTHIC lumped parameter model of the LST (Reference 9.1, Section 8.2) shows that the noding used can result in calculated velocities that differ from measured by an order of magnitude, showing that the particular test facility and noding used can have a strong influence on calculated velocities. Therefore, a bounding approach is used in the WGOTHIC Evaluation Model, as follows. The effects of predicted velocities in the containment pressure transient are eliminated by considering only free convection heat and mass transfer in the containment. This conservatively biases the Evaluation Model when forced convection would occur during the LOCA blowdown and the MSLB transients.

9. The lumped parameter method does not have the capability to predict the hydrogen distribution in a stratified containment atmosphere, as in HDR E11.2 with high-positioned release. In a break scenario with buoyant plume (released at about 50 percent of containment height), the steam and gas transport to the lower parts of the containment were over-predicted. (Artificial limitation of convective flows by decreasing flow areas improved predicted concentrations in the lower regions, but overestimated the containment pressure in upper compartments.)

Hydrogen distribution predictions are not a consideration for containment DBA (Reference 9.2, Section 4.4.2E).

9.2 LARGE-SCALE TEST RESULTS

In the passive containment design, interest is focused on how much the jet kinetic energy affects gradients inside containment. If the jet kinetic energy is sufficient to disrupt stable stratification, it may also be sufficiently energetic to virtually eliminate vertical gradients in the upper containment volume and to induce circulation between the above-deck and below-deck regions. The Westinghouse Large-Scale Test (LST) data was used to understand the effect of jet kinetic energy on stratification gradients above the operating deck.

The Westinghouse large-scale PCS test facility was built to provide integral test data for a geometrically similar model of the AP600 containment vessel and PCS. The tests provide experimental data that can be used for evaluating the physics in containment, determining the relative importance of various parameters that affect heat and mass transfer, and validating computer codes. Three series of tests (References 9.5 and 9.6) were run at the Westinghouse large-scale PCS test facility. The steady-state pressure, annulus air flow rate, water coverage, steam flow rate, injection velocity, location and orientation, and noncondensible gas concentration were varied between the tests.

It is desirable to use a Froude number formulation that relates momentum phenomena in both the AP600 and the LST to permit scaled inferences between the tests and the AP600. A volumetric Froude number can be defined as the square of the jet Reynolds number, divided by the containment Grashof number:

$$Fr_v = \frac{\rho_a U_o^2 d_o^2}{g(\rho_a - \rho_o)H^3}$$

where ρ_a = density of ambient containment
U_o = velocity of jet at source
d_o = hydraulic diameter of jet at source
g = gravitational acceleration
ρ_o = density of jet source
H = height of volume above steam source

The following sections first describe test configurations as they represent LOCA and MSLB configurations and then provide data that can be used to examine gradients in the above-deck region.

9.2.1 LOCA Configuration

Twenty-five LSTs were conducted in the LOCA configuration with the diffuser located under the steam generator model. A diffuser was used to provide a uniform velocity profile. The tests do not apply to the LOCA blowdown phase, but they do apply to the peak pressure and long-term phases. The volumetric Froude numbers ranged from approximately $5x10^{-6}$ to $5x10^{-3}$. Steam concentrations just above the deck and below the deck near the bottom of the vessel are presented in Figure 9-1, which can be used to see test-to-test variation in above-deck gradients. The plotted values are the ratios of the measured local steam partial pressure to the partial pressure of steam assuming perfect mixing. A value of 1.0 indicates perfect mixing. The values show the above-deck ratios generally range from 0.6 to 1.0 and below-deck values range from 0.1 to 0.4. The below-deck values are an indication of the distortion in the LST due to lack of a simulated steam generator compartment flow path. The distortion leads to an air-rich mixture in the LST below-deck.

Stratification data for LSTs with the diffuser under the simulated steam generator compartment are shown in Figures 9-2 through 9-25. Tests have been grouped by steam flow and plotted so that the temperature axis spans the same range for all the tests to simplify test-to-test comparison. For each group of tests, three plots are shown. First is the azimuthally-averaged temperature data from thermocouples located one inch inside the vessel shell, called the "fluid thermocouples." Data is available from nine elevations above the operating

deck; fluid thermocouple data was not taken below the deck. Second is a plot of the saturation temperature obtained based on the third plot of measured steam mole fractions, or pressure ratio (p_{stm}/P_{vessel}).

Also, a reference test to examine the physics of stratification (test 222.2), with an elevated diffuser, is included as Figures 9-26 through 9-28. These test data are reviewed in Section 9.2.3 to develop insight into an appropriate bounding stratification gradient.

9.2.2 MSLB Configuration

Phase 3 of the LST program included a series of tests designed to simulate a main steamline pipe rupture. LST data from baseline and Phase 2 tests suggested that noncondensible concentrations increase dramatically below the elevation of steam injection with considerable steam mixing above the operating deck. One could postulate that the effect of the higher steamline elevation could be to create a larger volume of rich air mixture which extends above the operating deck, and reduces the active heat transfer area. Test series 222 addressed the impact of the elevation and direction of the steamline break on the response of the test vessel and included a high flow transient to a steady-state condition. The kinetic energy available in an MSLB is seen to be an important parameter.

The four configurations in this test series were:

222.1 Low velocity steam flow from under the operating deck
222.2 Low velocity steam flow above the operating deck (a reference condition to examine the physics, not a realistic AP600 configuration)
222.3 High velocity steam flow with horizontal discharge above the operating deck
222.4 High velocity steam flow above the operating deck directed upward

Stratification data for LSTs with high kinetic energy above the operating deck are shown in Figures 9-29 through 9-34, also grouped by steam flow, and showing measured internal fluid temperature, saturation temperature, and measured steam pressure ratio, as described in Section 9.2.1 for the LOCA configuration. These data are referenced in the development of a bounding MSLB Evaluation Model (Section 9.4.2).

To understand the effects of kinetic energy on circulation and stratification, it is useful to note the stratification pattern observed for a test with a buoyant source (low Froude number) versus a test with a high Froude number. For example, test 222.4 can be used to assess the effects of steam releases with Froude numbers representative of an MSLB occurring above the steam generator. Test 222.4 is compared to test 222.2, which had a similar setup, but a diffuser was used to provide a low velocity elevated steam source. The

elevated buoyant source in test 222.2 produced a significantly stratified vessel, with very little steam penetration below the elevation of the break. In contrast, the high kinetic energy-elevated source of test 222.4 induced a substantial amount of circulation in the test vessel, including substantial steam ingress into the below-deck regions. The decrease in the steam concentration stratification for test 222.4 compared to test 222.2 is due to the high kinetic energy of the injected fluid because that is the only significant difference between the two tests.

Mass transfer data from LSTs with high velocity jets (forced convection) has been compared to that from the low velocity diffuser under the simulated steam generator (dominated by free convection) in Reference 9.9, Figure 3.9-5. The referenced figure includes shell condensation data above the operating deck for the elevated high momentum source LST compared to the mean of such data from the diffuser under the steam generator. The elevated diffuser LST is not included in the referenced figure due to its atypical condition of a low Froude number elevated source - the elevated releases which may be postulated for an MSLB are of a higher Froude number similar to that of the tests for which data are plotted, as described earlier in this section. Results indicate that in the LST forced convection effects enhanced the mass transfer rate by a factor of 1 to a factor of 10 in the direction the jet is directed.

9.2.3 Method to Address Distortions in LST Stratification Data

Internal momentum effects were distorted in the LST due to the lack of a simulated flow path for entrainment near the bottom of the steam generator compartment. Thus in the LOCA DECLG configuration, the LST effectively stratified into two regions – separated at the elevation of the steam generator compartment exit (Section 9.2.1). Therefore, the LST cannot be used to examine intercompartment circulation.

There is also a system level distortion in the LST with respect to power-to-volume and power-to-area (Reference 9.7, Section 11). Since only quasi-steady state data for circulation and stratification were used, there is no impact of power-to-volume distortion on this evaluation. The LST quasi-steady data was taken with a range of break flow rates, and the external wall boundary condition was ranged using controllable variables (turning external water and fan on and off). The internal release configuration also allowed varying the release elevation, momentum, and direction. Initial noncondensible content ranged from near vacuum to two atmospheres. Thus the LST provides a valuable database to examine the physics of potential stratification mechanisms that may be postulated to occur in a passive containment.

Because of the momentum-related distortions in the LST, available international test data has been reviewed (Appendix 9.C, Section 9.C.2) to supplement the database for examining stratification effects. The supplementing of LST data with additional tests at various scales, combined with the use of LST matrix tests, sufficiently addresses the system level power-to-area distortion. The following summarizes conclusions that may be drawn from LST and the international databases, leading to the selection of an extreme stratification gradient to be considered in thermal calculations of Appendix 9.B.

It is desired to gain insight into vertical steam concentration gradients that may occur within the region above the operating deck and within compartments below-deck during a LOCA. (The bounding approach for an MSLB is given in Section 9.4.2.) The region above the operating deck in the LST can be considered to be an enclosure with a plume and wall boundary layers (Appendix 9.C, Section 9.C.1.4.1). The relevant vertical profile data is presented in Figures 9-2 through 9-25. Comparisons of internal fluid thermocouple data (1-inch inside the vessel wall) and steam concentration measurements show that the gas is within a few degrees of saturation, so that the vertical temperature profiles provide a good measure of the vertical steam concentration gradient during the LSTs. Clearly, for the diffuser under the steam generator model, there is only about a 3 to 12°F temperature gradient from the steam generator exit elevation to the dome. The plotted data is at the fluid thermocouple location. A review of the internal rake temperature data shows that the bulk fluid vertical temperature difference is equal to or several degrees less than that given by the fluid thermocouples.

Comparison of the vertical temperature profile from the elevated diffuser case in the LST (Figure 9-26) shows that the stratification in the above-deck region is more pronounced than that in any of the tests with the LOCA configuration. Such stratification from an elevated diffuser is similar to that observed in the CVTR tests (Appendix 9.C, Section 9.C.2.3) which had a similarly elevated, low momentum source. Tests in the much larger HDR and NUPEC facilities indicate that stratification gradients from diffuse releases low in containment in fact produce temperature gradients above the operating deck similar in magnitude to those quoted above in the LST with a low diffuser. However, because of the distortions in LST mentioned above and uncertainties in transferring stratification data from HDR and NUPEC to AP600 and AP1000, an extreme stratification gradient, well beyond that which would occur in a containment with natural convection and a low elevation release, has been considered for thermal calculations.

The steam concentrations used for thermal calculations presented in Appendix 9.B assume a three region distribution — nearly pure steam at the top (steam fraction 0.98), the average value at the middle (steam fraction 0.63), and the balance of the air content at the bottom (steam fraction 0.28). The elevated diffuser case in the LST shows a steam pressure ratio (equal to steam mole fraction) of 0.10 near the operating deck and 0.90 under the dome. The distribution chosen is consistent with that indicated by the LST elevated diffuser, considering that the Appendix 9.B calculation represents an average steam concentration calculated for AP600 transient conditions. It should be noted that the LST elevated diffuser test produces an extreme, or bounding, test configuration for the real situation of a buoyant plume released low in containment, such as for the LOCA DECLG post-blowdown. Thermal calculations in Appendix 9.B are used to develop appropriate biases to bound the effects of stratification within the AP600 and AP1000 lumped parameter compartment nodes and the above-deck region.

9.2.4 Application of Modeling Methods Developed for NUPEC M-4-3 Lumped Parameter Model

The following is a brief summary of the experience gained in developing the WGOTHIC lumped parameter model of the NUPEC natural circulation test, M-4-3, and application of the experience to development of the WGOTHIC lumped parameter Evaluation Model. Justification is provided for using the lumped parameter Evaluation Model for performing sensitivity studies. The sensitivities are used to examine the effects of circulation in containment from a LOCA DECLG.

NUPEC Lumped Parameter Modeling Experience

Actual circulation was interpreted based on data provided by NUPEC for the detailed time history for gas temperature and hydrogen concentration as well as a video of processed data to aid visualization.

As shown in Figures 9.C.2-32 (flow pattern) and 9.C.2-38 (data for one circulation loop) of Appendix 9.C, the break flow rose from the affected steam generator loop, spread through the upper portion of the large vertical opening into the adjacent steam generator loop, and rose from those two compartments into the dome. The large-scale natural convection loop continued with continuity driving circulation down through the opposite steam generator compartments and other openings through the operating deck, and then down to the level of the break release. From the break release level, the convection loop was closed by entrainment into the rising plume. This result is consistent with results of international tests at several scales and is rather simple and straightforward. However, careful development of the lumped parameter noding structure is necessary to allow the code to predict the observed qualitative behavior, as follows.

It should first be noted that for the M-4-3 calculations, best estimate condensation correlations were used to better isolate the biases of lumped parameter noding on predicted parameter distributions and the effect of those biases on containment pressure.

For general application of WGOTHIC lumped parameter, it is necessary that the vertical noding be defined by a set of horizontal planes that cut through the entire modeled region, as described in Reference 9.4, Section 16.12.1. This is done to prevent artificial flows driven solely by the method used to estimate a static pressure profile using the single value of density available within a lumped parameter cell. The successful elimination of such artificial circulation is confirmed when a new model is developed by running a null problem (uniform temperatures in heat sinks and volumes, and no heat or mass source) and verifying that there is no predicted circulation.

(a,c)

[ ]

Application of NUPEC Test Experience to Containment Evaluation Model

The Evaluation Model has been verified to have no significant artificial flows in a null problem. In the further development of the WGOTHIC lumped parameter noding used in the containment pressure Evaluation Model, experience with the NUPEC tests was used qualitatively in representing the CMT compartment.

(a,c)

[ ]

Table 9-2 AP600 Flow Areas Connecting to North and South CMT Compartments (excluding Dead-Ended Compartment Connections)

Flow Path Number	Flow Path End A Node	Flow Path End B Node	Flow Area (ft^2)

(a,c)

+a,c

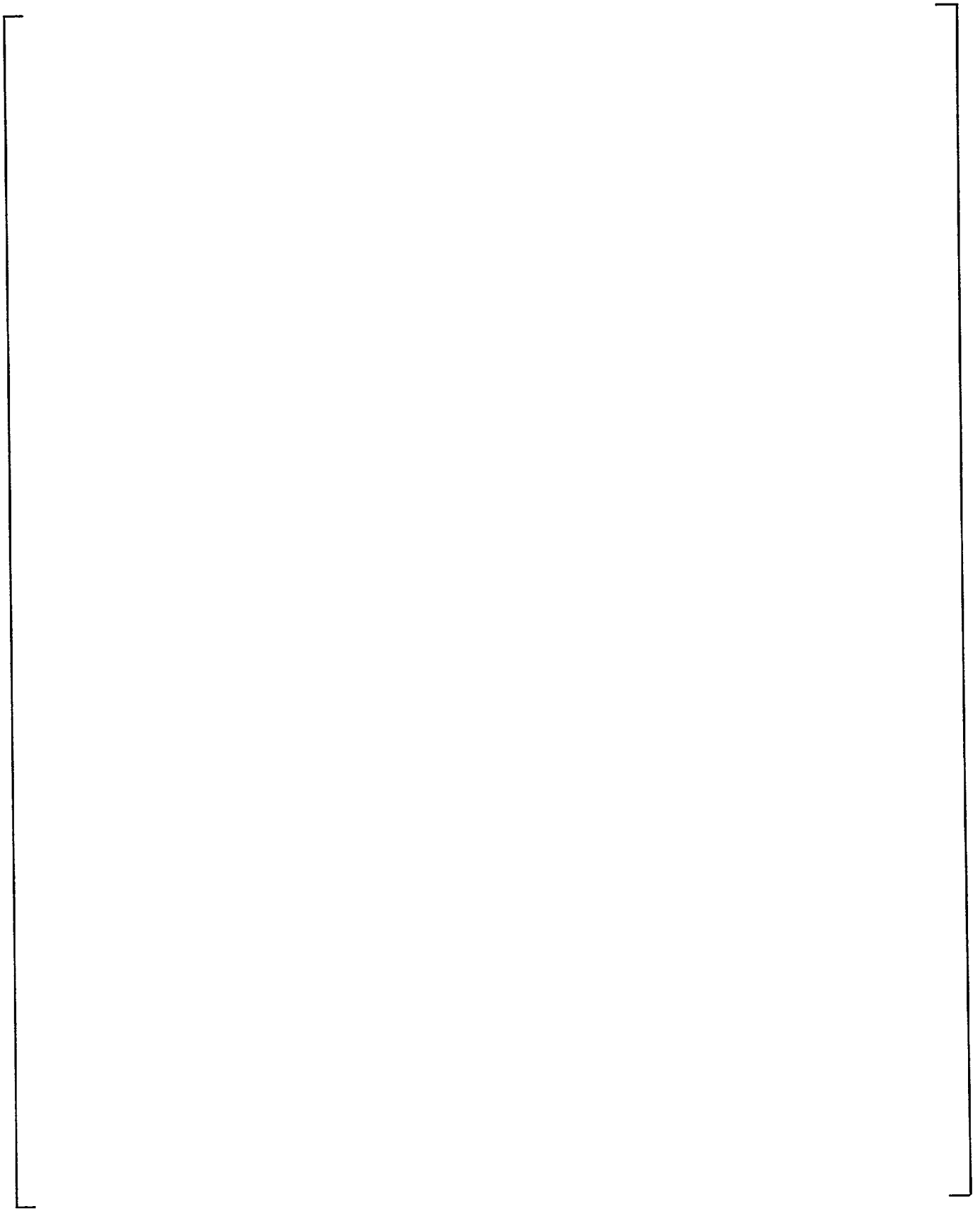

9.3 CIRCULATION AND STRATIFICATION ASSESSMENT FOR THE LOSS-OF-COOLANT ACCIDENT

The rupture of primary system piping can lead to a significant release of mass and energy into the containment. A containment analysis is performed to verify the ability of the passive containment systems to mitigate the consequences of a hypothetical LOCA. The WGOTHIC code, in conjunction with the Containment Evaluation Model, is used for the containment analysis. The effects of circulation and stratification must be bounded by the containment analysis calculations to ensure a conservative containment analysis. For purposes of evaluating the effects of circulation and stratification on the LOCA containment analysis, the LOCA event is divided into four temporal phases: the blowdown phase, the refill phase, the peak pressure phase, and the long-term phase, based on Section 3.4.2.2 of Reference 9.2.

The blowdown phase is the period immediately following the rupture of the primary system piping: For the design basis event, a double-ended, cold leg guillotine (DECLG) break is assumed, which results in the complete severance of the pipe. This phase is characterized by a rapid depressurization of the reactor coolant system (RCS), as the RCS inventory is expelled into the containment volume. The containment gas volume rapidly pressurizes due to the tremendous release of mass and energy. This phase is short in duration (about 30 seconds) and ends when the RCS pressure has equilibrated with containment.

The refill phase immediately follows blowdown. After blowdown, the accumulators refill the lower plenum of the reactor with a high flow rate of cold water. The resulting steam and water flow rates from the break are very low and increase with time. The mass and energy release rates are two orders of magnitude less than the blowdown rates, and can be approximated as 0 from approximately 30 to 90 seconds into the event. With a negligible steam source rate and a high condensation rate, the containment pressure drops by a few psi from its peak at the end of blowdown to the end of the refill phase at approximately 90 seconds. (It should be noted that the Evaluation Model used for sensitivity studies conservatively neglects the refill period.)

The phase following refill is the peak pressure phase. During the beginning of the peak pressure phase, a continuing pressurization of the containment building accompanies the release of mass and energy. Containment pressurization is mitigated by the containment volume and the presence of the substantial number of heat sinks inside containment. Hot steam condenses on the cold steel and concrete surfaces, which transfers energy into the heat sinks. As this phase continues, the temperature of the internal heat sinks increases and their effectiveness is reduced. By this time, however, water flow onto the containment shell has initiated. The PCS provides the path to the ultimate heat sink, and represents the only assumed path through which energy can be removed from inside the containment building. A key feature of the peak pressure phase is the second, more limiting, pressure peak. The combination of internal heat sinks and the PCS act to limit the containment pressurization, and containment pressure begins to drop. Later in this phase, the PCS becomes clearly dominant. The peak pressure phase extends from 90 seconds to about

1500 seconds when the containment pressure reaches its peak. During this phase, ADS Stage 4 actuates and becomes the source of mass and energy release.

The long-term phase is the period after the peak pressure occurs out to twenty-four hours and beyond. During the long-term phase, core decay heat continues to create steam, which exits the fourth stage automatic depressurization system (ADS) as a buoyant plume. The containment continues to depressurize as a result of energy removed by the PCS. As containment pressure drops, internal heat sinks may begin to reject some of their heat back into the containment atmosphere. Thus the long-term phase depressurization is governed by PCS heat removal.

To facilitate an understanding of the relative positions of the various compartments, a simplified AP600 compartment diagram is provided in Figure 9-36. Figure 9-36 shows the relative location of various important compartments, such as the steam generator compartment, the core makeup tank (CMT) compartment, and the above-deck volume. Noding used to represent these compartments within the Evaluation Model is described in Section 4. The compartment features are discussed in Section 4 and summarized in Table 3-1 of Reference 9.2.

Figure 9-35 presents a diagram of the CMT compartment. The CMT room contains most of the below-deck containment heat sinks (approximately 52 percent of below-deck heat sinks by area). Although 48 percent of the heat sinks are not in the CMT room, no other single below-deck compartment contains as many heat sinks. Also, the CMT room is the largest (volume) of the below deck compartments and contains many flow paths. These flow paths mean that the CMT room is of significant importance with respect to both above- and below-deck circulation patterns. Therefore, the effect of circulation and stratification on heat sink utilization in the CMT room plays an important part in the transient pressure mitigation.

9.3.1 LOCA Break Scenarios

The DECLG rupture is the design basis LOCA event for the AP600 and AP1000. The circulation and stratification patterns associated with this break will depend on the direction of the break jet momentum. Although leak-before-break has been implemented, the conservative design basis analysis evaluation assumes the broken pipe can be pointed in any direction from its nominal position. Three scenarios may be postulated: the jet momentum is locally dissipated in the steam generator compartment, the jet exits undissipated up through the steam generator compartment, or the jet momentum is dissipated in the reactor coolant drain tank (RDCT) cavity (stairwell).

9.3.1.1 Jet Momentum Locally Dissipated in Steam Generator Compartment

During the blowdown phase, a tremendous amount of mass is released as shown in Figures 4-96 and 4-98 of Section 4.5.2 for AP600. For the case where the jet momentum is locally dissipated, the source flow rate is so high that it increases the local pressure by several psi. This results in a high-pressure source in the break compartment, with the fluid flow distribution governed by the relative resistances through flowpaths. This forces the source mixture through the RCDT cavity, CMT room, the steam generator compartments, and into the above-deck volume. Pressurization will also drive steam into dead-ended compartments during blowdown (See subsection 9.3.2.1). As the event progresses into the peak pressure phase, the source flow rate drops by two orders of magnitude. The jet momentum locally dissipates. This brings the source flow velocity to near zero, including a local pressure increase that is the same order of magnitude as the buoyant forces. The pressure source may be opposed or aided by buoyancy in other flow paths. The resulting flow pattern is the solution to the flow in a network with buoyancy and heat/mass transfer in the network branches. Superimposed on the large-scale flow, the mixture within a given compartment is most likely stratified (Reference 9-8).

Within compartments, the gas may stratify with air concentrating in lower regions and steam concentrating in upper regions, resulting in a vertical steam concentration gradient. If the circulation is sufficient to entrain significant bulk mixture, the gradient may be expected to be small. Entrainment-driven circulation rates in the CMT room are shown, for example, in Section 9.3.1.3. Significant circulation occurs over the height of the CMT room.

Stratification is expected in the containment based on LST data. Low Froude numbers during the long-term indicate a low kinetic energy buoyant plume source. This type of plume is not sufficiently energetic to disrupt stratification. The physics of buoyant plumes and wall layers leads to the existence of recirculating stratification (Appendix 9.C, Section 9.C.1.4.1) in the above-deck region. Plumes rise from the release point and entrain significant volume of mixture as they rise. The heavier bulk air/steam mixture is drawn through the top of the CMT and other deck openings and through compartments to be entrained into the rising plume. Stratification is assumed to have a negligible impact on heat removal in compartments which experience the already air-rich downflow. A very conservative assessment of the effects of stratification on heat removal through the steel shell by the PCS has been performed (Appendix 9.B). An extreme stratification gradient is assumed, to bound the potential for distortions in test data (9.2.3). The homogeneous case total heat sink utilization results are nearly equal to those for the stratified case, with the homogeneous case giving less than 0.5 percent less instantaneous heat removal rates. A simple bias of removing operating deck floors is included in the Evaluation Model to bound this effect.

The containment pressure was calculated for this case using the WGOTHIC AP600 Evaluation Model, (Section 4). It was assumed that the jet was dissipated in the East steam generator compartment, so no

specific break orientation was modeled. The break was located in Volume [ ]$^{(a,c)}$ at elevation [ ]$^{(a,c)}$ The results are discussed in Section 9.3.2.5.

9.3.1.2 Jet Directed Up With No Dissipation

A jet directed upward, that passes through the steam generator compartment undissipated, is considered unlikely. Releases are initially from the break and, later in the transient, releases exit from the fourth stage ADS and the break pipe is covered with liquid. The containment design calls for a steel plate to cover half the flow area in the steam generator compartment above the cold leg pipe and ADS Stage 4 valves. This plate and other structures in the steam generator compartment such as gratings, supports, and the steam generator itself make it doubtful that the break jet could pass through the steam generator compartment unobstructed. Despite the improbability of this scenario, it will be considered as an extreme case to support the selection of a limiting scenario for circulation and stratification.

For the case in which a jet is postulated to pass undissipated up through the steam generator compartment, there is no entrainment into the Steam Generator compartment due to chimney or momentum effects because these effects would act to dissipate the jet. An undissipated jet would enter the above-deck region at the top of the Steam Generator compartment with approximately the same diameter as the broken cold leg pipe. This scenario is similar to two of the LST MSLB configuration tests 222.3 and 222.4. To assess the effects relative to the mass transfer in the above-deck region, volumetric Froude numbers (Fr_v) for the undissipated jet are determined and compared to the LST. An examination of the magnitude of AP600 pressure improvements is provided with sensitivities, relative to condensation results discussed in Reference 9.9, Section 3.9.

For a LOCA DECLG, a postulated undissipated jet will have the same mass flow rate as the design basis LOCA DECLG exiting the top of the steam generator compartment. The two cases differ in the flow area and exit velocity. For the design basis case, the flow area is the area at the top of the Steam Generator compartment. For the undissipated jet, the flow area is the area of the cold leg pipe. For a constant mass flow rate, the product of the flow area times the exit velocity will be equal for the two cases ($U_{DECL} \times A_{DECL} = U_{UNDIS} \times A_{UNDIS}$, where U is the velocity, A is the area, subscript $_{DECL}$ designates the design basis case, and subscript $_{UNDIS}$ designates the undissipated jet case). Fr_v defined in Section 9.2 is proportional to U^2d^2, and is therefore proportional to U^2A^2. For the two cases, the other terms in the Fr_v equation will be the same and $Fr_{v\text{-}UNDIS}$ can be expressed in terms of $Fr_{v\text{-}DECL}$, using $U_{DECL} \times A_{DECL} = U_{UNDIS} \times A_{UNDIS}$. The relationship is $Fr_{v\text{-}UNDIS} = Fr_{v\text{-}DECL} (A_{DECL} / A_{UNDIS})^2$. The area of the top of the Steam Generator compartment is approximately [ ]$^{(a,c)}$ and the area of the cold leg pipe is approximately [ ]$^{(a,c)}$ This results in $Fr_{v\text{-}UNDIS} \sim= Fr_{v\text{-}DECL} \times$ [ ]$^{(a,c)}$

Reference 9.7, Section 6.5.2 presents Fr_v as a function of time for the design basis LOCA in Figure 6-2. At 24 hours Fr_v is approximately 3E-06 (the minimum value during the transient excluding the refill phase). For an undissipated jet, Fr_v is estimated to be 3E-06 x [ ]$^{(a,c)}$ which equals [ ]$^{(a,c)}$. This value is at the lower end of the LST Fr range in the MSLB configuration as shown in Reference 9.7, Figure 6-3. For such high values of Fr, data from the LST in the MSLB configuration (Section 9.2.2) shows that there is minimal deviation from a homogeneous steam concentration in the above-deck region. For the MSLB, Reference 9.9, Figure 3.9-5 shows that use of the Evaluation Model free convection correlation underpredicts condensation on shell surfaces by a factor of [ ]$^{(a,c)}$ for the LST. A multiplier of [ ]$^{(a,c)}$ is a reasonable factor to assess based on the data. To address postulated uncertainty in scaling the LST condensation results to AP600, a range of potential forced convection benefits in AP600 shell heat transfer are considered by examining the sensitivity of predicted containment pressure to condensation multipliers in the Evaluation Model. A sensitivity study examined the effects on containment pressure of using condensation multipliers of [ ]$^{(a,c)}$ These sensitivity cases show that taking credit for improved condensation provides a significant benefit in the calculated containment pressure. The results are discussed in Section 9.3.2.5.

9.3.1.3 Jet into RCDT Cavity (Stairwell)

During the blowdown phase, a jet into the RCDT cavity will create a pressure source in the RCDT cavity compartment. As with the jet dissipation in the East steam generator compartment, the high-pressure source will force fluid through all available openings. The source mixture will flow into the above-deck volume through both the CMT room and steam generator compartments. Following the blowdown phase, the source will rise from the RCDT cavity as a buoyant plume and split, based upon flow areas and resistances, with part of the flow rising through the West steam generator compartment and the remaining fluid flowing through the CMT compartment.

The post-blowdown flow split between the West steam generator and the CMT compartment will depend on flow areas and loss coefficients associated with both flow paths. A range of flow splits can be postulated varying from all the fluid rising through the steam generator compartments to all of the fluid rising through the CMT room and everything in between.

The first scenario is an extreme case which postulates that all the fluid rises through the West steam generator compartment. This scenario is identical to the scenario that assumes the jet momentum is locally dissipated in the East steam generator compartment. The case of the jet momentum dissipated in the East steam generator compartment is discussed in Section 9.3.1.1. The buoyant plume rising from the RCDT cavity into the West steam generator compartment is essentially the same scenario.

The second scenario is a split of the flow entering the RCDT cavity, with part of the break flow rising through the West steam generator compartment and part rising through the CMT compartment. The flow split is dependent on the relative flow path resistances. In this scenario, both the steam generator compartments and the CMT compartment would be subjected to a steam-rich break plume. The CMT and steam generator compartments contain the majority of the below-deck heat sinks. The flow split will result in good heat sink utilization subjecting both the steam generator compartments and the CMT compartment to the steam source. Thus, the case with the jet momentum dissipated in the RCDT cavity and a plume flow split between the CMT and steam generator compartments, will not be limiting. This is confirmed in the sensitivity calculations of Section 9.3.2.5.

The third scenario is an extreme case which postulates that the plume from the RCDT cavity rises into the CMT room. For this scenario, the buoyant plume rises from the floor to the ceiling of the CMT room, entraining gas from the bulk concentration present in the CMT room. An examination of entrainment into a CMT plume can be used to gain insight into the potential for stratification.

Calculation of CMT Room Plume Entrainment Rates

For the case of the LOCA jet being dissipated in the CMT room, the rate of entrainment of mixture in the CMT into the incoming break flow plume, Q_e, can be estimated based on the work of Peterson (Reference 9.15). In particular, Peterson gives the following relation for the volumetric entrainment rate into a buoyant plume,

$$Q_e = k_\mu B^{1/3} z^{5/3} \qquad (9\text{-}1)$$

where k_μ is a constant equal to approximately 0.15, z is the height of the plume, and B is the buoyancy flux, given by:

$$B = g \frac{(\rho_a - \rho_o)}{\rho_a} Q_b \qquad (9\text{-}2)$$

In this equation, g is acceleration due to gravity, ρ_a and ρ_o are the ambient fluid and injected fluid densities respectively, and Q_b is the volumetric flow rate from the plume source.

Substitution of equation (9-2) into equation (9-1) gives:

$$Q_e = k_\mu \left[g \frac{(\rho_a - \rho_o)}{\rho_a} Q_b \right]^{1/3} z^{5/3} \quad (9\text{-}3)$$

The ratio of entrained flow to break flow is therefore:

$$\frac{Q_e}{Q_b} = k_\mu \left[g \frac{(\rho_a - \rho_o)}{\rho_a} \frac{1}{Q_b^2} \right]^{1/3} z^{5/3} \quad (9\text{-}4)$$

AP600 break flow rates for a LOCA DECLG at transient times of 460 seconds and 1,000 seconds are 1,070 ft^3/sec and 266 ft^3/sec respectively for steam. The injected fluid density is taken as the density of saturated steam at the CMT room pressure. These densities are 0.128 lb/ft^3 (based on 54.6 psia at 460 seconds) and 0.135 lb/ft^3 (based on 58 psia at 1,000 seconds). Ambient fluid density is taken as the total density of gas mixture in the CMT room at the times of interest. Inspection of the WGOTHIC output, from the sensitivity case which modeled the break in the CMT room (see Section 9.3.2.5), indicates densities of 0.158 lb/ft^3 at 460 seconds and 0.165 lb/ft^3 at 1,000 seconds in the CMT room. The height of the CMT room is 28.1 feet. Based on this data the applicable entrainment ratios, $Q_e \backslash Q_b$, are 0.68 at t=460 seconds, and 1.7 at t = 1000 seconds.

An entrainment-driven circulation time constant for the CMT room is calculated by dividing the entrainment flow rate into the volume of the CMT. From above $Q_e \backslash Q_b$ is 0.68 when Q_b is 1066 ft^3/sec and 1.7 when Q_b is 266 ft^3/sec. Solving for Q_e gives a range of 725 to 452 ft^3/sec for the entrainment rate. The volume of the CMT room is approximately 157200 ft^3 and the resulting circulation time constant ranges from 217 seconds to 348 seconds (3.6 to 5.8 minutes). This range is relatively short compared to the time of ADS Stage 4 actuation (approximately 1000 seconds), when the steam source is relocated to the steam generator compartments.

Assessment of CMT Room Entrainment Circulation

The entrainment rate for this case is relatively large, increasing to over a factor of two relative to break flow later in time. Thus, a significant amount of CMT room mixture is entrained into the break as the plume rises to the ceiling. It may be concluded that vertical concentration gradients in the CMT room would be relatively small due to circulation within the room. It also may be concluded that the break flow circulates within the room, significantly increasing the room average steam concentration. Thus, high steam concentrations are expected in the CMT room compared to other break scenarios. The high steam concentrations for this scenario will result in high heat sink utilization for heat sinks in this important room.

With such low density mixture in the North CMT room, the chimney effect induces flow to the room from connecting flow paths at the floor elevation. Connecting flow paths from the Section 4 Evaluation Model are [ ]$^{(a,c)}$ horizontally connecting to the steam generator compartments, and until the liquid level closes the path, [ ]$^{(a,c)}$ from the RCDT cavity (see Figure 9-47). The density head over almost 30 feet of height outside the CMT room strongly drives circulation through the CMT and upward in this scenario, suggesting that the flow should rise from the North CMT room into the above-deck region. There is little resistance to flow navigating past the CMT room pinch point to access the ceiling openings on the South CMT room opposite the stairwell, suggesting that flow would spread as it rises into the South CMT room, and then rise from all CMT deck openings. It is known from studies of building fires that very little pressure driving force is necessary to drive horizontal flow in a stratified room (References 9.10, 9.11, 9.12).

The effect of stratification on heat sink utilization is also evaluated. Room pressure, temperature, and steam concentrations were input into a separate calculation to assess the potential effect of stratification in the CMT room. For the calculation, the CMT room was divided vertically into three equal sections. Using free convection heat and mass transfer correlations, room heat sink energy removal was calculated for a room with a homogeneous steam concentration. The applied steam fraction was .63. For the second scenario, the CMT room was subjected to a stratified condition. The top region was assumed to be nearly all steam (steam fraction = 0.98), the middle region was assumed to have a nominal steam fraction (0.63), and the bottom region steam fraction was determined by conserving the total amount of steam in the total volume (0.28). Figure 9.B-3 shows the energy absorbed by the heat sinks in the CMT room for; 1) a stratified steam concentration with the CMT floor included, 2) a homogeneous steam concentration with the CMT floor included, and 3) a homogeneous steam concentration without the CMT floor included. As Figure 9.B-3 shows, the homogeneous concentration with the floor results in the most energy absorbed in the CMT room (top curve). The curve for the stratified concentration with the floor is close to the curve for the homogeneous concentration without the floor. The curve for the homogeneous concentration without the floor is more conservative (less energy absorbed) after 2000 seconds. Given the relative closeness of these two curves, and considering the extreme cases they represent, it is concluded that the lumped parameter Evaluation Model (which uses a homogeneous steam concentration in each volume) without floors provides a reasonably conservative model for heat sink utilization, accounting for the thermal effects of potential stratification. Information on the heat sink utilization calculations is presented in Appendix 9.B.

The break scenario with a buoyant plume flowing into the CMT compartment will not be a limiting scenario. The evaluation of this scenario has shown only small vertical concentration gradients are expected in the CMT compartment while a bias has nevertheless been implemented by removing the floor. Furthermore, high steam concentrations are expected in this compartment due to the large amount of entrainment and subsequent circulation driven by the break plume. The high steam concentrations will yield improved heat sink usage in this room. The scenario discussed in Section 9.3.1.1, with the jet momentum dissipated in the steam generator compartment, will have lower steam concentrations in the CMT room. Thus, the break scenario with a buoyant plume flowing into the CMT compartment will be bounded by the case with the break

jet locally dissipated. To further confirm this conclusion, the results of a WGOTHIC analysis using the AP600 Containment Evaluation Model (Section 4), for a buoyant plume flowing into the CMT compartment, are discussed in Section 9.3.2.5. The analysis confirms that the buoyant plume rising into the CMT compartment is not a limiting scenario.

9.3.2 WGOTHIC Containment Evaluation Model for LOCA

The WGOTHIC Containment Evaluation Model uses lumped parameter noding. Lumped parameter noding simplifies the calculation by assuming homogeneous conditions in each network node. Lumped parameter formulation uses what may be called a scalar form of the momentum equations as follows. Here, momentum flow into each volume is parallel to the junction, and the terms perpendicular to the junction are discarded while junction momentum is dissipated within the volume. Momentum orientation is not tracked, and no turning losses are represented. During the LOCA blowdown phase, the high break mass flow pressurizes the steam generator compartment and flow exits based on relative loss coefficients. Such pressure-driven flows are reasonably modeled by the lumped parameter node-network formulation. Lumped parameter reasonably represents buoyancy and pressure-driven flows and the resulting large-scale circulations. The effects of stratification within each compartment or region can then be superimposed on the large-scale circulation solution. The Containment Evaluation Models are described in Section 4 (AP600) and Section 13 (AP1000).

Comparison of lumped parameter GOTHIC results to test data, has shown lumped parameter noding to be acceptable for LOCA breaks occurring in low zones of containment. Reference 9.13 discusses the test results and subsequent GOTHIC evaluation of the German Heissdampfreaktor (HDR) hydrogen mixing and distribution experiment E11.5. This experiment simulated a large-break LOCA in the lowest region of the HDR containment. The authors conclude that accident scenarios initiated by large-break LOCAs in the low zones of containments can be reliably predicted by the GOTHIC lumped parameter model using only a modest number of nodes (Appendix 9.C, Section 9.C.3.3). The DBA LOCA case models the break in [ ]$^{(a,c)}$ (lower East steam generator compartment) at the [ ]$^{(a,c)}$ elevation.

The conclusions concerning the use of a lumped parameter for low breaks modeled by GOTHIC, can be readily applied to WGOTHIC because of the similarity between the two codes. WGOTHIC is a descendant of the GOTHIC code. The difference between the two codes relates to the heat and mass transfer correlations applied to WGOTHIC by Westinghouse, to model the PCS phenomena for the passive containment design. Thus, since the LOCA scenarios of interest are breaks in the lower region of containment, it is reasonable to use WGOTHIC lumped parameter to model these events.

As discussed previously, the LOCA event is divided into four phases: the blowdown phase, the refill phase, peak pressure phase, and the long-term phase. These phases are discussed in Subsections 9.3.2.1 through 9.3.2.4.

9.3.2.1 Blowdown Phase (0 to 30 seconds)

The lumped parameter solution during blowdown is a node-network solution, governed by pressure differences and flow resistances between nodes. The mass and energy release in the Evaluation Model acts as a high-pressure source that forces the steam out through flowpaths connected to the source node. The Evaluation Model also assumes only free convection on inner containment surfaces. Based on high kinetic energy during blowdown (Ref. 9.7, Figure 6-2) significant enhancement to mass transfer due to forced convection occurs (Section 9.2.2). The steam is driven into the below-deck region and the above-deck volume. Figure 9-37 shows the calculated steam concentration of various containment regions during the blowdown phase, using the Evaluation Model described in Section 4 with a dissipated break in the SG East compartment.

The paragraphs in this subsection describe several sensitivity cases and an evaluation performed to examine various aspects of the blowdown phase. The first sensitivity case examines the effect of modeling a containment with a homogeneous steam concentration on the calculated containment pressure. The second sensitivity case examines the effect of removing all internal heat sinks on the calculated containment pressure. Following this sensitivity case, an evaluation of heat sink utilization in dead-ended compartments is performed. The final sensitivity case examines the effect of varying the flow pattern and steam concentrations on the calculated containment pressure.

To show the relative insensitivity to stratification, or heat and mass transfer coefficient during blowdown, a comparison is needed between the containment pressure response predicted by this node-network solution, and the containment response predicted for a homogeneous containment. Section 8, Figure 8-1 compares the LOCA blowdown pressure results of a one-node WGOTHIC AP600 model to the node-network solution. The one-node model assumes the same total containment volume and containment heat sinks as the multi-node model. Both models predict essentially identical containment pressure responses during the blowdown phase. Therefore, the details of the flow connections and heat mass transfer rates for the multi-node Evaluation Model are not important with respect to the containment pressure results because volume compliance is the dominant pressure mitigator during blowdown.

During the blowdown phase, the mass and energy release is mitigated primarily by containment volume via the rapid pressurization of the containment building. Figure 8-2 shows a comparison of the AP600 Evaluation Model results for the blowdown phase versus an identical model with all internal heat sinks removed. At the end of blowdown (30 seconds), the difference between these two cases is about 3 psi, accounting for only 10 percent of the pressurization. Thus, in the Evaluation Model, the blowdown mass and energy release increases containment pressure by about 35 psi, while the containment heat sinks absorb approximately 3 psi worth of energy. Clearly, the dominant mechanism during blowdown is the pressurization of containment.

The heat sink effectiveness in the presence of a stratification gradient is evaluated in Appendix 9.B. To conservatively account for the reduced effectiveness of heat sinks in lower room areas, floors are eliminated in the WGOTHIC Containment Evaluation Model throughout the transient.

The effectiveness of heat sinks in dead-ended compartments is also evaluated. Since only one opening exists for these compartments, interaction with overall containment volume is expected to be minimal unless the compartments have non-uniform temperatures. During blowdown, these compartments pressurize along with the rest of containment. Steam/air mixture from the bulk containment volume flows into the dead-ended compartments during the initial pressurization. Once pressurized, additional steam/air flow into the dead-ended compartments only occurs to make up for steam condensing in the compartment. Analysis of the Nuclear Power Engineering Corporation (NUPEC) natural circulation test, M-4-3, showed that asymmetric heating of dead-ended compartment walls can lead to natural circulation flows within the compartment (Reference 9.14). However, a conservative evaluation of dead-ended compartments would consider no thermally driven circulation. In such a case, inside the compartments, the condensation of steam leaves behind a heavier air-rich mixture. The air flows to the bottom and blankets the lower heat sinks. The poor circulation within the dead-ended compartments leaves the air-rich layer relatively undisturbed. As steam continues to condense, the air-rich layer continues to build up and will result in significant stable stratification within the dead-ended compartments. Although the heat sinks in the dead-ended compartments will contribute somewhat to containment heat removal, to conservatively bound the effects of stratification, condensation and convection on the heat sinks in the dead-ended compartments are neglected after 30 seconds in the Evaluation Model.

Based on the results of the evaluation, it has been demonstrated that blowdown pressure history is relatively insensitive to the effects of circulation and stratification. The internal heat sinks do heat up during blowdown, however, as discussed above, containment volume pressurization is the dominant mechanism for absorbing the energy released. Since volume pressurization is the governing process, blowdown pressure response is not sensitive to circulation and stratification effects. The Evaluation Model utilizes a conservative lower estimate of containment free volume. Thus, the uncertainties in heat and mass transfer or stratification, and flow path effects, do not significantly impact the LOCA blowdown pressure history and the Evaluation Model adequately models the LOCA blowdown phase.

To assess the effects of varying the steam concentrations and flow rates on the calculated containment pressure, a sensitivity was performed which varied several loss coefficients in the Evaluation Model. This sensitivity shows how changes in conditions during the blowdown phase affect the later phases and, in particular, the calculated containment pressure. For this sensitivity, the AP600 Containment Evaluation Model (Section 4), with a dissipated jet in the SG East compartment, was used and the loss coefficients [

]$^{(a,c)}$

Figure 9-38 shows the pressure transient for this sensitivity case. The maximum calculated pressure is 43.8 psig, which is 0.1 psi less than the 43.9 psig reported in Section 9.3.2.5.

Circulation plots for this sensitivity case are presented in Figures 9-39 through 9-42. Compared to the circulation plots for the dissipated jet in the SG East compartment (Figures 9-47 through 9-50), the effects of the revised loss coefficients are evident. At 20 seconds, Figure 9-39 shows that most of the break flow goes from the SG East compartment to the SG West compartment, and through the RCDT cavity to the North CMT room. At 1000 seconds (Figure 9-40), flow is rising from both SG compartments and a steam/air mixture is flowing down into the North and South CMT volumes. Figure 9-48, shows flow rising only from the SG East compartment. At 1550 and 80050 seconds (Figures 9-41 and 9-42) the ADS Stage 4 valves are the source of the steam releases and the flow patterns are similar to those in Figures 9-49 and 9-50. This sensitivity altered the flow patterns and steam concentrations early in the transient by changing some of the flow path loss coefficients. The change in calculated maximum pressure was negligible.

9.3.2.2 Refill Phase (30 to 90 seconds)

The refill phase immediately follows blowdown. After blowdown, the accumulators refill the lower plenum of the reactor with a high flow rate of cold water. The resulting steam and water flow rates from the break are very low and increase with time. The mass and energy release rates are two orders of magnitude less than the blowdown rates, and can be approximated as 0 from approximately 30 to 90 seconds into the event. With a negligible steam source rate and a high condensation rate, the containment pressure drops by a few psi from its peak at the end of blowdown to the end of the refill phase at approximately 90 seconds. For the calculation of maximum containment pressure, the Evaluation Model conservatively neglects the refill period.

9.3.2.3 Peak Pressure (90 to 1200 seconds)

During the peak pressure phase, the location of the steam releases changes from the break to the ADS Stage 4 valves in both steam generator compartments. The Evaluation Model includes this change in steam release location. In addition, the lower compartments begin to fill with liquid from the break. The reduced heat transfer area due to filling is accounted for in the Evaluation Model. Figure 9-43, for a jet dissipated in the SG East compartment, shows that the condensation on the steel becomes the dominant mechanism for heat removal towards the end of the peak pressure phase.

The evaluation of break scenarios in Section 9.3.1 led to the conclusion that the case with jet momentum dissipated in the steam generator compartment may lead to stratification within compartments after the blowdown phase. Given this possibility, it is necessary to show that the Evaluation Model bounds the possible effects of this stratification. Lumped parameter models assume no gradients within each volume of the network. Thus, in the Evaluation Model, all heat sinks within a compartment volume see identical environmental conditions. In contrast, actual conditions may lead to a stratified compartment with a region of higher steam concentration on top and lower steam concentration near the bottom. For the effects of stratification on heat sink utilization, the most significant heat sinks are the above-deck region (containment shell) and the CMT room (steel and jacketed concrete). The compartment features are discussed in Sections 4 and 13 and summarized in Table 3-1 of Reference 9.2. In Section 9.3.1.3, the CMT room was assessed for its sensitivity to stratification. In this calculation, heat sink usage was calculated for a homogeneous room and a severely stratified room. A bias has been defined to bound the potential effects of stratification in compartments as discussed in 9.3.1.3. In Section 9.3.1.1, the containment shell was assessed for its sensitivity to stratification. A bias has been defined to bound the potential effects of stratification above-deck as discussed in Section 9.3.1.1. Appendix 9.B discusses the calculations performed.

Based upon the results of the evaluation, a method to bound circulation and stratification effects for the peak pressure phase has been developed. In the Evaluation Model, all floors are neglected throughout the transient and condensation and convection on all heat sinks in dead-ended compartments are neglected after 30 seconds (refer to Section 9.3.2.1).

9.3.2.4 Long-Term Phase (1200 seconds to 24 hours)

Figure 9-43 shows the condensation on the steel shell remains the dominant mechanism for heat removal during the long-term. The results shown are from the AP600 Containment Evaluation Model (Section 4) with a dissipated jet in the SG East compartment. During early portions of the transient, internal heat sinks are the primary path of containment heat removal. As the transient progresses, the temperature of the heat sinks increases and their heat removal effectiveness is reduced. PCS heat removal, which dominates in the long-term, is dependant on steam concentrations. The effects of stratification on the containment shell heat removal have been evaluated in Section 9.3.1.1 and a bias of removing operating deck floors has been included in the Evaluation Model.

In addition, WGOTHIC predicts a slight gradient between the upper and lower compartments (excluding dead-ended compartments). Figure 9-44 shows WGOTHIC predicted steam concentrations for various compartments in the AP600, using the Evaluation Model (Section 4) with a dissipated jet in the SG East compartment. As Figure 9-44 shows, at 24 hours WGOTHIC predicts a homogeneous above-deck region.

However, WGOTHIC predicts a slightly lower steam concentration below the operating deck, excluding the SG compartments which continue to have steam release through the ADS Stage 4 valves.

The trend over time for the WGOTHIC calculations leads to a very small steam density gradient between above- and below-deck compartments. The WGOTHIC predicted average steam concentration above the operating deck is approximately 0.47 at 24 hours. Below the operating deck, the average is approximately 0.46 at 24 hours excluding the SG compartments. The calculated steam concentration for a homogeneous condition between the above-deck region and the below-deck open compartments is approximately 0.468. There is a negligible change between the WGOTHIC calculated above-deck steam concentration and the calculated homogeneous concentration (excluding dead-ended and SG compartments). Since the predicted stratification is slight, and since the volume of the above-deck regions is significantly greater than the below-deck open compartments, mixing the above-deck volume with the below-deck open compartments does not significantly change the above-deck steam concentrations. Thus, the WGOTHIC predictions as the transient calculation passes through 24 hours are essentially similar to the assumption of a homogeneous containment. It is conservative to not include the steam generator compartment steam concentration in the homogeneous calculation.

It is concluded that WGOTHIC predicts a slight segregation between the above- and below-deck regions, but the deviation from the homogeneous assumption is insignificant. Based upon the results of the evaluation, it has been shown that the Evaluation Model adequately bounds the effects of circulation and stratification during the long-term phase.

9.3.2.5 Evaluation Model Results

Sensitivities have been performed using the lumped parameter AP600 Containment Evaluation Model (Section 4) for several postulated, plausible break locations. An evaluation of the sensitivities leading to selection of a limiting scenario for design basis accident calculations follows.

It has been determined that to bound circulation and stratification effects, floors are neglected throughout the transient, and condensation and convection on all heat sinks in the dead-ended compartments are neglected after blowdown. The stratification of steam and air within compartments may reduce heat sink effectiveness. These biases are included in the Evaluation Model used to perform sensitivities.

Undissipated Jet Rising in SG East Compartment

The postulated, undissipated jet directed up the Steam Generator compartment results in increased heat and mass transfer, possibly as high as a factor of [ ]$^{(a,b)}$ over the steel shell surface based on the LST,

compared to that using the free convection correlation in the Evaluation Model, as discussed in Section 9.3.1.2. To estimate the potential benefit for AP600, the heat transfer coefficient multipliers for the inner surfaces of the clime conductors (that is, only the steel shell mass transfer is enhanced) were increased to [ ]$^{(a,c)}$ times the Evaluation Model values. The Evaluation Model with the break in the steam generator East compartment was used for the sensitivity cases. The postulated, undissipated jet will only occur until the ADS Stage 4 valves are opened at approximately 1000 seconds. Therefore the containment pressure response is plotted for the first 1000 seconds of the LOCA. The containment pressure sensitivity results are shown in Figure 9-45, along with the Evaluation Model results. The results show that the pressure response during the blowdown phase is the same for all cases. This is expected because volume compliance is the dominant pressure mitigator during blowdown (Section 9.3.2.1). Compared to the Evaluation Model results at 1000 seconds, the calculated containment pressure for the [

]$^{(a,c)}$ These results show that a substantial benefit in containment pressure is gained when the heat transfer coefficient is increased to account for the forced convection from an undissipated jet. Therefore, this case will be less limiting than the other postulated break scenarios in which the jet is dissipated.

Dissipated Jet Rising in SG East Compartment

Another postulated break scenario, the design basis case, is a dissipated jet in the SG East compartment (Volume 107, elevation 100 ft.). Figure 9-46 shows the results of the WGOTHIC AP600 Containment Evaluation Model which includes the circulation and stratification biases. Assuming the break momentum is dissipated in the broken loop steam generator compartment, a maximum containment pressure of 43.9 psig is calculated, which is below the design pressure of 45 psig. The pressure transients for compartments directly connected to the SG East compartments are shown in Figure 9-46A. Figures 9-47 through 9-50 show the circulation pattern predicted by WGOTHIC for this case at different times during the transient. The figures show the Evaluation Model flow path connections for the below-deck volumes, the flow rates and directions, volume steam pressure ratio, and liquid level. Figure 9-51 is a depiction of each of the flow connections to the above-deck volumes. In subsequent figures, total flows through the ceiling of each compartment are shown for simplicity. Flow paths that have been grouped have the same flow direction. Figure 9-47 presents data at 20 seconds which is near the end of blowdown. Flow is forced into all of the below-deck volumes and into the above-deck volumes from the East and West steam generator compartments and the North and South CMT rooms. Figure 9-48 presents data at 1000 seconds which is near the time of maximum pressure and prior to ADS Stage 4 valve actuation. Flow to the dead-ended compartments has stopped. The general circulation pattern is fluid from the break flowing up through the SG East compartment while a steam/air mixture is drawn into and through the SG West compartment, the North and South CMT rooms, and the RCDT cavity into the SG East compartment. At 1500 seconds, Figure 9-49 shows the change in circulation pattern due to the actuation of the ADS Stage 4 valves. The steam releases

flow up through both steam generator compartments while a steam/air mixture is drawn into and through the CMT rooms and the RCDT cavity. This flow pattern develops less than 2 minutes after ADS Stage 4 activation. Figure 9-50 shows the circulation pattern near 24 hours. The flow rate out of the ADS Stage 4 valves is approximately one-fourth of the flow at 1500 seconds. The flow pattern remains out of the SG compartments and into the CMT rooms, however, flow through the RCDT cavity has ceased, due to liquid level rising above the top of the flow path.

Plume Rising in CMT Room

In Section 9.3.1.3, the LOCA with jet dissipation in the RCDT cavity was postulated. It was postulated that the entire buoyant plume rises into the North CMT compartment. The evaluation concluded this scenario was not limiting because of the higher steam concentrations expected in the CMT compartment, which would result in better internal heat sink utilization. Furthermore, the evaluation concluded that the relative steam densities would drive the steam to navigate the bend in the CMT compartment. This would lead to a steam-rich environment for the heat sinks in the south end of the CMT room opposite the stairwell. To confirm that this scenario is not bounding, a WGOTHIC calculation was performed using the AP600 Containment Evaluation Model (Section 4). The calculation assumed a LOCA where the jet plume dissipates and rises into the North CMT compartment. This was simulated by applying the break boundary conditions to the North CMT node (Volume 6, elevation 107 ft.), the only change made to the Evaluation Model. The circulation and stratification biases of neglecting floors throughout the transient and condensation and convection in dead-ended compartments following blowdown were included. The containment pressure results of this evaluation are shown in Figure 9-52. The maximum pressure was calculated to be 43.7 psig. As expected, this pressure is below the previous scenario where momentum is dissipated in the East steam generator compartment. The circulation pattern predicted by WGOTHIC is shown in Figures 9-53 and 9-54.

Figure 9-53 presents data at 1000 seconds which is near the time of maximum pressure and prior to ADS Stage 4 valve actuation. Compared to Figure 9-48 (break in SG East compartment), Figure 9-53 shows flow out of the North and South CMT rooms into the above-deck region, while a steam/air mixture flows down into both SG compartments and up through the RCDT cavity into the North CMT room. Figure 9-54, at 1400 seconds, shows the change in flow pattern due to ADS Stage 4 valve actuation. The flow rates and pattern are similar to those in Figure 9-49, as expected. Figure 9-55 shows the heat sink utilization for this sensitivity case. As expected, Figure 9-55 shows a greater CMT room (Volumes 6 and 104) heat sink utilization than that shown in Figure 9-43 for a break in the SG East compartment. Both figures show that the PCS shell is the dominant heat sink at the time of maximum containment pressure and beyond.

Plume Rising in RCDT Cavity

In Section 9.3.1.3, a LOCA with jet dissipation in the RCDT cavity was postulated. This scenario assumed the break flow splits between the CMT and steam generator compartments. The evaluation concluded that good below-deck heat sink utilization is expected because of the high steam concentrations in the CMT and steam generator compartments. A WGOTHIC calculation was performed for this scenario using the AP600 Containment Evaluation Model (Section 4). The calculation simulated the flow split by placing the break boundary condition directly in the RCDT cavity [ ]$^{(a,c)}$ The circulation and stratification biases were included. The pressure prediction from the evaluation is shown in Figure 9-56. The maximum pressure was calculated to be 43.4 psig. This pressure is below both of the previously discussed sensitivities. The WGOTHIC predicted circulation pattern is shown in Figures 9-57 and 9-58.

Figure 9-57 presents data at 1000 seconds which is near the time of maximum pressure and prior to ADS Stage 4 valve actuation. With the break in the RCDT cavity, the bulk flow distribution is based on the path areas and loss coefficients. Consequently, at 1000 seconds, the steam flow from the break goes up through the CMT rooms, while a steam/air mixture flows down through both SG compartments and into the North CMT room and RCDT cavity. Figure 9-58, at 1500 seconds, shows the change in flow pattern due to ADS Stage 4 valve actuation. The flow rates and pattern are similar to those in Figure 9-49, as expected. Figure 9-59 shows the heat sink utilization for this sensitivity case. Compared to Figure 9-43 for a break in the SG East compartment, Figure 9-59 shows a small delay in the heat absorption from the SG East compartment and the CMT rooms. The heat absorption from the SG West compartment starts a little sooner in Figure 9-59. The effects are due to the break location differences. Consistent with the other cases, Figure 9-59 shows that the PCS shell is the dominant heat sink at the time of maximum containment pressure and beyond.

9.3.2.6 Evaluation of Drops During a LOCA

Drops, or fog particles, are created when the blowdown break source steam velocity is large enough to disperse a fraction of the break liquid along with the gas. As discussed in Reference 9.2, Section 4.4.2D and Reference 9.7, Section 7.1, drops will be formed during the LOCA blowdown phase. For the post-blowdown phases of a LOCA and for the main steamline break (MSLB), there will not be any significant drop formation. The thermal and circulation effects of drops on LOCA containment pressure are examined in Appendix 9.A and summarized below.

Drop fall times for various size drops were determined in Appendix 9.A, which only account for the gravitational effects on the drops. Fall times range from seconds to hours depending on the drop size and fall height. This provides an indication that the drops will exist long enough that their effect on containment

pressure must be considered. In addition, Appendix 9.A estimated plume entrainment rates for 0 percent and 100 percent of the break liquid converted to drops. The entrainment rates and subsequent circulation time constant for both 0 and 100 percent drops show that a large fraction of the containment volume will be entrained in the plume within a few minutes, which is relatively short compared to the time to reach maximum pressure (at approximately 1200 seconds), and very short compared to long-term cooling. A relatively large entrainment rate within the above-deck region indicates that the steam density gradients above-deck are not large whether drops exist or not. Therefore, the presence of drops will not significantly affect the general circulation and stratification patterns in the containment atmosphere.

Section 5.8 shows the results of sensitivity cases to assess the Evaluation Model treatment of the thermal effects of drops with respect to containment pressure. The results that show the Evaluation Model assumption of 50 percent of the break liquid being converted into drops provides essentially the same containment maximum calculated pressure as assuming 100 percent of the liquid is converted into drops. The 50 and 100 percent drop fractions are both more limiting with respect to maximum pressure than assuming none of the break liquid is converted into drops.

The formation of drops during the LOCA blowdown phase is a physically real phenomenon which may influence the maximum containment pressure calculated by the Evaluation Model. Drop formation increases the effective density of the containment atmosphere due to the close coupling between small drops and gas by shear forces, making the post-blowdown releases relatively more buoyant. A small percentage ($\geq 5\%$) of the blowdown break liquid formed into drops is sufficient to saturate the containment atmosphere, at which point, additional drop density has a minor thermal effect. The Evaluation Model treatment of drops, as described in Section 4.5.2.1 and Section 13.5.2.1 and Section 13.5.2.1, provides a sufficiently bounding calculation for maximum and long-term containment pressure.

9.4 MAIN STEAMLINE BREAK (MSLB)

The main steamline transports steam from the steam generators within the containment building to the turbine generators in the auxiliary building. The main steamline path begins at the top of the steam generator, where it bends 180° and follows a downward path to the CMT room. In the CMT room, the steamline bends 90°, crosses through the CMT room, and exits the building through a penetration in the containment shell. Rupture of the main steamline inside containment would release high energy steam into the containment. To confirm the design adequacy of the containment, various MSLB scenarios are examined to develop a conservative model accounting for the effects of circulation and stratification in the containment pressure calculations.

9.4.1 Break Locations

An evaluation of circulation and stratification must allow for the consideration of possible break locations. For the MSLB, two distinct break locations may be postulated: a break in the steamline above the operating deck or a break in the steamline in the CMT compartment.

9.4.1.1 MSLB Above the Operating Deck

An MSLB above the operating deck could occur anywhere in the steamline piping from the top of the steam generator to the operating deck penetration into the CMT compartment.

The design basis MSLB mass and energy releases for containment pressure assume a 1.388 ft^2 break (due to integral flow limiters). The MSLB event is characterized by a high energy release of short duration. Reference 9.7, Figure 6-3 shows the calculated Froude numbers for the event compared to Froude numbers calculated for the LST. The high Froude numbers indicate a high kinetic energy source which is expected to drive circulation above and below the jet source elevation. High Froude numbers also indicate that a significant forced convection enhancement to mass transfer occurs during an MSLB.

An examination of releases from smaller sized breaks in main steamlines indicates that the reduction in mass flow is more than offset by the reduction in exit flow area. Therefore, the larger size breaks have the lowest Froude numbers. The double-ended rupture MSLB has the limiting combination of mass and energy release and Froude numbers.

9.4.1.2 MSLB in the CMT Compartment

A steamline rupture in the CMT compartment would propel a high momentum steam jet into the CMT room. Since the break is within an enclosed compartment, momentum from the jet would be dissipated by the

equipment, walls, floors, and ceilings of the CMT room. The effect would create a pressure source in the CMT compartment with the fluid following the path of resistance through the node network into adjacent compartments and the above-deck volume.

The steam source in the CMT compartment will create a steam-rich environment for this room which contains many heat sinks. The high steam concentration will result in excellent heat sink utilization for this scenario.

The MSLB in the CMT compartment case is bounded by the scenario of an MSLB occurring above the operating deck. While the break above the operating deck does produce substantial circulation, the steam concentrations in the CMT compartment will not approach the steam levels for a break directly within the CMT room. Thus, the MSLB in the CMT compartment is not the bounding scenario. To confirm this conclusion, Section 9.4.3 presents the results of a WGOTHIC analysis for a break in the CMT compartment. As expected, the containment peak pressure is lower for the MSLB in the CMT compartment than for an MSLB above the operating deck.

9.4.2 WGOTHIC Containment Evaluation Model for MSLB

In creating an appropriate and conservative Evaluation Model, it is necessary to understand how the code handles circulation, to bias the model to produce bounding but reasonably representative results. Investigation of the lumped parameter AP600 Containment Evaluation Model (Section 4) has shown that this noding structure tends to mix upwards from the break elevation.

The lumped parameter calculational bias may be attributed to the use of multiple, relatively large lumped parameter nodes to represent the above-deck region in the Evaluation Model. Lumped parameter formulation uses what may be called a scalar form of the momentum equations, as follows. Here, momentum flow into each volume is parallel to the junction, and the terms perpendicular to the junction are discarded while junction momentum is dissipated within the volume. Momentum orientation is not tracked, and no turning losses are represented. This momentum dissipation is the characteristic of the lumped parameter noding which results in the calculated stratification above/below the jet. With momentum diffused throughout the volume node, the vigorous circulation from the high kinetic energy jet does not occur in the model. Circulation above the jet source in the lumped parameter model is driven by the density head terms in the momentum equation which cannot drive flow below the source. Thus, lumped parameter noding predicts a steam-rich atmosphere above the assumed source elevation, and a steam-deficient atmosphere below this source elevation (simulating stratification).

With an understanding of both the physics, and lumped parameter model biases, a WGOTHIC representation is constructed which conservatively represents the accident scenario. The high kinetic energy of the MSLB will tend to circulate steam through the above-deck portion of the containment vessel and lead to forced convection conditions for the shell. The lumped parameter Evaluation Model, however, calculates a steam-rich region above the injection point and an air-rich region below this point. Figure 9-60 shows the steam concentration results of a WGOTHIC MSLB calculation using the AP600 Containment Evaluation Model with the source entering [ ]$^{(a,c)}$ which is just above the operating deck (refer to Section 4.5.2.2). The model predicts a small steam density gradient above-deck, consistent with the expectation of only small gradients in the AP600, based on LST data (see Section 9.2.2). Evaluation has shown that the effect on shell mass transfer of even extreme stratification, beyond that expected for the AP600 or AP1000 (see Section 9.3.1.3), is very small. Very little steam penetrates into the below-deck region in the model. Steam access into the below-deck compartments in the model is governed only by the volume pressurization. As the mass and energy releases pressurize the above-deck region, a steam/air mixture from above-deck is pushed into the below-deck compartments. The use of the WGOTHIC lumped parameter model, with an injection point just above the operating deck, results in a conservative Evaluation Model for the steam line break as a result of reduced steam access to the below-deck heat sinks. The reduced steam access is due to the momentum dissipation in the model which reduces the calculated circulation to the nodes below the operating deck. The Evaluation Model neglects any heat and mass transfer contribution from forced convection, so above-deck velocity predictions become unimportant. Mass transfer is seen to be underestimated by as much as a factor of [ ]$^{(a,c)}$ on the steel shall surface relative to forced convection in the LST. To add an additional conservative bias, the stratification heat sink biases developed for LOCA scenarios are also included

9.4.3 MSLB Sensitivity Results

Based on an evaluation of circulation and stratification, an MSLB Evaluation Model has been constructed to bound circulation and stratification effects. The limiting MSLB scenario assumes a pipe break above the operating deck. In this scenario, test data indicates that the high kinetic energy source jet induces circulation above and below the jet elevation, including substantial steam penetration into below-deck compartments. The lumped parameter Evaluation Model, that bounds circulation and stratification, places the break source directly above the operating deck [ ]$^{(a,c)}$ This results in a well-circulated upper region with little steam access to the heat sinks below the operating deck. To further bound circulation and stratification effects, stratification heat sink biases developed for LOCA scenarios are included (see Table 9-1). Figure 9-61 shows the results of the AP600 WGOTHIC MSLB Evaluation Model described above. A containment peak pressure of 44.8 psig is calculated, which is below the design pressure of 45 psig.

In Section 9.4.1.2, the MSLB in the CMT compartment scenario was evaluated, concluding that increased circulation below the operating deck would reduce the calculated containment pressure. This scenario was determined not to be the limiting scenario, because of the high steam concentrations expected in the CMT compartment. The high steam concentration would result in improved heat removal rates by the heat sinks in the CMT compartment. To confirm this hypothesis, a WGOTHIC analysis was performed for a break in the CMT compartment [ ]$^{(a,c)}$ As with the break above the operating deck, LOCA stratification biases were included. Figure 9-62 shows the results of the WGOTHIC calculation. A containment peak pressure of 43.2 psig is calculated, which is 1.6 psi less than the peak pressure for the MSLB above the operating deck. As expected, the Evaluation Model predicts the MSLB above-deck to be the limiting location.

9.5 CONCLUSIONS

A WGOTHIC Containment Evaluation Model is used which considers circulation and stratification in the calculation of LOCA and MSLB containment pressures and temperatures. The effects of circulation and stratification on the calculated containment pressure have been examined, and biases have been defined for the Evaluation Model. The Evaluation Model input deck and specific biases are described in Sections 4 and 13. In addition, break locations have been examined for LOCA and MSLB to determine the limiting location for each transient with respect to calculated containment pressure.

The following biases have been incorporated into the Evaluation Model for the LOCA analysis based on the circulation and stratification evaluations documented in this section:

- Heat and mass transfer from floors of compartments and the operating deck have been removed to bound the potential reduction in heat transfer due to stratification. Refer to Sections 9.3.1.1, 9.3.1.3, and Appendix 9.B.

- Condensation and convective heat transfer in dead-ended compartments are turned off after 30 seconds (i.e., after blowdown) to bound the potential reduction in heat transfer due to stratification. The basis for this bias is provided in Section 9.3.2.1.

- The lumped parameter Evaluation Model considers only free convection for internal heat sinks and shell surfaces and, therefore, conservatively neglects the increase in mass transfer to the containment steel shell due to forced convection during blowdown. Refer to Section 9.3.2.1.

Ranges of LOCA break locations and jet directions were evaluated to determine the limiting case with respect to containment pressure. The limiting scenario is the DECLG break in the East steam generator compartment with the jet momentum locally dissipated. Other break locations, or jet directions, result in increased heat sink utilization which results in lower calculated containment pressures. Based on the results presented in Section 9.3.5.2, the calculated maximum LOCA containment pressure from a dissipated jet is not very sensitive to the break location since internal heat sinks "reach maximum effectiveness" well before the time of maximum pressure.

The following biases have been incorporated into the Evaluation Model for the MSLB analysis based on the circulation and stratification evaluations documented in this section:

- The break is placed in a node at the operating deck level to minimize circulation and steam access to below-deck heat sinks, which bounds the potential reduction in heat transfer in below-deck compartments due to stratification. This is discussed in Section 9.4.2.

- The lumped parameter Evaluation Model considers only free convection for internal heat sinks and shell surfaces and, therefore, conservatively neglects the increase in mass transfer to the containment steel shell due to forced convection during the entire transient. Refer to Section 9.4.2.

- The above listed LOCA biases (relative to floors and dead ended compartments) have been included in the MSLB Evaluation Model to further conservatively bound potential reductions in heat transfer due to stratification. Refer to Section 9.4.3.

Based on the routing of the steamline pipe, two MSLB locations were evaluated; a break above the operating deck and a break in the CMT room. As discussed in Section 9.4.3, the break above-deck resulted in the higher calculated containment pressure. The break in the CMT room had increased heat sink utilization in the CMT room which resulted in the lower calculated containment pressure.

The above biases are incorporated into the Evaluation Model as described in Sections 4.2 and 13.2, subsections entitled "Special Modeling Assumptions." Therefore, the effects of circulation and stratification have been conservatively bounded in the WGOTHIC containment pressure calculations.

9.6 REFERENCES

9.1 WCAP-14382, "WGOTHIC Code Description and Validation," May 1995.

9.2 WCAP-14812, "Accident Specification and Phenomena Evaluation for AP600 Passive Containment Cooling System," Revision 2, April 1998.

9.3 NTD-NRC-95-4563, "GOTHIC Version 4.0 Documentation, Enclosure 2: Technical Manual," September 21, 1995.

9.4 NTD-NRC-95-4563, "GOTHIC Version 4.0 Documentation, Enclosure 3: User Manual," September 21, 1995.

9.5 WCAP-13566, "AP600 1/8th Large-Scale Passive Containment Cooling System Heat Transfer Test Baseline Data Report," October 1992.

9.6 WCAP-14135, "Final Data Report for PCS Large-Scale Tests, Phase 2 and Phase 3," Revision 1, April 1997.

9.7 WCAP-14845, "Scaling Analysis for AP600 Containment Pressure During Design Basis Accidents," Revision 3, March 1998.

9.8 Wolf, L., Gavrilas, M., Mun, K., 1996, "Overview of Experimental Results for Long-Term, Large-Scale Natural Circulations in LWR-containments after Large LOCAs," DOE - Project, Order Number: DE-AP07-96ID10765, University of Maryland at College Park, July 1996.

9.9 WCAP-14326, "Experimental Basis for the AP600 Containment Vessel Heat and Mass Transfer Correlations," Revision 2, April 1998.

9.10 Jaluria, Y. "Buoyancy Driven Wall Flows in Enclosure Fires," Twenty-first Symposium (International) on Combustion, The Combustion Institute, 151-157 (1986).

9.11 Goldman, D., Jaluria, Y., "Effect of Opposing buoyancy on the Flow in Free and Wall Jets," *Journal of Fluid Mechanics*, 166, 41-56 (1986).

9.12 Jaluria, Y., Cooper, L.Y., "Negatively Buoyant Wall Flows Generated in Enclosure Fires," Progress in Energy and Combustion Science, 15, 159-182 (1989).

9.13 Fisher, K., Schall, M., and Wolf, M., "Simulations of GOTHIC Large-Scale Containment Experiments," published by Battelle Ingenieurtechnik GmbH, October 1995.

9.14 Ofstun, R.P., Woodcock, J., Paulsen, D.L., "Westinghouse - GOTHIC Modeling of NUPEC's Hydrogen Mixing and Distribution Test M-4-3," Third International Conference on Containment Design and Operation, October 1994, Toronto, Canada.

9.15 Peterson, P.F., "Scaling and Analysis of Mixing in Large Stratified Volumes," *International Journal of Heat and Mass Transfer*, Vol. 37, Suppl. 1, pp 97-106, 1994.

(a,c)

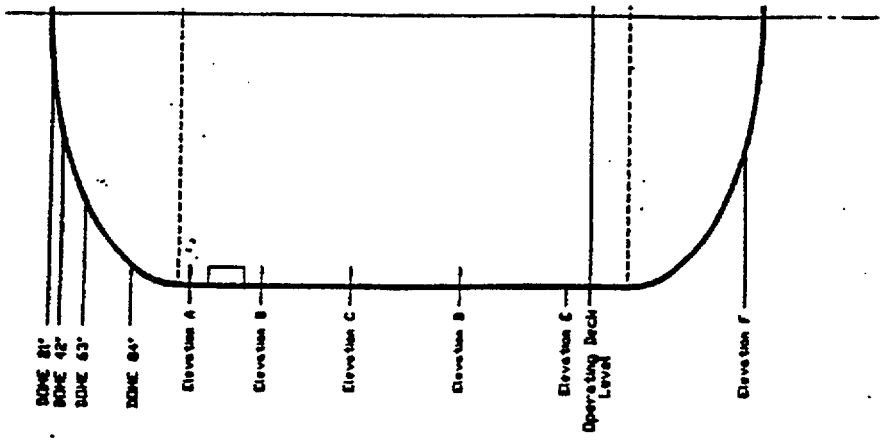

Figure 9-1 Measured Steam Concentrations for LST

(a,b)

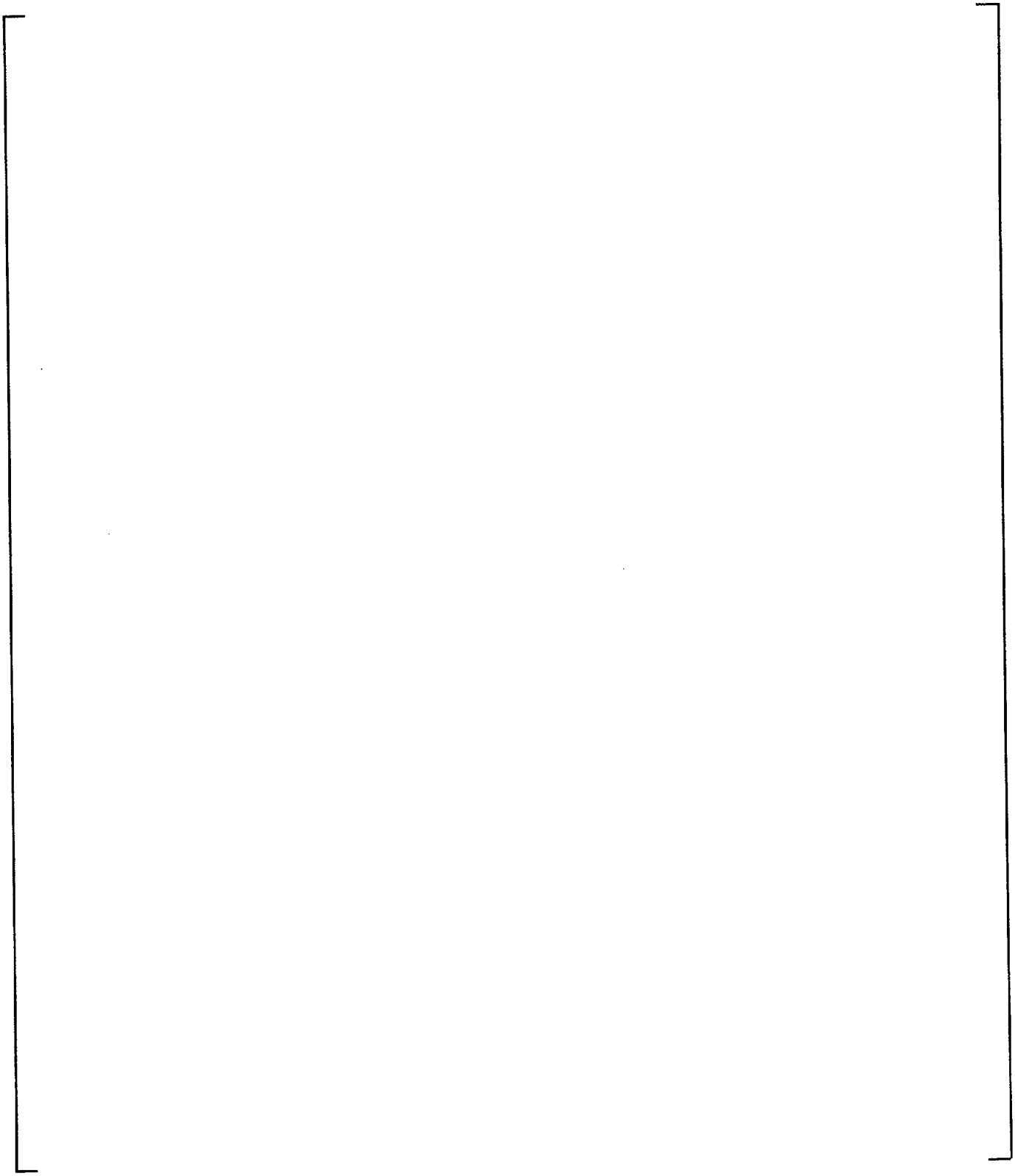

Figure 9-2 **LST with Diffuser Under Steam Generator - Steam Flow 0.11-0.17 lb/sec - Internal Fluid Temperature - Group 1**

(a,b)

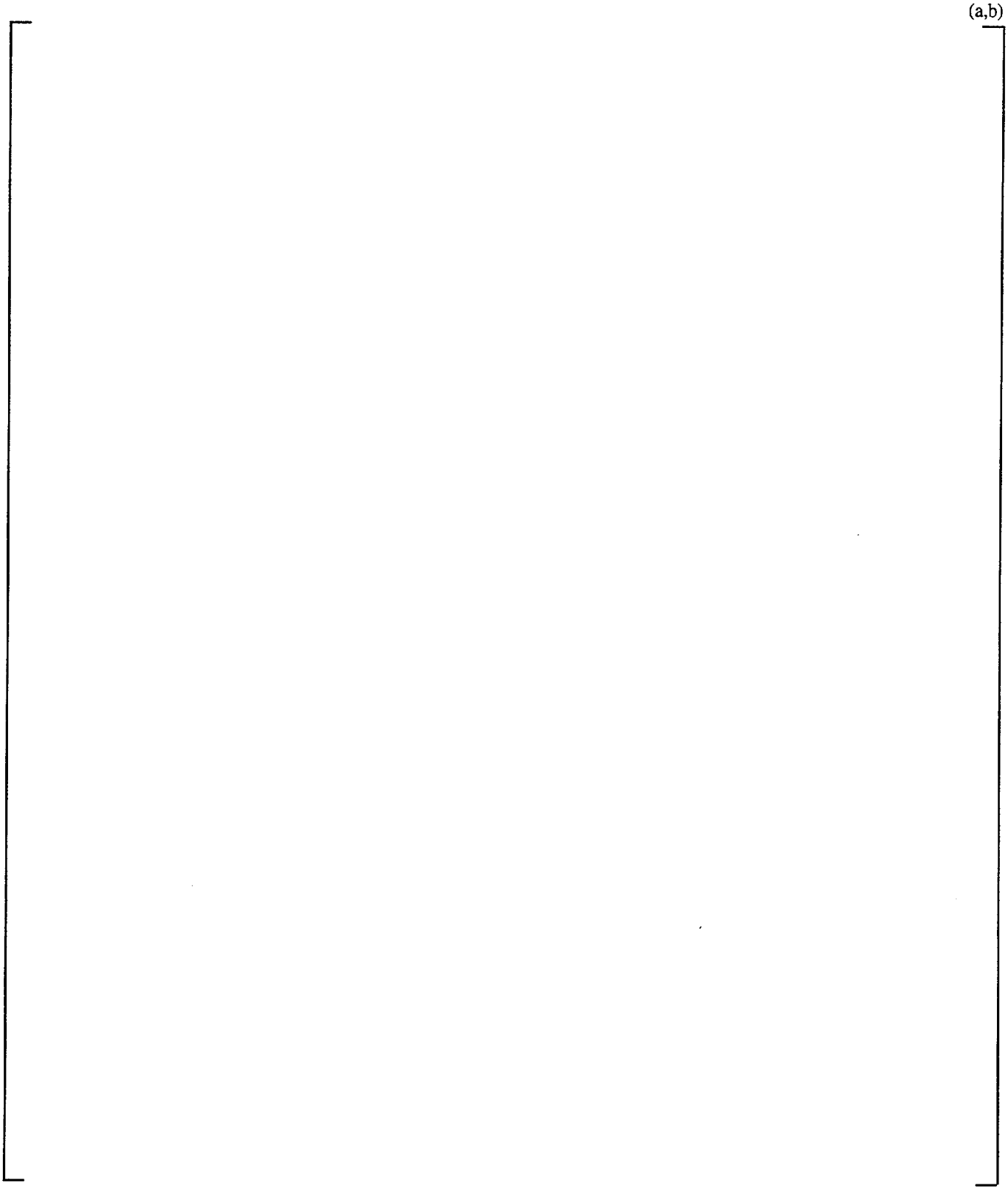

Figure 9-3 LST with Diffuser Under Steam Generator - Steam Flow 0.11-0.17 lb/sec - Saturation Temperature - Group 1

(a,b)

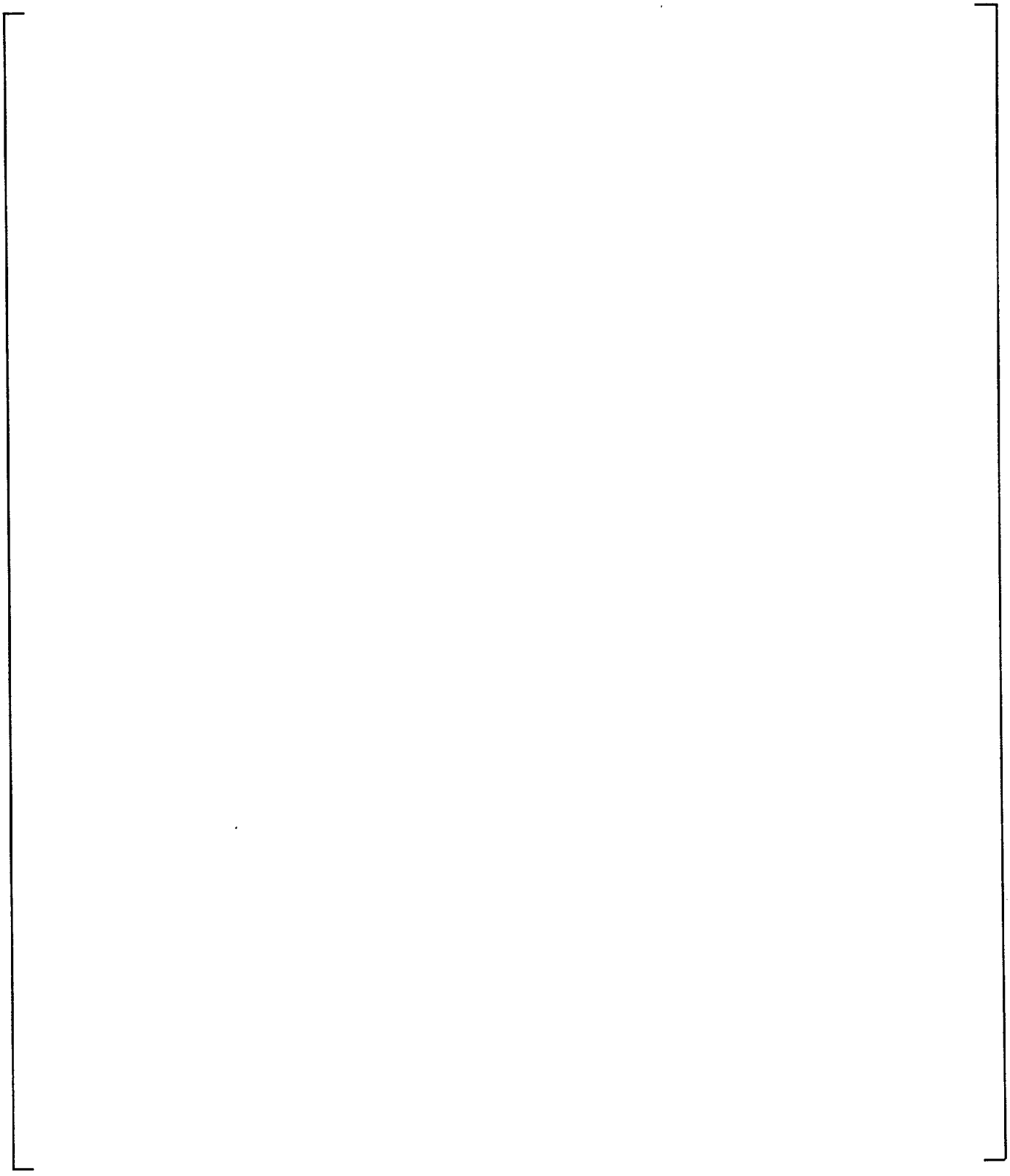

Figure 9-4 **LST with Diffuser Under Steam Generator - Steam Flow 0.11-0.17 lb/sec - Internal Steam Pressure Ratio - Group 1**

(a,b)

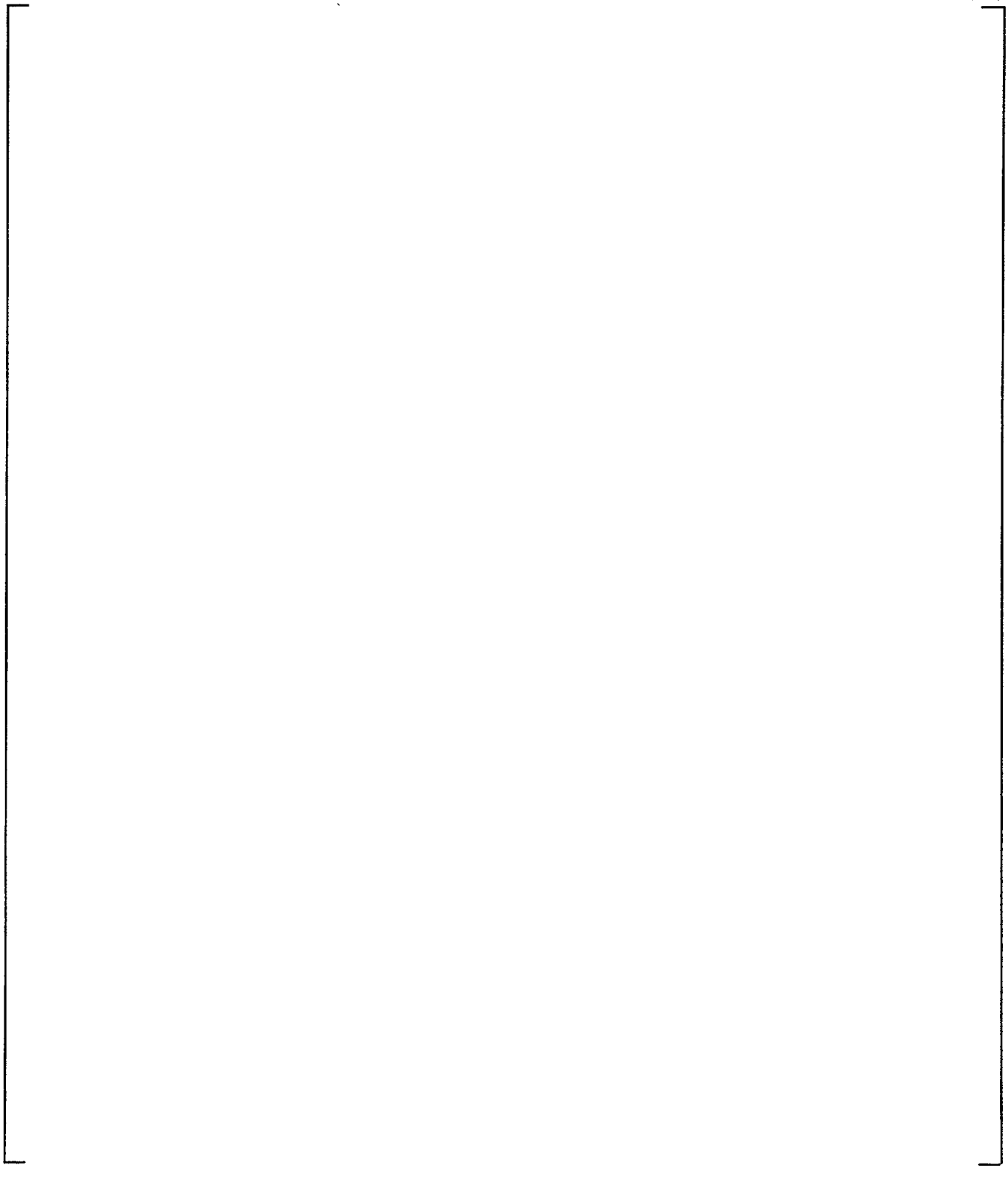

Figure 9-5 LST with Diffuser Under Steam Generator - Steam Flow 0.11-0.17 lb/sec - Internal Fluid Temperature - Group 2

(a,b)

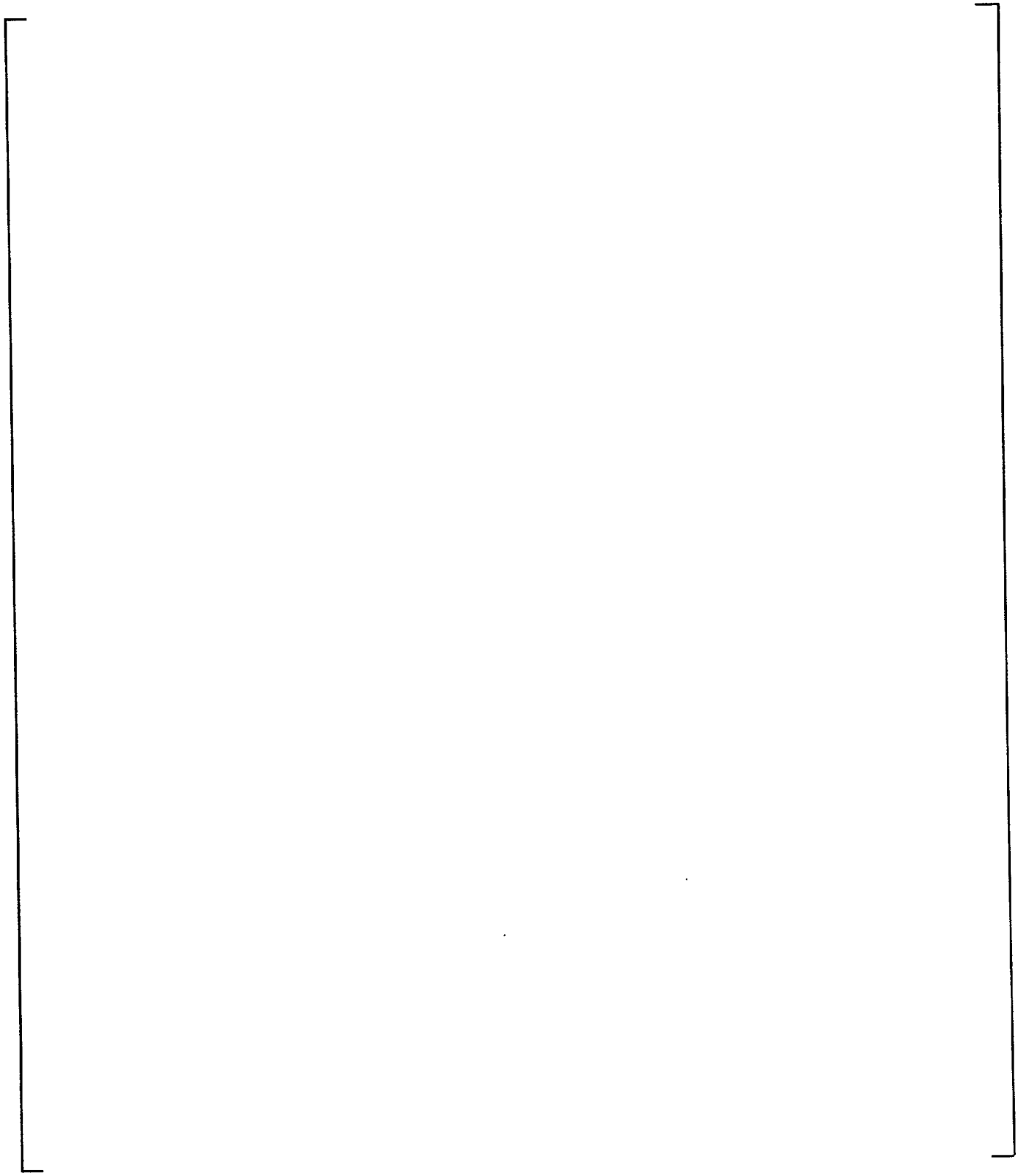

Figure 9-6 **LST with Diffuser Under Steam Generator - Steam Flow 0.11-0.17 lb/sec - Saturation Temperature - Group 2**

(a,b)

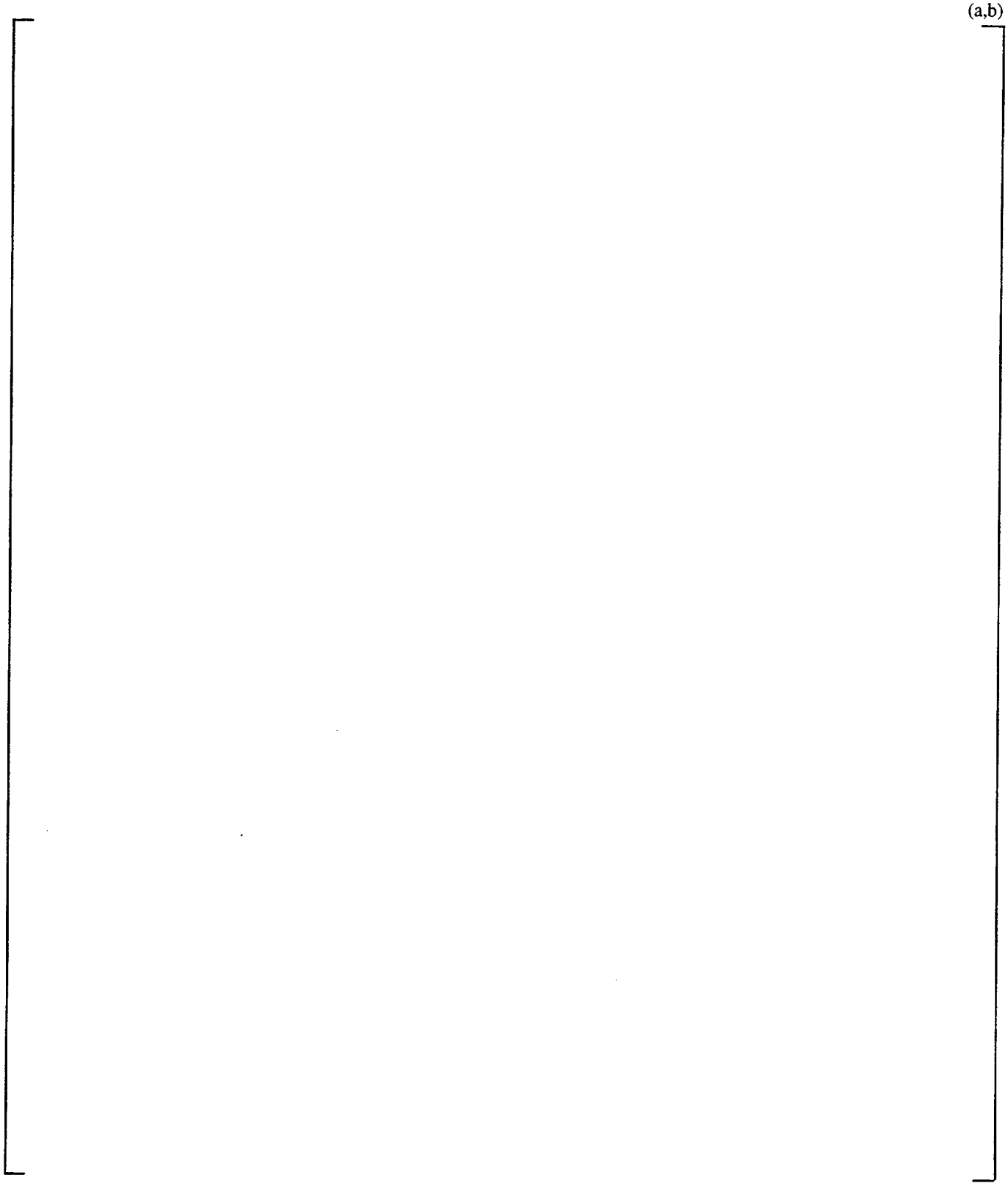

Figure 9-7 **LST with Diffuser Under Steam Generator - Steam Flow 0.11-0.17 lb/sec - Internal Steam Pressure Ratio - Group 2**

(a,b)

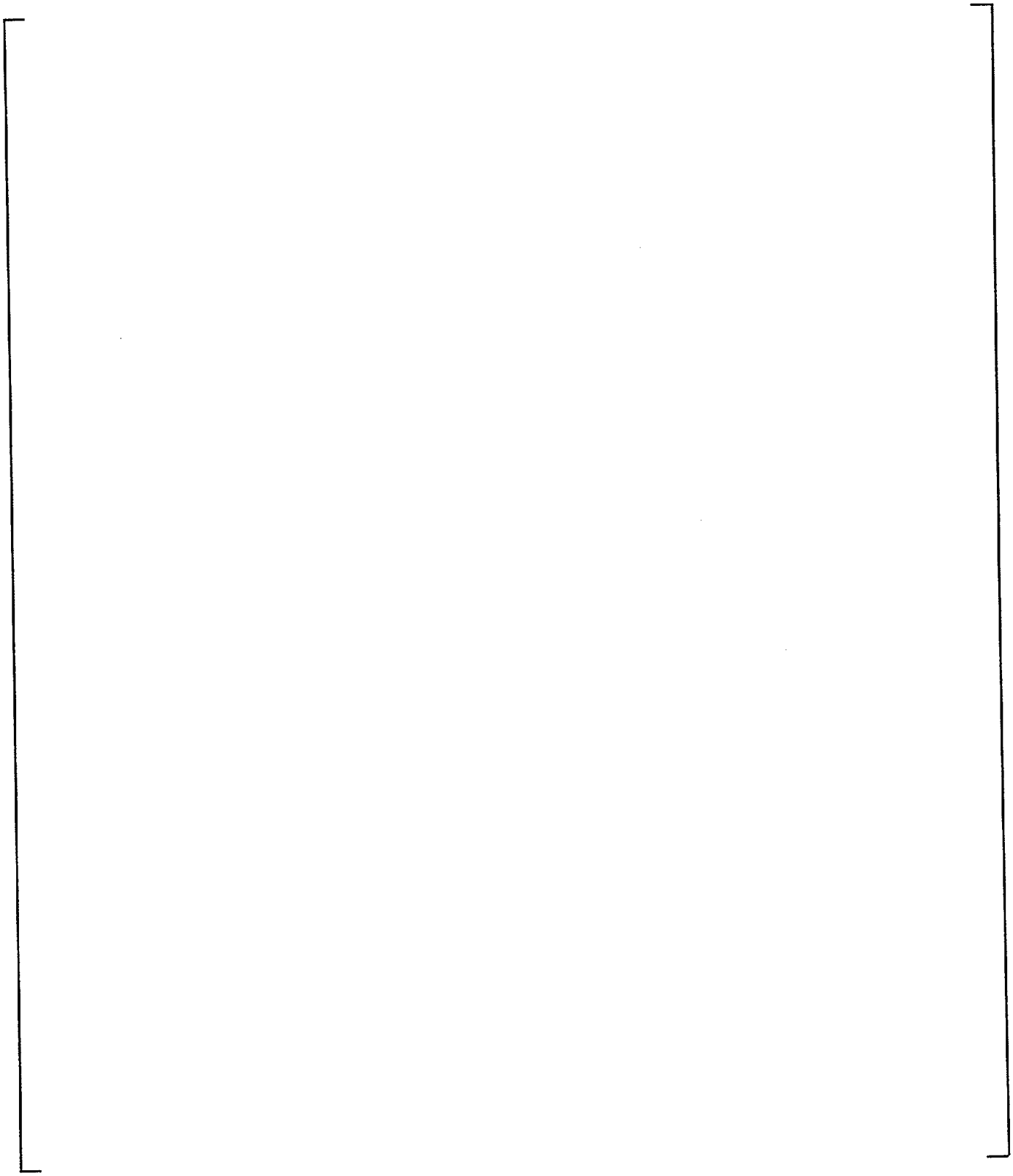

Figure 9-8 **LST with Diffuser Under Steam Generator - Steam Flow 0.27-0.36 lb/sec - Internal Fluid Temperature**

(a,b)

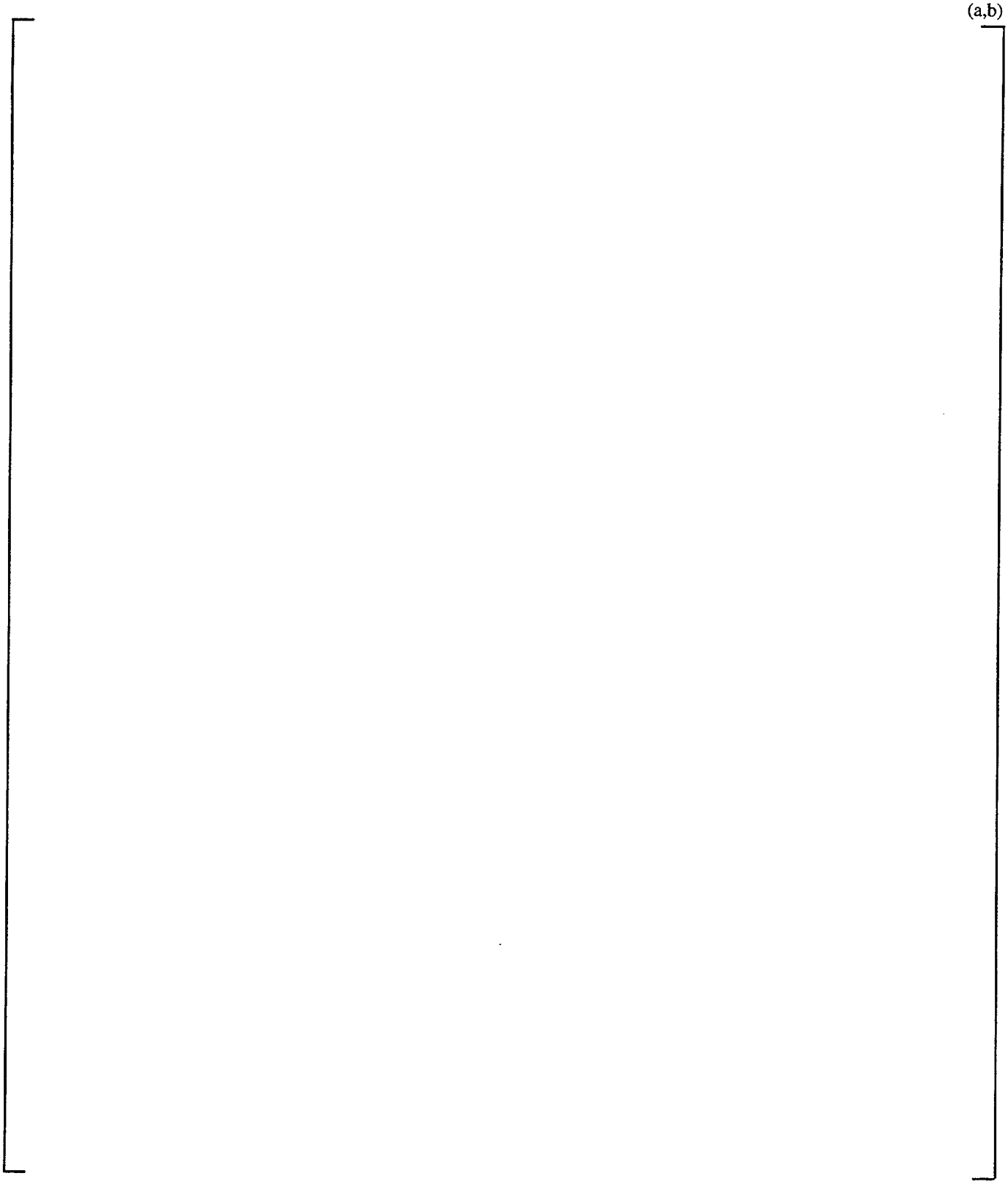

Figure 9-9 **LST with Diffuser Under Steam Generator - Steam Flow 0.27-0.36 lb/sec - Saturation Temperature**

(a,b)

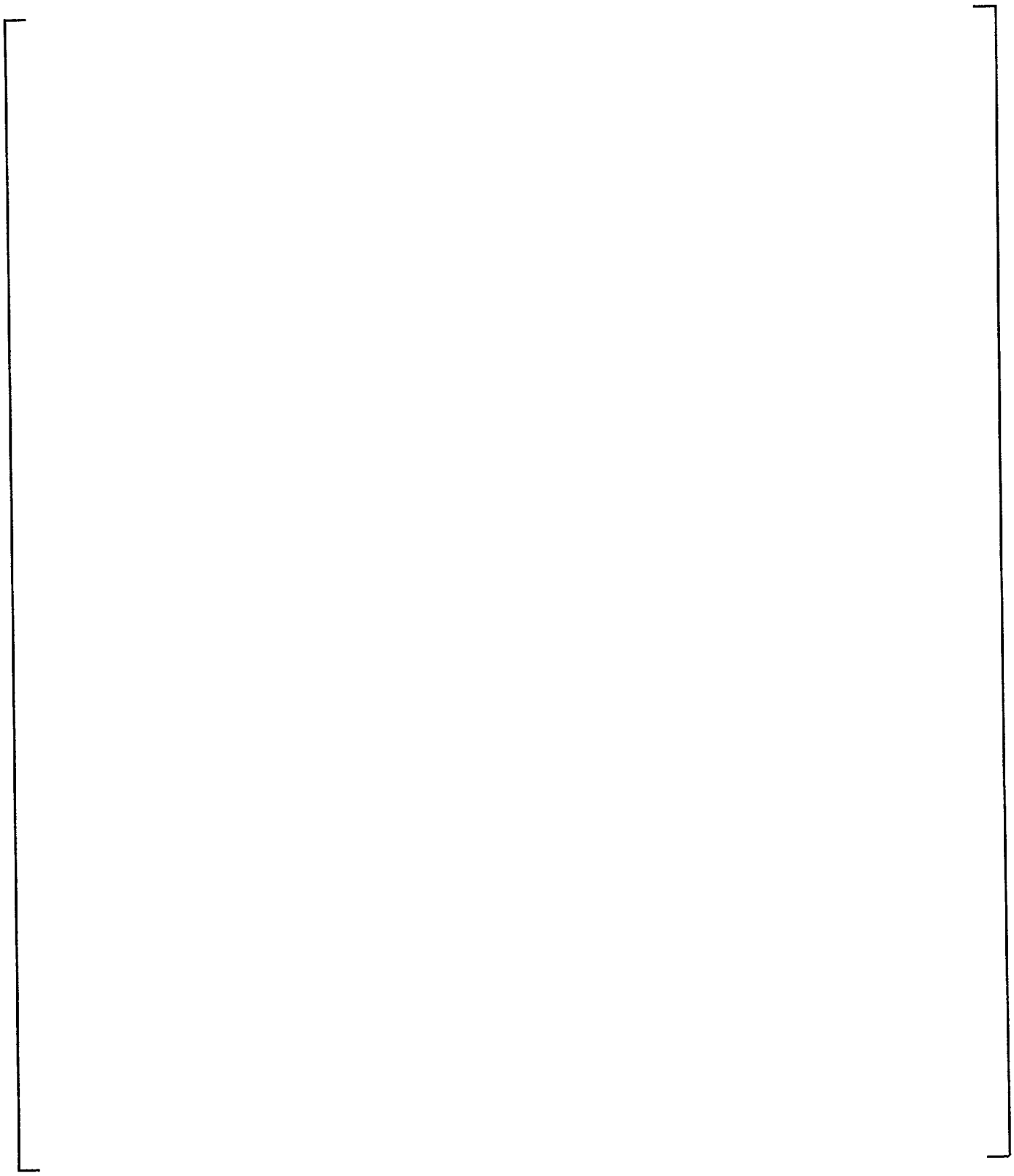

Figure 9-10 **LST with Diffuser Under Steam Generator - Steam Flow 0.27-0.36 lb/sec - Internal Steam Pressure Ratio**

(a,b)

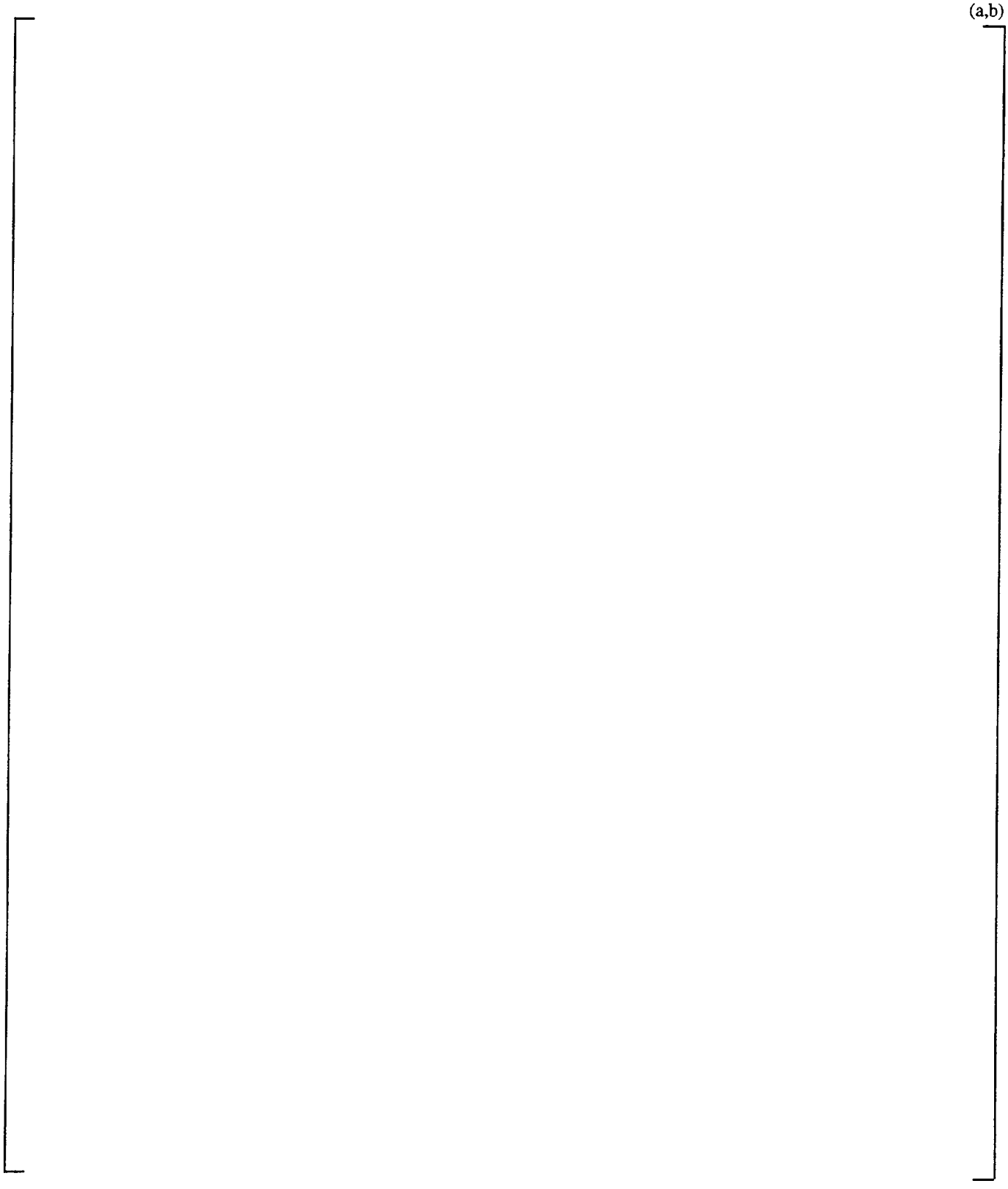

Figure 9-11 **LST with Diffuser Under Steam Generator - Steam Flow 0.49-0.62 lb/sec - Internal Fluid Temperature - Group 1**

(a,b)

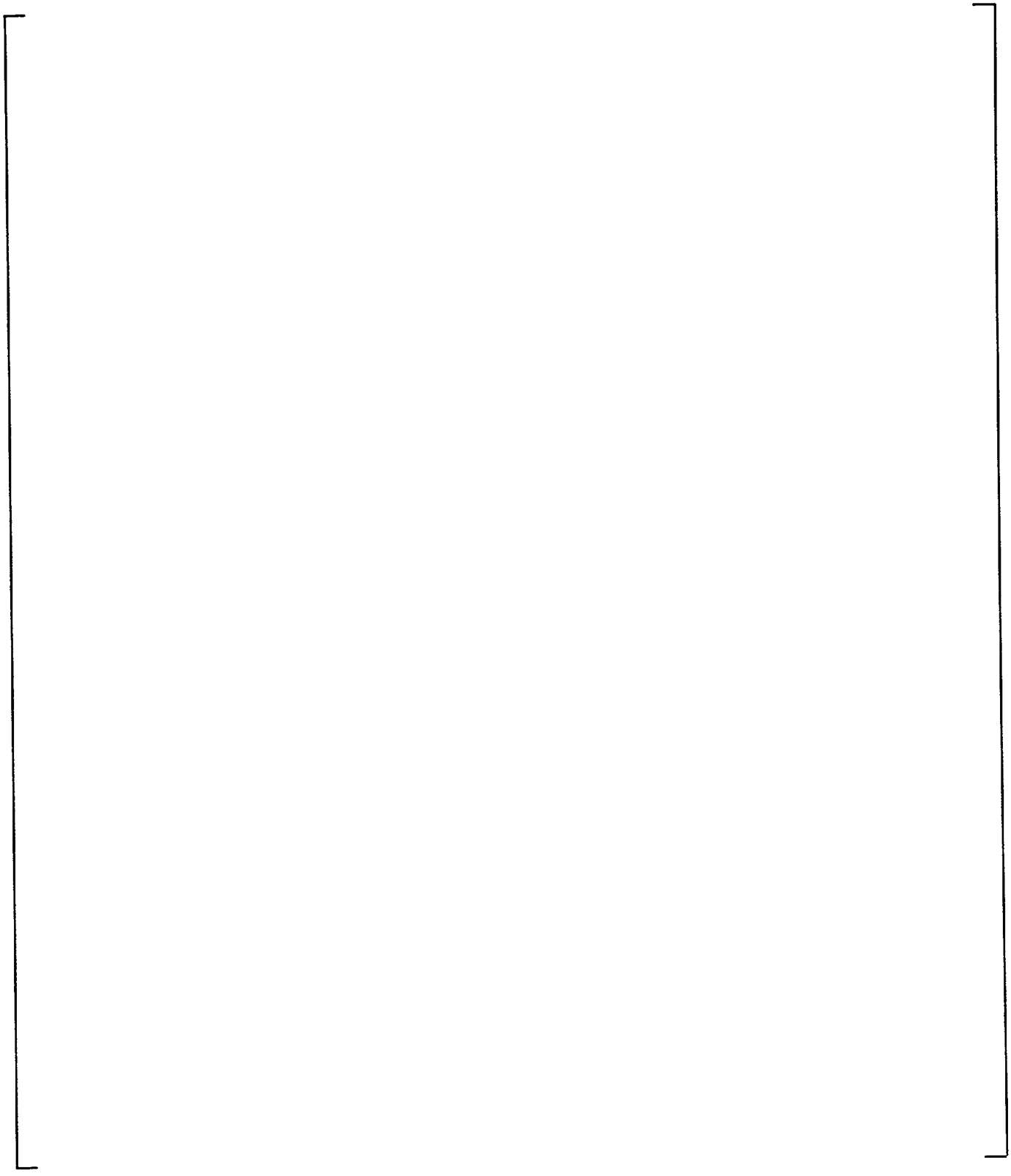

Figure 9-12 LST with Diffuser Under Steam Generator - Steam Flow 0.49-0.26 lb/sec - Saturation Temperature - Group 1

(a,b)

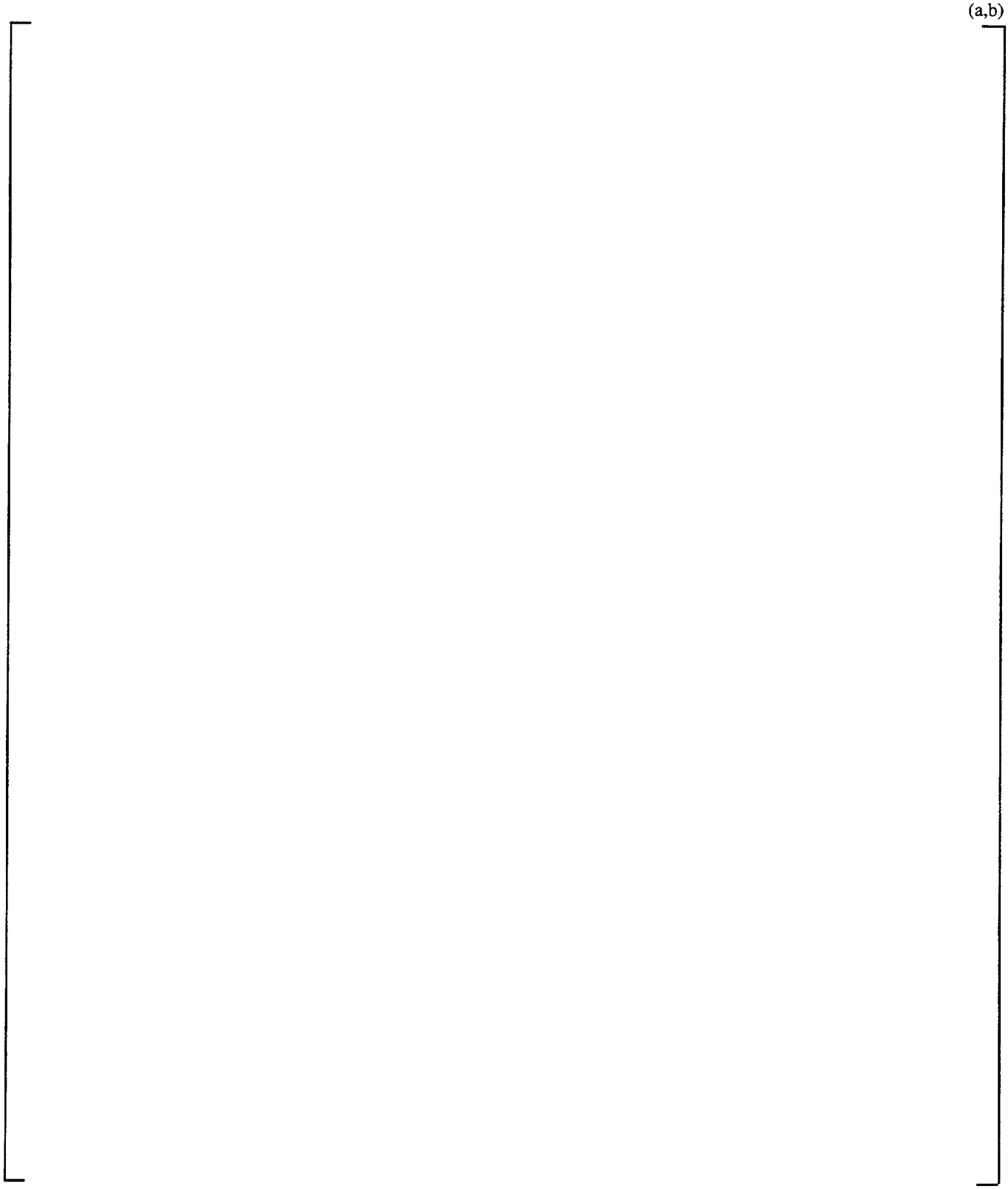

Figure 9-13 LST with Diffuser Under Steam Generator - Steam Flow 0.49-0.62 lb/sec - Internal Steam Pressure Ratio - Group 1

(a,b)

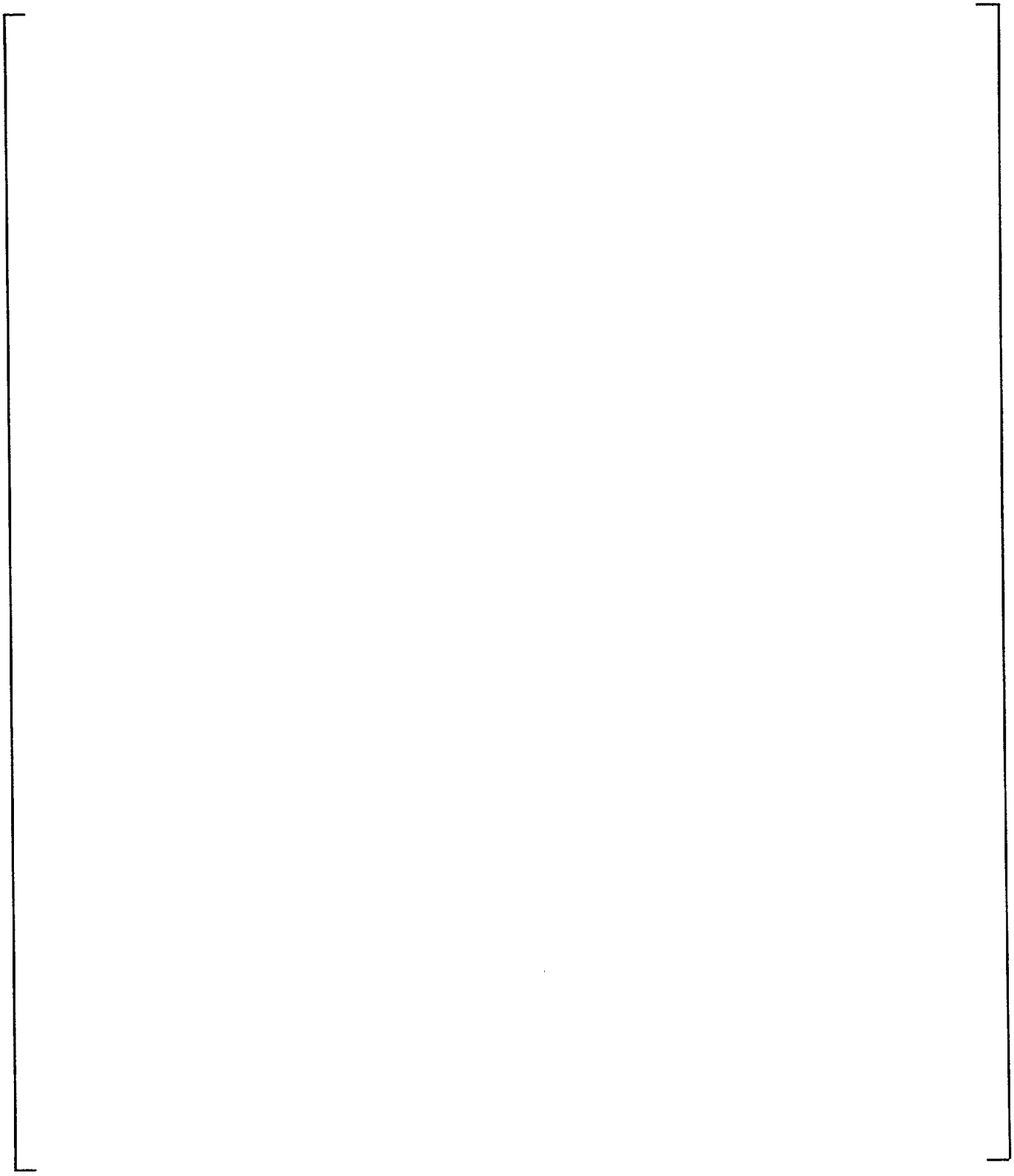

Figure 9-14 **LST with Diffuser Under Steam Generator - Steam Flow 0.49-0.62 lb/sec - Internal Fluid Temperature - Group 2**

(a,b)

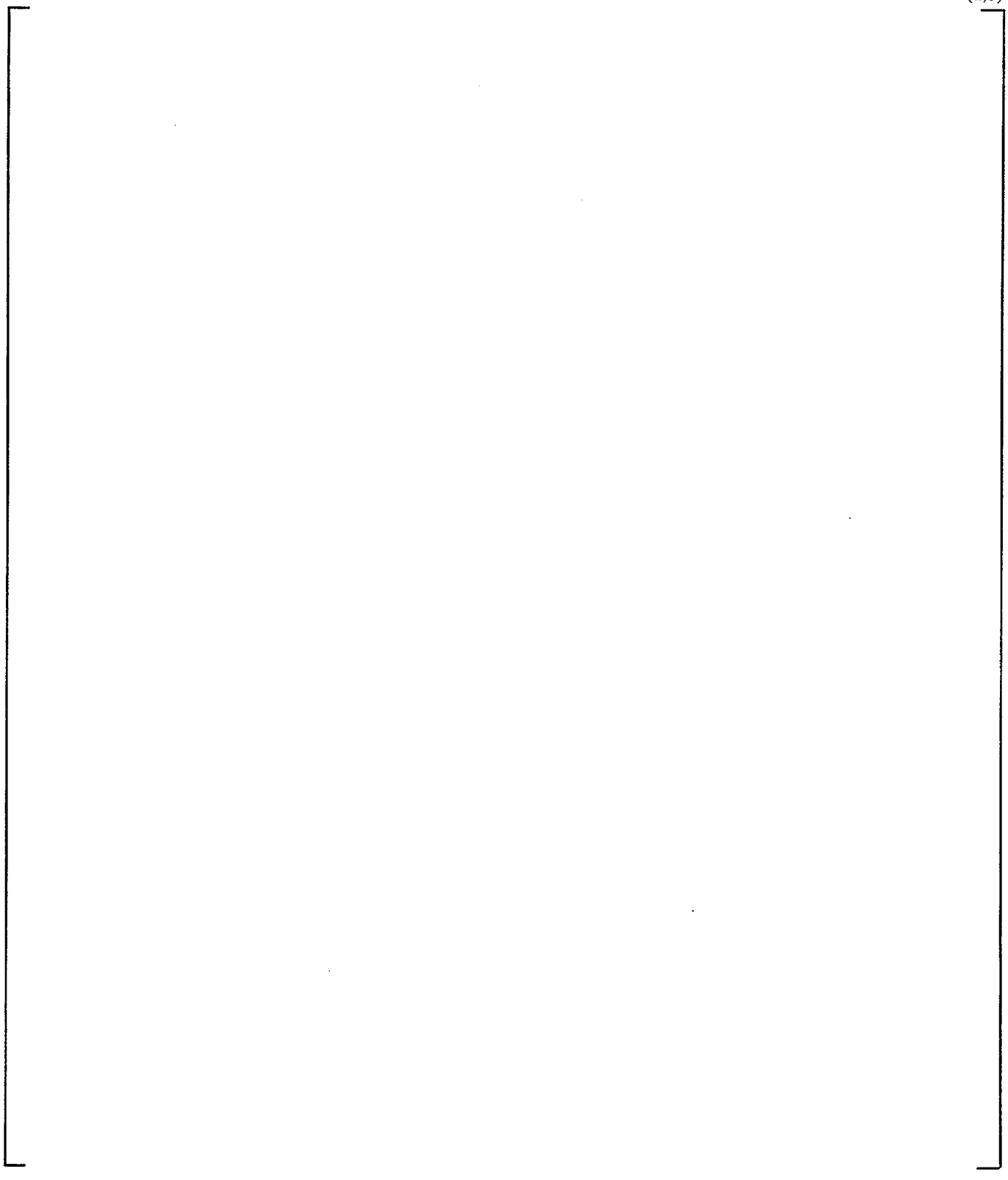

Figure 9-15 LST with Diffuser Under Steam Generator - Steam Flow 0.49-0.62 lb/sec - Saturation Temperature - Group 2

(a,b)

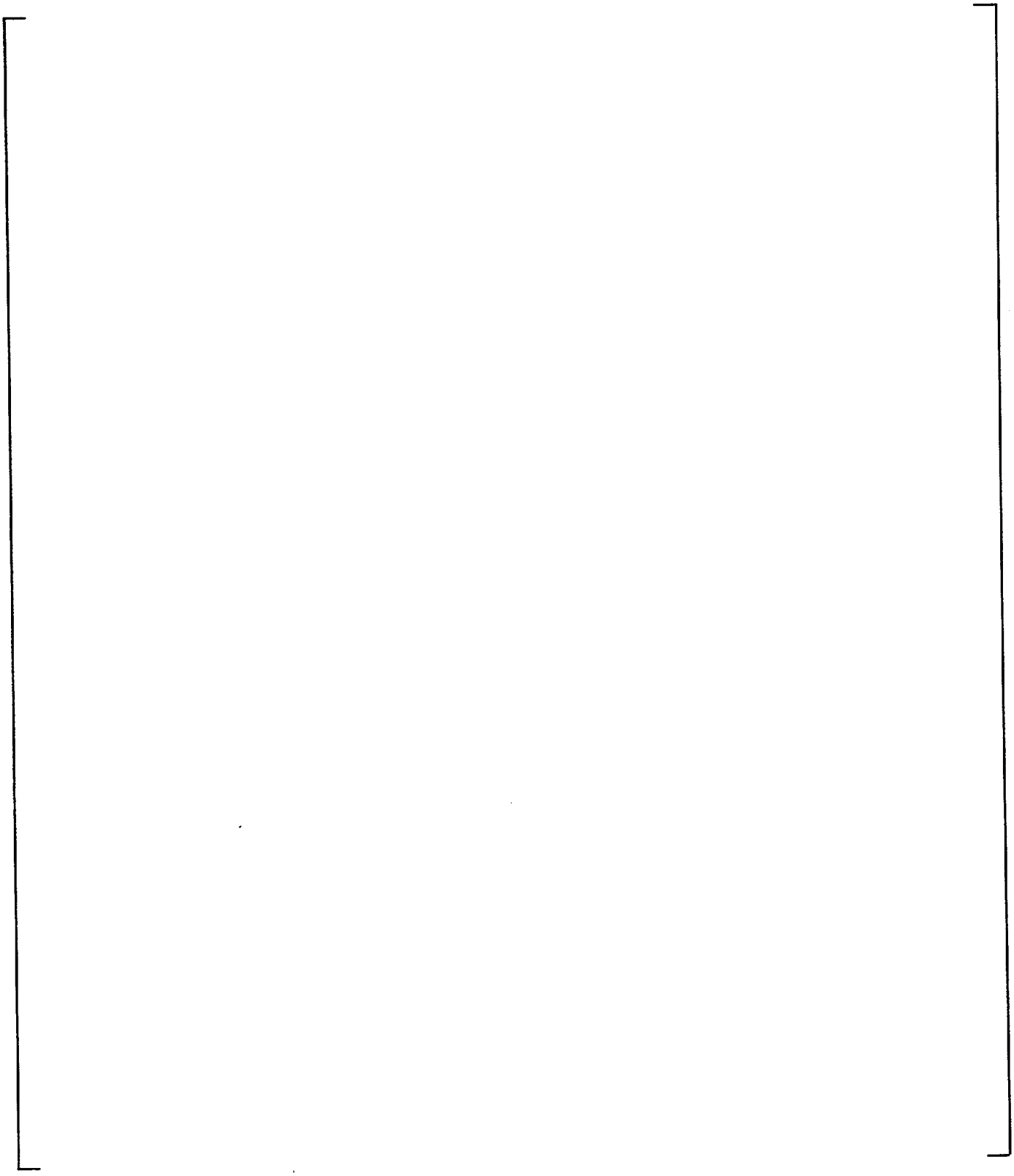

Figure 9-16 **LST with Diffuser Under Steam Generator - Steam Flow 0.49-0.62 lb/sec - Internal Steam Pressure Ratio - Group 2**

(a,b)

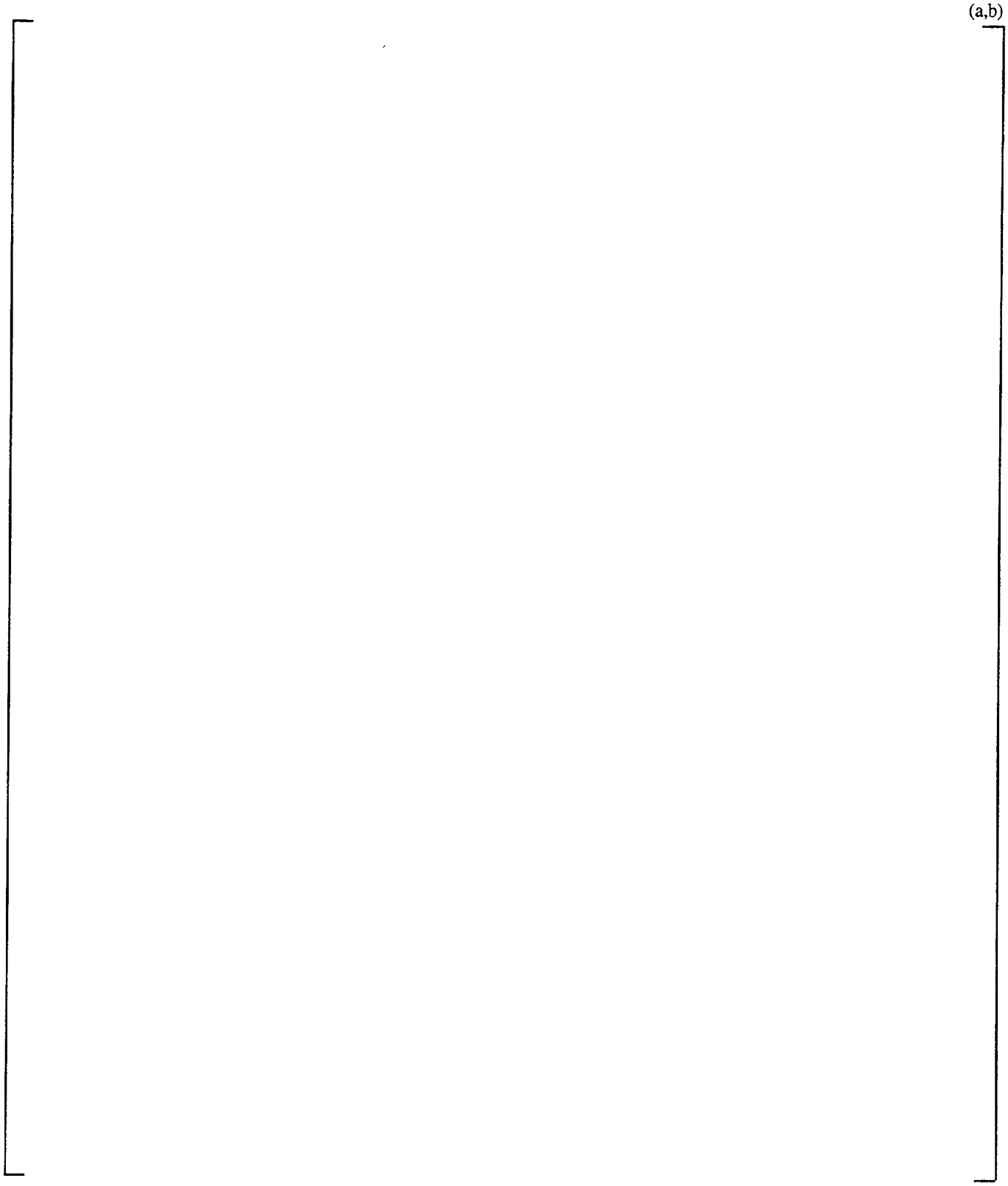

Figure 9-17 LST with Diffuser Under Steam Generator - Steam Flow 0.76-0.84 lb/sec - Internal Fluid Temperature

(a,b)

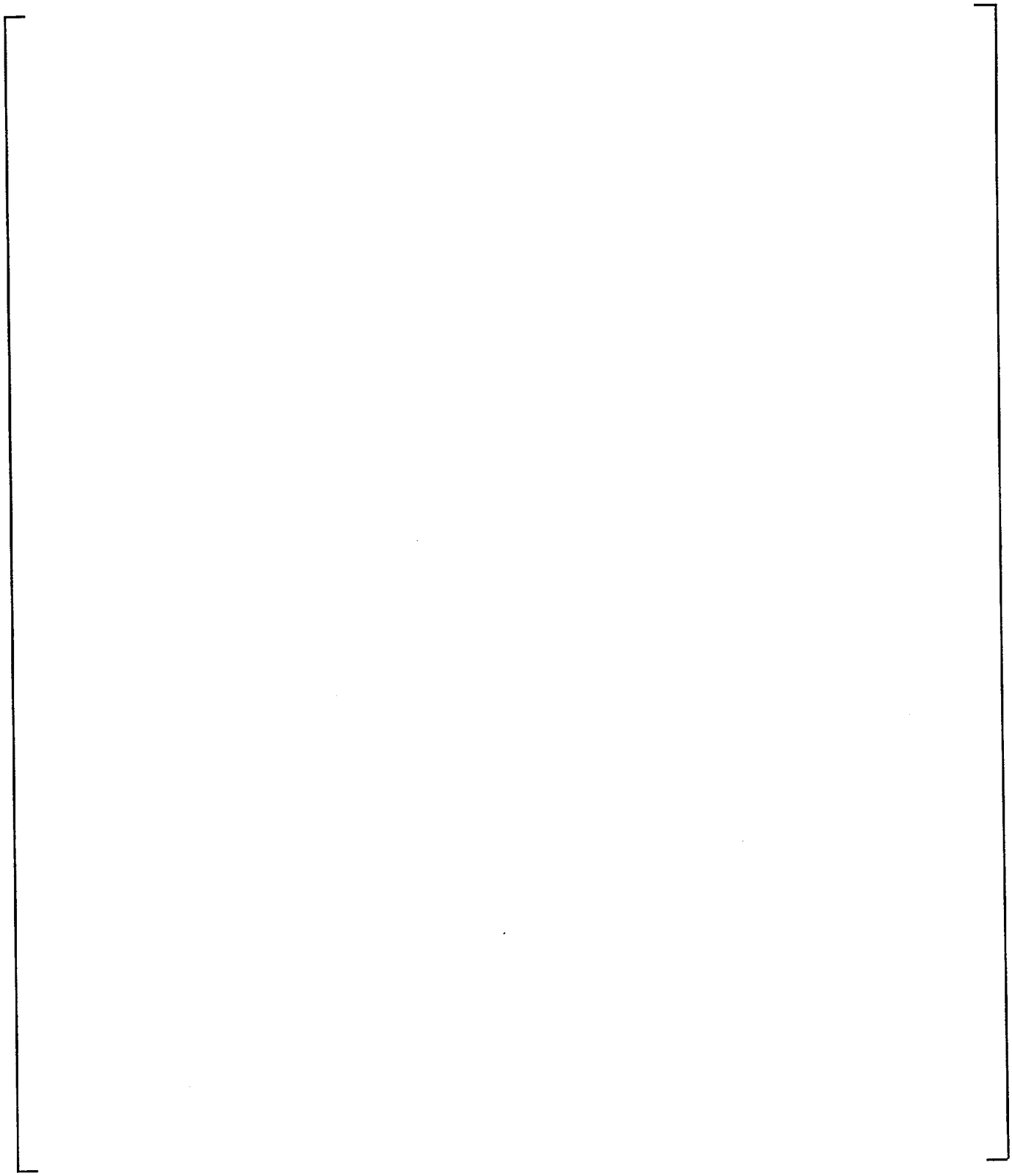

Figure 9-18 **LST with Diffuser Under Steam Generator - Steam Flow 0.76-0.84 lb/sec - Saturation Temperature**

(a,b)

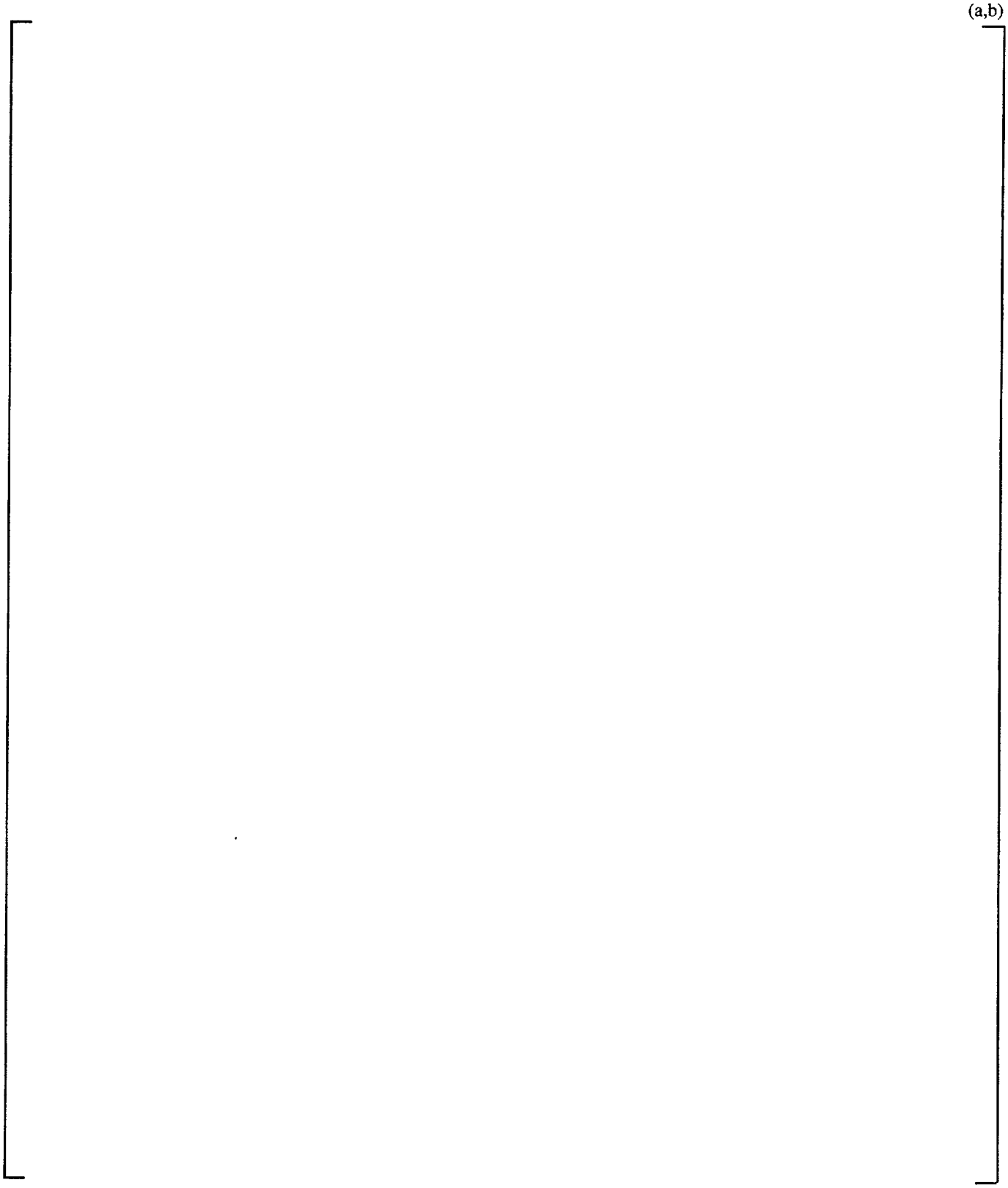

Figure 9-19 LST with Diffuser Under Steam Generator - Steam Flow 0.76-0.84 lb/sec - Internal Steam Pressure Ratio

(a,b)

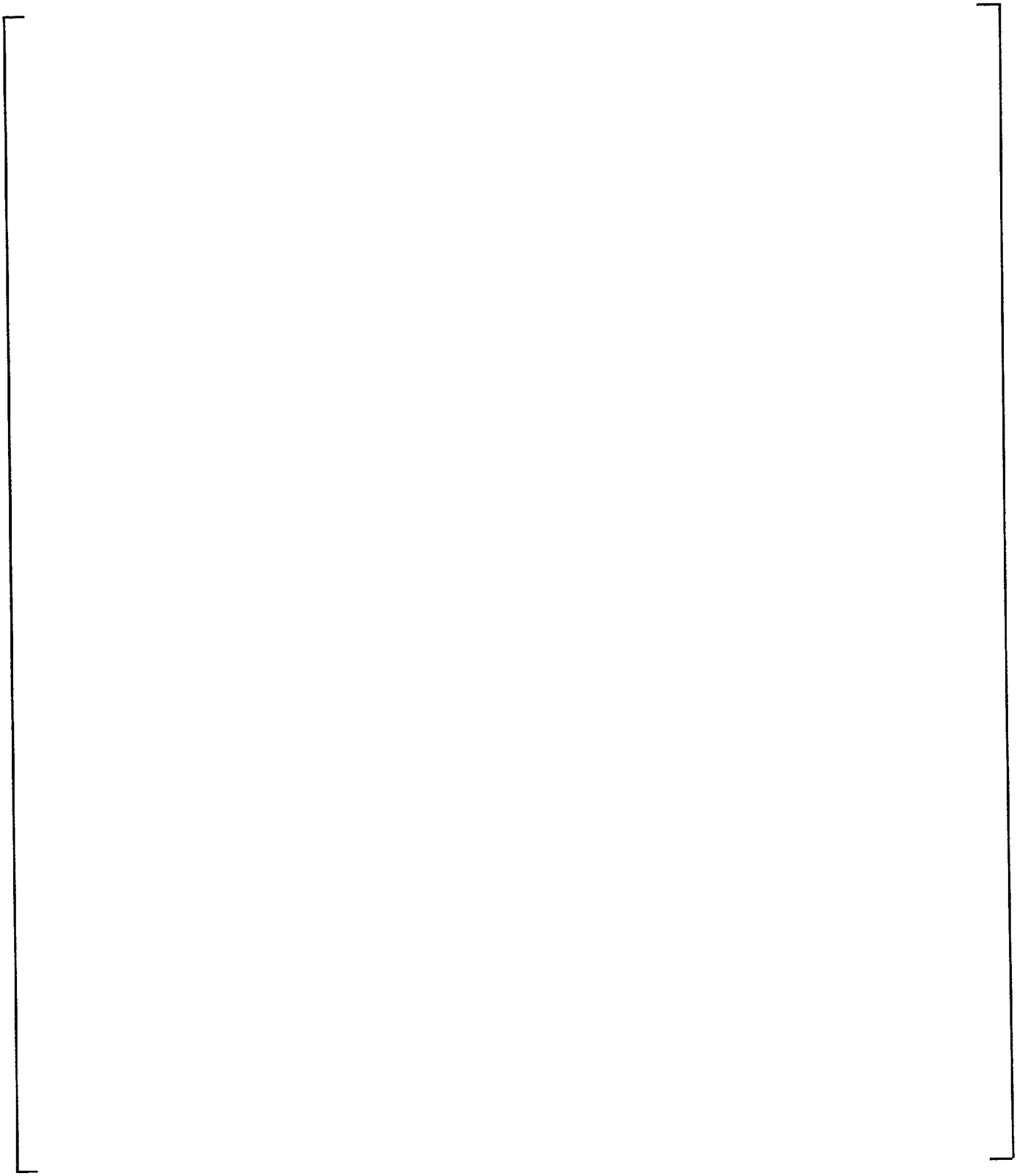

Figure 9-20 LST with Diffuser Under Steam Generator - Steam Flow 1.10-1.20 lb/sec - Internal Fluid Temperature

(a,b)

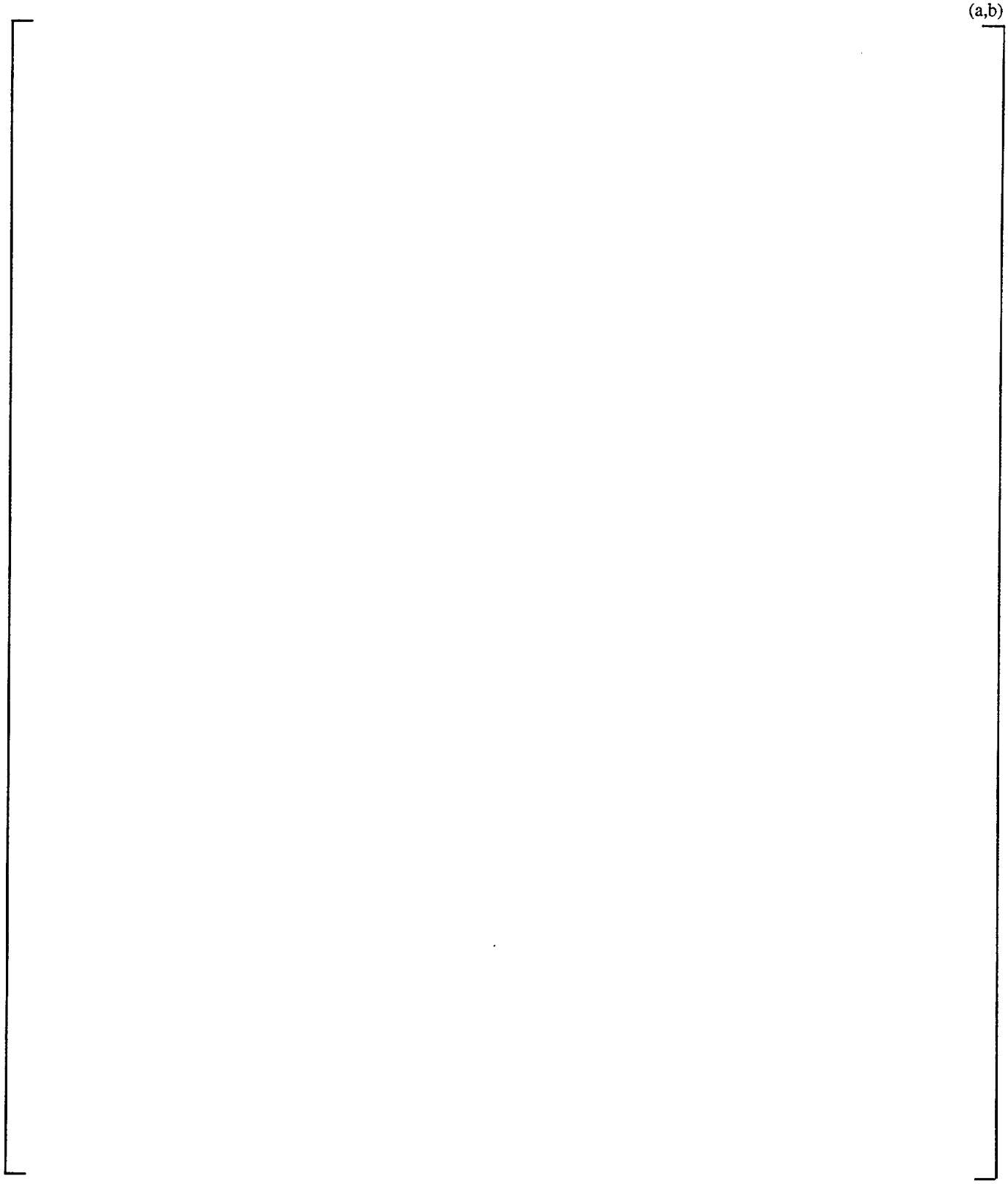

Figure 9-21 LST with Diffuser Under Steam Generator - Steam Flow 1.10-1.20 lb/sec - Saturation Temperature

(a,b)

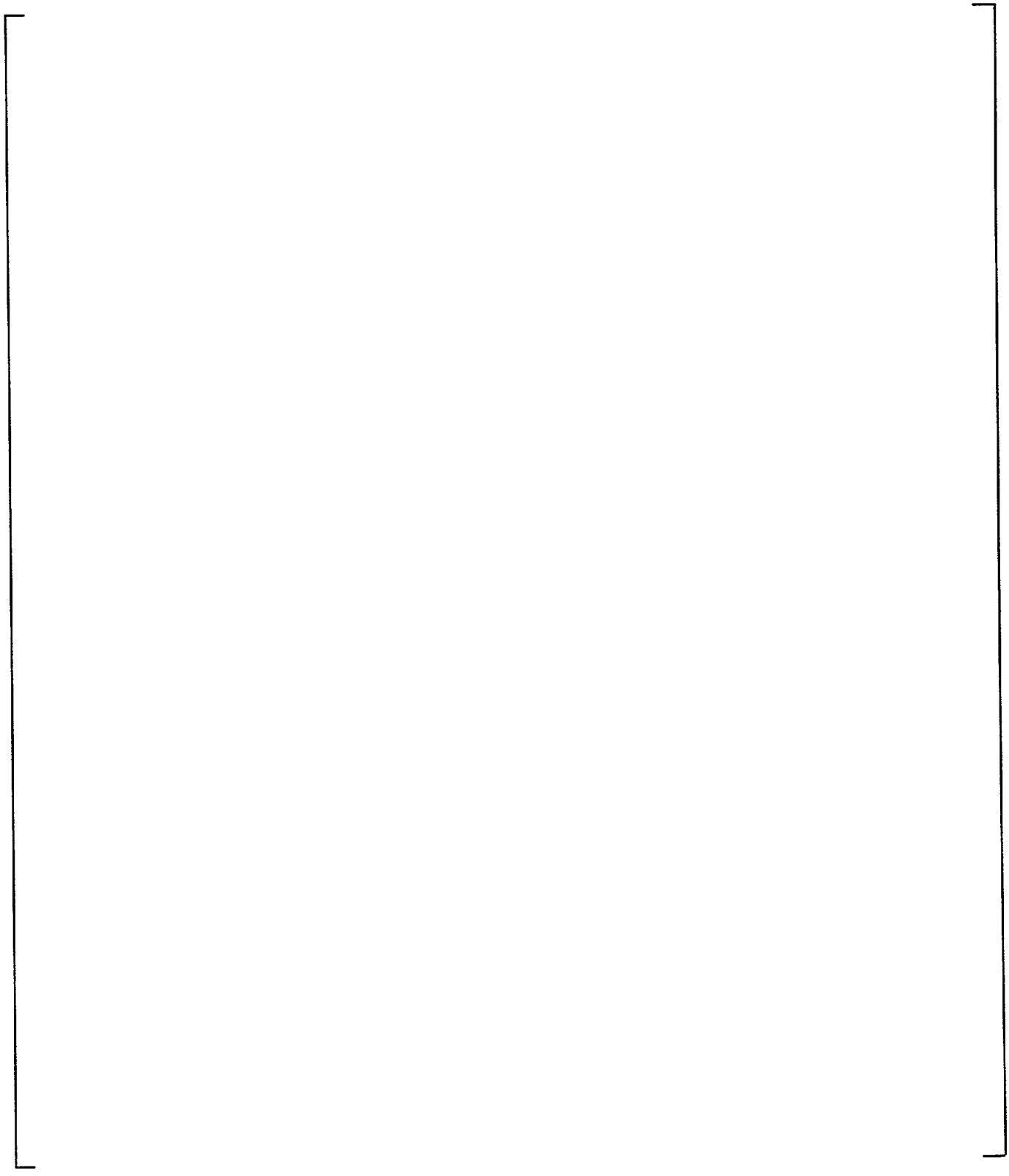

Figure 9-22 **LST with Diffuser Under Steam Generator - Steam Flow 1.10-1.20 lb/sec - Internal Steam Pressure Ratio**

(a,b)

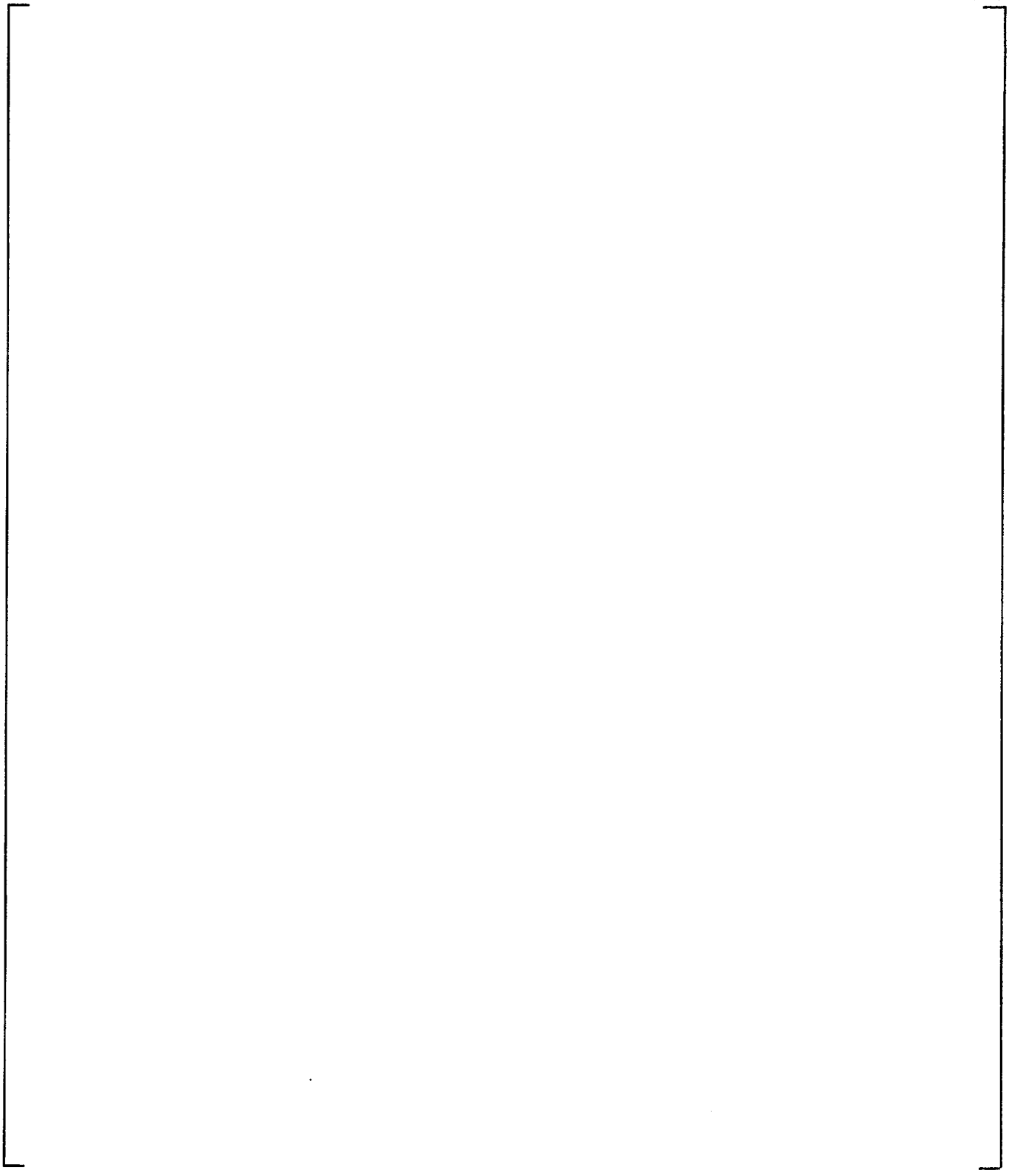

Figure 9-23 LST with Diffuser Under Steam Generator - Steam Flow 1.54-1.68 lb/sec - Internal Fluid Temperature

(a,b)

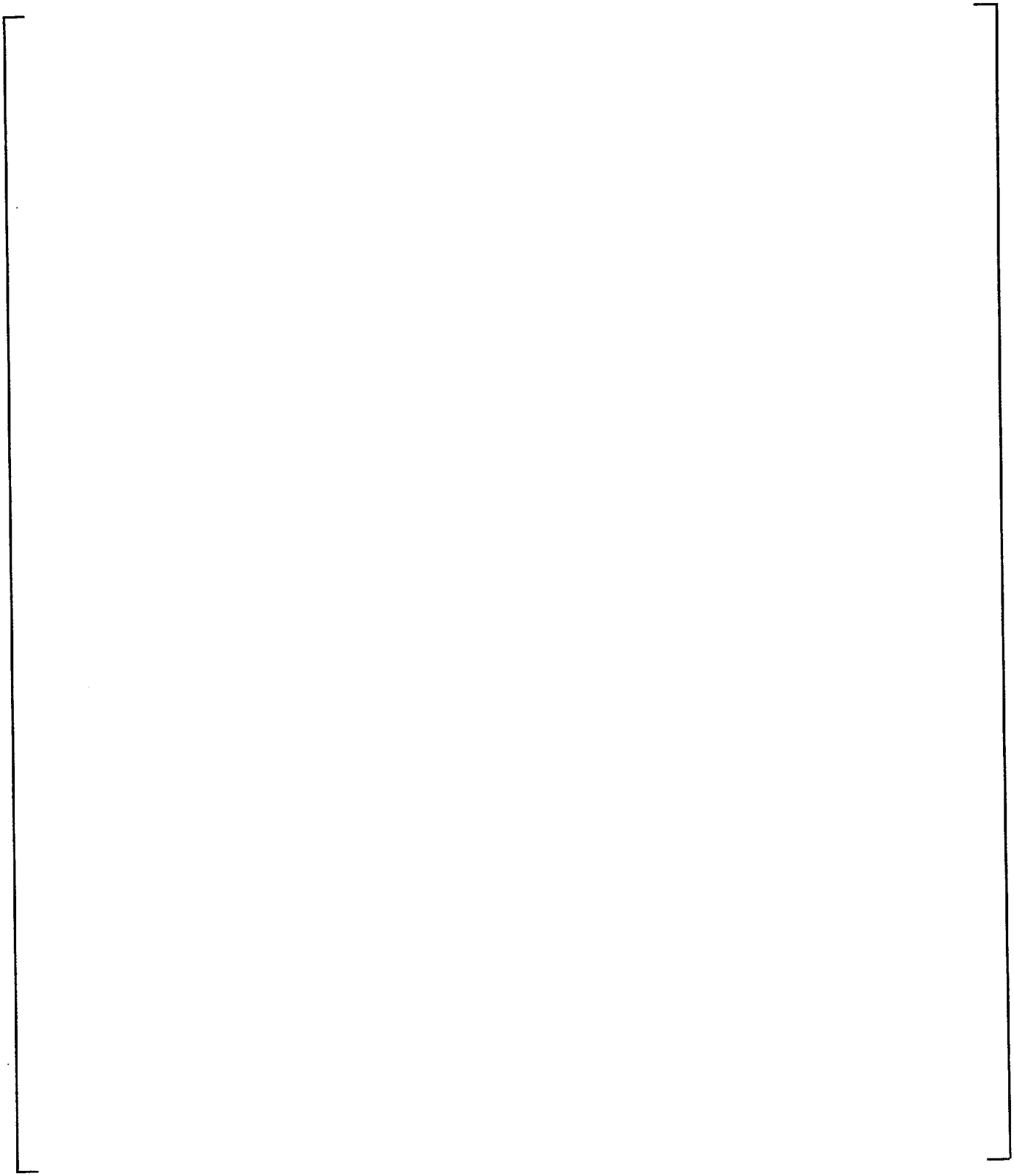

Figure 9-24 **LST with Diffuser Under Steam Generator - Steam Flow 1.54-1.68 lb/sec - Saturation Temperature**

(a,b)

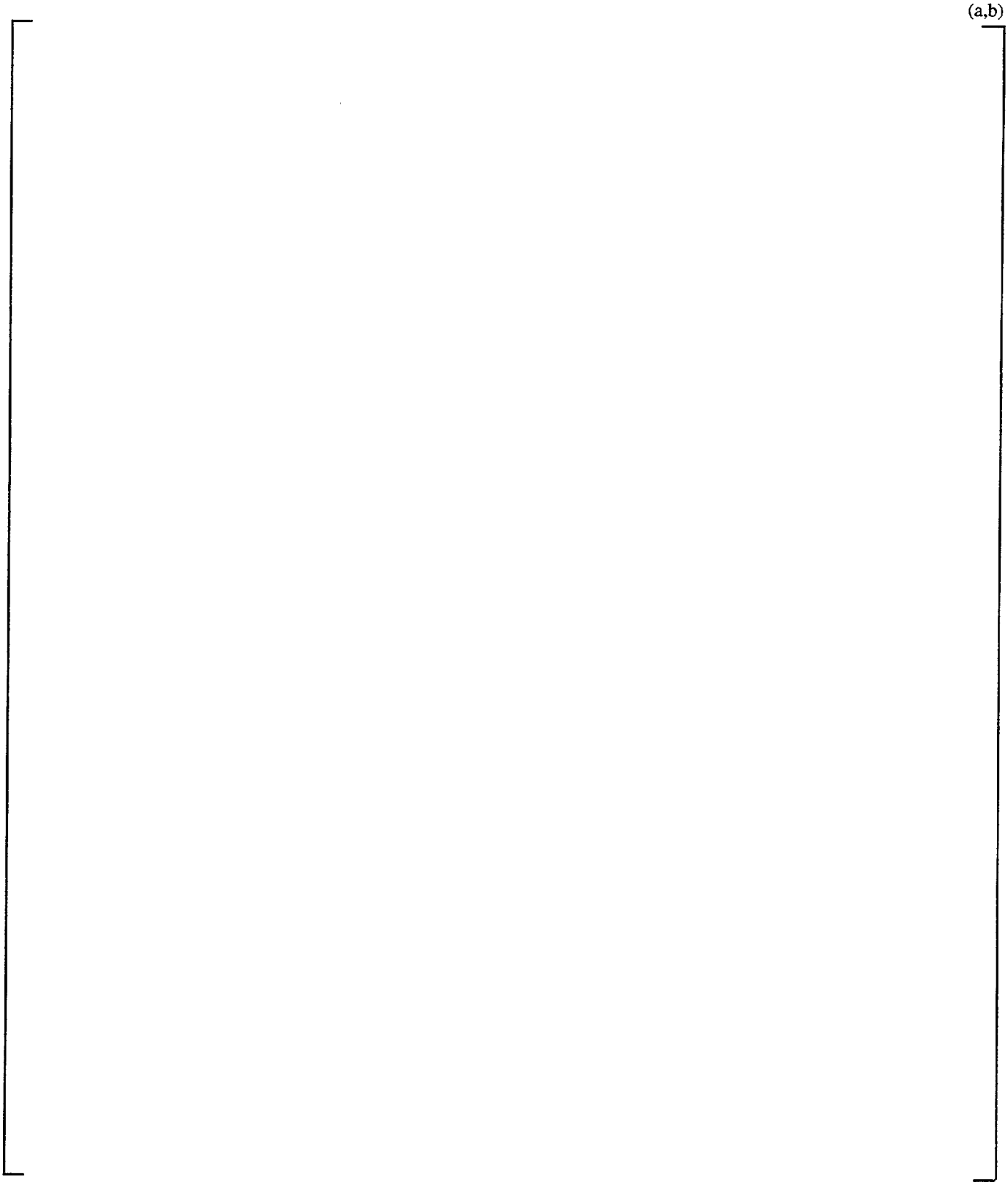

Figure 9-25 LST with Diffuser Under Steam Generator - Steam Flow 1.54-1.68 lb/sec - Internal Steam Pressure Ratio

(a,b)

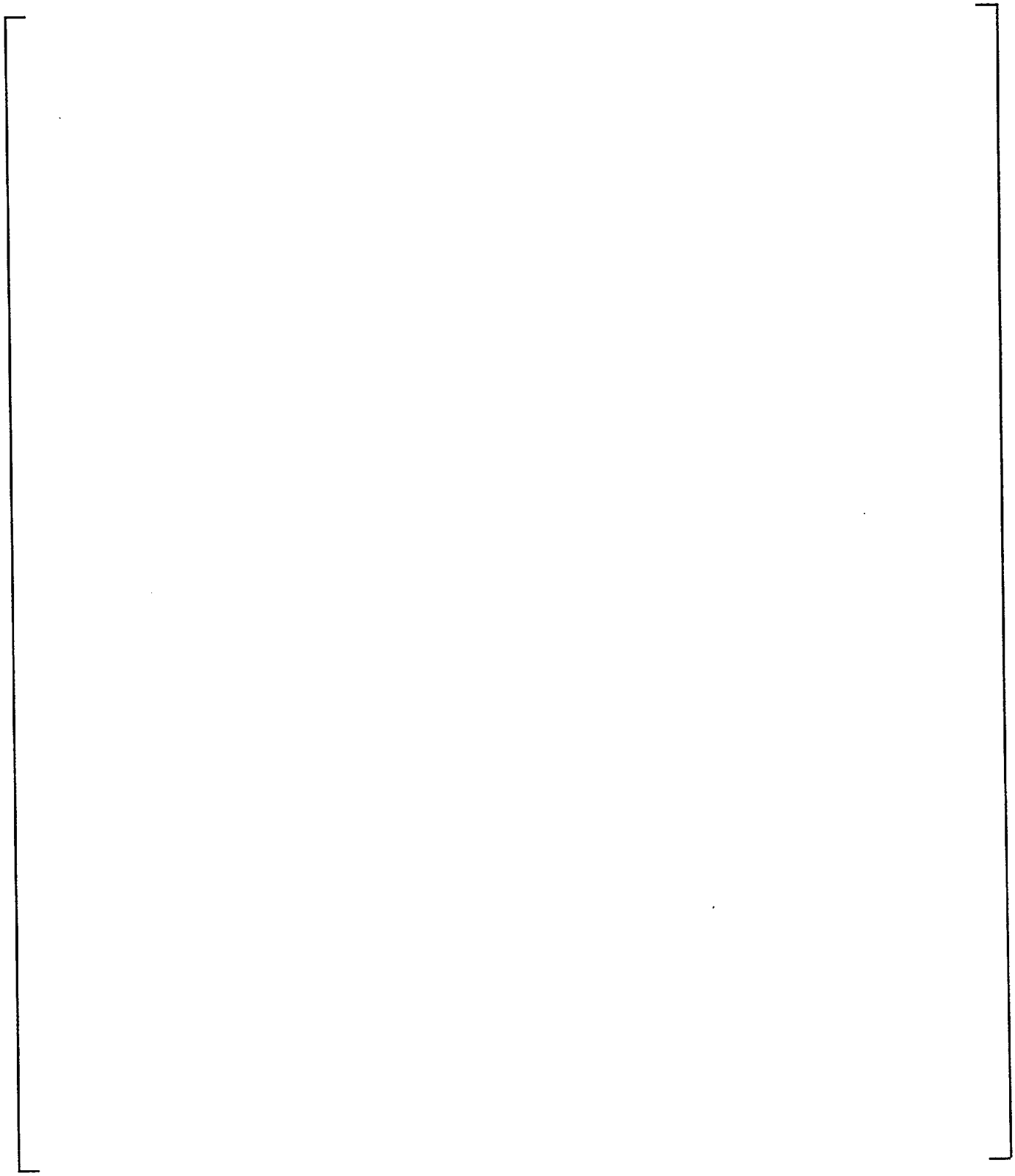

Figure 9-26 **LST with Diffuser Up 6 Feet - Steam Flow 0.76 & 1.68 lb/sec - Internal Fluid Temperature**

(a,b)

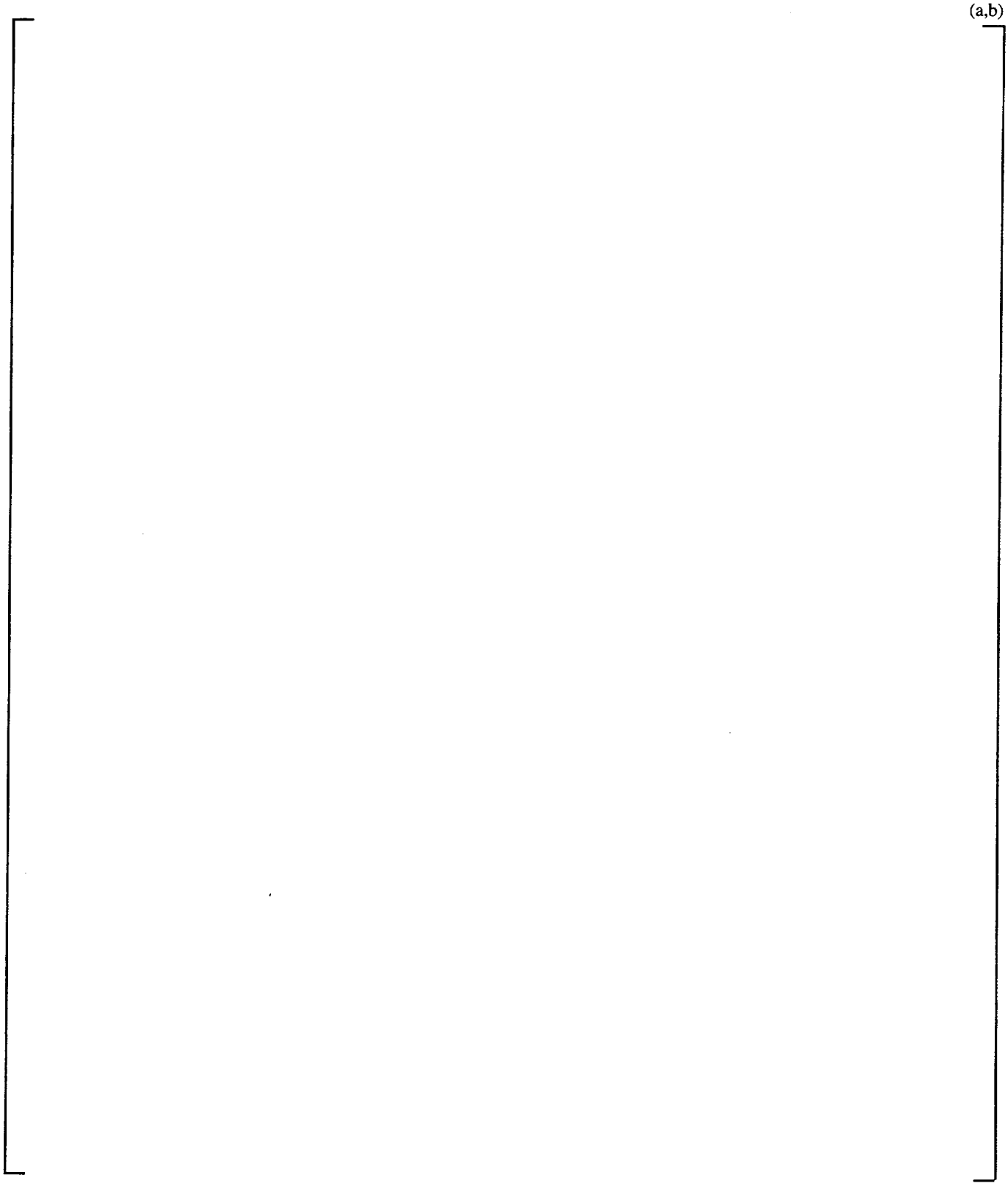

Figure 9-27 LST with Diffuser Up 6 Feet - Steam Flow 0.76 & 1.68 lb/sec - Saturation Temperature

(a,b)

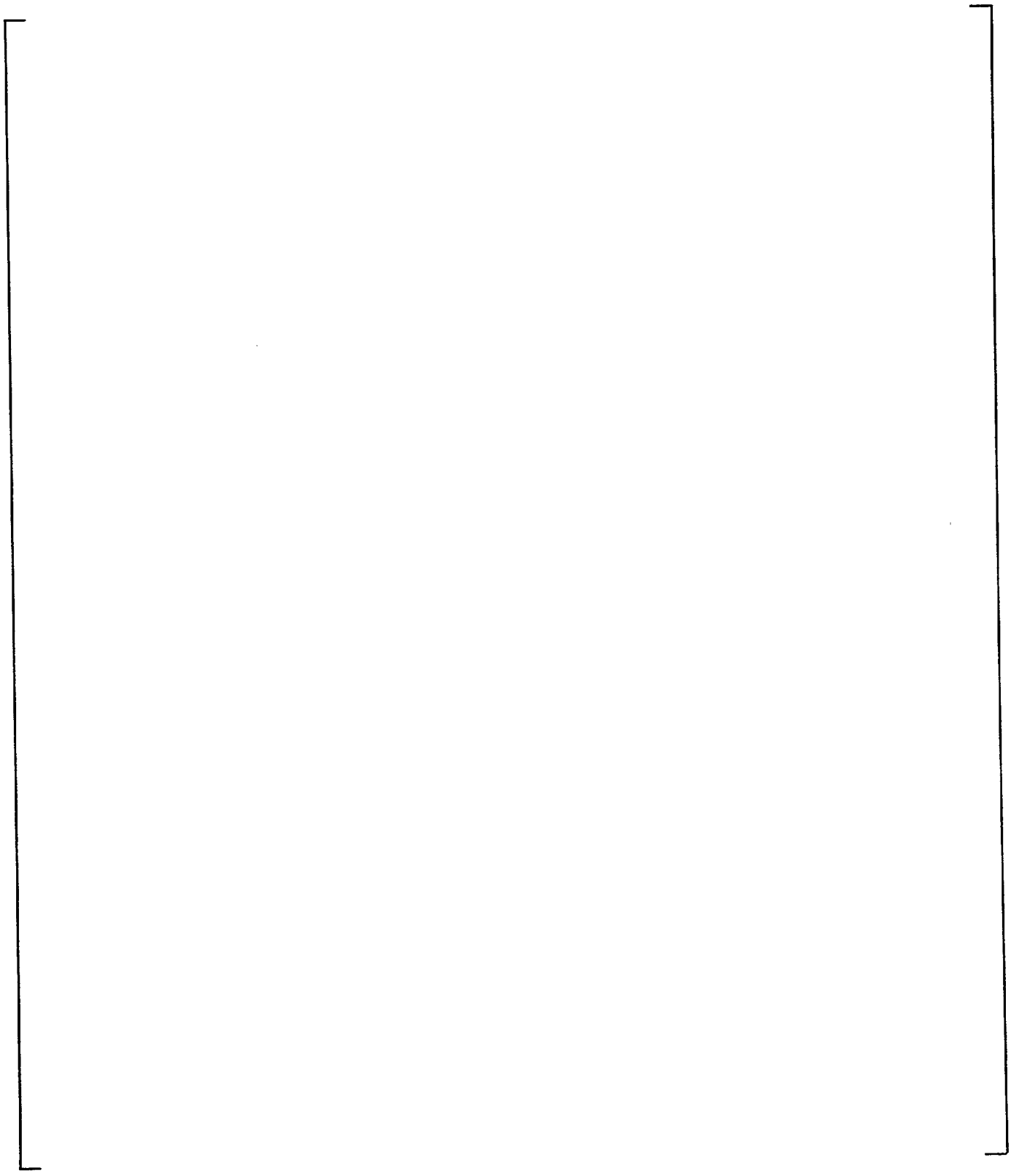

Figure 9-28 **LST with Diffuser Up 6 Feet - Steam Flow 0.76 & 1.68 lb/sec - Internal Steam Pressure Ratio**

(a,b)

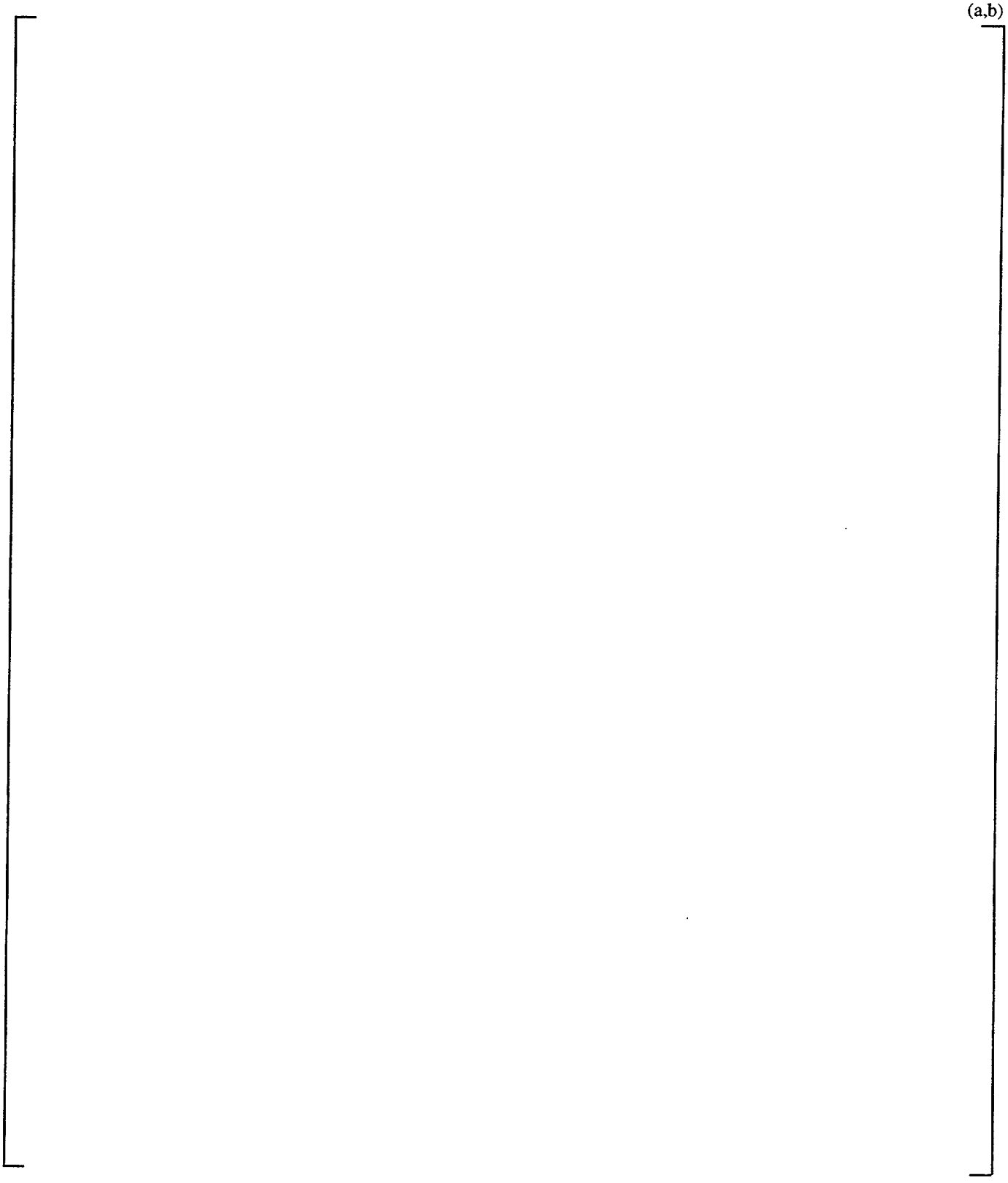

Figure 9-29 **LST with Steam Injection: 3 Inch Pipe - Steam Flow 0.76 - 0.95 lb/sec - Internal Fluid Temperature**

(a,b)

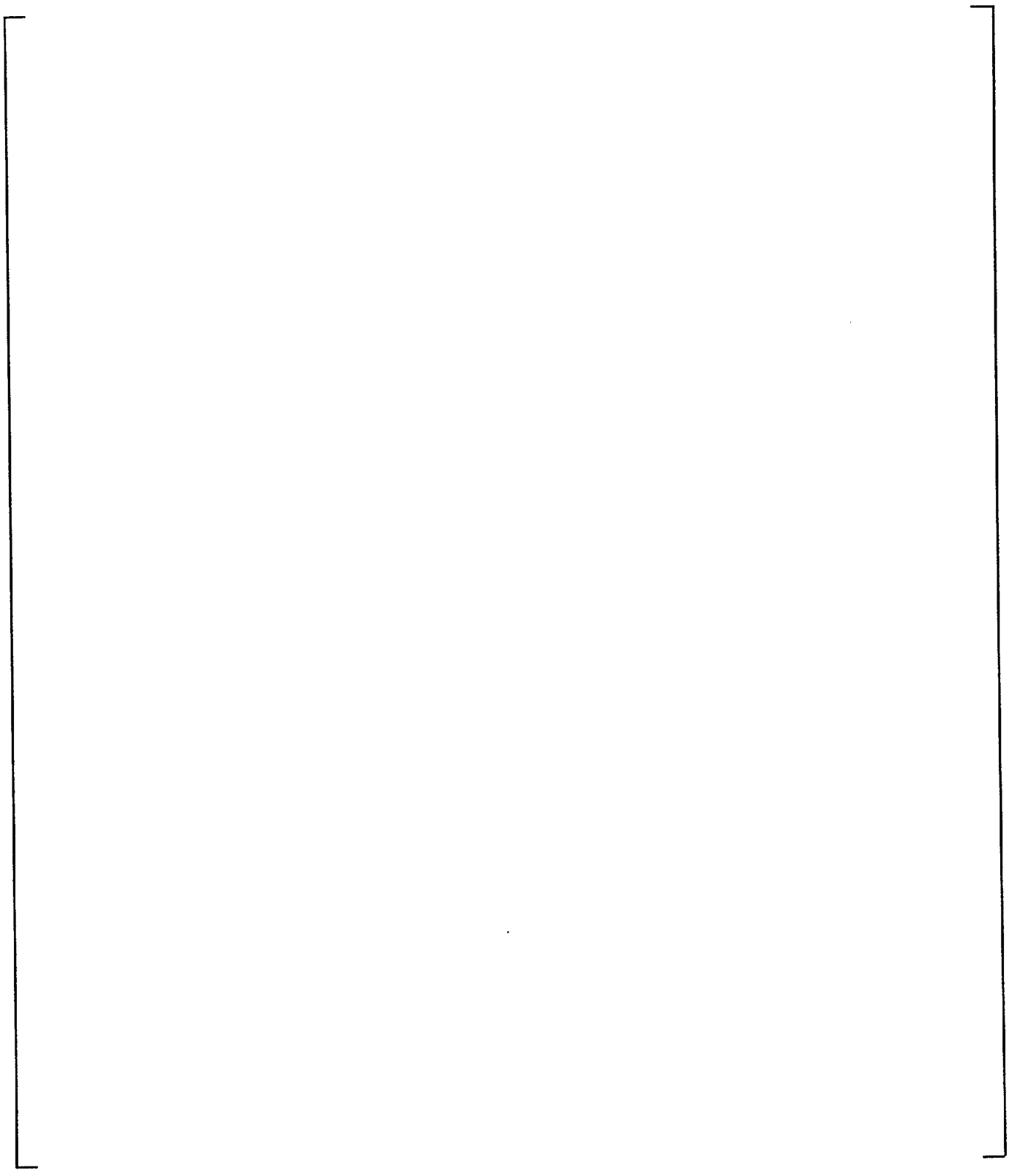

Figure 9-30 **LST with Steam Injection: 3 Inch Pipe - Steam Flow 0.76 - 0.95 lb/sec - Saturation Temperature**

(a,b)

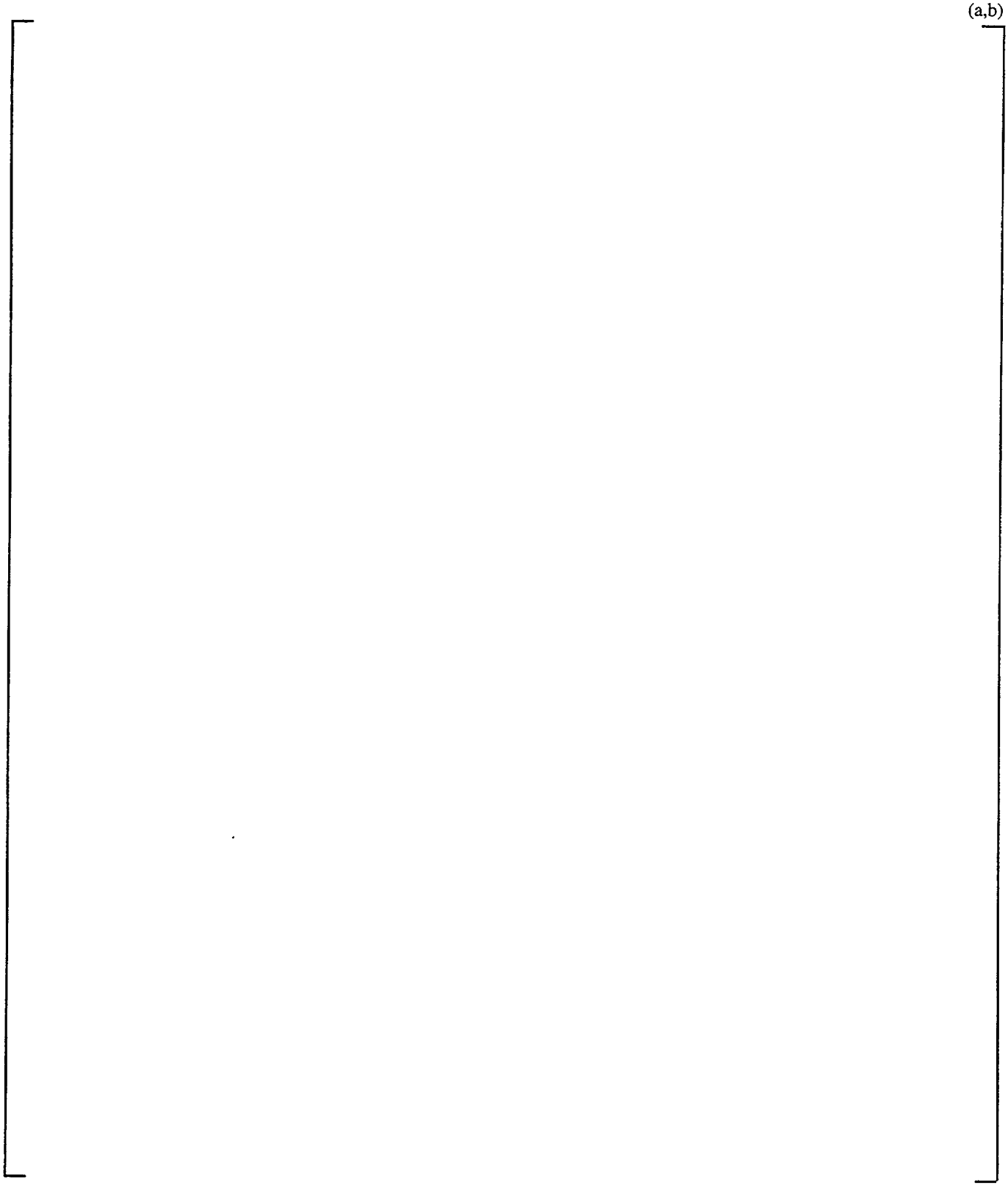

Figure 9-31 LST with Steam Injection: 3 Inch Pipe - Steam Flow 0.76 - 0.95 lb/sec - Internal Steam Pressure Ratio

(a,b)

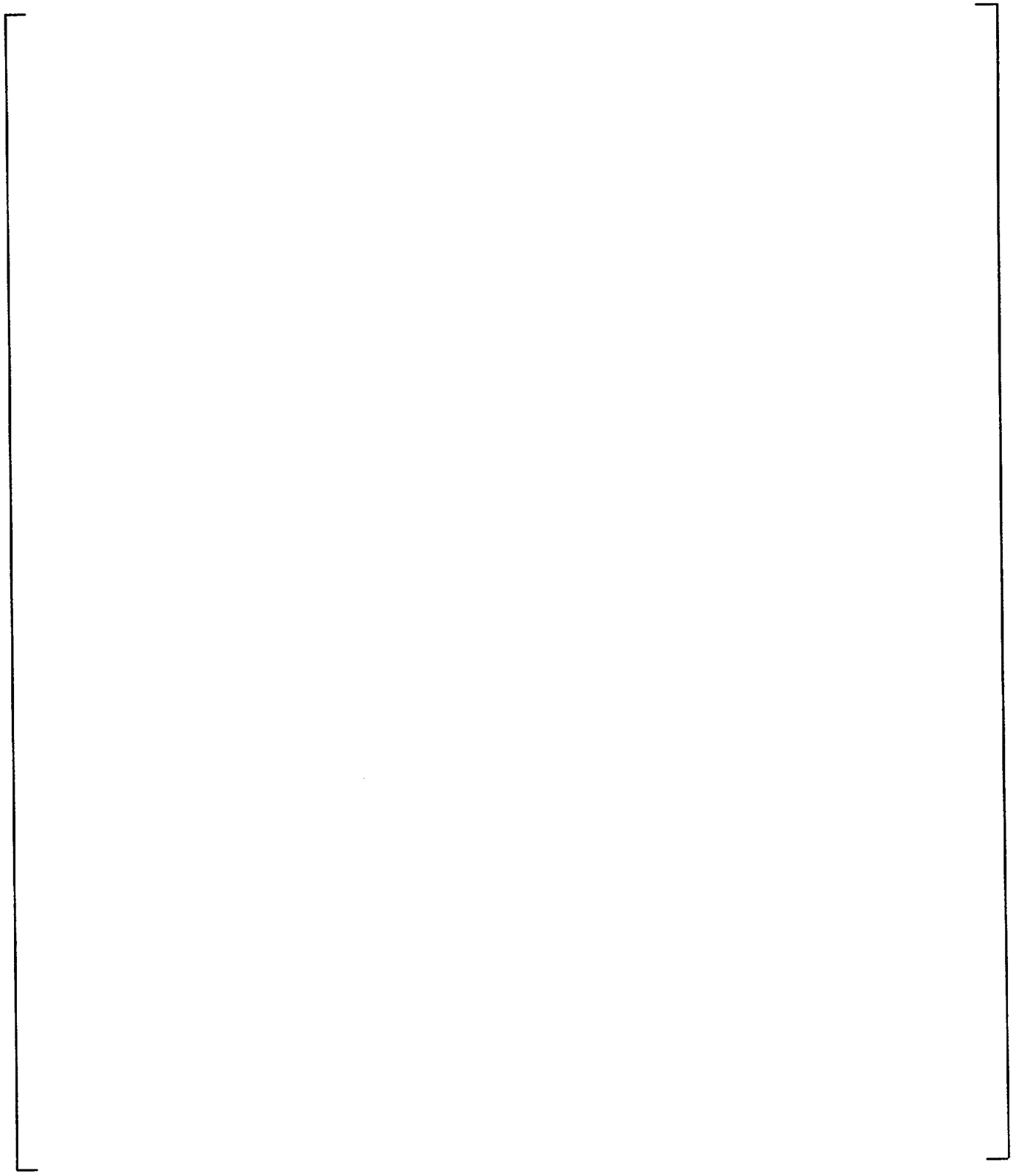

Figure 9-32 **LST with Steam Injection: 3 Inch Pipe - Steam Flow 1.25 - 1.31 lb/sec - Internal Fluid Temperature**

(a,b)

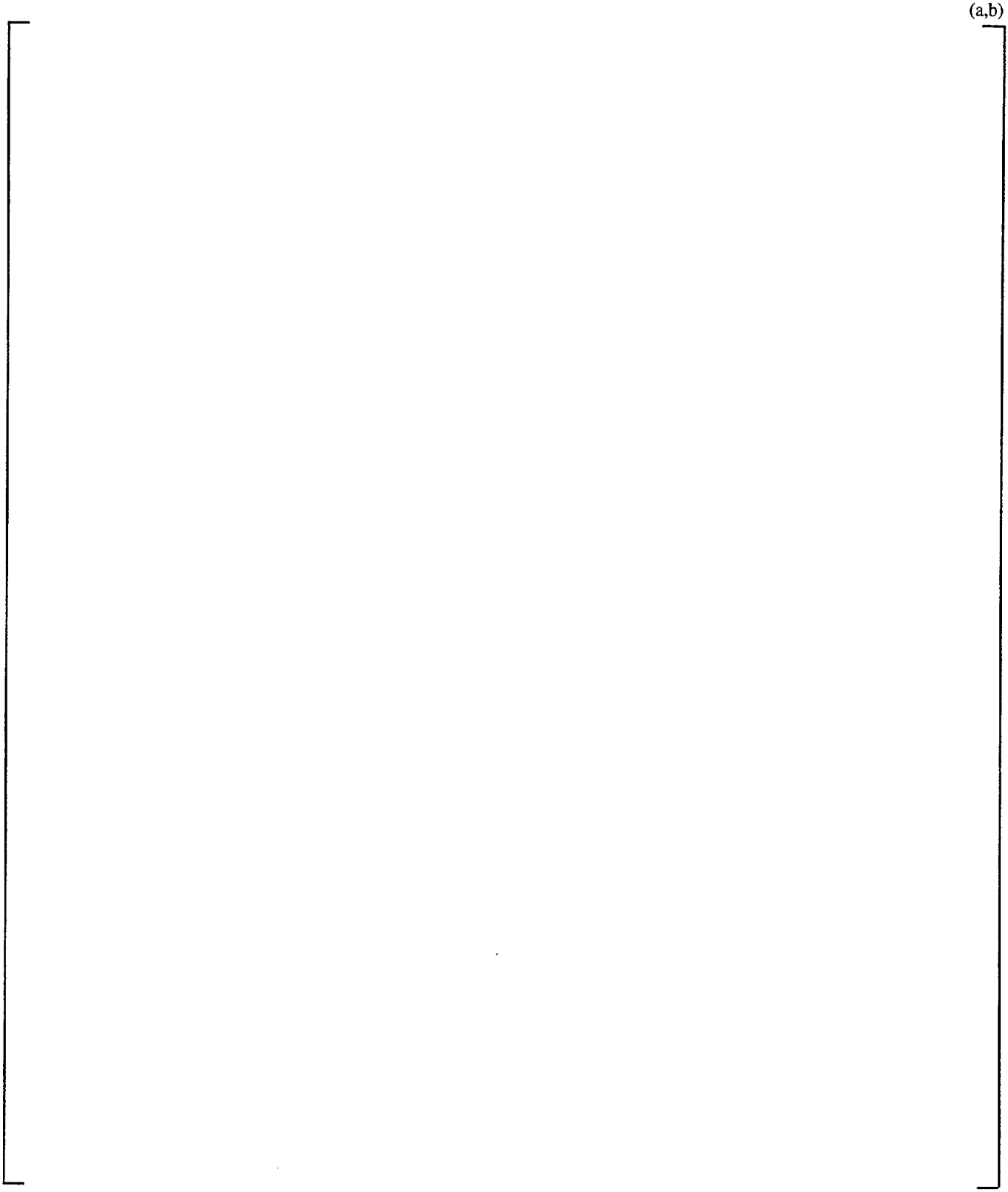

Figure 9-33 LST with Steam Injection: 3 Inch Pipe - Steam Flow 1.25 - 1.31 lb/sec - Saturation Temperature

(a,b)

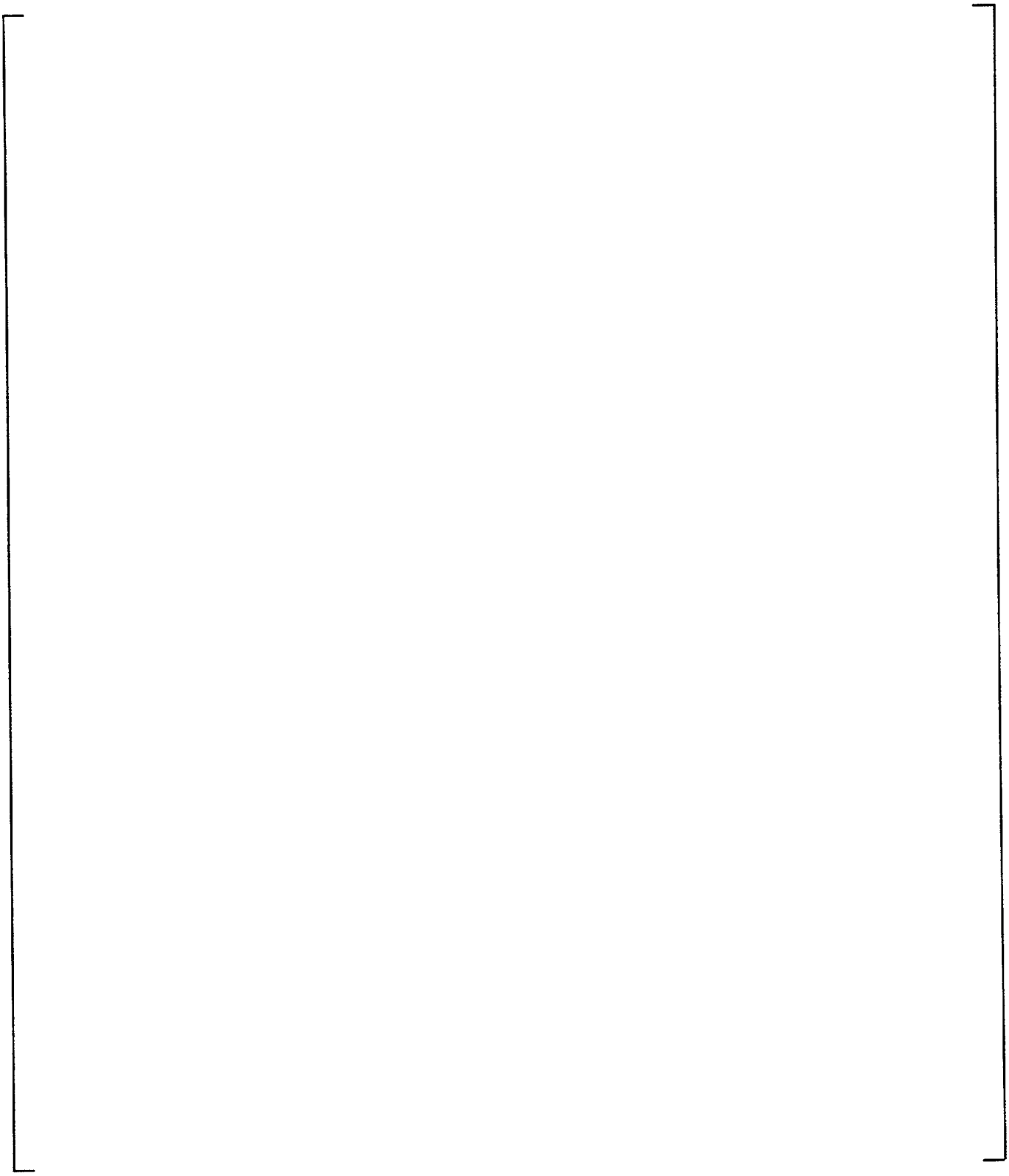

Figure 9-34 **LST with Steam Injection: 3 Inch Pipe - Steam Flow 1.25 - 1.31 lb/sec - Internal Steam Pressure Ratio**

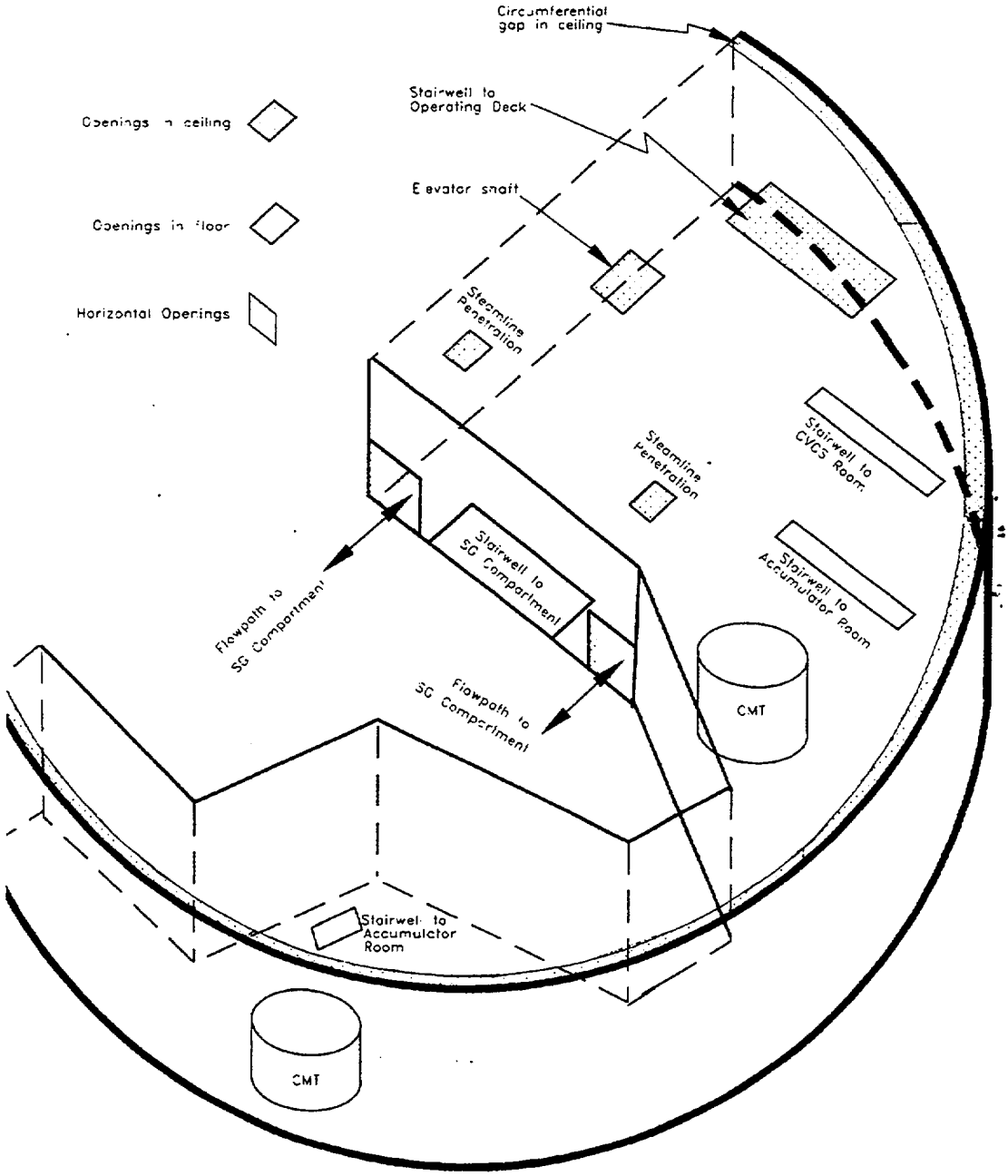

Figure 9-35 CMT Compartment Layout

(a,c)

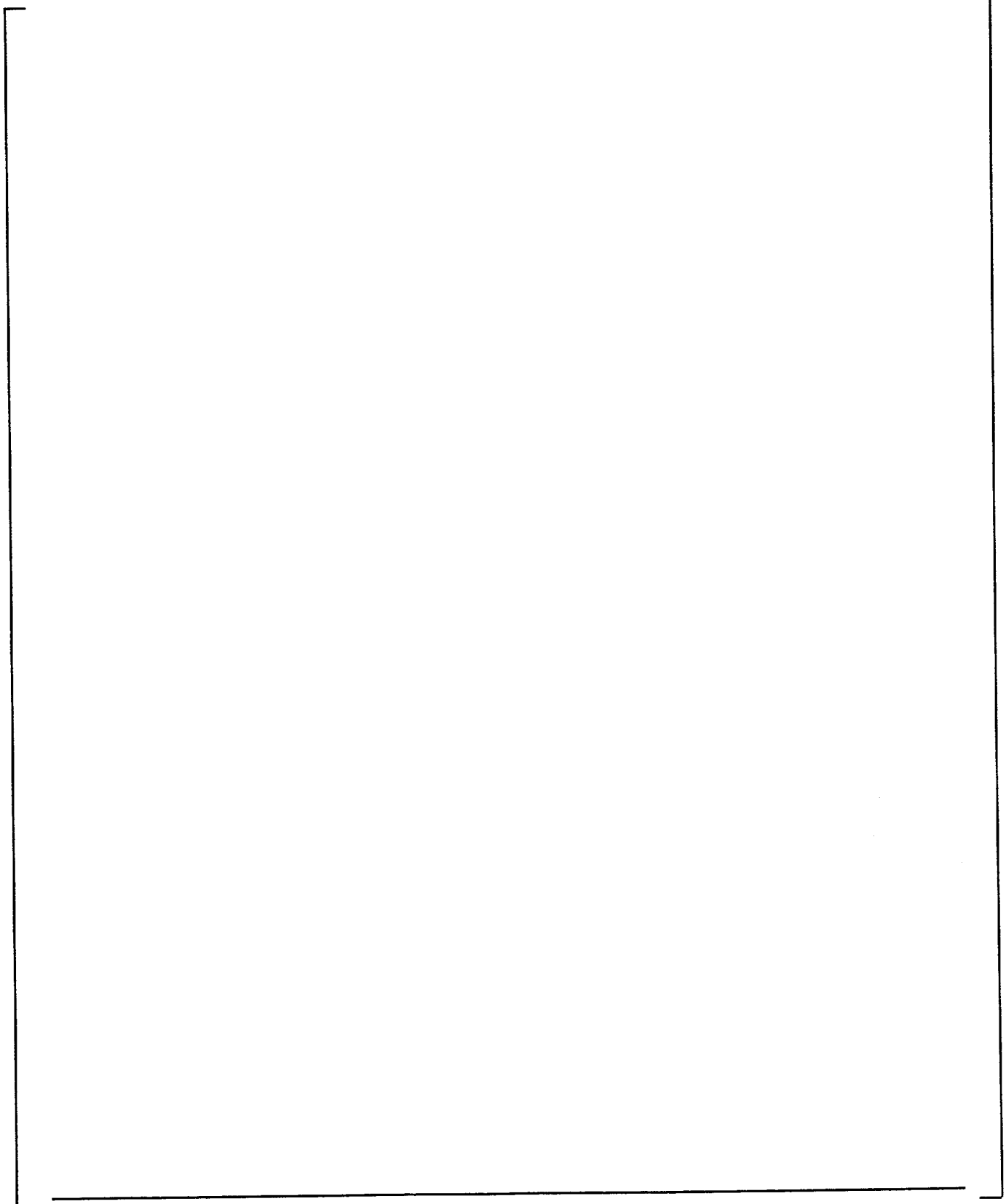

Figure 9-36 Simplified AP600 Containment Diagram

(a,c)

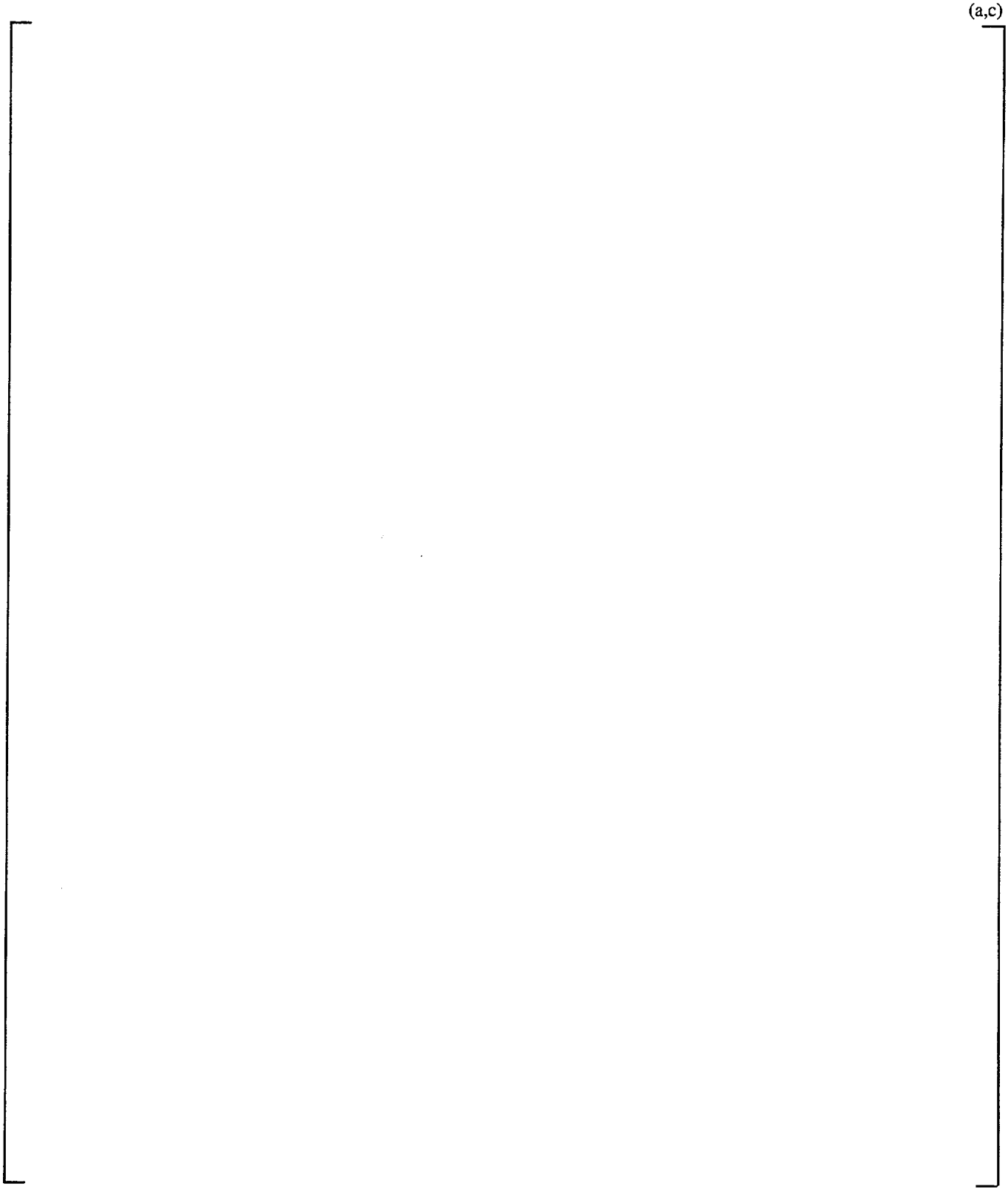

Figure 9-37 **WGOTHIC Calculated LOCA Blowdown Steam Pressure Ratio for Jet Momentum Dissipated in SG East Compartment**

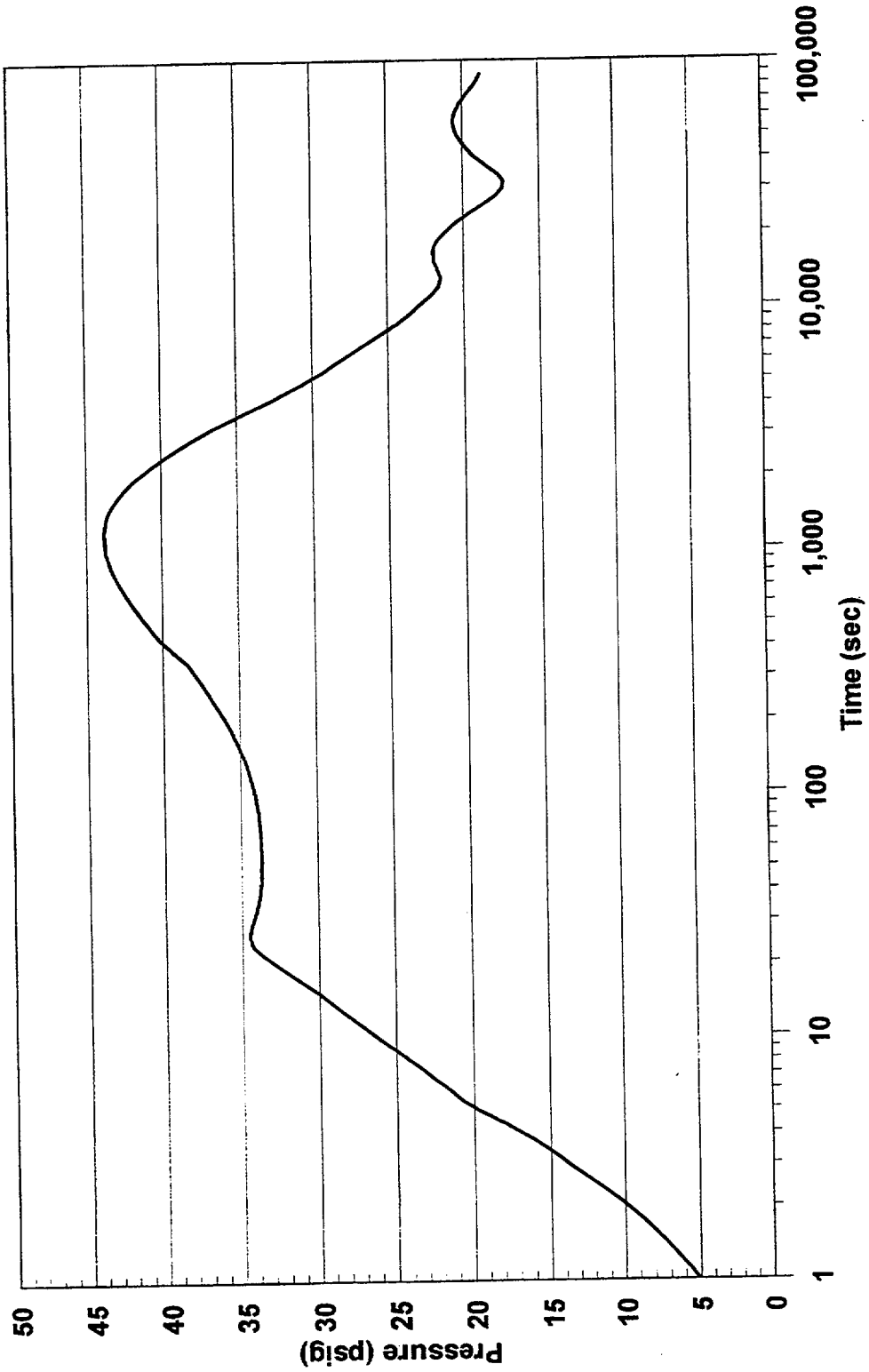

Figure 9-38 **WGOTHIC Calculated AP600 Containment Pressure - Sensitivity to Loss Coefficients for LOCA Jet Momentum Dissipated in SG East Compartment**

(a,c)

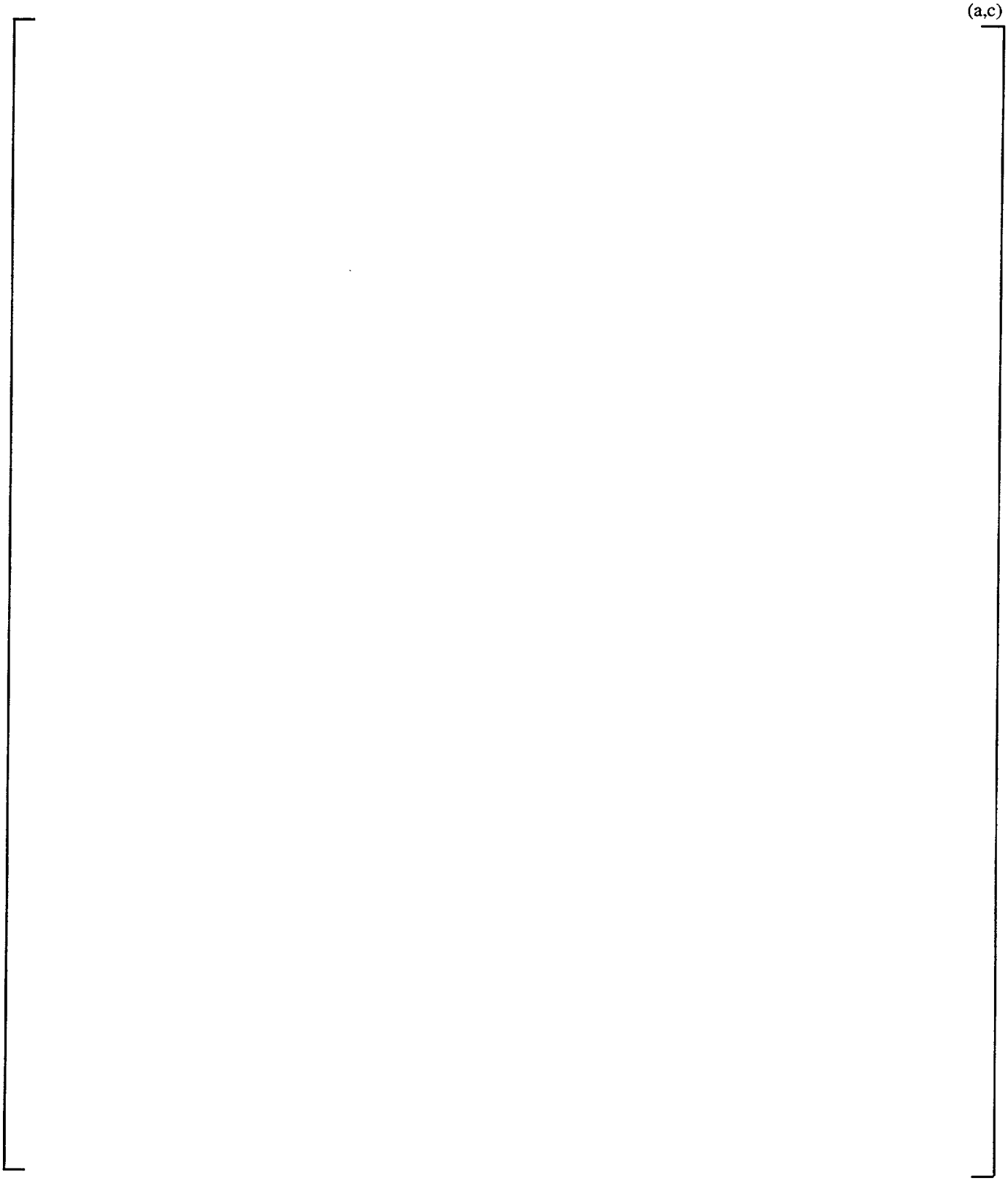

Figure 9-39 **WGOTHIC Calculated Flow Pattern - Sensitivity to Loss Coefficients for LOCA Jet Momentum Dissipated in SG East Compartment at 20 Seconds**

(a,c)

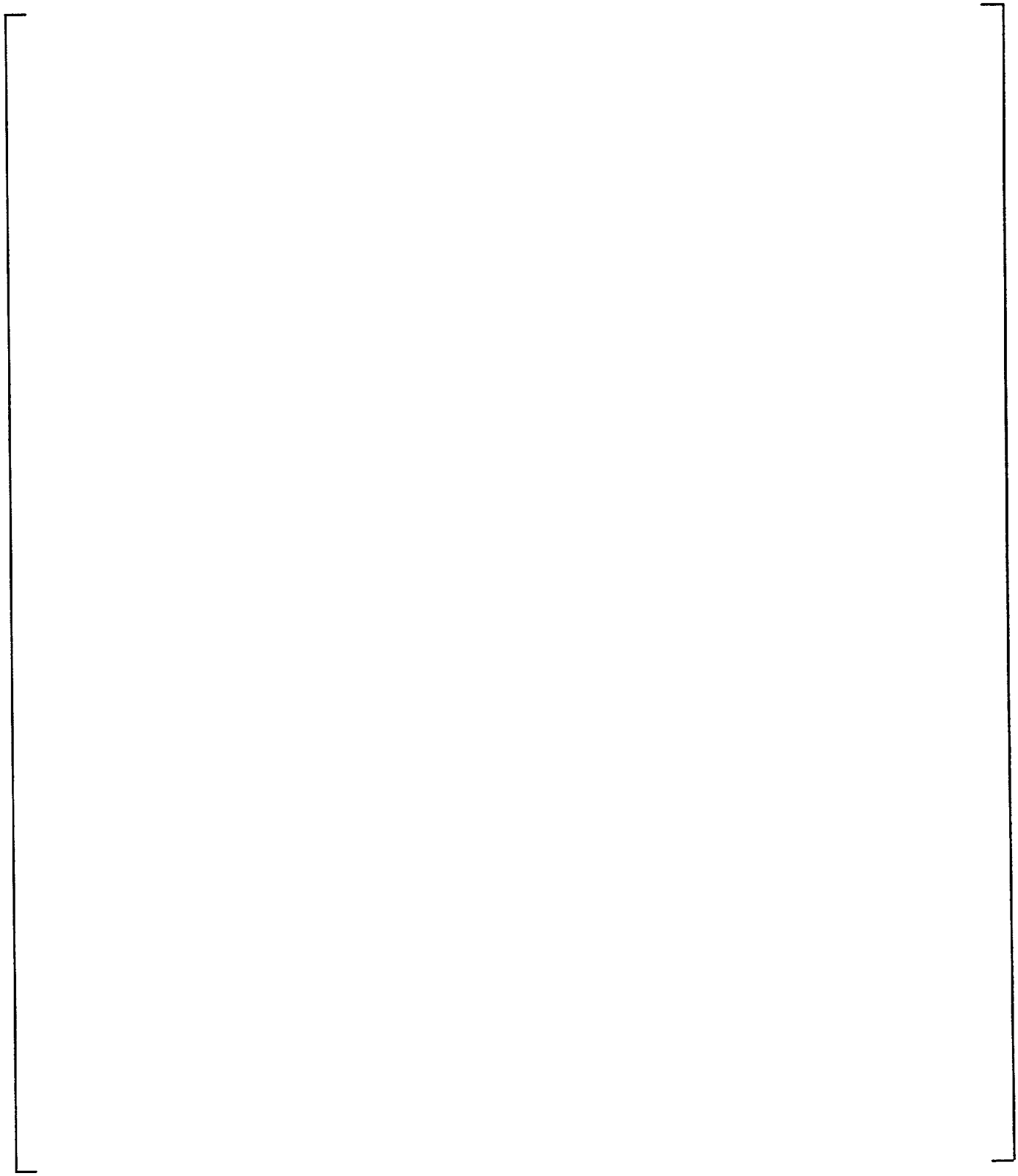

Figure 9-40 **WGOTHIC Calculated Flow Pattern - Sensitivity to Loss Coefficients for LOCA Jet Momentum Dissipated in SG East Comp. at 1000 Seconds**

(a,c)

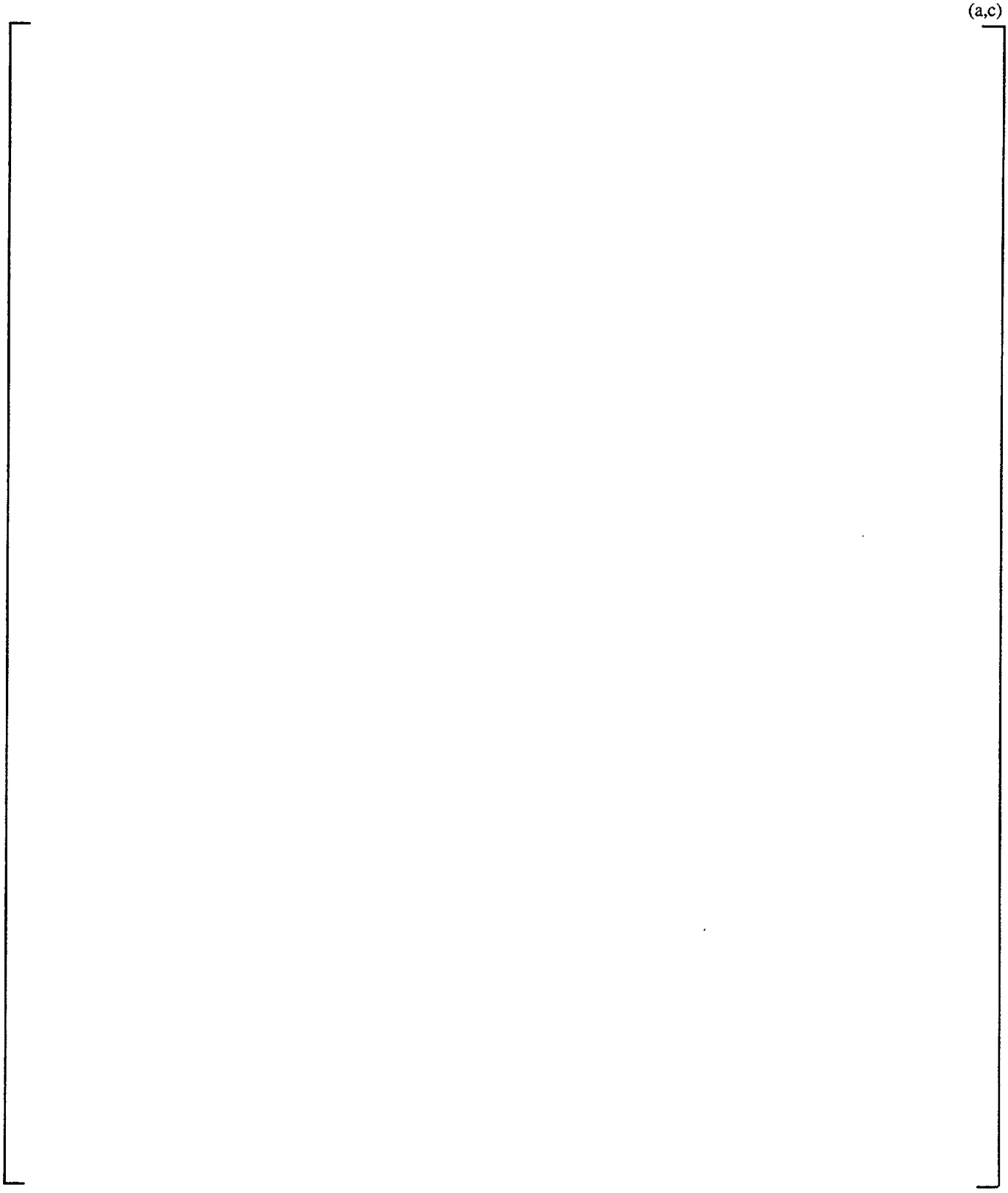

Figure 9-41 **WGOTHIC Calculated Flow Pattern - Sensitivity to Loss Coefficients for LOCA Jet Momentum Dissipated in SG East Comp. at 1550 Seconds**

(a,c)

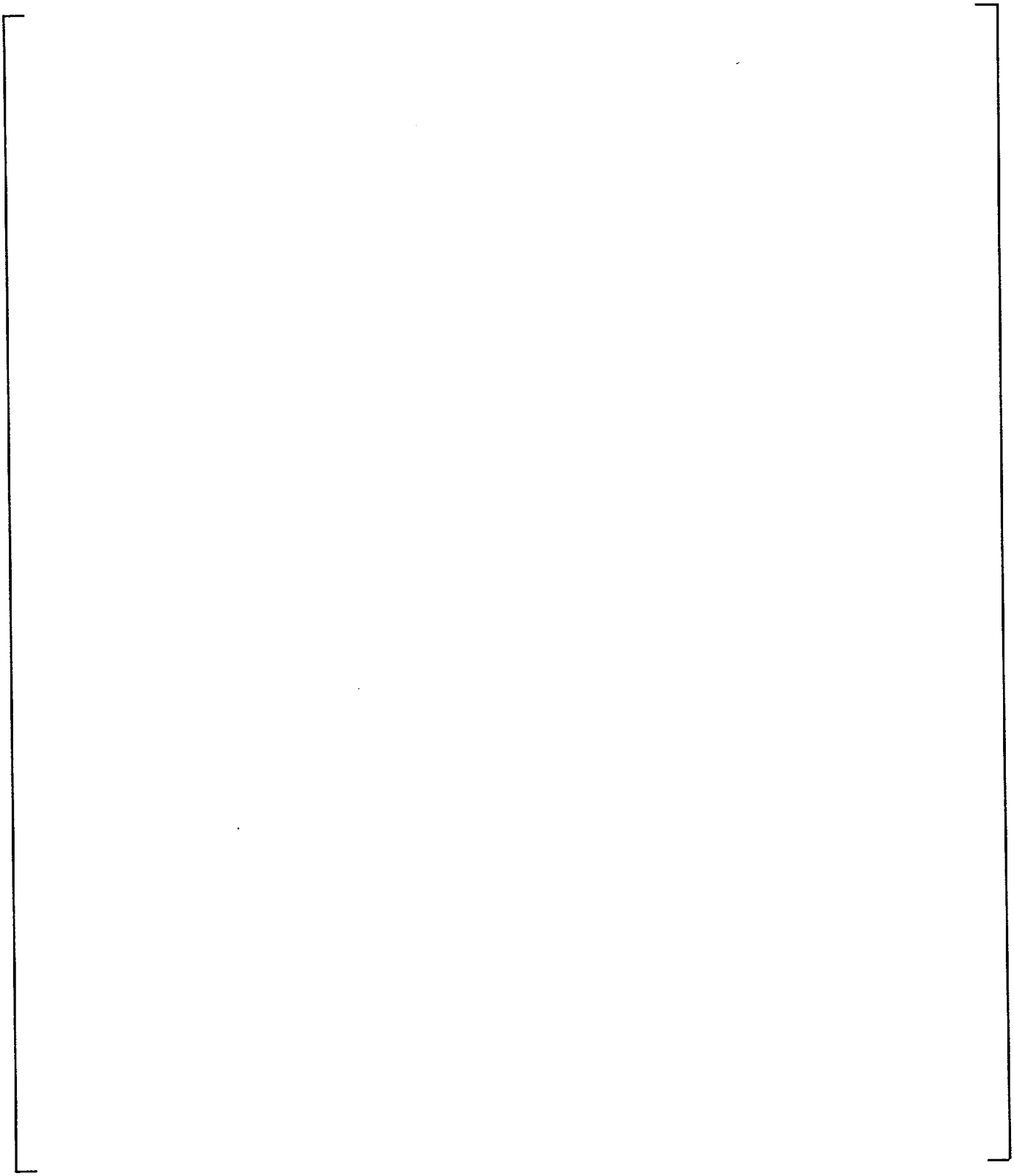

Figure 9-42 **WGOTHIC Calculated Flow Pattern - Sensitivity to Loss Coefficients for LOCA Jet Momentum Dissipated in SG East Comp. at 80050 Seconds**

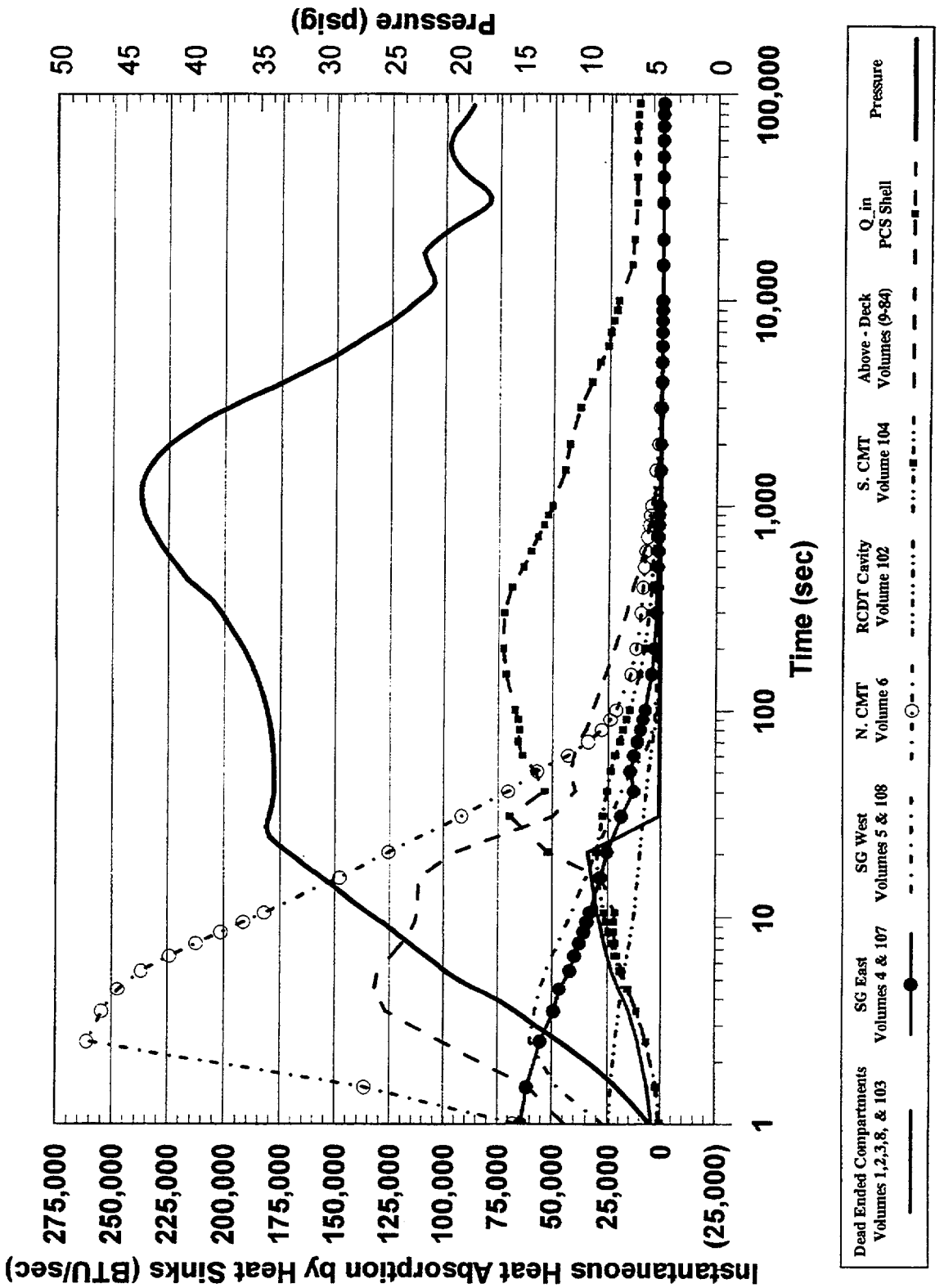

Figure 9-43 WGOTHIC Calculated AP600 Containment Heat Removal Rates - LOCA Jet Momentum Dissipated in SG East Compartment

(a,c)

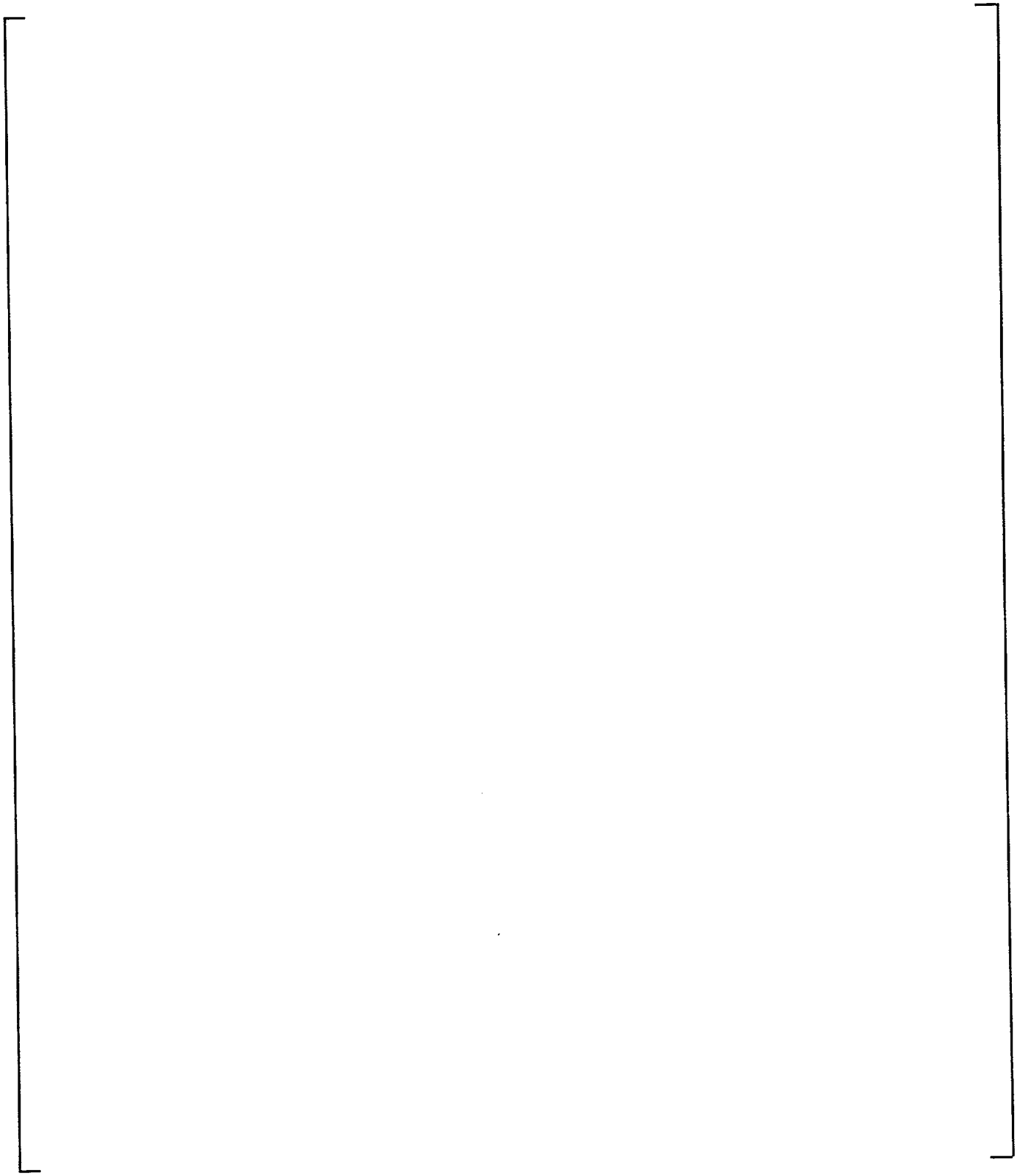

Figure 9-44 WGOTHIC Calculated AP600 Containment Steam Pressure Ratio for LOCA Jet Momentum Dissipated in SG East Compartment

(a,c)

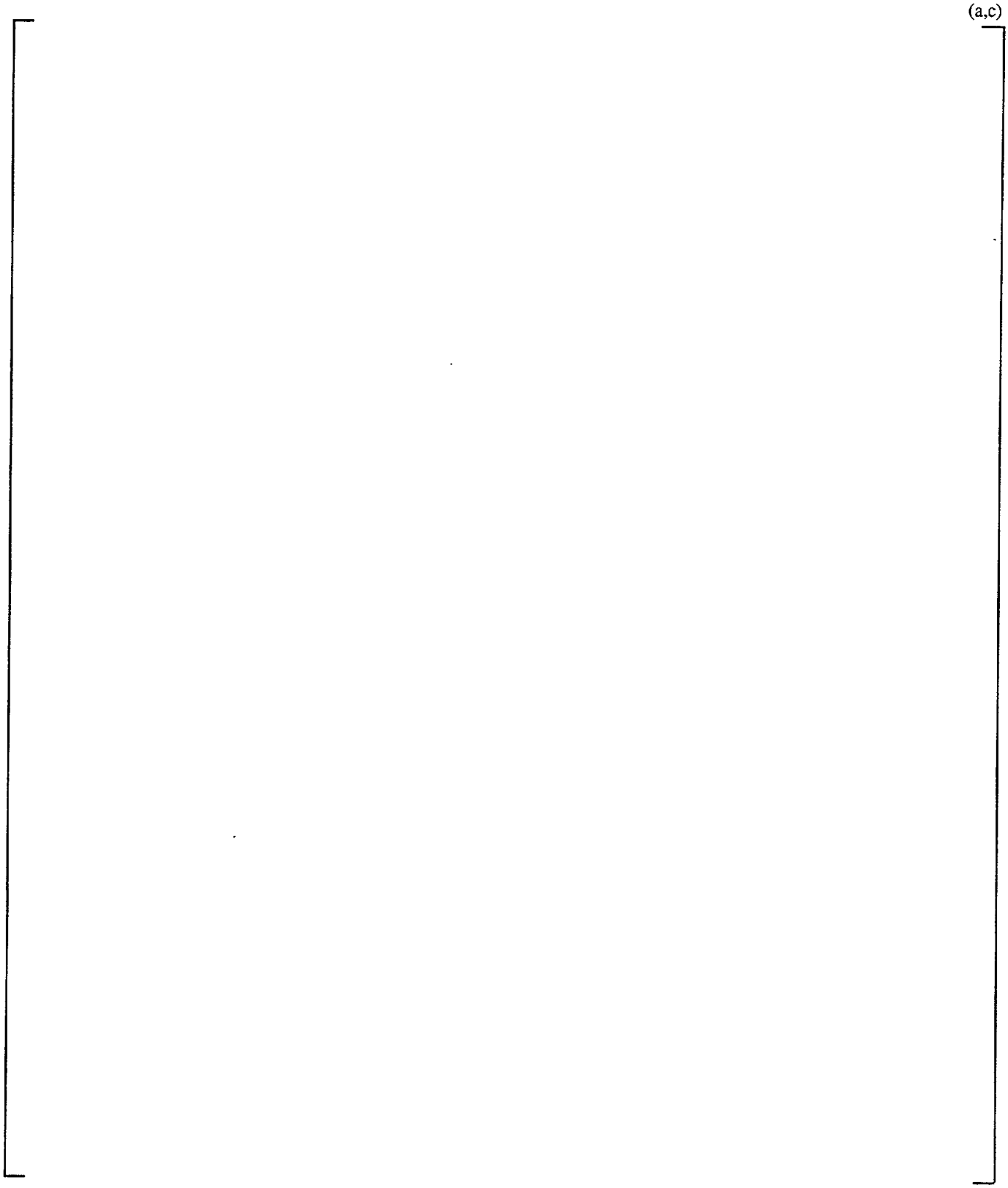

Figure 9-45 **WGOTHIC Calculated AP600 Cont. Pressure - Sensitivity to Heat Transfer Coefficient for Study of Undissipated Jet Effects During a LOCA**

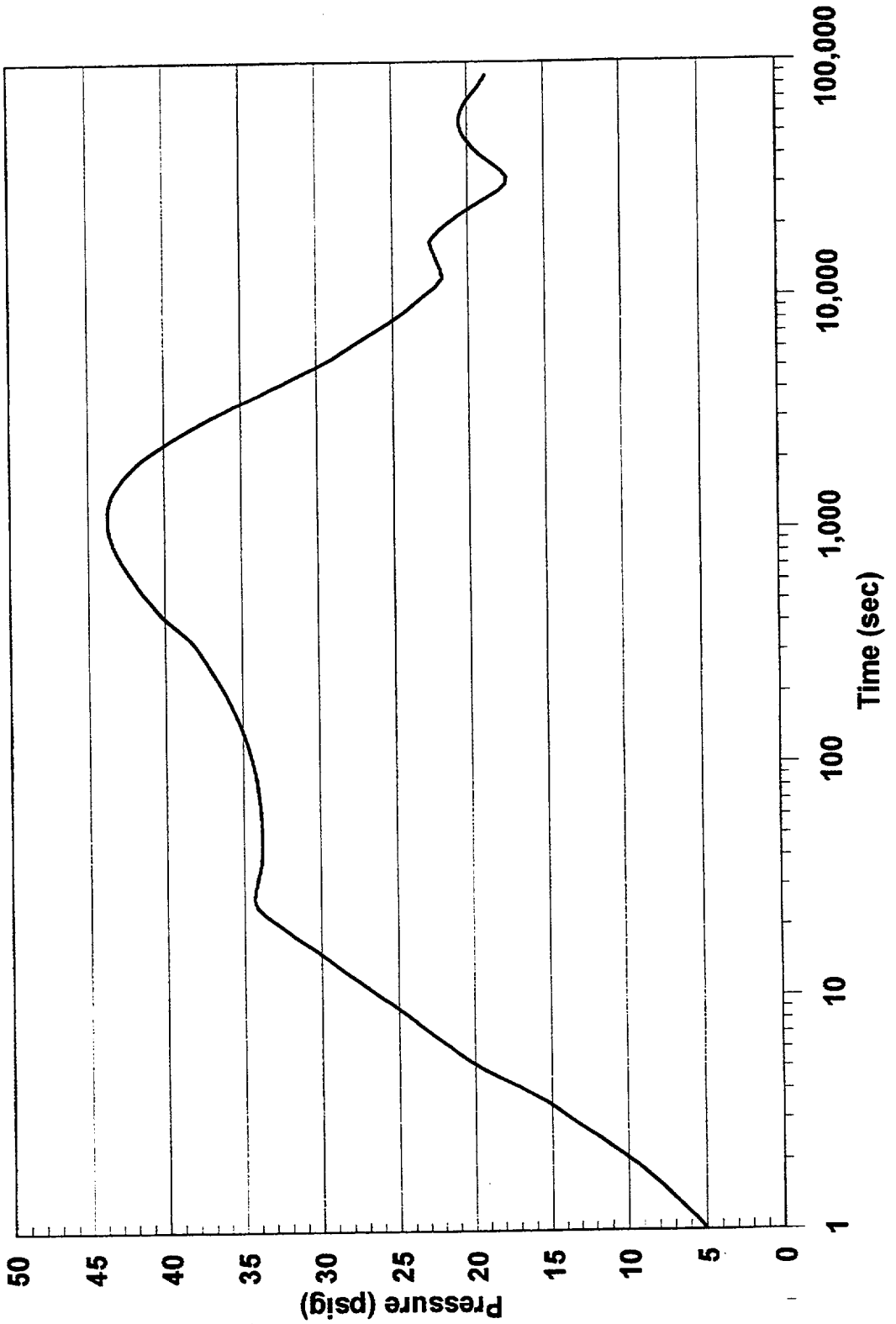

Figure 9-46 **WGOTHIC Calculated AP600 Containment Pressure-LOCA Jet Momentum Dissipated in SG East Compartment**

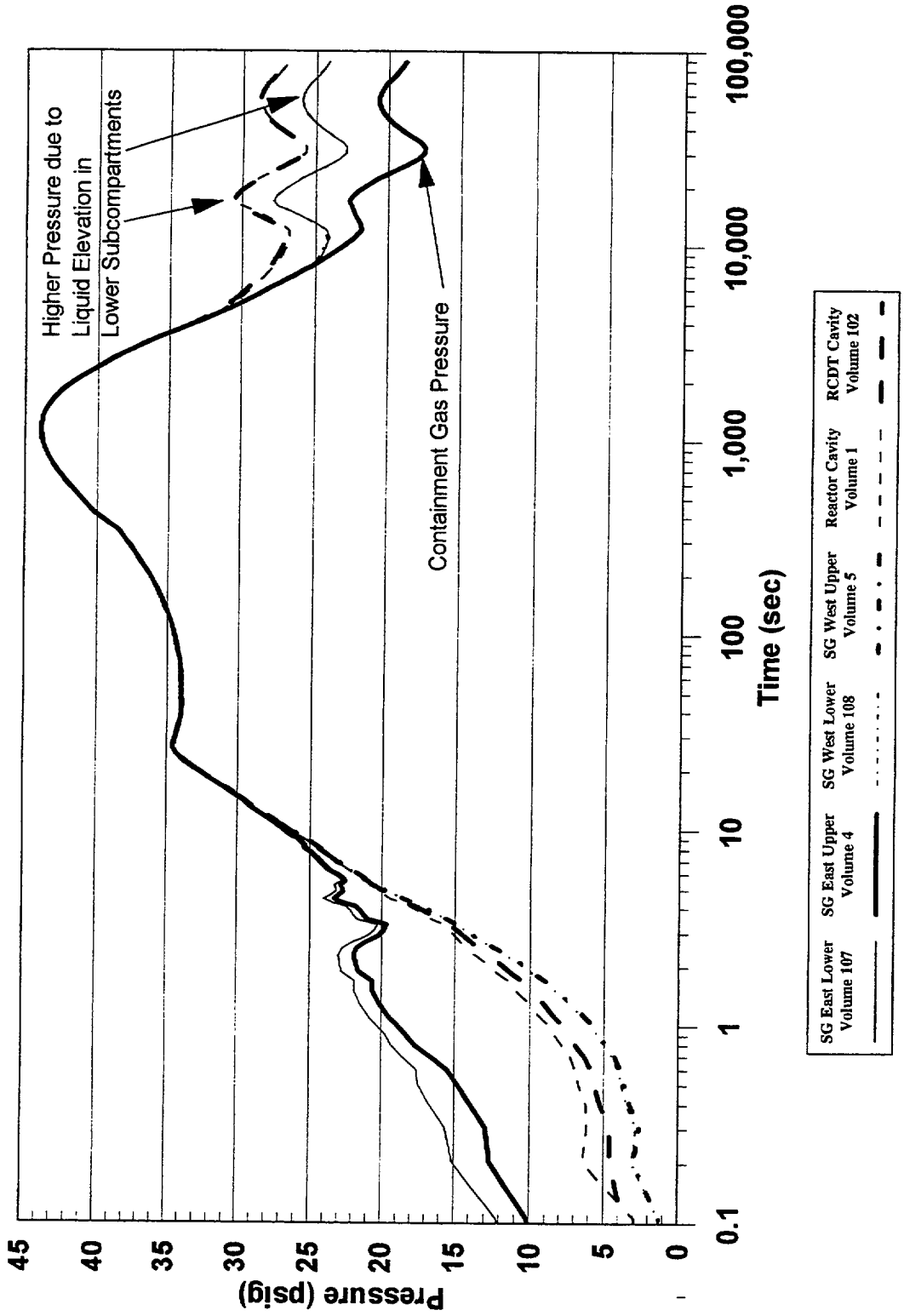

Figure 9-46A WGOTHIC Calculated AP600 Containment Below-Deck Compartment Pressure for LOCA Jet Momentum Dissipated in SG East Compartment

(a,c)

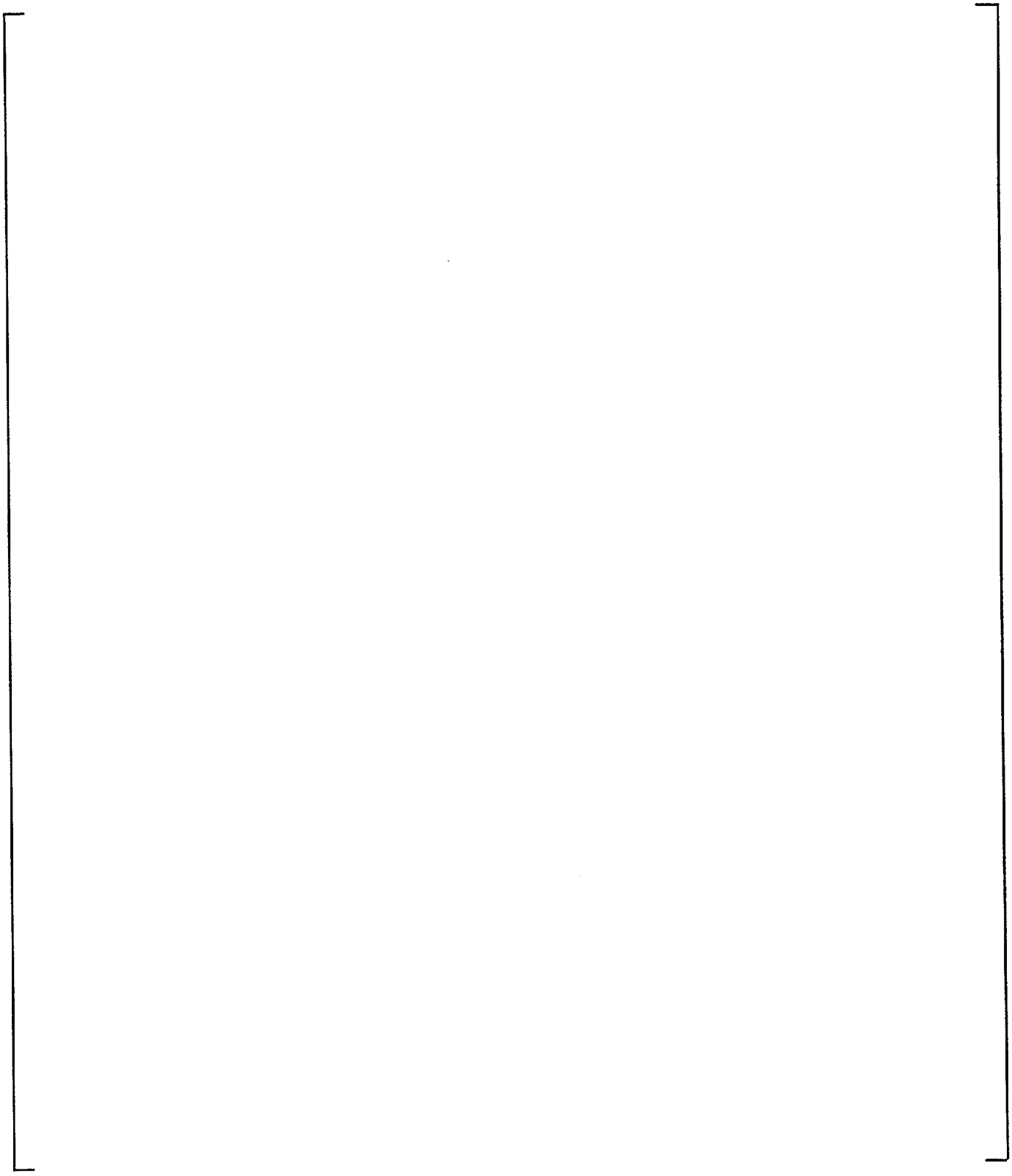

Figure 9-47 **WGOTHIC Calculated Flow Pattern - LOCA Jet Momentum Dissipated in SG East Compartment at 20 Seconds**

(a,c)

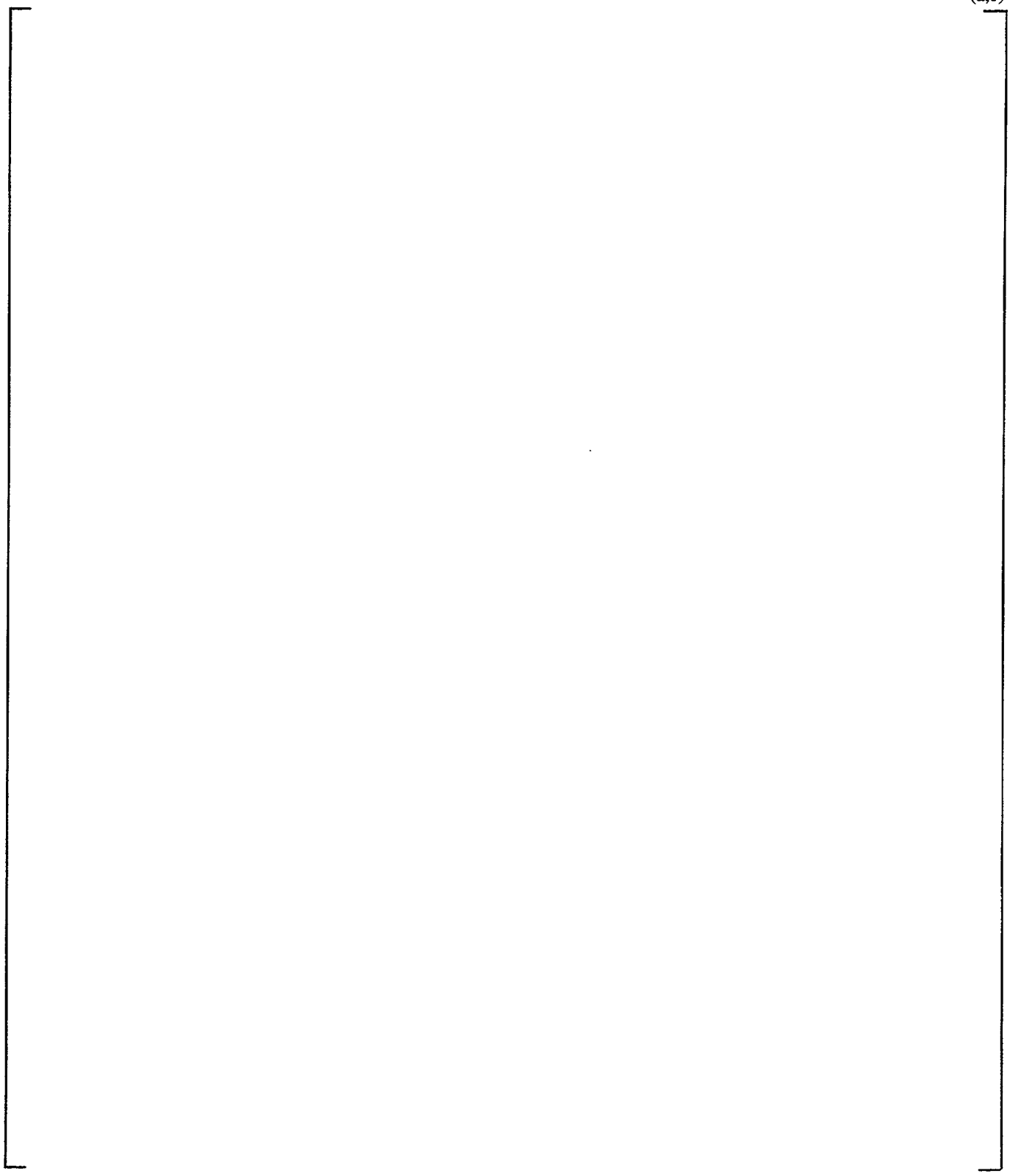

Figure 9-48 **WGOTHIC Calculated Flow Pattern - LOCA Jet Momentum Dissipated in SG East Compartment at 1000 Seconds**

(a,c)

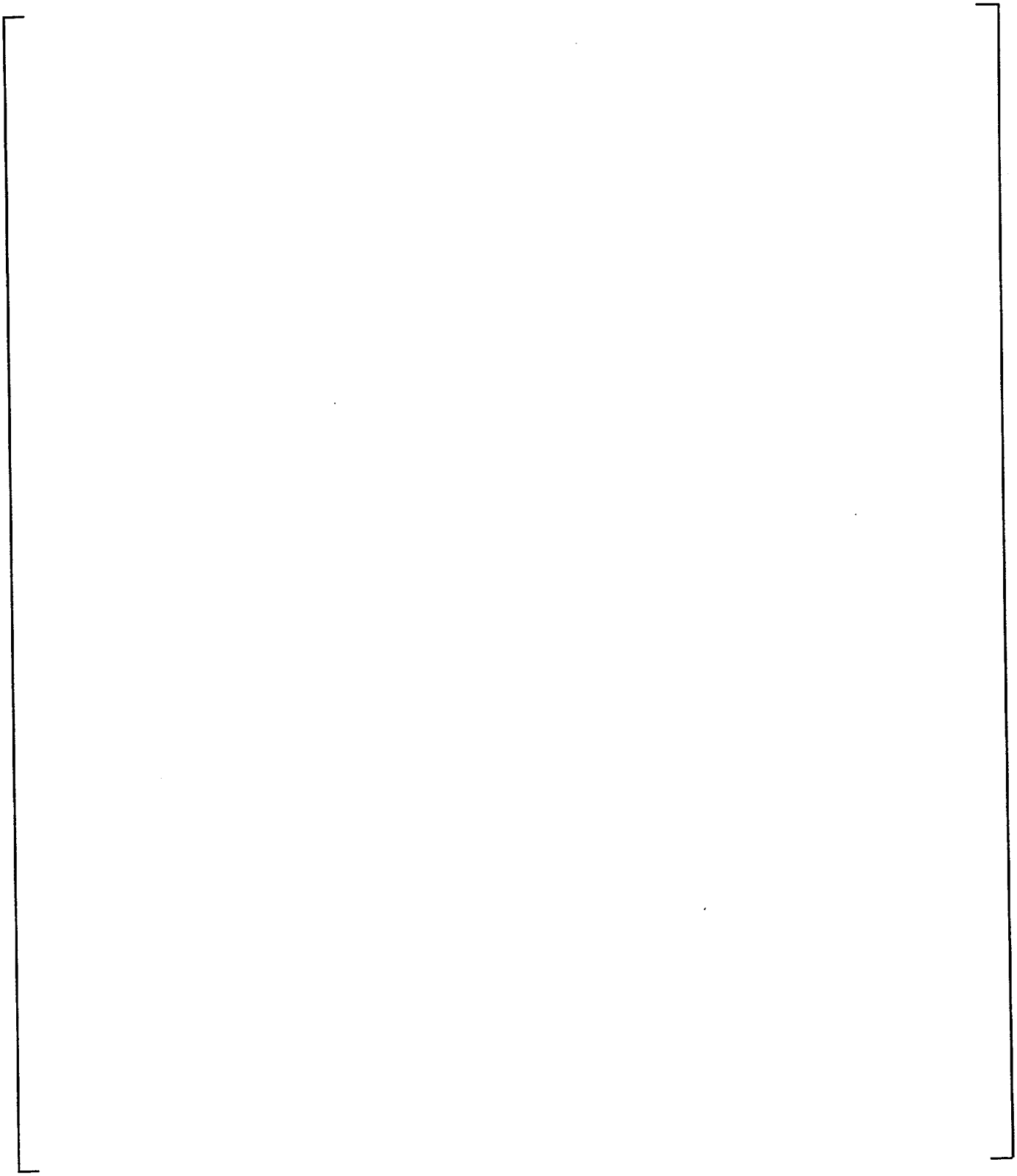

Figure 9-49 **WGOTHIC Calculated Flow Pattern - LOCA Jet Momentum Dissipated in SG East Compartment at 1500 Seconds**

(a,c)

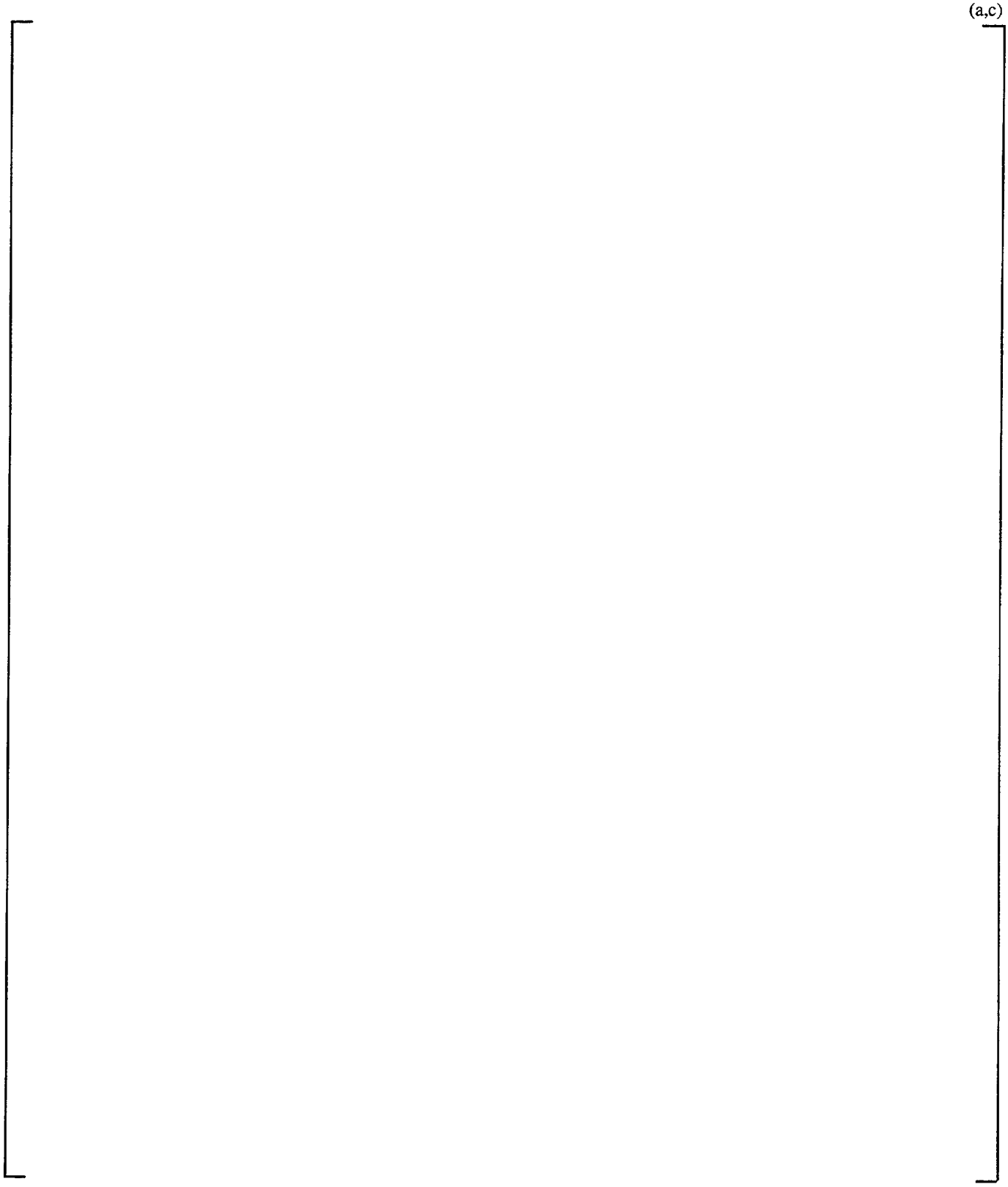

Figure 9-50 WGOTHIC Calculated Flow Pattern - LOCA Jet Momentum Dissipated in SG East Compartment at 8000 Seconds

(a,c)

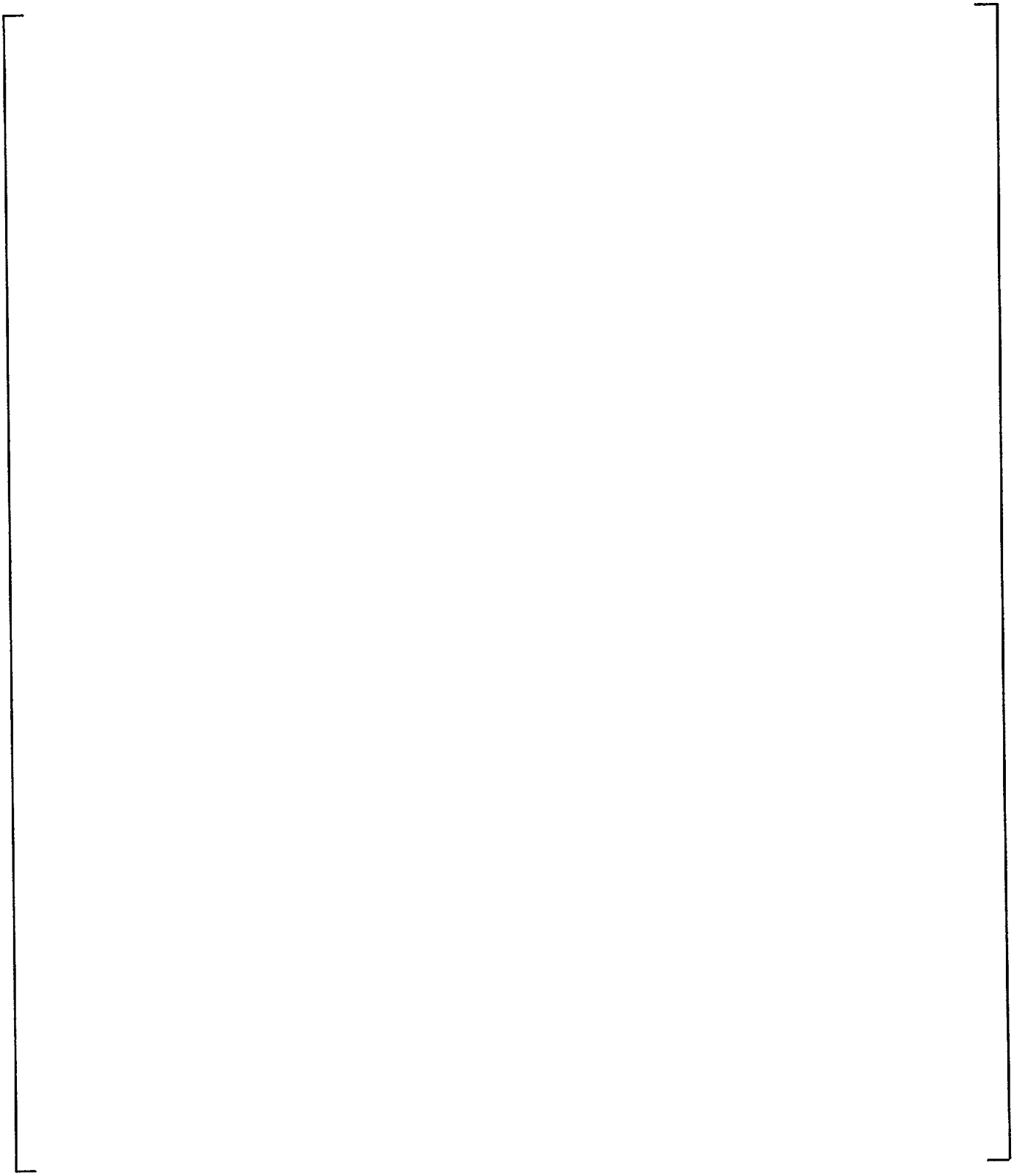

Figure 9-51 **Details of WGOTHIC Flow Paths to Above-Deck Region from CMT, Refueling Canal, and IRWST**

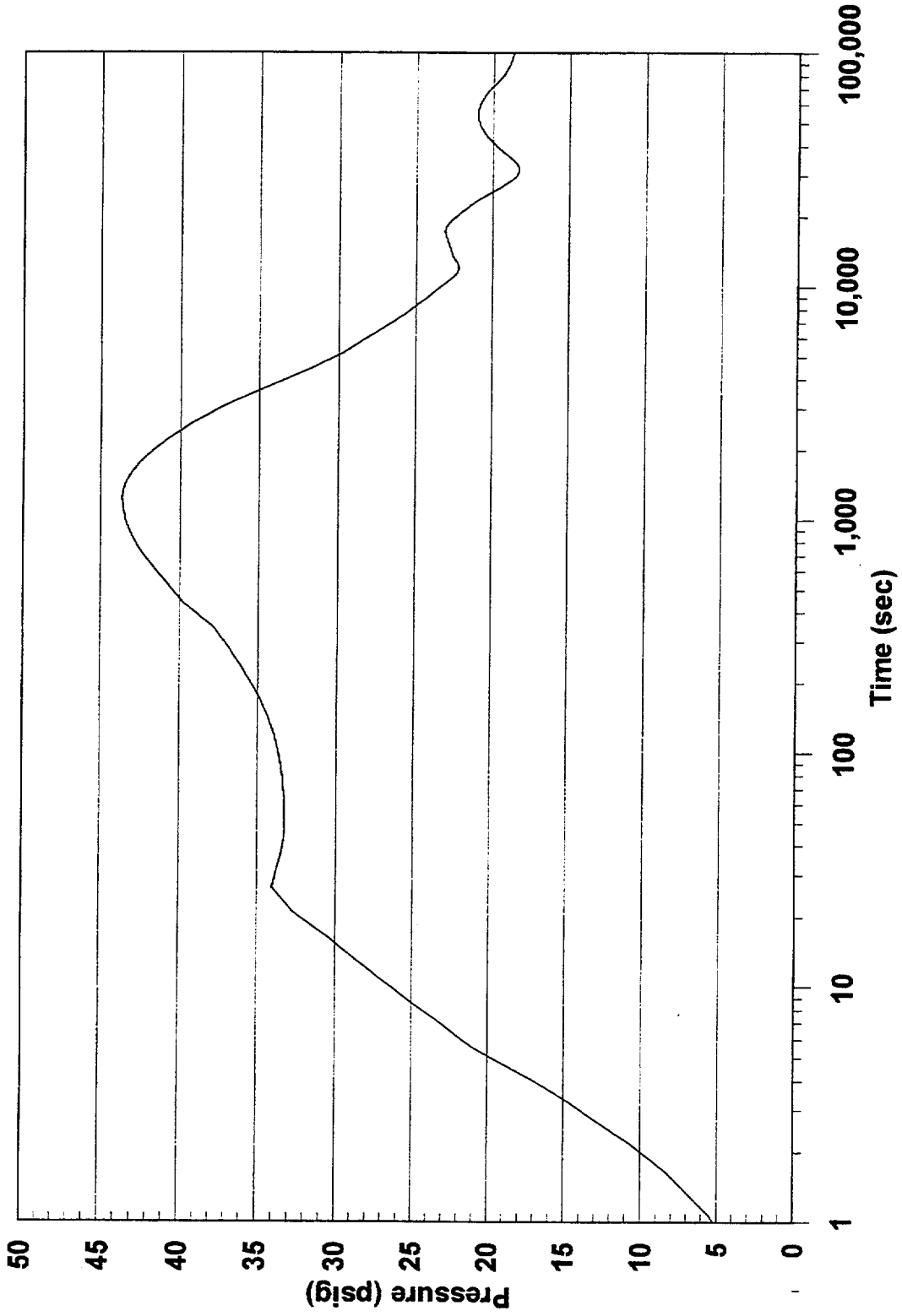

Figure 9-52 WGOTHIC Calculated AP600 Containment Pressure - LOCA Plume Rising into CMT Room

(a,c)

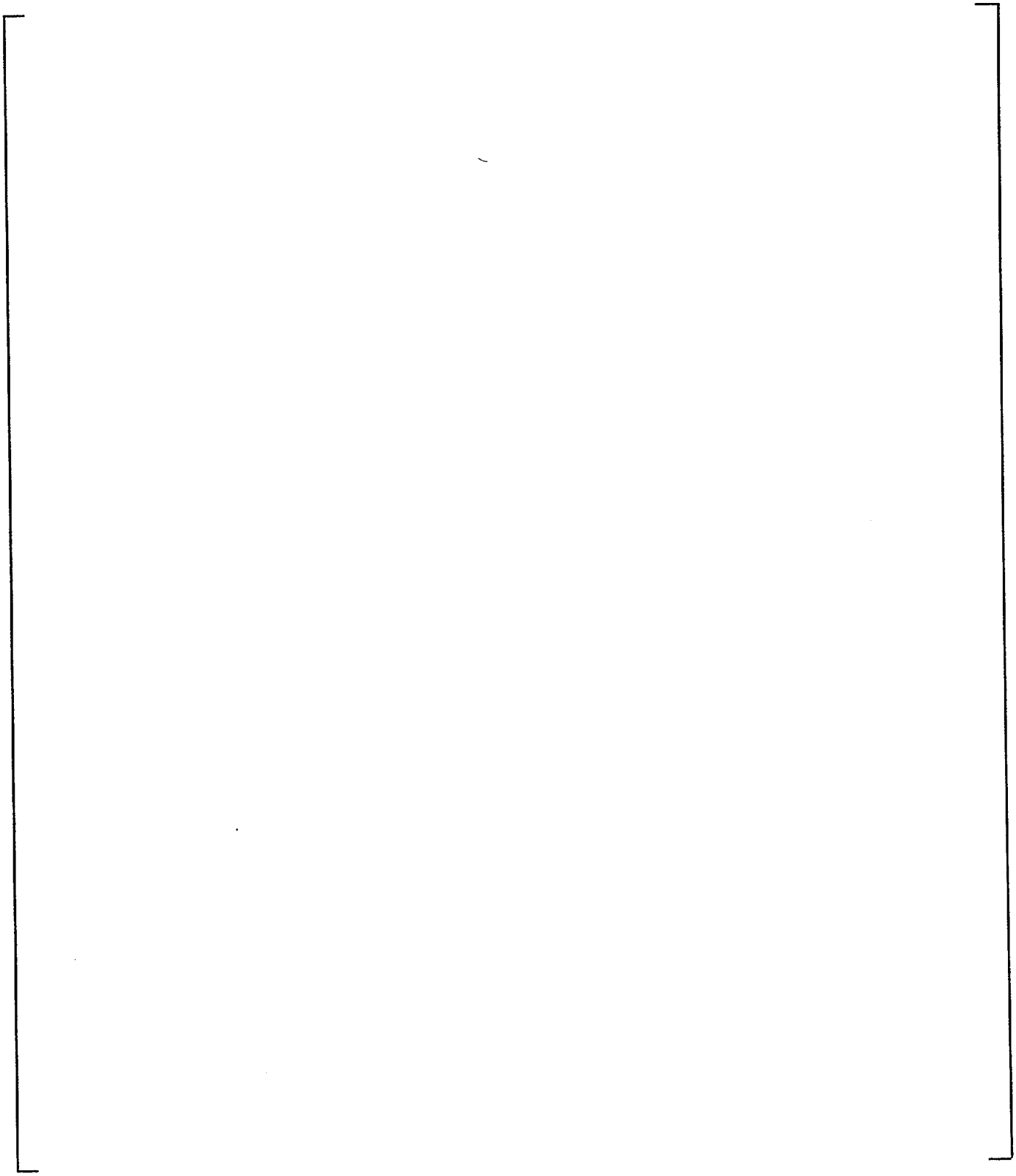

Figure 9-53 WGOTHIC Calculated Flow Pattern - LOCA Plume Rising into CMT Room at 1000 Seconds

(a,c)

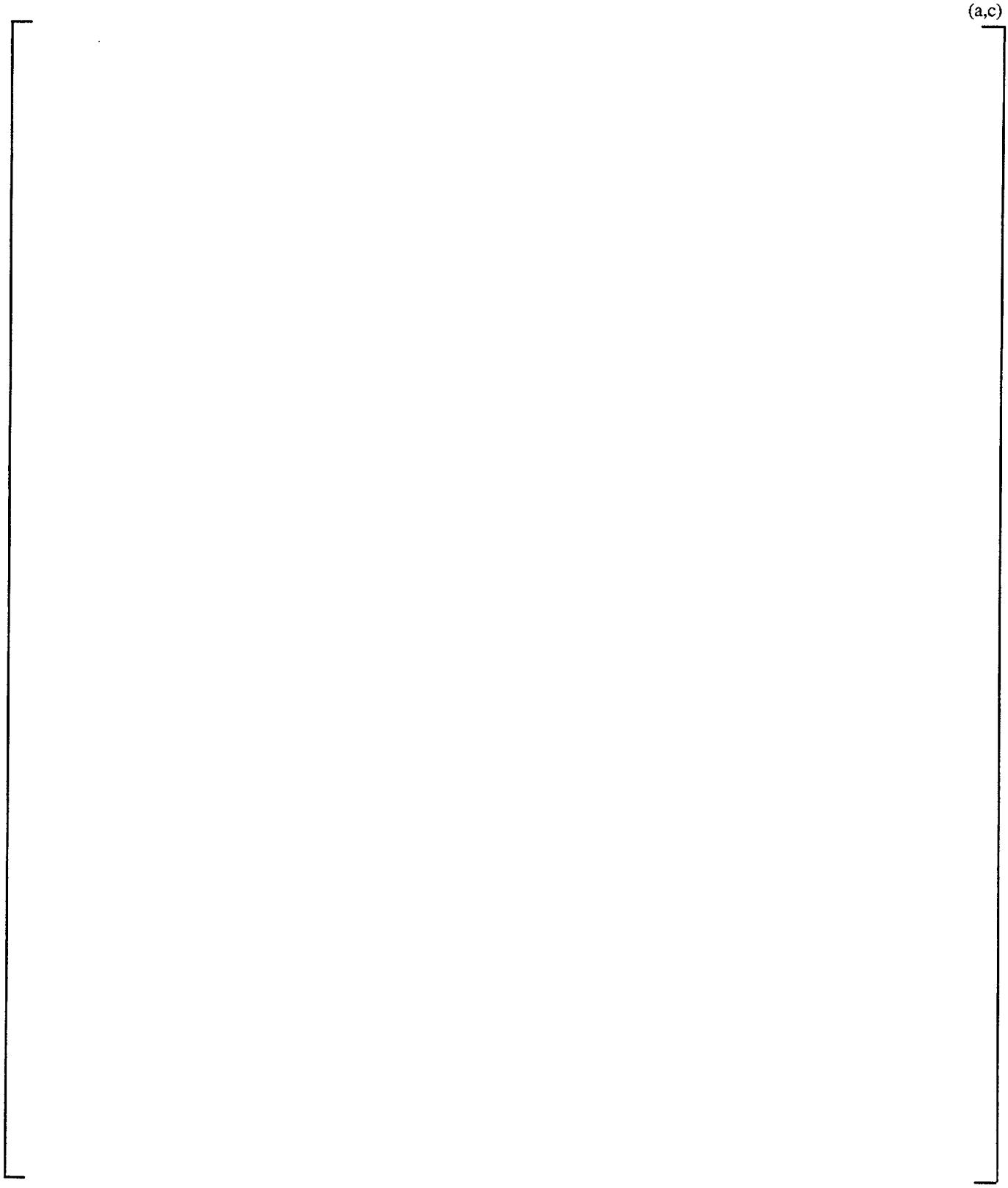

Figure 9-54 **WGOTHIC Calculated Flow Pattern - LOCA Plume Rising into CMT Room at 1400 Seconds**

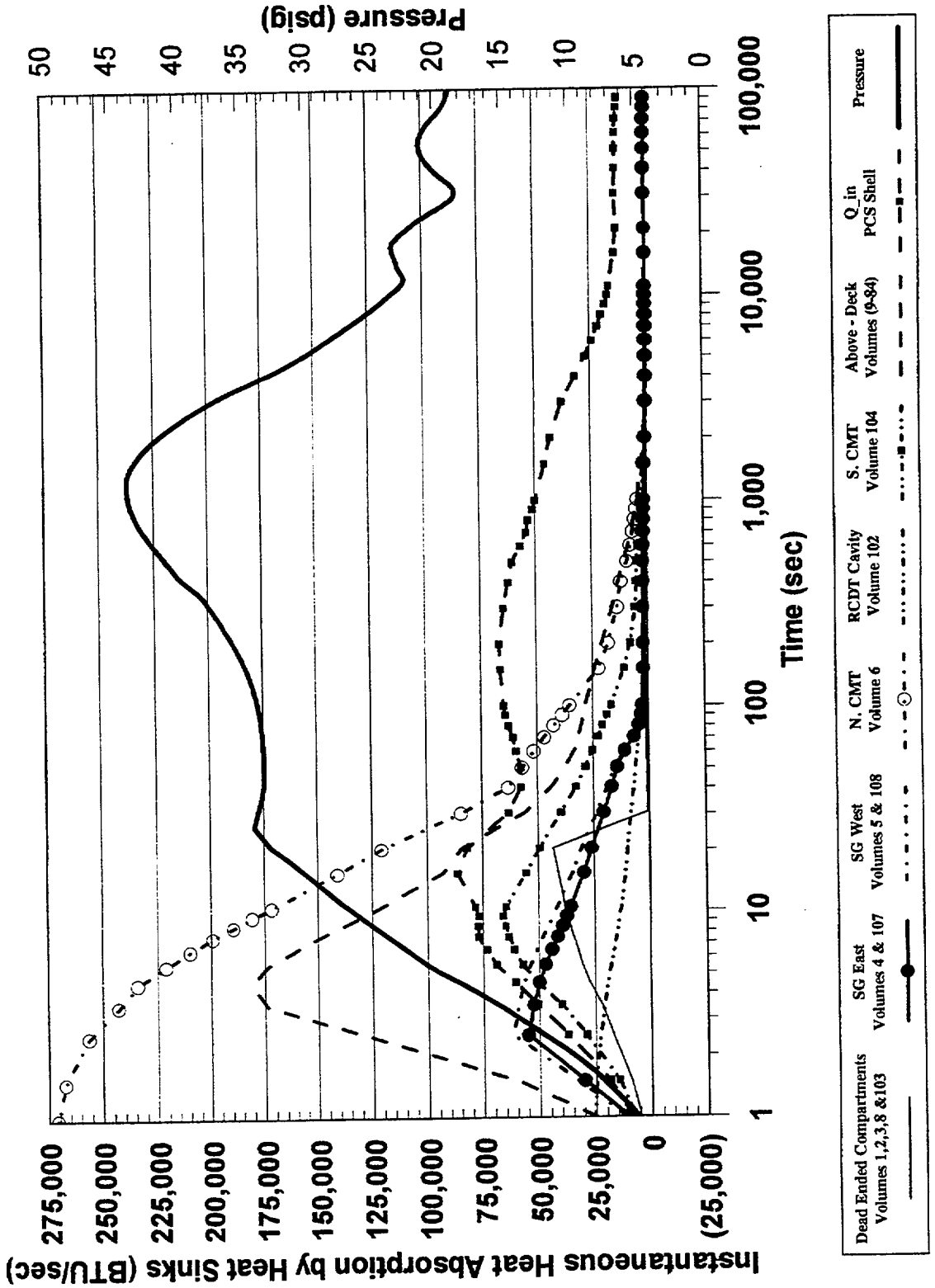

Figure 9-55 WGOTHIC Calculated AP600 Containment Heat Removal Rates - LOCA Plume Rising into CMT Room

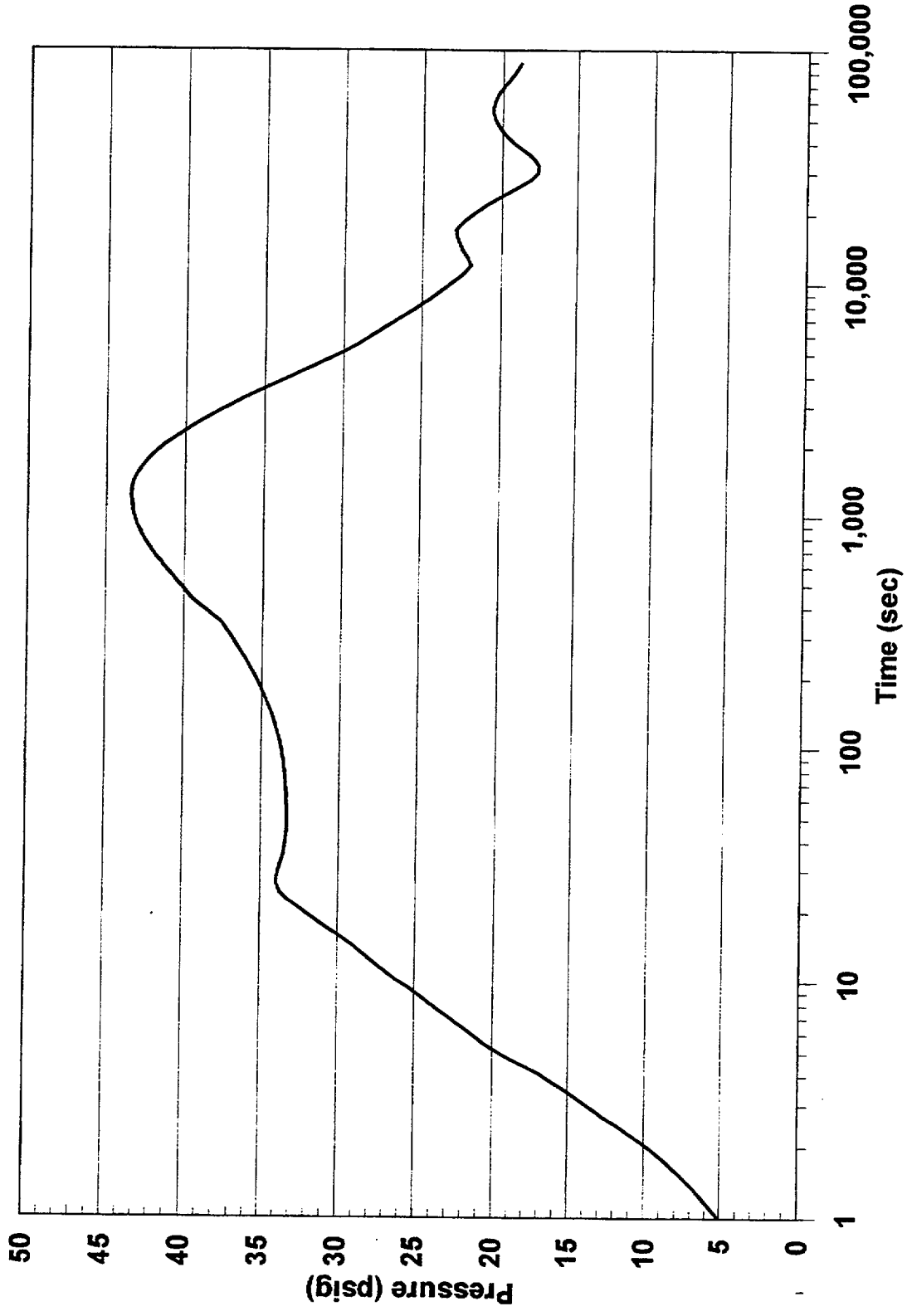

Figure 9-56 **WGOTHIC Calculated AP600 Containment Pressure - LOCA Plume Rising into CMT Room and SG Compartments**

(a,c)

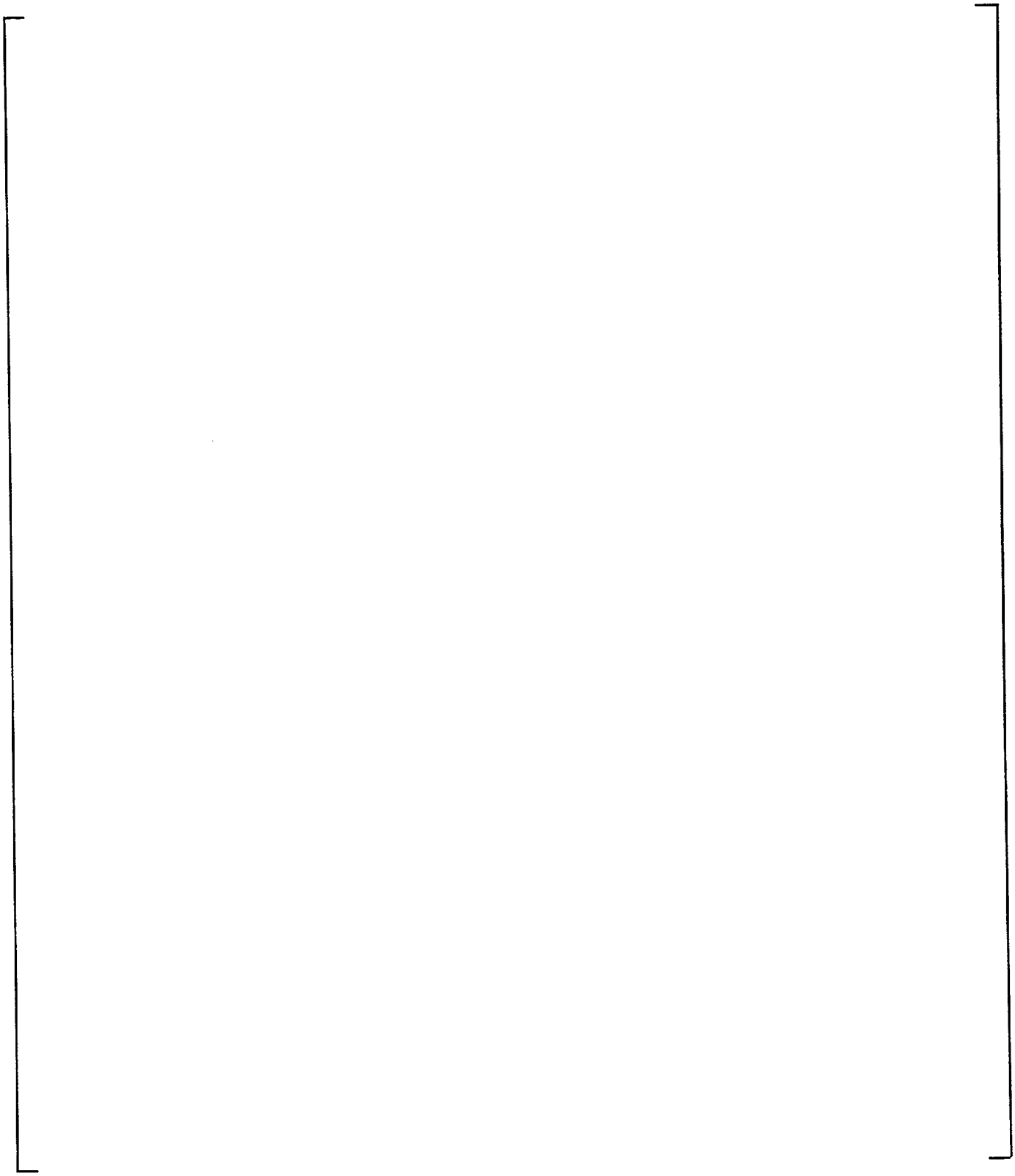

Figure 9-57 **WGOTHIC Calculated Flow Pattern - LOCA Plume Rising into CMT Room and SG Compartments at 1000 Seconds**

(a,c)

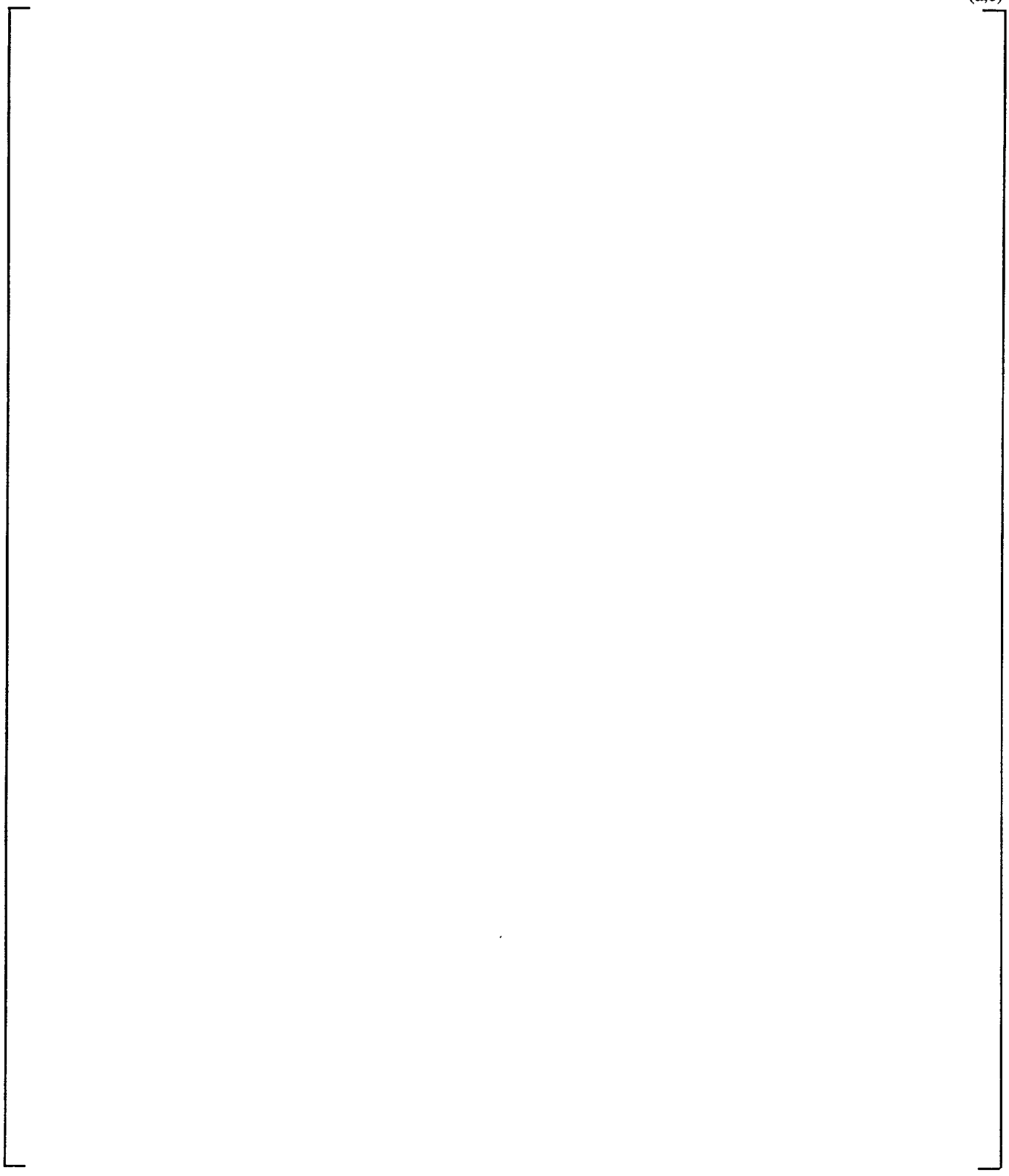

Figure 9-58 WGOTHIC Calculated Flow Pattern - LOCA Plume Rising into CMT Room and SG Compartments at 1500 Seconds

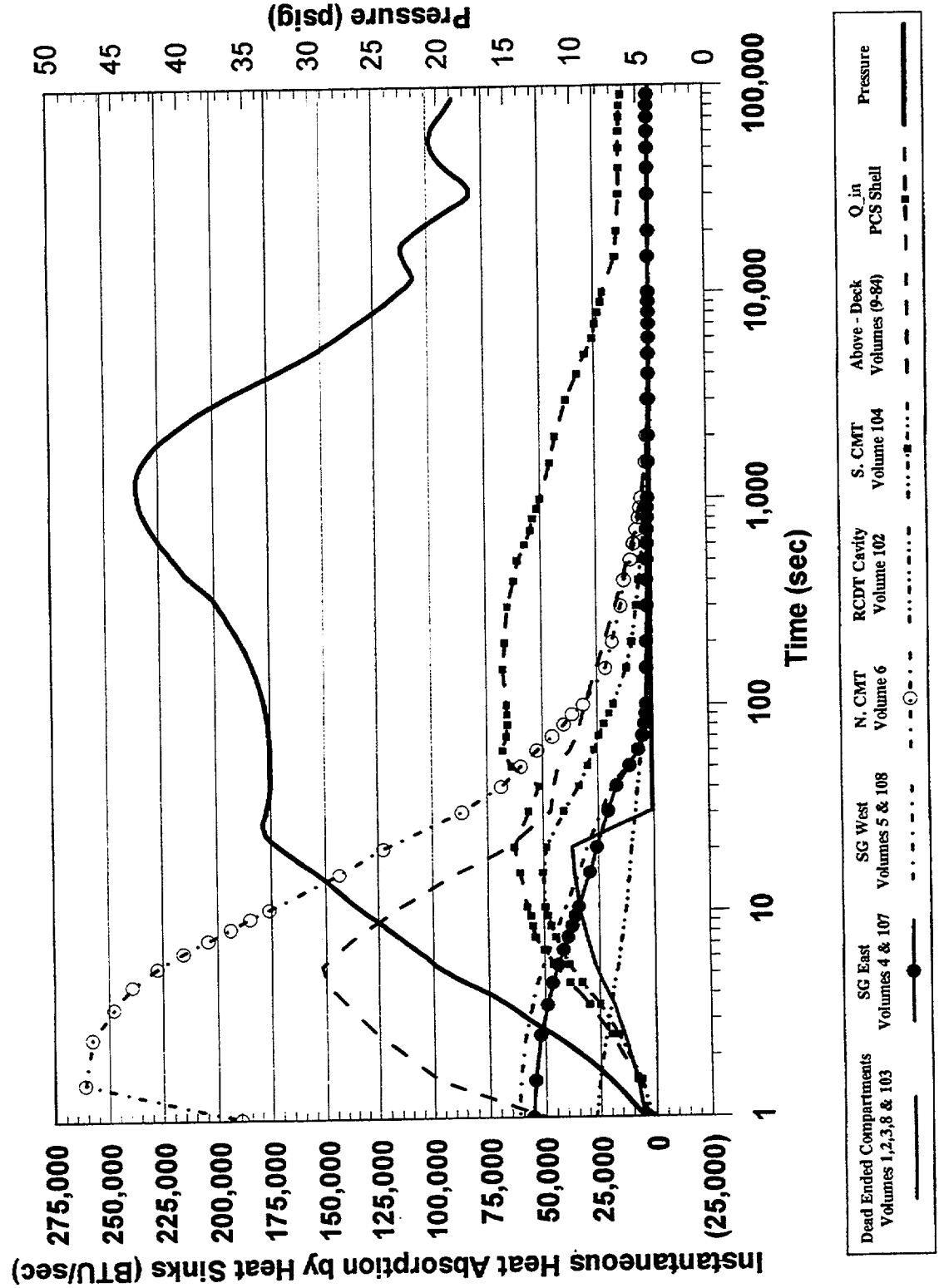

Figure 9-59 WGOTHIC Calculated AP600 Containment Heat Removal Rates - LOCA Plume Rising into CMT Room and SG Compartments

(a,c)

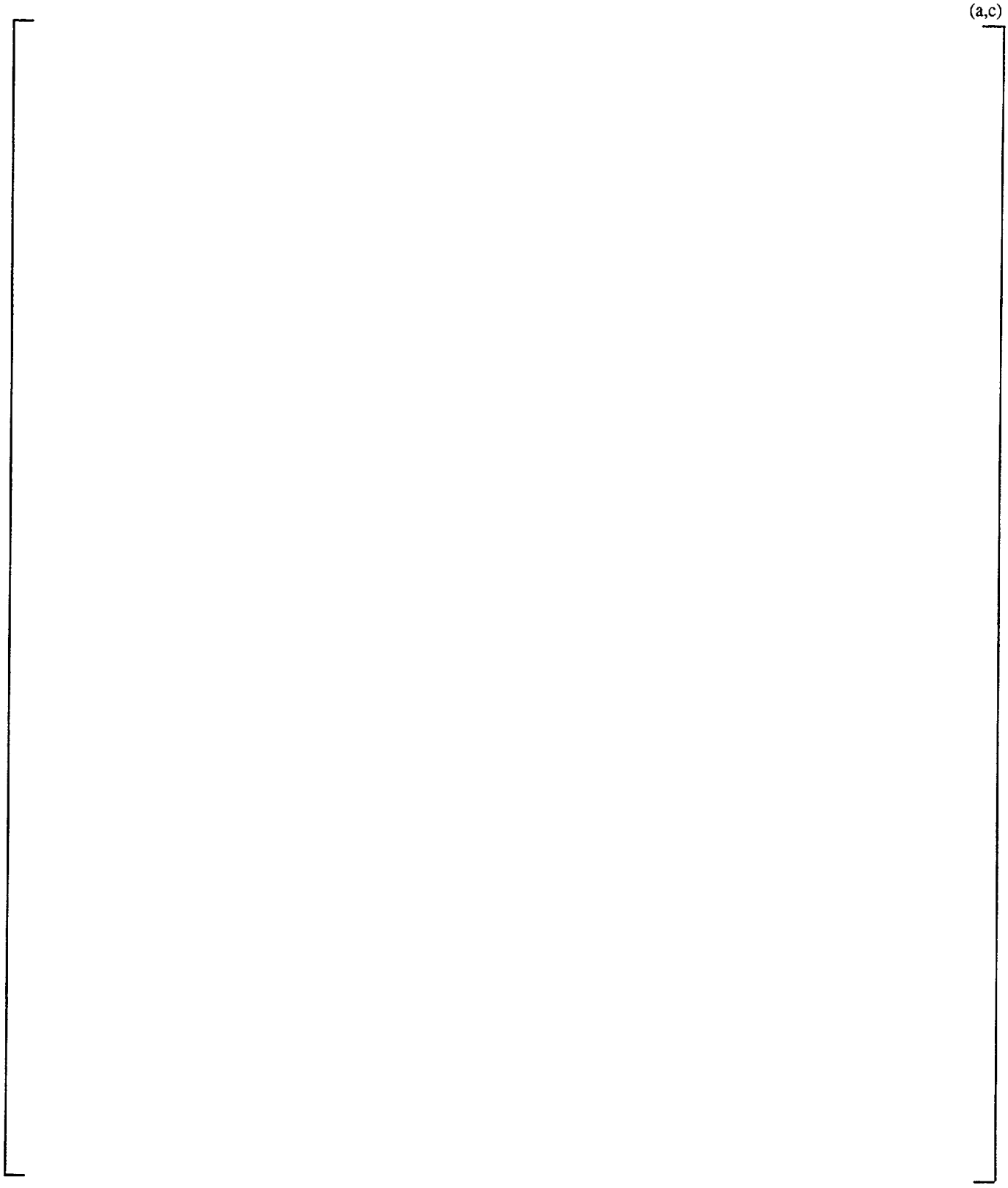

Figure 9-60 **WGOTHIC Calculated AP600 Containment Steam Pressure Ratio for MSLB Above-Deck**

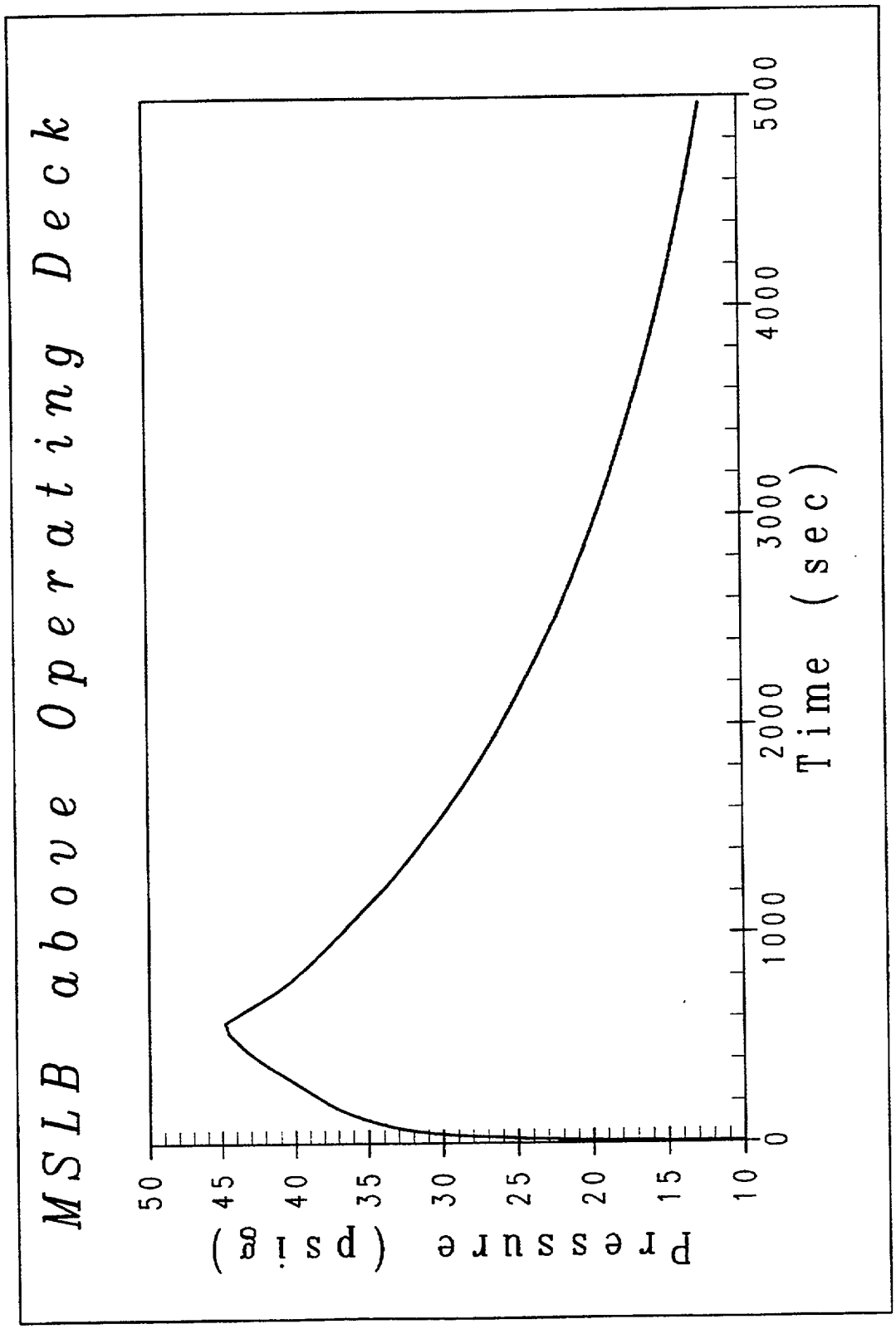

Figure 9-61 WGOTHIC Calculated AP600 Containment Pressure - MSLB Above Operating Deck

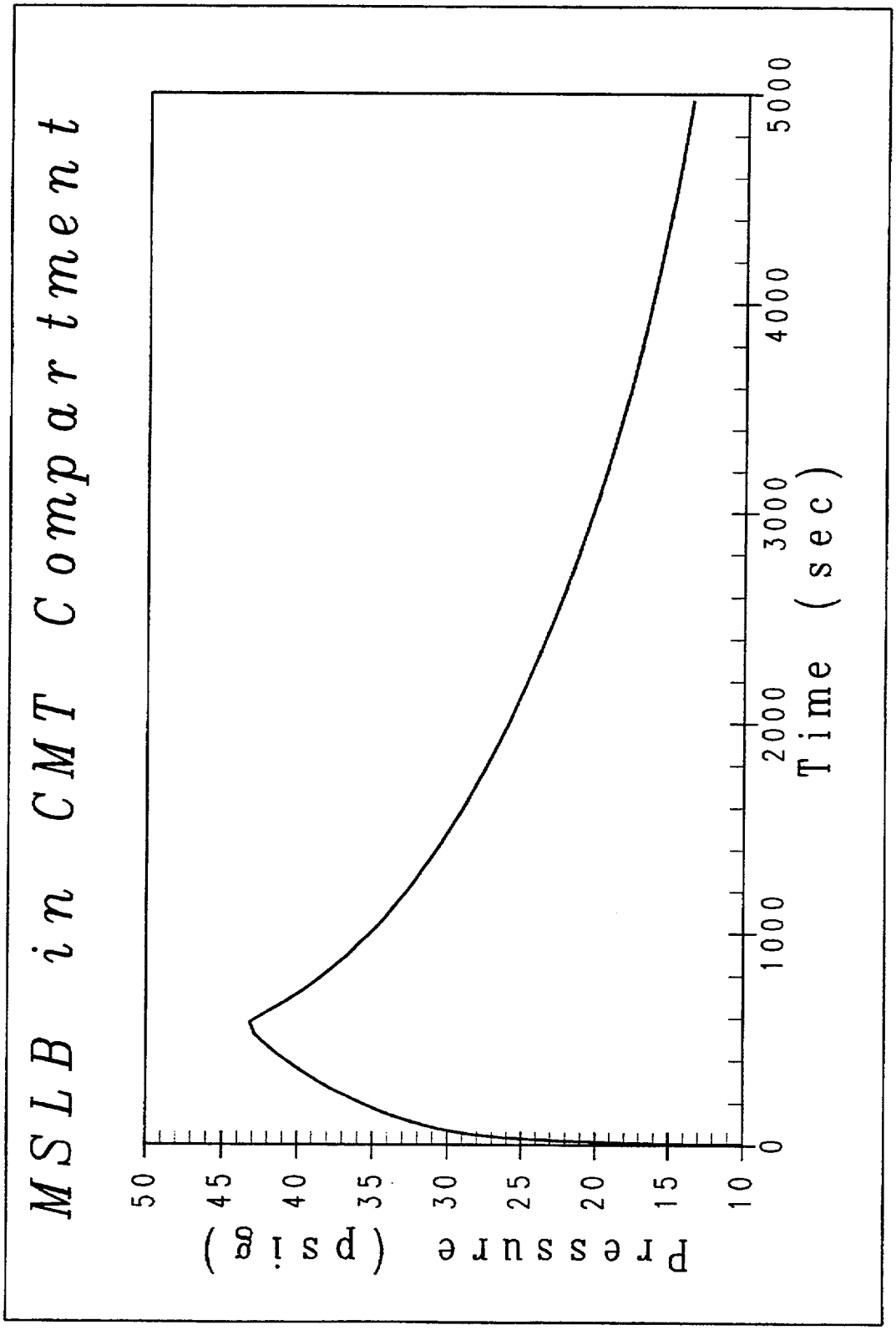

Figure 9-62 **WGOTHIC Calculated AP600 Containment Pressure - MSLB in CMT Room**

Appendix 9.A

Thermal and Circulation Effects of Drops During a LOCA

TABLE OF CONTENTS

9.A THERMAL AND CIRCULATION EFFECTS OF DROPS DURING A LOCA 9.A-2

LIST OF TABLES

9.A-1 Estimated Drop Fall Times 9.A-2

9.A THERMAL AND CIRCULATION EFFECTS OF DROPS DURING A LOCA

Drops, or fog particles, are created when the blowdown break source steam velocity is large enough to disperse a fraction of the break liquid along with the gas. As discussed in Section 4.4.2D of Reference 9.A.1 and Section 7.1 of Reference 9.A.2, drops will be formed during the LOCA blowdown phase. For the post-blowdown phases of a LOCA and for the MSLB, there will not be any significant drop formation. The thermal and circulation effects of drops on LOCA containment pressure are examined in this section.

The limiting DBA analysis LOCA is a DECLG break. The source flow from the reactor side of the break has more energy than the source flow from the steam generator side of the break, so more drops are expected from the reactor side. During blowdown, a range of drop sizes will be produced. The percentage of liquid converted to drops will also be within some range, the theoretical limits being 0 and 100 percent, although it is anticipated that a significant fraction of the liquid will form drops.

Many factors affect the length of time that the drops will be present in the atmosphere, such as shear coupling to the moving gas, coalescence, de-entrainment at walls and other surfaces, and the drop size (affecting its fall time). To estimate the fall time for various size drops, a simple calculation was performed which only accounts for the gravitational effects on the drops. Using the terminal velocity versus drop diameter information in Section 7.6 of Reference 9.A.3, fall times range from seconds to hours depending on the drop size and fall height. Table 9.A-1 shows estimated fall times for drops with diameters of 0.001, 0.01, and 0.1 inches. This provides an indication that the drops will exist long enough that their effect on containment pressure must be considered.

Table 9.A-1 Estimated Drop Fall Times

Drop Size (in)	Terminal Velocity (ft/sec)	Fall Time (sec) 30 ft	100 ft
0.001	.08	375	1250
0.01	8	3.8	12.5
0.1	20	1.5	5

Thermal Effects

The drops flash when they enter the containment atmosphere, reaching saturation very quickly. Section 7.1 of Reference 9.A.2 estimates 3.5 percent of a given drop flashes to steam. Section 7.1 also estimates that the drop diameter only decreases 5 percent due to evaporation in later phases. The drops are strongly coupled to the containment atmosphere temperature due to the large surface area of the total drop population. This strong coupling results in the drop temperature closely following the containment atmosphere temperature as it changes during the transient. Sensitivities using WGOTHIC show that if 5 percent or more of the liquid is converted into drops, then the containment atmosphere will be saturated quickly. Given the high velocity of the blowdown releases, much greater than 5 percent is anticipated to be converted into drops. With the atmosphere saturated, thermal effects such as superheating will not occur and the effect of larger drop fractions does not significantly affect the pressure response. The effects of drops on the Evaluation Model calculation of containment pressure is investigated with a sensitivity study described in Section 5.8.

Circulation and Stratification Effects

The presence of drops increases the density of the containment atmosphere, which makes the post-blowdown steam release relatively more buoyant. An estimate of the effect of drops on circulation and stratification is made by calculating the plume entrainment rate and resulting circulation time constant for the conditions at the end of the blowdown phase of the DBA LOCA. As discussed in Section 7.1 of Reference 9.A.2, well-accepted models are not available to predict the mass of the drops created during blowdown, so the bounds of 0 percent and 100 percent of the liquid will be considered.

To estimate the volume entrained into the plume (Q_{ent}, in ft^3/sec), Peterson's equations (Reference 9.A.4) can be used:

$$Q_{ent} = 0.15 * B^{1/3} * Z^{5/3}$$

where: Z = elevation (ft.)

$$B = g * Q_{st} * (\rho_{amb} - \rho_{st})/\rho_{amb}$$

g = gravitational acceleration = 32.2 ft/sec^2

Q_{st} = volumetric steam flow (ft^3/sec)

ρ_{amb} = containment ambient density (lbm/ft^3)

ρ_{st} = steam density (lbm/ft^3)

The entrainment is calculated for a height of 100 feet above the top of the steam generator compartment, so Z = 100 ft. The steam release at the beginning of the peak pressure phase is estimated to be 1870 ft^3/sec (Q_{st}). For the case assuming 0 percent of the liquid is released as drops, the $(\rho_{amb} - \rho_{st})/\rho_{amb}$ term is approximately 0.275. For the case assuming 100 percent of the liquid is released as drops, the density term

is approximately 0.60. Using the above equation, the estimated entrainment rate is Q_{ent} = 8239 ft^3/sec (0 percent drops) and 10695 ft^3/sec (100 percent drops). The estimated entrainment at the end of blowdown is approximately four times the steam flow (Q_{st}) for the case without drops, and slightly less than six times the steam flow for the case with drops.

Knowing the entrainment rate, a circulation time constant can be calculated for the containment free volume. This time constant will change with time, but it provides an indication of the amount of circulation expected for the releases after the refill phase. The circulation time constant is the volume divided by the entrainment rate, and for 0 percent drops it is 206 seconds and for 100 percent drops it is 159 seconds. It should be noted that the estimated times conservatively neglect volumetric entrainment into the wall layers. These time constants increase as the steam flow decreases, but this estimation shows that a large fraction of the containment volume will be entrained in the plume within a few minutes, which is relatively short compared to the time to reach maximum pressure (at approximately 1200 seconds), and very short compared to long-term cooling. A relatively large entrainment rate within the above-deck region indicates that the steam density gradients above-deck are not large whether drops exist or not. Therefore, the presence of drops will not significantly affect the general circulation and stratification patterns in the containment atmosphere.

Evaluation Model Drop Sensitivity Study

The AP600 Containment Evaluation Model, with the LOCA jet dissipated in the steam generator compartment, was used to determine the effect of drops on the calculation of containment pressure. The treatment of drops in the AP600 Containment Evaluation Model is described in Section 4.5.2.1. The Evaluation Model converts all of the liquid from the reactor side of the break to drops, and none of the liquid from the steam generator side of the break. Sensitivity cases were analyzed for comparison to the Evaluation Model results. The sensitivity cases are discussed in Section 5.8. One case modeled no drop formation and one case modeled 100 percent of the liquid converted into drops.

The containment pressure, as a function of time, was calculated for the sensitivity case. The maximum containment pressure, calculated with the Evaluation Model, is greater than the maximum pressure calculated assuming no drop formation. The presence of drops does have a slight influence on the Evaluation Model pressure calculation. Drop formation is expected during the blowdown phase and the sensitivity study indicates that drop formation should be modeled to provide a bounding calculation for containment pressure.

Conclusions

The formation of drops during the LOCA blowdown phase is a physically real phenomenon that may influence the maximum containment pressure calculated by the Evaluation Model. Drop formation increases the density of the containment atmosphere making the post-blowdown releases relatively more buoyant. A small percentage of the blowdown break liquid formed into drops is sufficient to saturate the containment atmosphere, at which point additional drop density has a minor thermal effect. The Evaluation Model treatment of drops, provides a sufficient bounding calculation for maximum and long-term containment pressure.

References

9.A.1. WCAP-14812, "Accident Specification and Phenomena Evaluation for AP600 Passive Containment Cooling System," Revision 2, April 1998.

9.A.2. WCAP-14845, "Scaling Analysis for AP600 Containment Pressure During Design Basis Accidents," Revision 3, March 1998.

9.A.3. NTD-NRC-95-4563, "GOTHIC Version 4.0 Documentation, Enclosure 2: Technical Manual," September 21, 1995.

9.A.4. Peterson, P., "Scaling and Analysis of Mixing in Large Stratified Volumes," *International Journal of Heat and Mass Transfer*, Vol. 37, Supplement 1, pp 97-106, 1994.

Appendix 9.B

Effects of Stratification on Heat Sink Utilization

TABLE OF CONTENTS

9.B.1 INTRODUCTION 9.B-2
9.B.2 HEAT SINK ANALYSIS 9.B-2
9.B.3 CONDENSATION BOUNDARY CONDITIONS 9.B-2
9.B.4 HEAT CONDUCTION MODELS 9.B-5
9.B.5 RESULTS 9.B-7
9.B.6 CONCLUSIONS 9.B-11

LIST OF TABLES

9.B-1 Concrete Model Nodal Thickness 9.B-6
9.B-2 AP600 Assumed Room Heat Sink Distribution 9.B-9

LIST OF FIGURES

9.B-1 Condensation Heat Transfer Coefficients vs. T_{surf} 9.B-13
9.B-2 Containment Shell Heat Sink Results 9.B-14
9.B-3 CMT Room Heat Sink Results 9.B-15

9.B.1 INTRODUCTION

An analysis was performed to determine the impact of stratification on the relative effectiveness of containment heat sinks during a postulated LOCA. Models were developed to study transient heat conduction effects for steel and concrete structures under a variety of containment atmosphere boundary conditions. The models were then used to determine the effects of stratification of steam in the containment atmosphere on heat sink utilization in the CMT room and in the above-deck region.

9.B.2 HEAT SINK ANALYSIS

The condensation heat transfer in the containment atmosphere has been characterized as a function of the steam fraction, and has been used as boundary conditions to determine the transient heat absorption rate of the heat sink structures. The results of these analyses are used to estimate the relative effects of stratification on the heat sinks located on the PCS steel shell and in the CMT room.

The purpose of the analysis is to obtain relative effects of stratification for reasonably representative conditions to assess the magnitude of the bias. An extreme stratification gradient is assumed from which the relative effect of stratification on total heat sink energy removal in a region can be assessed. A bias is developed to bound the non-conservative effects of stratification.

9.B.3 CONDENSATION BOUNDARY CONDITIONS

These sensitivity calculations are performed to examine the relative effect of a gas mixture that is homogeneous (as in a lumped parameter node) and a gas mixture that is stratified. To keep the calculations simple, boundary conditions are assumed constant with time, and the following homogenous atmosphere conditions are assumed:

T_{atm} = 276°F

P_{atm} = 59.7 psia

f_{st} = 0.63 (homogeneous steam mole fraction)

These parameters represent approximately time-averaged values over the first hour of the LOCA, since the CMT room steam concentration is relatively constant (Figure 9-44).

The heat transfer from the containment atmosphere and the structure is assumed to be dominated by condensation so that convection and radiation are neglected. The condensation heat transfer is determined by first determining the mass transfer for turbulent free convection (Reference 9.B.1, Section 4.3):

$$\dot{m}'' = 0.13^{*} \frac{\rho_{stm} D_v \Delta P_{stm}}{(\upsilon^2/g)^{1/3} P_{lm,air}} \left(\frac{\Delta\rho Sc}{\rho} \right)^{1/3} \quad (9.B\text{-}1)$$

where

$\dot{m}''$ is the condensation mass flux
ρ_{stm} is the density of steam at the total pressure and boundary layer temperature
ΔP_{stm} is the difference in the steam partial pressure atmosphere - surface
ν is the mixture kinematic viscosity
g is gravity
$P_{lm,air}$ is the log mean pressure difference atmosphere - surface
$\Delta\rho$ is the mixture density difference atmosphere - surface
ρ is the bulk mixture density
Sc is the mixture Schmidt number (typically ~0.51)

and D_v is the air-steam diffusion coefficient which is given by (Reference 9.B-1, Section 4.3.2)

$$D_v = 0.892 \frac{14.2 \text{ psi}}{P} \left(\frac{T_{surf} + T_{atm}}{2 \times 460^{\circ}R} \right)^{1.81} \quad (9.B\text{-}2)$$

The steam partial pressure in the atmosphere is given by:

$$P_{stm\text{-}atm} = f_{st} * P \quad (9.B\text{-}3)$$

where f_{st} is the steam mole fraction in the atmosphere and P is the total pressure.

The steam partial pressure at the condensing surface is given by:

$$P_{stm\text{-}surf} = P_{sat}(T_{surf}) \quad (9.B\text{-}4)$$

where P_{sat} is the saturation pressure corresponding to T_{surf}.

The log mean pressure difference between the atmosphere air pressure and the air pressure at the surface is given by:

$$P_{lm-air} = \frac{(P_{air-surf} - P_{air-atm})}{\ln (P_{air-surf} / P_{air-atm})} \quad (9.B\text{-}5)$$

where $P_{air-surf}$ is the air partial pressure at the heat sink surface, $P - P_{stm-surf}$ and $P_{air-atm}$ is the air partial pressure in the atmosphere, $(1 - f_{st}) * P$.

The densities of air and steam at the atmospheric and surface pressures and temperatures are determined from the ideal gas law.

To determine the effect of the steam fraction, three distinct regions based on equal volume are assumed. The top region is assumed to be nearly all steam with $f_{st-top} = 0.98$. The middle region is assumed to be at the nominal conditions with $f_{st-mid} = 0.63$. The bottom region steam fraction is determined by conserving the total amount of steam in the total volume.

$$f_{st-bot} = 3^* f_{st-nom} - f_{st-top} - f_{st-mid} = 0.28 \quad (9.B\text{-}6)$$

Applying these three steam mole fractions along with the above containment atmosphere conditions, a relationship can be determined for the condensation heat transfer coefficient as a function of heat sink surface temperature. An equivalent condensation heat transfer coefficient is calculated from $\dot{m}''$ for use as a boundary condition for heat sink condensation, described later. The equivalent condensation heat transfer coefficient is calculated by:

$$h_{cond} = \frac{m^* h_{fg}}{(T_{atm} - T_{surf})} \quad (9.B\text{-}7)$$

where h_{fg} is the difference between the steam and liquid saturation enthalpy. The relationships for equivalent heat transfer coefficient are shown graphically in Figure 9.B-1.

The condensation heat transfer coefficient varies considerably with respect to the steam fraction in the containment atmosphere, f_{st}, and the surface temperature, T_{surf}. For each steam fraction, the heat transfer coefficient increases with increasing T_{surf} until the saturation temperature that corresponds to the steam partial

pressure at the surface is reached. At this point the condensation heat transfer drops to zero, and is zero for all surface temperatures greater than this temperature.

For the case of $f_{st} = 0.98$, $T_{sat} = 291\,°F$, which is greater than the containment atmosphere temperature. Thus, the condensation heat transfer coefficient increases with surface temperature and no cutoff is reached. For the case of $f_{st} = 0.63$, $T_{sat} = 264\,°F$, and the heat transfer coefficient drops to zero at this temperature. For the case of $f_{st} = 0.28$, 217 °F, the heat transfer coefficient drops to zero.

9.B.4 HEAT CONDUCTION MODELS

Several models were developed to calculate heat transfer to the heat sinks. These include:

- Steel structures of varying thickness
- Concrete structures
- Steel-jacketed concrete structures
- Steel containment shell

A description of each model is given as follows.

Steel Structures

The one-dimensional model consists of a 1 ft. by 1 ft. section of steel, modeled by ten nodes of equal thickness, representing one-half the heat sink thickness. For example, for a one-half inch thick steel plate, the model has ten nodes, each 0.025 in. thick. A convective boundary condition is applied to one surface, while the other surface is assumed to be adiabatic. Connections between the nodes are defined by the area of the interface (1 ft^2), and the distance from the node center to the interface (0.0125 in.). The properties for steel are listed below:

$\rho = 490.7$ lbm/ft^3
C = 0.107 Btu/lbm-°F
k = 30 Btu/hr-ft-°F

A zero-volume node is attached to the steel at the surface exposed to the atmosphere. The boundary conditions for the three steam fractions are described in the previous section.

Concrete Heat Sinks

The concrete heat sinks have much lower thermal conductivity and are modeled differently than the steel heat sink. The thermal properties of the concrete are given as:

$\rho = 140$ lbm/ft^3
C = 0.19 Btu/lbm-°F

k = 0.83 Btu/hr-ft-°F

Once again, ten nodes are used to represent one-half the concrete thickness. For this case, the nodes are not equal volume with the nodes nearest the convecting surface having small thicknesses, and the thickness increasing geometrically as the nodes progress inward to the adiabatic boundary. The thicknesses are summarized for each node in Table 9.B-1.

(a,c)

As for the steel model, Node #1 is connected to a zero-volume surface node, which is in turn connected to the boundary temperature. The heat transfer coefficient is defined in the previous section as a function of the surface temperature for the three steam fractions considered.

Steel-Jacketed Concrete Heat Sinks

The steel-jacketed concrete heat sinks combines the two-foot thick concrete model previously described with a one-half inch steel plate. The condensation boundary condition is attached to the outside of the steel plate, that is represented by 10 nodes, 0.05 in thick. The inside steel node is attached to the first concrete node with an assumed gap of 0.036 in. The gap conductance is given by

$$h_{gap} = k_{mix} / \delta_{gap} \qquad (9.B\text{-}8)$$

where δ_{gap} is the gap thickness
and k_{mix} is the thermal conductivity of the containment atmosphere mixture

$$k_{mix} = 0.5^{*} (k_{air} + k_{stm}) \quad (9.B\text{-}9)$$

For $T_{atm} = 276°F$, and $f_{st} = 0.5$, $k_{mix} = 0.03$ Btu/hr-ft-°F, and $h_{gap} = 10$ Btu/hr-ft^2-°F.

The concrete is represented by 10 nodes with thicknesses shown in Table 9.B-1.

Steel Containment Shell

The steel containment shell model is somewhat more complex in that the inside boundary condition is the same as the other models while the outside boundary condition is not adiabatic, but is representative of the outer shell evaporative heat transfer. The steel shell is assumed to be [ ]^{a,c} in. thick. For this case, a [ ]^{a,c} The inner-most node is connected to a zero-volume node upon which the condensation boundary condition is assumed. The outer-most node is also connected to a zero-volume node upon which an evaporation boundary condition is assumed. The outside boundary temperature is assumed to be an average between the inlet air temperature at the bottom of the Passive Containment Cooling System annulus, and the outlet air temperature at the top.

$$T_{air\text{-}avg} = 142°F$$

and $h_{evap} = 113$ Btu/hr-ft^2-°F

Note that the assumption of a constant value of h over the entire shell surface is very conservative, since in the stratified case, the shell adjacent to the steam-rich top would heat up and significantly increase the evaporation rate on the outside. No credit is taken in this analysis for the associated increase in external heat transfer coefficient.

For this model, there is a short period of time during which the shell heats up from the initial temperature. After this time, a steady-state condition is established as heat is transferred at a nearly constant rate from the inside to the outside of the shell.

9.B.5 RESULTS

For each of the models described above, three transient calculations were performed representing each of the three steam fraction conditions. The results of these calculations were used to examine heat absorption effects for each of the conditions. Since the models represent one square foot of heat sink area, the results

can be used to estimate the heat sink behavior in a typical room by multiplying the integrated heat removal by the total area for a particular heat sink type.

Containment Steel Shell Heat Sink Stratification Sensitivity

Figure 9.B-2 shows the heat removal rate for the containment shell. The areas for the top, middle, and bottom of the shell are not weighted equally (as in Equation 9.B-10). The volume of the containment above the operating deck is divided into three regions of equal volume, and the associated surface area for each volume is used. For the AP600 containment,

Elevation of operating deck = 135.25 ft

Elevation of spring line = 218.71 ft

Elevation of top of dome = 256.4 ft

Containment radius = 65 ft

Gas Volume in dome = 336,963 ft^3

Surface area of dome = 15,552 ft^2

Total volume of gas above deck = 1.45 x 10^6 ft^3

The two lower regions both consist of a cylindrical gas volume = 481,582 ft^3. This corresponds to a cylindrical section 36.28 feet in length with a surface area = 14,776 ft^2. The upper region gas volume is also 481,582 ft^3, and consists of the dome and a cylindrical section 11.1 feet in length. The total surface area associated with this volume is 19,898 ft^2.

Thus, the equivalent integrated heat removal rate through one square foot of the shell is weighted by surface area as

$$\dot{Q}_{3\text{-Region}} = (19{,}898^{*}\ \dot{Q}_{top} + 14{,}776^{*}\dot{Q}_{mid} + 14{,}776^{*}\dot{Q}_{bot})/49{,}450 \qquad (9.B\text{-}10)$$

The results show that the higher weighting of the upper, steam-rich region nearly compensates for the lower heat removal rates in the bottom region, and the heat removal rate is slightly (~0.5% after 200 seconds) higher for the homogeneous case.

Results for the steel shell assessment are presented in terms of instantaneous rate since the external boundary condition never allows the steel to saturate. The results also allow interpretation of stratification effects during the quasi-steady, long-term, while the steel shell is the dominant heat sink and the balance between instantaneous source and sink heat rates governs the containment pressure. Since the stratification penalty on the steel shell heat removal rate is nearly negligible, a simple bias is introduced into the Evaluation Model by removing the non-grating operating deck floors to bound the effect. The stratification effect is exaggerated due to the use of an extreme gradient, well beyond what has been observed in the LST (Section 9.2.1 and 9.2.3) and in the international containment database (Appendix 9.C.2).

Simulated Room Heat Sink Stratification Sensitivity

These models were applied to heat sinks which reasonably represent the AP600 CMT room. The heat sinks for the AP600 CMT room (North and South sections) are summarized in Table 9.B-2.

Table 9.B-2 AP600 Assumed Room Heat Sink Distribution

Heat Sinks in Simulated Room	Thickness	Surface Area	Region
Steel-Jacketed Concrete - Ceiling (single-sided)	0.5 in. / 24 in.	5398.87 ft^2	Top
Steel-Jacketed Concrete - Floors (single-sided)	0.5 in. / 24 in.	5601.44 ft^2	Bottom
Steel-Jacketed Concrete - Walls (double-sided)	0.5 in. / 24 in.	4596.11 ft^2	1/3 in each region
Steel-Jacketed Concrete - Wall (double-sided)	0.5 in / 48 in	673.99 ft^2	1/3 in each region
Concrete - Bulk (double-sided)	48 in.	3287.36 ft^2	1/3 in each region
Steel - CMT (single-sided)	4.874 in.	1848.8 ft^2	1/3 in each region
Steel - Containment Shell Wall (single-sided)	1.57 in.	11385.53 ft^2	1/3 in each region
Steel - Columns (double-sided)	0.39 in.	1656.5 ft^2	1/3 in each region
Steel - Floor Grating (double-sided)	0.39 in.	3781.69 ft^2	1/3 in each region
Steel - Elevator (double-sided)	0.2 in.	218.96 ft^2	1/3 in each region
Steel - Platform (double-sided)	0.144 in.	11254.2 ft^2	1/3 in each region
Steel - Stair & Rails (double-sided)	0.132 in.	181.59 ft^2	1/3 in each region

As was discussed previously, each heat sink was analyzed using three different steam fractions representing the top, middle, and bottom thirds of the room which is a bounding gradient when the plume rises through the CMT compartment. There is expected to be no significant stratification penalty in the CMT room with

downflow in the Evaluation Model, where the plume rises from the steam generator compartment. For each individual heat sink, a homogeneous case and three-region averaged result was obtained for a 1 ft^2 section of the heat sink. The energy removal by each heat sink is determined by calculating the heat removal for 1 ft^2, and multiplying by the appropriate surface area.

Where appropriate, the heat sinks that are located in a specific volume (i.e., ceilings and floors) are not averaged for the three-region, but are analyzed solely with the steam fraction of that volume. This becomes important for the ceilings since these heat sinks are located within the high steam fraction volume and higher heat transfer is expected when the room is stratified. The opposite is expected when considering floors. Refer to Table 9.B-2 for the region designation.

Figure 9.B-3 shows the integrated heat removal by all the heat sinks in the CMT room for a one hour transient. As will be discussed below, the stratification bias for this case is a function of the total energy absorbed. This is because the adiabatic boundary condition results in heat sinks reaching a maximum thermal absorption governed by the saturation temperature for the given steam concentration in a volume. Therefore, results for this scenario are presented in terms of integrated total heat absorption.

The results show the CMT room heat sinks including the floors for the homogeneous and stratified cases. In addition, the case where the floors are not included for the homogeneous case is also shown. The stratified, three-region results are lower than the homogeneous case results by 10-15% when all heat sinks are considered. The homogeneous case with floors excluded is slightly conservative when compared to the stratified case with the floors included. Thus, the combination of assuming homogeneous conditions and neglecting the floors in the total heat sink area results in total heat sink utilization that is neutral at the time of peak pressure, and over the longer term is slightly conservative relative to the expected conditions.

The assessment of stratification effects is very conservative because a conservatively low benefit for the uppermost region is used, and the gradient is much more extreme than what has been observed in the LST (9.2.1 and 9.2.3) and in the international containment database (Appendix 9.C.2). The choice of stratified conditions to examine for this sensitivity are conservative and the results bound other, less extreme postulated stratification gradients. The room temperature is assumed to be 276 °F in the stratified case, the same temperature as in the base case homogeneous room. One could, for example, postulate a less extreme, thermodynamically consistent, gradient of 0.77 for the top, 0.63 for the middle, and 0.49 for the bottom. The saturation temperature for a region at 59.7 psia and a steam mole fraction of 0.98 (psat of 58.5 psia) is 291 °F. The upper region then would be about 15 °F hotter than assumed. Therefore, the upper region conditions are thermodynamically inconsistent in a way that minimizes heat absorption in the upper region of the room, and thus maximizes the stratification bias.

The bias for the CMT room is governed by the air content in the lowest region. Results indicate that steel heat sinks, and the steel on jacketed concrete, reach a maximum for integrated heat absorption well within

the one-hour time frame of the calculation. The concrete continues to absorb heat over a very long term, on the order of days. However, the transient skin temperature of concrete increases due to its relatively poor thermal conductivity and a gap between the steel jacket and concrete reduces concrete effectiveness, so that the magnitude of concrete heat absorption is not significant relative to the steel. The integrated heat absorption by heat sinks is then primarily a function of the maximum bulk steel temperature rise, which is related to the saturation temperature of the adjacent region. While a less severe assumed stratification gradient would result in less rapid heat absorption by sinks in the upper region, the upper heat sinks would still reach their maximum well within the one- hour time frame. The lower region integrated heat absorption is limited by the saturation temperature for the assumed steam concentration. Therefore, the stratification bias is controlled by the lower region steam concentration and is maximized by the assumption of the extreme stratification gradient.

Since the exaggerated effect of stratification for the case of a plume rising through the CMT shows a bias on total integrated heat removal, a bias is introduced into the Evaluation Model by removing heat sinks associated with floors in compartments. As an additional conservatism, that bias is retained for the Evaluation Model with a plume rising through the steam generator compartment, as well as all sensitivity cases performed, even though most situations result in downflow through the CMT compartment.

For the case of the steel containment shell above the operating deck, the dome surface area weights the upper, steam-rich volume more heavily than the lower volumes, and compensates for the lower heat removal rates. Thus, the homogeneous case results are nearly equal to those for the stratified case, with the homogeneous case giving less than 0.5% less instantaneous heat removal rates. A simple bias of removing operating deck floors is included in the Evaluation Model to bound this effect.

9.B.6 CONCLUSIONS

For the case of the steel containment shell above the operating deck, the dome surface area weights the upper, steam-rich volume more heavily than the lower volumes, and compensates for the lower heat removal rates. Thus, the homogeneous case results are nearly equal to the stratified case, with the homogeneous case giving less than 0.5 percent less instantaneous heat removal rates. A simple bias of removing operating deck floors is included in the Evaluation Model to bound this effect.

The results of the heat sink utilization analysis for below-deck compartments indicate that in general, the assumption of homogeneous compartment volumes predicts higher overall heat removal by the heat sinks compared to stratified volumes. This is primarily due to the propensity of the condensation heat transfer to fall off as the heat sink surface temperature approaches the local saturation temperature in the lower steam fraction volumes. Stratification gradients are not expected to be nearly as extreme as assumed in this evaluation. The results of the homogeneous case gives 15-20% higher integrated heat removal than the

stratified results. Therefore, a bias is introduced in the Evaluation Model to account for this difference, implemented by removing heat sinks representing floors from the Evaluation Model.

References

9.B-1. WCAP-14845, "Scaling Analysis for AP600 Containment Pressure During Design Basis Accidents," Revision 3, March 1998.

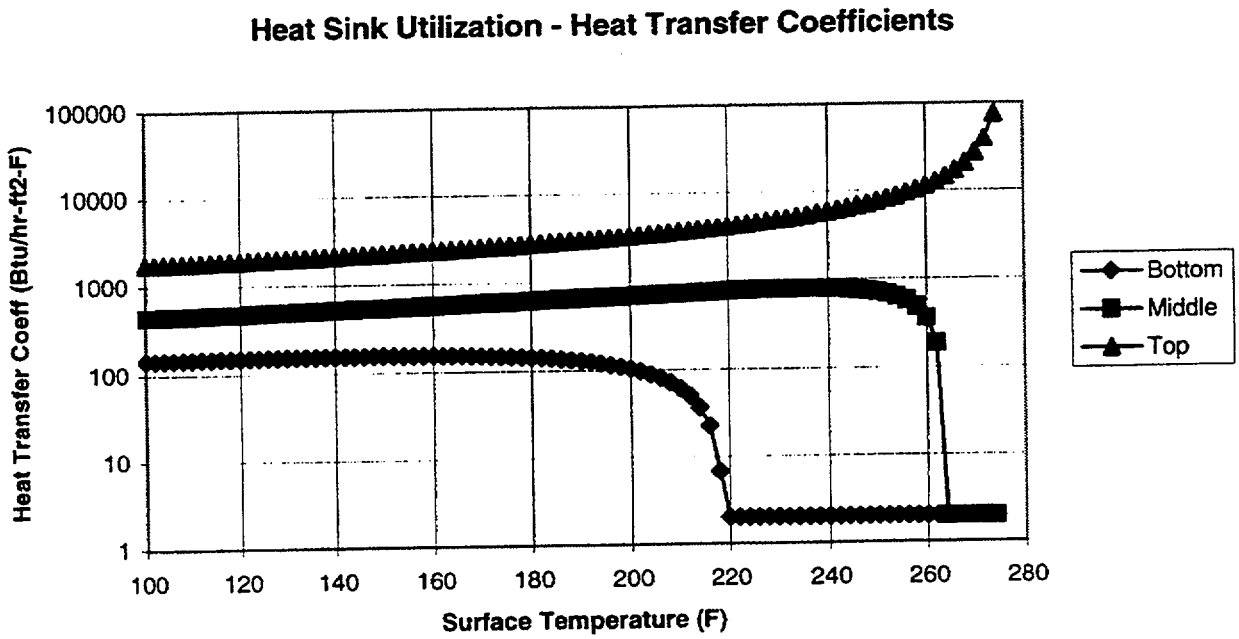

Figure 9.B-1: Condensation Heat Transfer Coefficients vs. T_{surf}

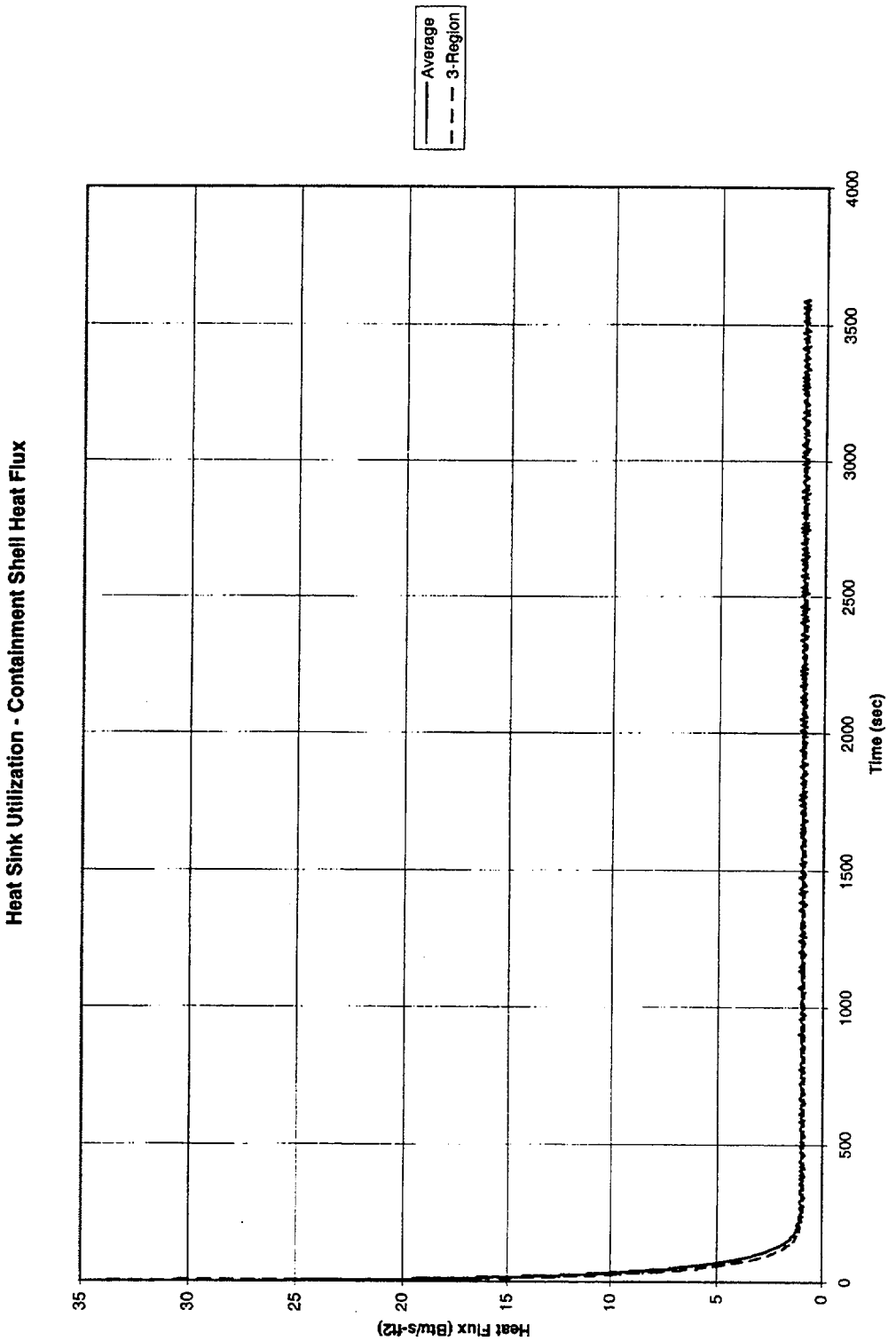

Figure 9.B-2: Containment Shell Heat Sink Results

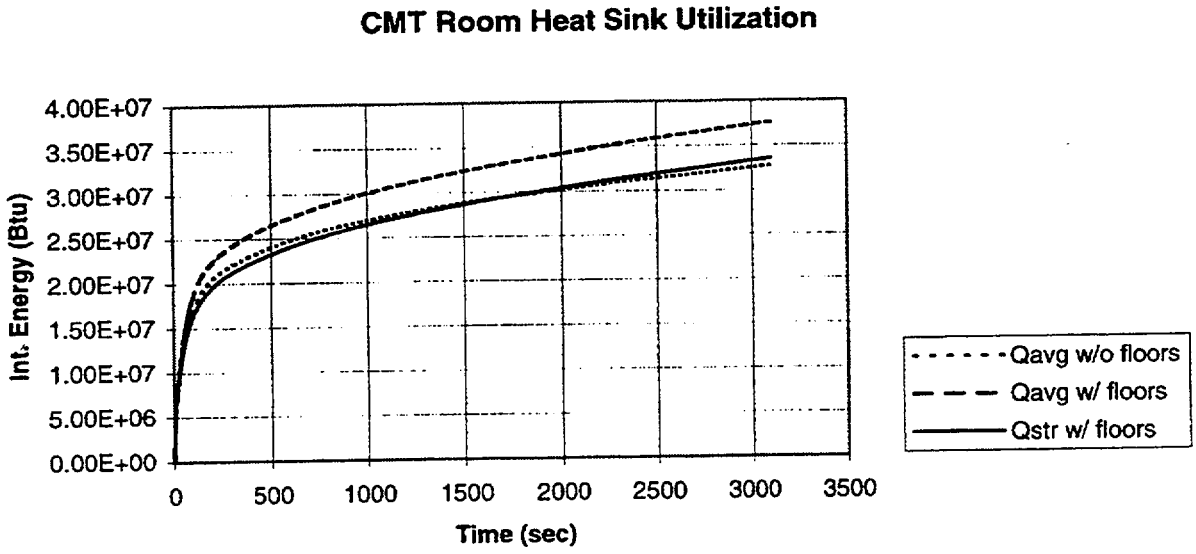

Figure 9.B-3: CMT Room Heat Sink Results